IDENTIFYING NOVEL ROLES FOR THE IMMUNOPROTEASOME IN THE RETINA

A DISSERTATION
SUBMITTED TO THE FACULTY OF THE GRADUATE SCHOOL
OF THE UNIVERSITY OF MINNESOTA
BY

STACY ANN HUSSONG

IN PARTIAL FULFILLMENT OF THE REQUIREMENTS
FOR THE DEGREE OF
DOCTOR OF PHILOSOPHY

Dr. Deborah A. Ferrington, Ph.D., Advisor

October 2010

Acknowledgments

First I would like to thank my advisor and mentor, Deb Ferrington. She has helped shape me into the person I am today. She always has unswerving optimism and patience, even when experiments go sideways. Deb always has her door open and has been ready to answer any questions I have. I couldn't have asked for a better advisor, mentor, and friend.

I would also like to thank everyone who has worked in the Ferrington lab, past and present. In particular, I would like to thank Pabalu Karunadharma, my fellow toiler in graduate school, and Becky Kapphahn. I would also like to thank Elizabeth Lockamy, the honorary member of the Ferrington lab. They have all been with me since the beginning. The people you work with can make or break you and I was lucky enough to be made by them.

I would also like to thank Machelle Pardue. She made a journey all the way up to Minnesota just to teach me how to do ERGs. I have spent many hours in the dark because of her, literally.

I would like to thank my family as well. They have always been willing to listen to what I have been doing in lab. I would especially like to thank my sister April, for all the hours she has spent in the car with me listening to me talk about Western blots and for giving up her Sunday to help me format my thesis.

This work was supported in part by grants from the National Institutes of Health T32-AG029796 (SAH), EY014176, EY013623, AG032391 (DAF), P30-EY11374 (Core Grant for Vision Research, HR), EY011542 (DSG), T32-EY07133 (CME), and AG025392 (TWO), a Career Development Award from the American Federation for Aging Research and Foundation for Fighting Blindness (DAF), American Health Assistance Foundation, Minnesota Medical Foundation, the University of Minnesota Academic Health Center and Graduate School, the Fesler-Lamper Foundation, and an unrestricted grant to the Department of Ophthalmology from the Research to Prevent Blindness Foundation and the Minnesota Lions Clubs.

Dedication

I would like to dedicate this thesis to my parents. They have always told me I could do anything I set my mind to. Thanks for always being there to support and encourage me.

Abstract

Immunoproteasome is a proteasome sub-type that is known to produce antigenic peptides for MHC class I presentation. However, immunoproteasome is present in the immune-privileged brain and retina and is upregulated with disease in human retina and injury in mouse retina and brain, suggesting functions unrelated to its role in the immune system. The goal of this thesis is to define novel roles for the immunoproteasome in the retina.

Potential functions of the immunoproteasome were defined by comparing the stress response of wild-type and knock-out mice missing one (*lmp7*$^{-/-}$(L7)) or two (*lmp7*$^{-/-}$ /*mecl-1*$^{-/-}$(L7M1)) of the three immunoproteasome subunits. Aging was used as a model system for chronic stress. Chronic peroxide exposure in cultured retinal pigment epithelial (RPE) cells developed from wild-type mice was used as an additional stress model. In wild-type retinas and RPE cells, upregulation of immunoproteasome was observed in response to both models of chronic stress. To determine the consequence of eliminating immunoproteasome, the retinas and RPE cells from KO mice were examined. L7M1 retina had significantly elevated levels of photoreceptor apoptosis that further increased with age. In addition, L7M1 cell lines were more susceptible to oxidant-induced death. Together these data suggest immunoproteasome is protective against oxidative stress.

The localization of immunoproteasome to the outer plexiform layer in wild-type retina suggested a role in retinal function. Electroretinography was used to test the hypothesis that immunoproteasome is required for maintaining normal visual transmission. Data indicated that immunoproteasome-deficient mice had a decreased bipolar cell response as compared to wild-type. Evaluation of several retinal synapse proteins by Western blot revealed no significant difference in protein content across strains. In addition, gross retinal morphology and bipolar cell density were not different. In conclusion, immunoproteasome-deficiency causes a decrease in visual transmission but the mechanism is still unclear.

In summary, these data provide compelling evidence that immunoproteasome has a role in retinal stress response, specifically in protecting against oxidative stress.

Furthermore, immunoproteasome-deficient mice have a decreased bipolar cell response as measured by ERG. Altogether, data from this thesis strongly support the hypothesis that immunoproteasome has additional functions in the retina that do not involve immune function.

Table of Contents

List of Tables

List of Figures

Chapter 1

Chapter 2

Chapter 3

Chapter 4

Chapter 5

Chapter 1

Introduction

1.1. Proteasome

The proteasome was first discovered in the 1970s simultaneously in two labs [1, 2]. In the early 1980s, this protease was further characterized and coined the multicatalytic proteasome (MCP) complex [3-5], but eventually became known simply as the proteasome. From its discovery to the present, the number of publications regarding the proteasome has increased exponentially (17,729 publications as of October 2010), largely due to the ever-expanding functions and linkage to disease that is attributed to this essential complex. Recently, attention to the proteasome has shifted to the immunoproteasome sub-type. Originally, the immunoproteasome was thought to function exclusively in creating antigenic peptides for immune surveillance. An increasing number of studies have shown that immunoproteasome has a more general physiological role in the cell [6-11]. This thesis focuses on functions for the immunoproteasome in the retina that go beyond its role in the immune system.

1.1.1. Cellular functions of the proteasome

Although cellular protein homeostasis is maintained through both the lysosomal and proteasomal pathways [12], the proteasome is responsible for the majority of regulated protein degradation in the cell [12, 13]. The proteasome regulates many processes essential for cell survival, such as signal transduction, gene expression, protein quality control, and cell cycle control. Because of proteasome's involvement in cell cycle regulation (degradation of cyclins), proteasome inhibitors are now being used as cancer treatments [14]. Additionally, many nascent proteins rely on the proteasome for post-translational processing of the precursor protein to its mature form. For example, NFκB transcription factors p50 and p52 are produced as propeptides p105 and p100, respectively, that must be proteolytically processed to become active. An additional way the proteasome activates the NFκB transcription factor is through the degradation of the inhibitor IκB.

1.1.2. 20S proteasome structure

The 20S catalytic core of the proteasome contains four 7-membered rings of subunits that form a barrel-like structure (Figure 1.1A). The outer two rings of the

Figure 1.1. 20S proteasome structure

(A) The 20S proteasome core is composed of four 7-membered rings of α and β subunits. The outer two rings are made of the α subunits (α1-α7), while the inner two rings are comprised of the β subunits (β1-β7). Three of the β subunits have catalytic function (β1, β2, β5). These three subunits can be replaced by their inducible counterparts (β1i, β2i, β5i) to form the immunoproteasome. (B) A diagram of a vertical section through the 20S proteasome. The active sites (black spheres) of the catalytic subunits are sequestered to the center of the proteasome.

Figure 1.1. 20S proteasome structure

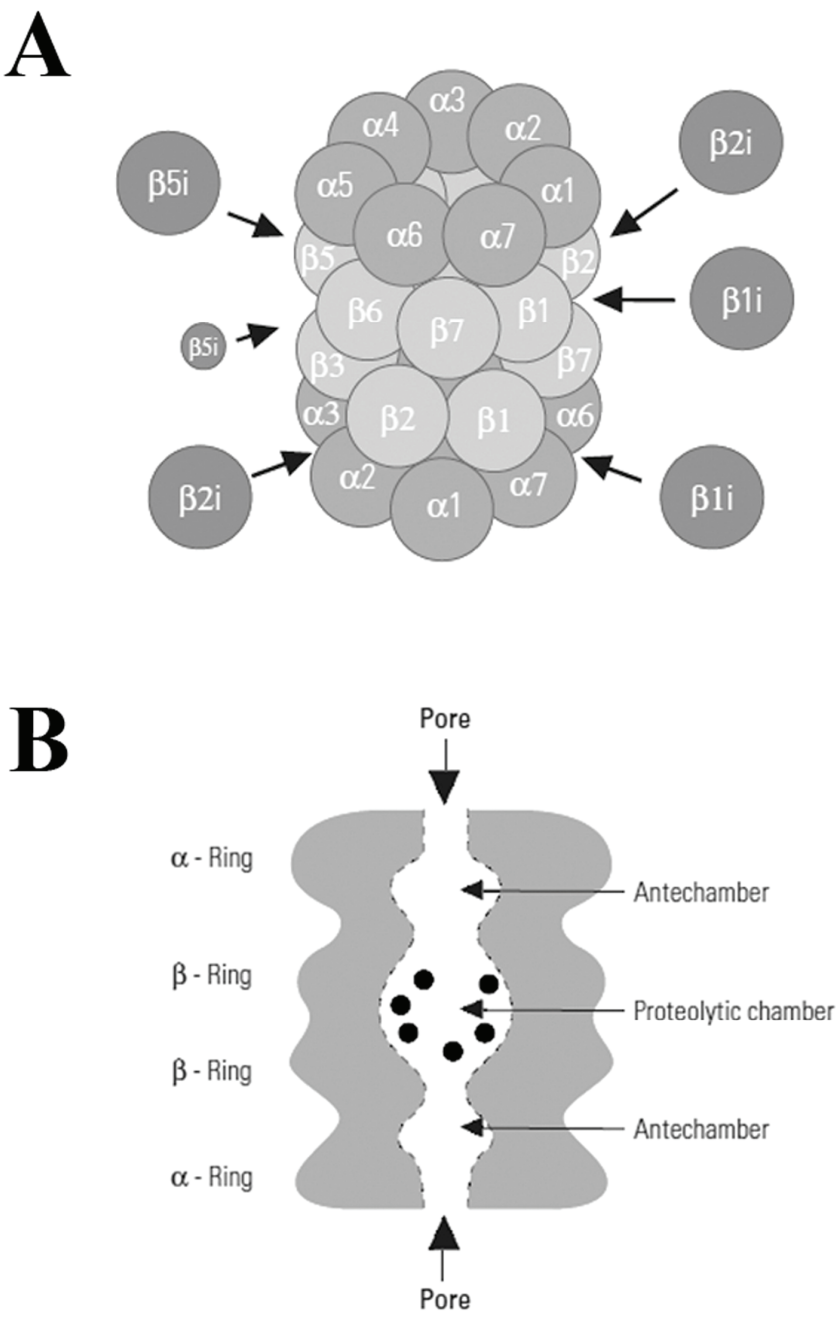

Figure is adapted from [15].

structure are comprised of α-subunits (α1-α7) and the inner two rings are formed from the catalytic β-subunits (β1-β7). The active sites face the interior of the 20S proteasome, which sequesters the catalytic activity of the proteasome to the interior chamber of the 20S core (Figure 1.1B). This isolation of the active sites is one mechanism that allows for controlled degradation of proteins by the proteasome. The structure of the proteasome also helps regulate degradation. The opening of the proteasome 'barrel' is only ~13 Å allowing only unfolded proteins to enter the catalytic chamber [16].

There are three major subtypes of proteasome that are defined by the composition of catalytic subunits. The standard proteasome contains the β1 (20SY), β2 (20SZ), and β5 (20SX) catalytic subunits. These three subunits can be replaced by their inducible forms β1i (LMP2), β2i (MECL-1), and β5i (LMP7) to form the immunoproteasome. The third proteasome subtype, the intermediate-type or mixed proteasome, contains a mixture of standard and immunoproteasome subunits [17].

The proteasome and its subunit composition were described by many different research groups working in different organisms. This led to multiple names being attributed to the same proteins. For example β2i subunit is also known as MECL-1 (human), Lmp10, and Psmb10 (yeast). The published literature is an amalgam of different nomenclatures. Scientists are now starting to use the more standardized nomenclature of subunits α1-α7 and β1-β7 [15]. This thesis uses a mixture of the old and new nomenclature.

1.1.3. Proteasome catalytic activity

The three sets of catalytic subunits each have a unique, specific activity. The β1 and LMP2 subunits have caspase-like activity and cleave peptides after acidic residues. Subunits β2/MECL-1 and β5/LMP7 exhibit trypsin-like and chymotrypsin-like activity, respectively, and cleave after basic and hydrophobic amino acids. The catalytic β subunits are translated as inactive propetides. During assembly of the 20S core, the N-termini are cleaved, exposing a threonine-type active site in the center of the proteolytic chamber, thereby activating the catalytic subunits (Figure 1.1B) [18]. The catalytic active sites cleave proteins by nucleophilic attack on the carbonyl moiety of the peptide bond [19-21].

Although the standard and immunoproteasome subunits have the same cleavage specificity, the rate of peptide hydrolysis between the two types of catalytic subunits is quite different. Traditionally, the immunoproteasome was thought to have greater chymotrypsin-like and trypsin-like activities and lower caspase-like activity, a property that allowed it to produce peptides that were better suited to MHC class I incorporation (i.e., hydrophobic amino acid at the C-terminus) [22, 23]. However, the literature is conflicting about the relative cleavage rates of standard and immunoproteasome subunits and appeared to depend on cell treatment and/or cell type studied [22-27].

Proteasome activity measures in tissue homogenates from immunoproteasome knock-out (KO) mice have produced more reliable data. In wild-type (WT) spleen and viral-infected liver tissues, the proteasome population is mainly immunoproteasome. In KO mice, the standard proteasome subunit takes the place of the immunoproteasome subunit(s) that has been genetically ablated [6]. Thus, spleen and viral-infected liver are optimal tissues to study because they have nearly complete populations of either immunoproteasome in WT, and standard proteasome in immunoproteasome KO.

Results from viral-infected liver in *lmp2*$^{-/-}$ and *mecl-1*$^{-/-}$ (which also have reduced LMP2 content) KO mice indicate that peptide hydrolysis rates of β1 are greater than LMP2 [28, 29]. In *lmp7*$^{-/-}$ KO spleen, there was an increase in chymotrypsin-like activity, reflecting that β5, which replaces LMP7, has higher activity than its immunoproteasome counterpart [30]. In addition, in *lmp7*$^{-/-}$*/mecl-1*$^{-/-}$ spleen that contains reduced levels of LMP2 as well, shows an increase in all three catalytic activities of the proteasome [6]. Taken together these results show that the standard proteasome subunits have higher peptide hydrolysis rates as compared to immunoproteasome (this is shown in further detail in Chapter 4).

Changes in subunit composition also change the cleavage site preference of the proteasome. Standard and immunoproteasome cleave after different peptides in a model substrate [28, 30]. These differences result in a unique subset of peptides created by each proteasome subtype. It has been proposed that some of the peptides created by the proteasome could be biologically active. Therefore, standard and immunoproteasomes

could have distinctive functions in cellular signaling depending on the array of peptides generated [31].

1.1.4. Immunoproteasome gene regulation

The LMP2 and LMP7 subunits of the immunoproteasome are encoded by the MHC class II region (mouse chromosome 17), whereas the *mecl-1* gene is located on mouse chromosome 8. The promoter regions of the immunoproteasome subunits are not well characterized, but there are some known similarities and differences. All of the immunoproteasome genes contain IFN-γ response elements in their promoter regions and therefore are transcribed following IFN-γ stimulation [32]. LMP2, LMP7, and MECL-1 all have Sp1 binding sites as well [33-35]. Both LMP2 and LMP7 have cAMP regulatory sites in their promoter regions [34, 35]. The promoter region of the LMP2 subunit also includes binding sites for AP-1, Zif268, and NFκB [35-38]. These differences in promoter regions suggest that each immunoproteasome subunit is expressed differently depending on the stimuli and/or cellular conditions.

1.1.5. Proteasome assembly

Proteasome assembly is a chaperone-mediated process that begins with the formation of the heptameric α-subunit rings (Figure 1.2). In mammals, proteasome-assembly chaperones 1 and 2 (PAC1-PAC2) form a dimer that aids in the binding of the α subunits in the correct formation while inhibiting dimer formation between other α-rings [39]. PAC3 and PAC4 additionally bind to forming α-rings to facilitate correct assembly and to join the ends of the ring together. PAC3/4 also initiates the β-ring formation by recruiting the first subunit, β2, to its proper position [40, 41]. With the incorporation of the β3 subunit, the PAC3/4 complex is released [40]. The completion of 20S proteasome assembly requires the proteasome maturation protein (POMP) (mammalian orthologue to Ump1 in yeast). Ump1/POMP stabilizes the proteasome intermediate and assists with the incorporation of the β-ring subunits. Once the β-ring is complete, Ump1/POMP aids in the assembly of two of the newly formed half-proteasomes (15S). Once the 20S proteasome is formed, the N-termini of the catalytic β-subunits undergo autolysis to expose their threonine active sites and Ump1/POMP and PAC1/2 are degraded [21].

Figure 1.2. Proteasome assembly

Proteasome α-subunit assembly is facilitated by two proteasome-assembly chaperones (PAC) complexes: PAC1-PAC2 and PAC3/4. PAC3/4 recruits β2 to the complex and then is released. Ump1, also known as POMP (proteasome maturation protein), binds to the proteasome intermediate to stabilize the complex and aid in the assembly of the β-ring of subunits. Two half-proteasomes (15S) are then joined together, the catalytic subunits autocatalytically expose their threonine active sites, and the chaperones Ump1 and PAC1-PAC2 are degraded to form the mature 20S proteasome.

Figure 1.2. Proteasome assembly

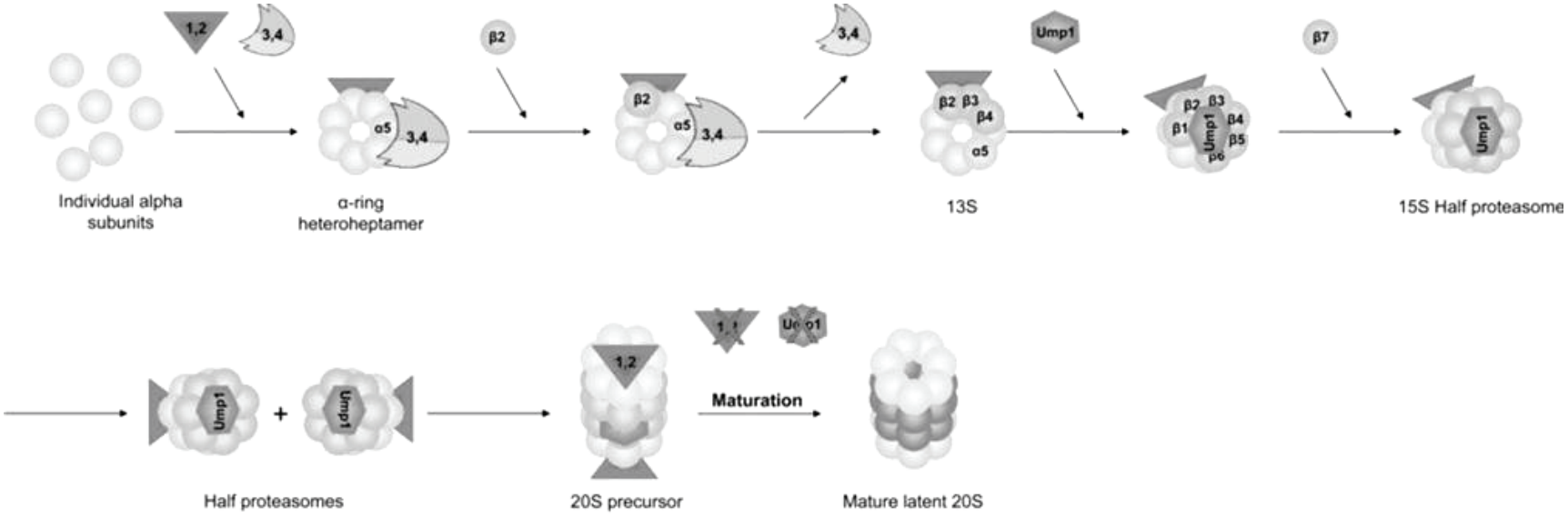

Figure is adapted from [42].

1.1.6. Immunoproteasome subunit incorporation

Previous work hypothesized that nascent proteasomes preferentially assembled either all standard or all immunoproteasome subunits into the 20S core [43, 44] and that mixtures of the subtypes in the 20S core or intermediate-type proteasomes did not form. This hypothesis was known as cooperative assembly. Work from several labs indicated that the MECL-1 and LMP2 subunits were both required to incorporate into 15S (half-proteasome) and the LMP7 subunit was required for maturation [43, 44]. With the use of chimeric proteins, research showed that cooperative assembly is influenced mainly by the propeptide sequence that is cleaved during the final steps of assembly of the 20S core. The propeptide on the first β subunit (β2/MECL-1) incorporated into nascent proteasomes influences whether the standard or immunoproteasome form of the remaining catalytic subunits are incorporated [45].

In refute of this hypothesis, *mecl-1*$^{-/-}$ and *lmp7*$^{-/-}$*/mecl-1*$^{-/-}$ KO mice contain the normal amounts of LMP2 in lymphocytes, cultured RPE cells, and young retina (Chapter 4) under normal conditions [6, 45]. However, recent data (Chapter 4) shows that the degree of subunit incorporation is dependent on the presence of the other immunoproteasome subunits [6]. When immunoproteasome is expressed at high levels (i.e., under stress or in immune tissue), subunit incorporation of the immunoproteasome subunits not genetically ablated in KO mice is diminished as compared to WT [6, 29].

1.1.7. Proteasome regulatory complexes

The 20S catalytic core is capable of degrading oxidized and unfolded proteins [46, 47]. However, with the addition of different regulatory complexes, the activity of the proteasome can be modified to degrade other substrates (Figure 1.3). The 19S (PA700) cap is the most well-described proteasome regulatory complex. The 20S core complex bound to two 19S complexes forms the 26S proteasome. The 26S proteasome is capable of degrading ubiquitin-modified substrates. The 19S cap is a multi-subunit complex that has both deubiquitinating and ATPase activity. Ubiquitin-modified proteins are recognized by the 19S cap (subunit S5a) [48] and deubiquitinated (subunits Uch37 and Rpn11) [49-51]. The 19S complex's ATPase activity then unfolds the protein so that it can enter the 20S core for degradation.

Figure 1.3. Proteasome regulatory complexes

Several different complexes associate with the 20S core to regulate its activity. The 19S (PA700) regulatory complex allows the proteasome to degrade ubiquitin-modified substrates. The 11S (PA28) regulatory complex is typically associated with the immunoproteasome and enhances antigenic peptide processing. PA200 is a nuclear proteasome activator and is hypothesized to be involved in DNA repair. PI31 is an inhibitory complex that binds to both complete and half-formed proteasome, inhibiting both activity and assembly of the immunoproteasome.

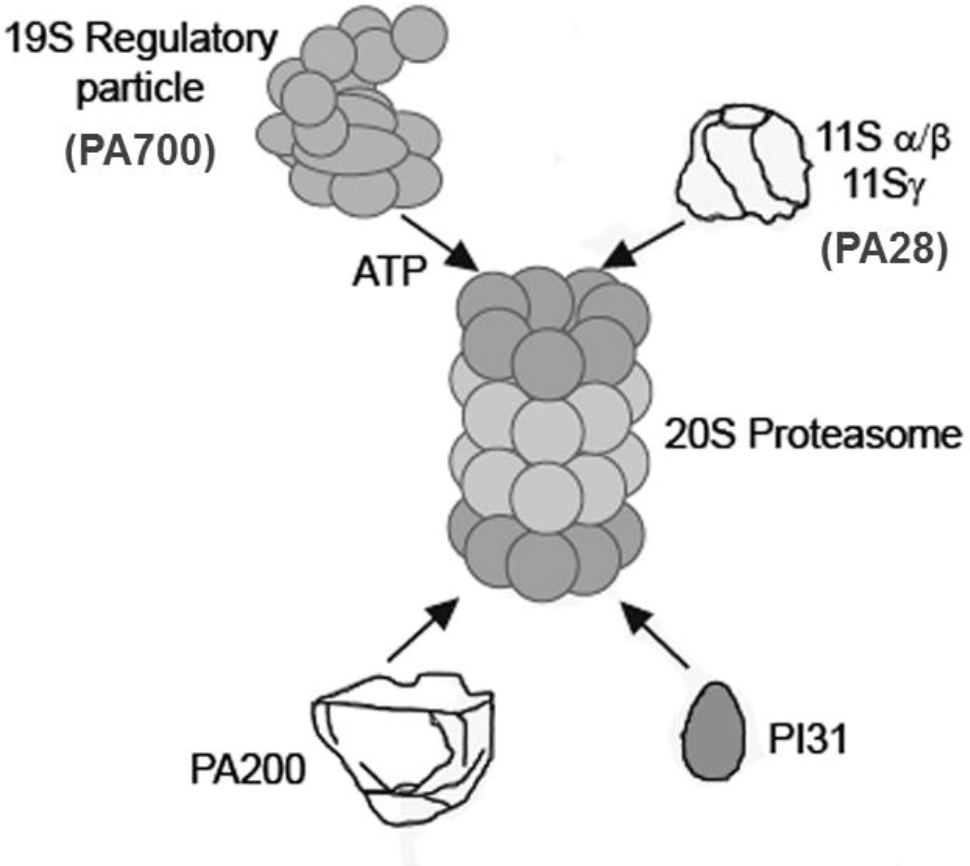

Figure is adapted from [15].

The 11S (PA28) regulatory complex is most often associated with the immunoproteasome but can bind to either the standard or immunoproteasome 20S core [52]. The PA28 complex is a heptameric ring structure containing two different homologous subunits: REGα and REGβ [53]. PA28 activates peptide production by the proteasome and also increases the number of peptides available for MHC class I presentation [52, 54].

The most recently discovered proteasome activator is PA200. This regulatory complex has been localized to the nucleus and has been shown to activate peptide hydrolysis by the proteasome [55]. PA200 was first hypothesized to be involved in DNA repair [55]. Later studies refuted this hypothesis, showing that null mutations of PA200 did not lead to increased sensitivity to DNA damage [56, 57]. PA200 does appear to have a role in spermatogenesis, although the mechanism still remains unclear [56].

A fourth regulatory complex is the PI31. Unlike the previously mentioned complexes, PI31 is a proteasome inhibitor. *In vitro* studies showed that PI31 inhibited proteasome activity by binding to the α subunits of the proteasome and blocking association of the 20S core with PA28 and PA700 [58, 59]. *In vivo* cell culture studies showed that the overexpression of PI31 had little effect on 26S proteasome function [60]. However, PI31 does impair antigen peptide processing by inhibiting immunoproteasome assembly and maturation [60].

Other proteins tightly associate with the proteasome and may influence its activity. For example, Hsp90 is a protein chaperone that often co-purifies with the 20S proteasome. Data has indicated that Hsp90 may be involved in targeting proteins for proteasomal degradation [61]. *In vitro* assays have also shown that Hsp90 has a direct effect on proteasome activity and have demonstrated that purified 20S proteasome requires Hsp90 to efficiently degrade oxidized calmodulin [62]. Conversely, in cell lysates from lens and pituitary, Hsp90 was inhibitory [63, 64]. In spleen homogenates containing mainly immunoproteasome, Hsp90 did not affect proteasome activity. Overall, Hsp90's direct effect on proteasome is unknown. But in regards to immunoproteasome function, Hsp90 has also been hypothesized to facilitate the transport of peptides to the endoplasmic reticulum (ER) for MHC class I presentation [65].

1.2. Immunoproteasome

1.2.1. Immunoproteasome function

As indicated by its name, the immunoproteasome's function was originally described in the immune system (Figure 1.4). Both native and foreign (if the cell is infected by a virus or bacterium) proteins are degraded by the proteasome as part of immune surveillance. The catalytic function of the specific immunoproteasome subunits (LMP2, LMP7, MECL-1) creates peptides that are better suited for MHC class I antigen presentation. For example, immunoproteasome generates peptides that are slightly longer and of adequate size for incorporation into MHC class I molecules [66, 67]. Additionally, initial studies showed that immunoproteasome produced an enhanced selection of peptides with hydrophobic amino acids at the C-terminal end, which are better suited to MHC class I presentation [22, 23]. This hypothesis was confirmed by overexpression studies that showed increasing immunoproteasome subunit content enhances antigen presentation [68]. The PA28 regulatory subunit bound to immunoproteasome increases antigen presentation [52, 54].

Once created by the proteasome, antigenic peptides are transported into the endoplasmic reticulum by the transporter associated with antigenic processing (TAP). In the ER, the peptides are loaded into the MHC class I molecules. Once the peptides are loaded, the MHC class I molecules are exported to the Golgi apparatus for further processing before being shuttled to the cell surface. At the cell surface, the peptides are presented to $CD8^+$ T cells. If the peptide is recognized as foreign, the cell is then targeted for killing by cytotoxic T lymphocytes (CTL).

1.2.2. Immune system in the retina

The immune system of the eye is designed to protect against pathogens while inhibiting inflammation. Tissue inflammation causes significant collateral damage to surrounding cells and therefore is avoided in the retina since the retina is a post-mitotic tissue and has limited ability to replace lost cells. Therefore, it is important to limit cell death to only the pathogen-infected cells. This dampened immune response is referred to as immune privilege.

Figure 1.4. Major histocompatibility complex class I antigen processing

As part of immune surveillance, proteins are degraded by the proteasome to create peptides. Some of these peptides are transported to the endoplasmic reticulum (ER) via the transporter associated with antigen processing (TAP). In the ER, peptides are loaded into major histocompatibility complex (MHC) class I molecules. The MHC class I molecules are then exported to the Golgi apparatus for further processing before being presented at the cell surface for T cell recognition. T cell receptor (TCR).

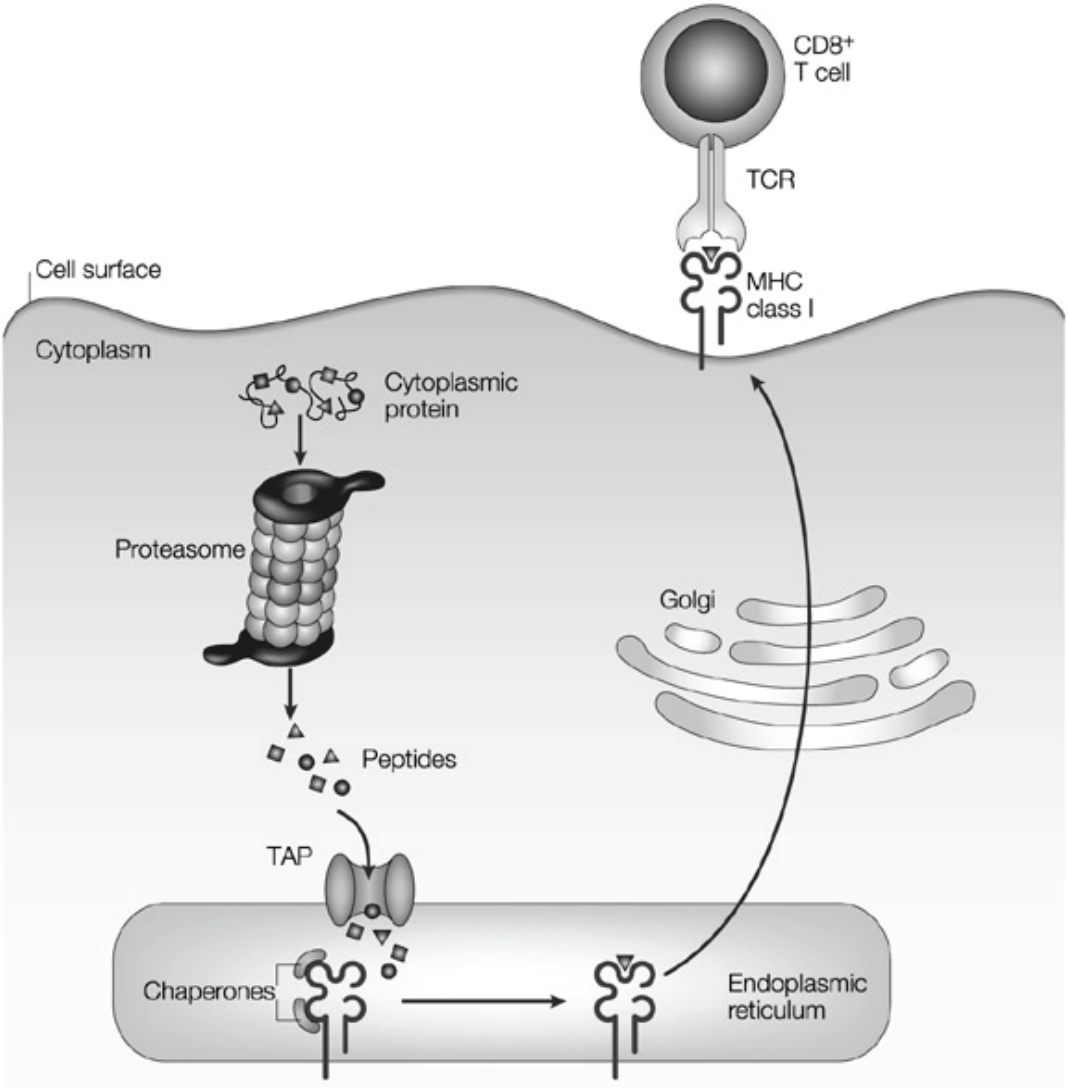

Figure is adapted from [69].

The eye utilizes many different mechanisms to maintain an immune-privileged environment. First, the eye contains many different immunosuppressive factors, including neuropeptides, complement inhibitors [70] and macrophage inhibitory factor [71]. Secondly, the retinal pigment epithelium (RPE), a monolayer of cells at the posterior of the retina, is able to convert active T cells (able to kill infected cells) into regulatory T cells, which further serve to suppress immune function [72, 73]. In addition, RPE cells are able to directly inhibit the activation of T cells [74]. Third, Fas ligand, which is able to cause apoptosis without inflammation, is expressed throughout the eye and functions to induce cell death of immune cells that encroach the blood-retina barrier [75]. Lastly, the retina has limited MHC class I expression [76, 77]. Therefore, the normal pathway for antigen presentation and recognition is suppressed in the retina, making it an ideal tissue for studying alternative roles of the immunoproteasome.

1.2.3. Alternative roles for the immunoproteasome

Immunoproteasome is expressed in most tissues of the body including the immune-privileged retina and brain [6-8, 78-86]. The ubiquitous expression of immunoproteasome, even in immune-privileged tissues, suggests that immunoproteasome may have a more general role in cellular function. Notably, a recent surge of papers has reported an increasing number of functions that are attributed to the immunoproteasome. Some of these alternative roles of immunoproteasome are discussed below.

- **Immunoproteasome and stress response**

One of the strongest arguments for immunoproteasome's involvement in the stress response is that cells respond to stress, injury, and disease by increasing immunoproteasome content. For example, a comparison of immunoproteasome content in the retina and brain showed that immunoproteasome is expressed in 2-fold higher abundance in the retina (Chapter 3) [8]. The higher content of immunoproteasome in the retina versus the brain is a direct correlation to the greater level of strain experienced by the retina due to its unique environment (e.g., high light exposure) and physiology (e.g., high metabolic rate and oxygen tension) [87]. Numerous other studies have shown that immunoproteasome is upregulated in neurodegenerative diseases, including age-related

macular degeneration (AMD, Chapter 2), Huntington's disease, amyotrophic lateral sclerosis (ALS), and Alzheimer's disease [83, 85, 86, 88].

Immunoproteasome is also upregulated with oxidative stress in cultured cells [6, 89-91]. This upregulation appears to be a protective mechanism in cells, as studies have shown that immunoproteasome-deficient cells are more susceptible to oxidation-induced damage (increased oxidized proteins) and cell death (Chapter 4) [6, 92]. A recent study proposed that the mechanism for this protective effect is that immunoproteasome degrades oxidized proteins more efficiently than standard proteasome [93, 94]. Under oxidative stress conditions, immunoproteasome was shown to degrade polyubiquitinated and oxidized proteins more efficiently than cells deficient in immunoproteasome subunits (LMP2 and/or LMP7) [94]. An *in vitro* study using isolated proteasome and model substrates confirmed these findings [93]. Taken together, these data suggest that the immunoproteasome subtype is preferentially upregulated in response to oxidative stress to cope with the levels of oxidant-damaged proteins.

Targeted cytotoxic T lymphocyte (CTL) injury to the retina and brain also causes the upregulation of immunoproteasome (Chapter 3) [8]. In this technique (section 1.5.1), CTLs are specifically targeted to kill astrocytes or photoreceptors of the brain and retina, respectively.

- **Immunoproteasome and signaling pathways**

Immunoproteasome may also have an integral role in several in cell signaling pathways. Several studies have shown that immunoproteasome is involved in both the proteolytic processing and activation of NFκB [9-11, 95, 96]. The p50 and p52 transcription factors (TF) of the NFκB family are translated as the precursors, p105 and p100, respectively (Figure 1.5). The precursor proteins require proteolytic processing by the proteasome to become active. Additional regulation of NFκB is through the binding of the inhibitor, IκB, with the NFκB TF dimers, which sequesters the TF in the cytosol. The NFκB TFs are activated via proteasomal degradation of IκB, which allows the TF to translocate to the nucleus.

Inflammatory bowel disease increased content of the LMP2 and MECL-1 immunoproteasome subunits and was correlated with increased processing of the NFκB

Figure 1.5. NFκB signaling pathway

Proteasome can activate the NFκB pathway through the proteolytic processing of the precursors p105 and p100 to form the transcription factors p50 and p52, respectively. Proteasome degradation of the inhibitor, IκB, allows the NFκB transcription factor to become active and translocate into the nucleus where it binds to promoter regions of genes.

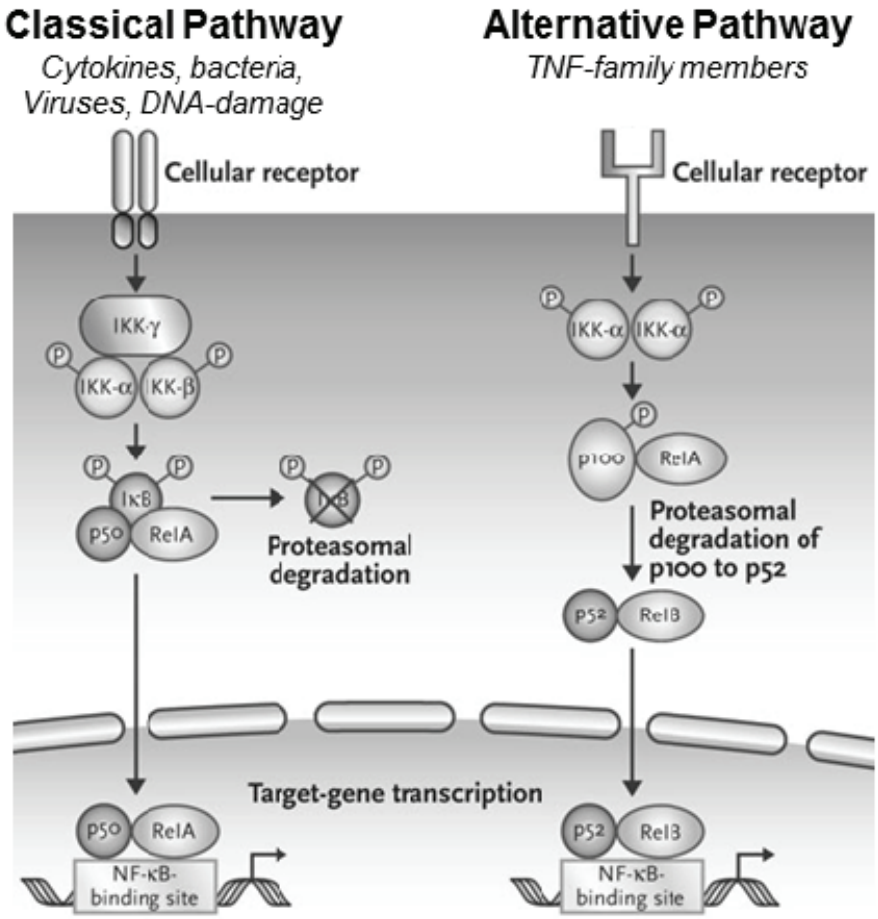

Figure is adapted from [97].

precursor [96]. Spleen tissue from *lmp2*$^{-/-}$ and non-obese diabetic mice (which have decreased LMP2) also showed a decrease in p105 processing and IκB degradation [10, 11]. This data was confirmed in *lmp2*$^{-/-}$ kidney epithelial and B cells, which also showed inhibited IκB degradation [9, 95]. Taken together, these data indicate that immunoproteasome, specifically the LMP2 subunit, plays an important role in the NFκB signaling pathway.

LMP2 is also required for efficient phosphatase and tensin homolog (PTEN) degradation and subsequent activation of pAkt (Figure 1.6). Ischemic preconditioning in the heart causes the activation of pAkt through the degradation of PTEN [98]. Activated pAkt inhibits apoptosis by phosphorylating Bax and Bad, converting them to their inactive forms. Bax is a pro-apoptotic protein and Bad inhibits the anti-apoptotic protein, Bcl-2. Therefore, the activation of pAkt is ultimately a protective mechanism. In *lmp2*$^{-/-}$ mice, PTEN degradation is inhibited and this inhibits the activation of pAkt. As such, in *lmp2*$^{-/-}$ mice, ischemic preconditioning does not lead to cardioprotection [98].

Another hypothesized role for the immunoproteasome is the production of biologically active peptides. Neuropeptides are proposed to modulate intercellular signaling in the retina by controlling neurotransmitter release and the opening of ion channels [99]. The immunoproteasome and the standard proteasome each produce a distinct subset of peptides [28, 30]. Therefore, the immunoproteasome could potentially produce unique, biologically active peptides [31]. These signaling peptides could be essential for normal retinal function.

The assembly rates and half-life of immunoproteasome also suggest a possible role in signaling. Immunoproteasome is assembled approximately four times faster than standard proteasome (21 vs. 82 minutes half-time assembly) in IFN-γ-treated, cultured cells [100]. This difference allows immunoproteasome to be rapidly upregulated in response to changes in cellular conditions. In addition, immunoproteasome also has a half-life that is approximately 20% of the standard proteasome [100]. This is similar to many signaling proteins that must be degraded in order to quench the signal.

- **Immunoproteasome and retinal function**

  Immunoproteasome is located in the outer plexiform layer (OPL) of the retina

Figure 1.6. IGF-1/pAkt signaling pathway

Insulin-like growth factor 1 (IGF-1) binds to the insulin-like growth factor receptor (IGFR) at the cell surface. The receptor is autophosphorylated and subsequently phosphorylates the insulin receptor substrate -1 (IRS-1). IRS-1 activates phosphatidylinositol 3-kinase (PI3K). PI3K phosphorylates phosphatidylinositol (3,4)-bisphosphate (PIP_2) to form phosphatidylinositol (3,4,5)-trisphosphate (PIP_3). This reaction can be reversed by phosphatase and tensin homolog (PTEN). PIP_3 formation allows for the phosphorylation of Akt by phosphoinositide-dependent protein kinase-1 (PDK-1). pAkt promotes prosurvival pathway by inhibiting the pro-apoptotic proteins Bax and Bad. Proteasome degrades PTEN to promote pAkt activation.

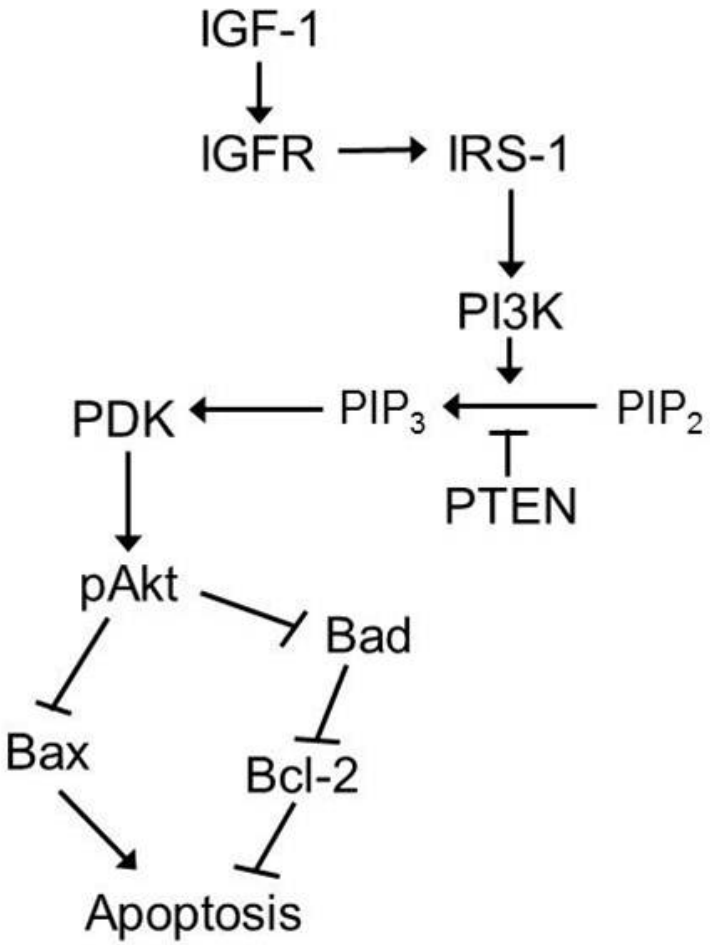

Figure is adapted from [101-103].

(synapses between the photoreceptors and bipolar cells) as well as the synapses of the brain [8, 104]. The localization of immunoproteasome to the synapse suggests a role in visual transmission. In support of this idea, electroretinogram measurements in Chapter 5 (see Section 1.5.3 for technique) indicate immunoproteasome-deficient mice have a decreased bipolar cell response to light as measured by the b-wave [7].

1.2.4. Immunoproteasome knock-out mice

Knock-out (KO) mice have been developed for each of the three subunits specific to the immunoproteasome. The *lmp2*$^{-/-}$ (L2) and *lmp7*$^{-/-}$ (L7) strains were developed in the 1990s with the *mecl-1*$^{-/-}$ being developed a decade later [28, 29, 105]. An 800 bp region spanning exon 2 and intron 2 of the LMP2 gene was deleted in the L2 mice [28]. The L7 mice are devoid of the LMP7 protein by eliminating exons 1-5; this accounts for 247 of 276 amino acids [105]. The *mecl-1*$^{-/-}$ mouse was produced by targeting exons 5-7 of *mecl-1* [29]. In addition, a double KO mouse was developed by crossing *lmp7*$^{-/-}$ with *mecl-1*$^{-/-}$ to produce mice with both the *lmp7* and *mecl-1* subunits (L7M1) genetically ablated [106].

These mice, generated as whole organism KOs, have no overt phenotype and breed and develop normally. Although immunoproteasome's main function has been attributed to creating antigenic peptides, initial characterization of the immunoproteasome KO mice has shown that the genetic deletion results in a mild phenotype with regards to immune function (Table 1.1). These changes include altered MHC class I expression, T cell populations, and T cell proliferation. None of the immunoproteasome KO mouse strains show evidence of being immune-compromised and respond more or less normally to a viral infection [106, 107], although a recent paper reported *lmp2*$^{-/-}$ mice had defects in B cell development and a lower response to antibody [9].

This thesis utilizes the immunoproteasome KO mice L7 and L7M1 to determine alternative roles for the immunoproteasome. The effects of age on the retina were assessed using proteasome content and activity along with retinal morphology (Chapters 4 and 5). The response to an oxidant challenge was evaluated in cultured retinal pigment epithelial cells isolated from the L7 and L7M1 mice.

Figure 1.7. Gene deletion in immunoproteasome KO mice

The targeted constructs of the mutated genes are shown below. (A) L2 KO mice have an 800 bp region spanning exon 2 and intron 2 removed from the LMP2 gene. (B) The L7 mice are devoid of the LMP7 protein by eliminating exons 1-5. (C) The *mecl-1*$^{-/-}$ mouse was produced by targeting exons 5-7 of *mecl-1*.

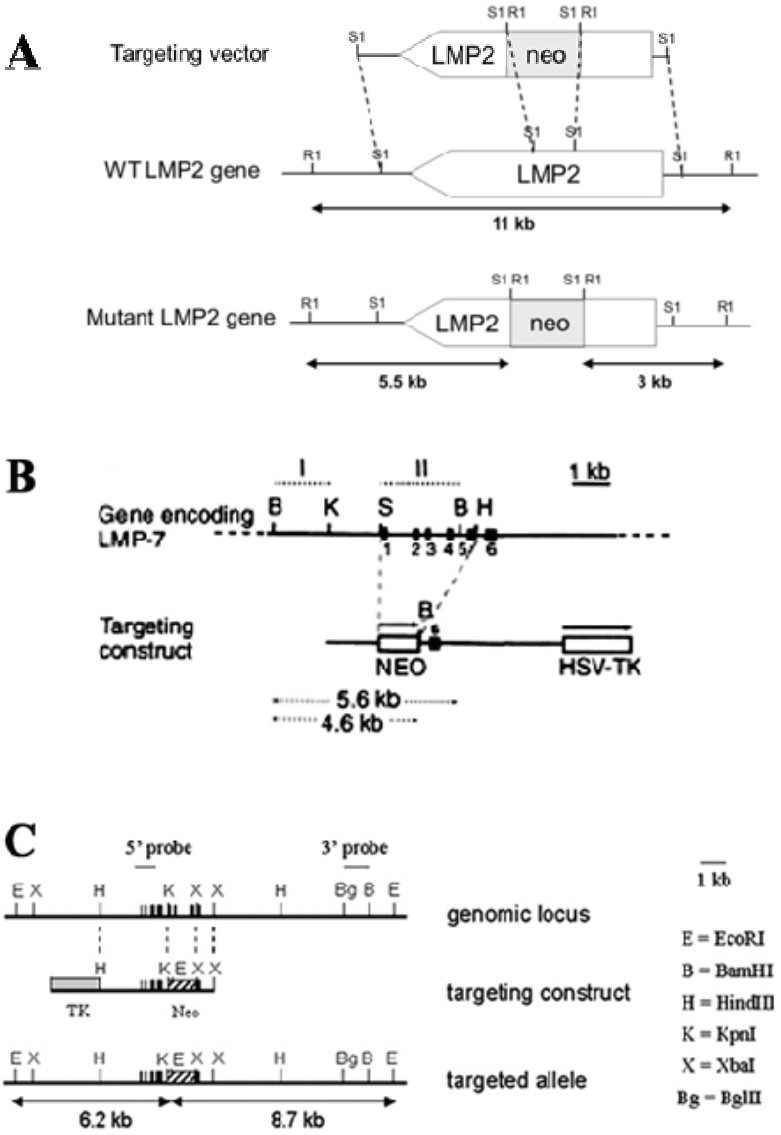

Figure is adapted from [28, 29, 105].

Table 1.1. Immune system phenotype of immunoproteasome KO mice

Strain	Lymphoid MHC Class I Expression	Splenic $CD4^+$:$CD8^+$	T-cell proliferation	% $CD8^+$ cells with memory phenotype
lmp7$^{-/-}$ *mecl-1*$^{-/-}$ (L7M1)	~60% decrease [106]	~150% increase [106]	Increased [106]	~2-fold increase [106]
mecl-1$^{-/-}$ (M1)	Normal [106]	~150% increase [106]	Normal [106]	Normal [106]
lmp7$^{-/-}$ (L7)	~60% decrease [105, 106]	Normal [105, 106]	Normal [106]	Normal [106]
lmp2$^{-/-}$ (L2)	Normal [28]	~150% increase [28, 106]	Normal [106]	~1.4-fold increase [106]

Table is adapted from [106].

1.3. Retina

1.3.1. Overview of mouse eye anatomy

The anatomy of the mouse eye is similar to that of the human eye (Figure 1.8). The outer surface of the eye is called the cornea. Light passes through the cornea, entering the iris and pupillary opening to the lens. Unlike the human eye, in the mouse eye, the lens takes up a large proportion of the eye volume. Light passing through the lens then strikes the retina, which is located at the posterior of the eye. The retina detects light and converts it into a neural signal that is transmitted through the optic nerve to the brain.

1.3.2. Retinal anatomy

The retina is a complex tissue made of three different cell types that are stratified into different layers. Neurons are the predominant cell type in the retina. The neurons are segregated into three layers of the retina: the outer nuclear layer (ONL), the inner nuclear layer (INL), and the ganglion cell layer (GCL) (Figure 1.9). The distinct localization of retinal cell types within these layers provides the opportunity to monitor the loss of specific cell types with age or following a specific injury. For example, in Chapter 5, an age-related decrease of photoreceptors was determined by counting the nuclei of the ONL.

The primary neurons or photoreceptors comprise the ONL. There are two photoreceptor types: rods and cones. Rod photoreceptors are highly sensitive to light and function well in low-light conditions, whereas cones function in higher light levels and are responsible for color vision. The mouse retina is rod dominant, with 97% rod photoreceptors and only 3% cone photoreceptors [108]. These neurons are highly specialized to capture light energy and convert it into a neural impulse. The nuclei of the photoreceptors are tightly packed in the ONL with the inner and outer segments projecting towards the posterior of the retina.

The second nuclear layer, which contains the secondary neurons of the retina, is the inner nuclear layer (INL). This layer of the retina contains bipolar (41%), amacrine (39%), and horizontal cells (3%) [108]. The remaining 16% of nuclei of the INL are Müller glia cells. The horizontal cells of the retina function to average the signal from

Figure 1.8. Diagram of the mouse eye

Light passes through the cornea and lens before reaching the retina. The retina is located at the posterior of the eye. The optic nerve transmits the neural signal from the retina to the brain.

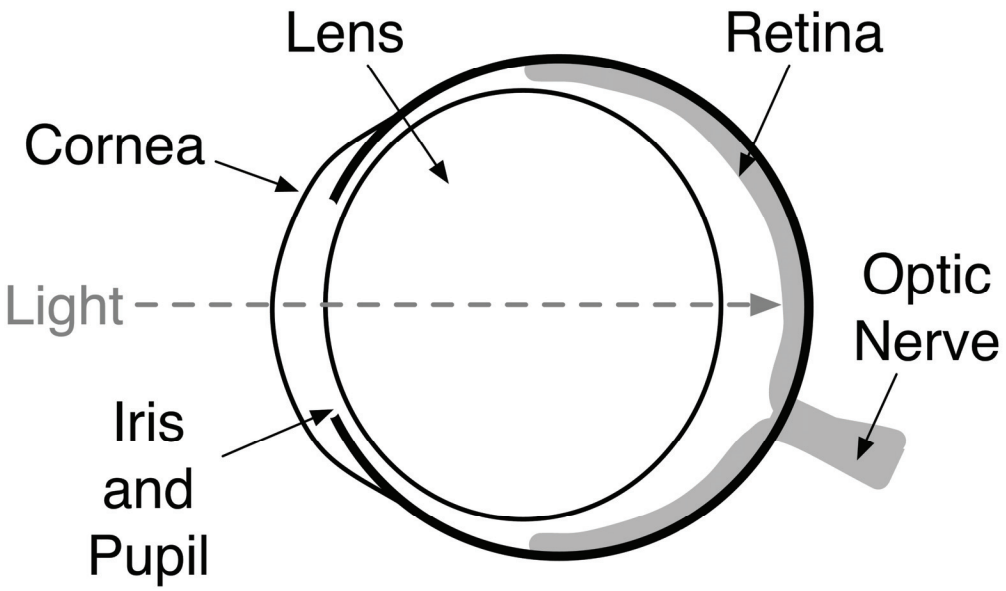

Figure is adapted from [109].

Figure 1.9. Structure of the mouse retina

On the left is a hematoxylin and eosin (H&E) stained section of a wild-type mouse retina. The cartoon diagram on the right defines the different layers and cell types that are found in the retina. As illustrated, the retina is complex tissue containing many different cell types. Light passes through the inner retina before being detected by the rod and cone photoreceptors at the posterior of the retina. The retinal pigment epithelium (RPE) forms a monolayer of cells at the back of the retina. Adjacent to the RPE are the photoreceptors whose nuclei are located in the outer nuclear layer (ONL). The outer plexiform layer (OPL) contains the synaptic connections between the photoreceptors and horizontal and bipolar cells. The nuclei of these cells comprise the inner nuclear layer (INL). Also found in the INL are Müller and amacrine cells. A second synaptic layer (inner plexiform layer, IPL) is formed between the INL and the ganglion cell layer (GCL). The GCL includes retinal ganglion cells (RGC), displaced amacrine cells, and astrocytes.

Figure 1.9. Structure of the mouse retina

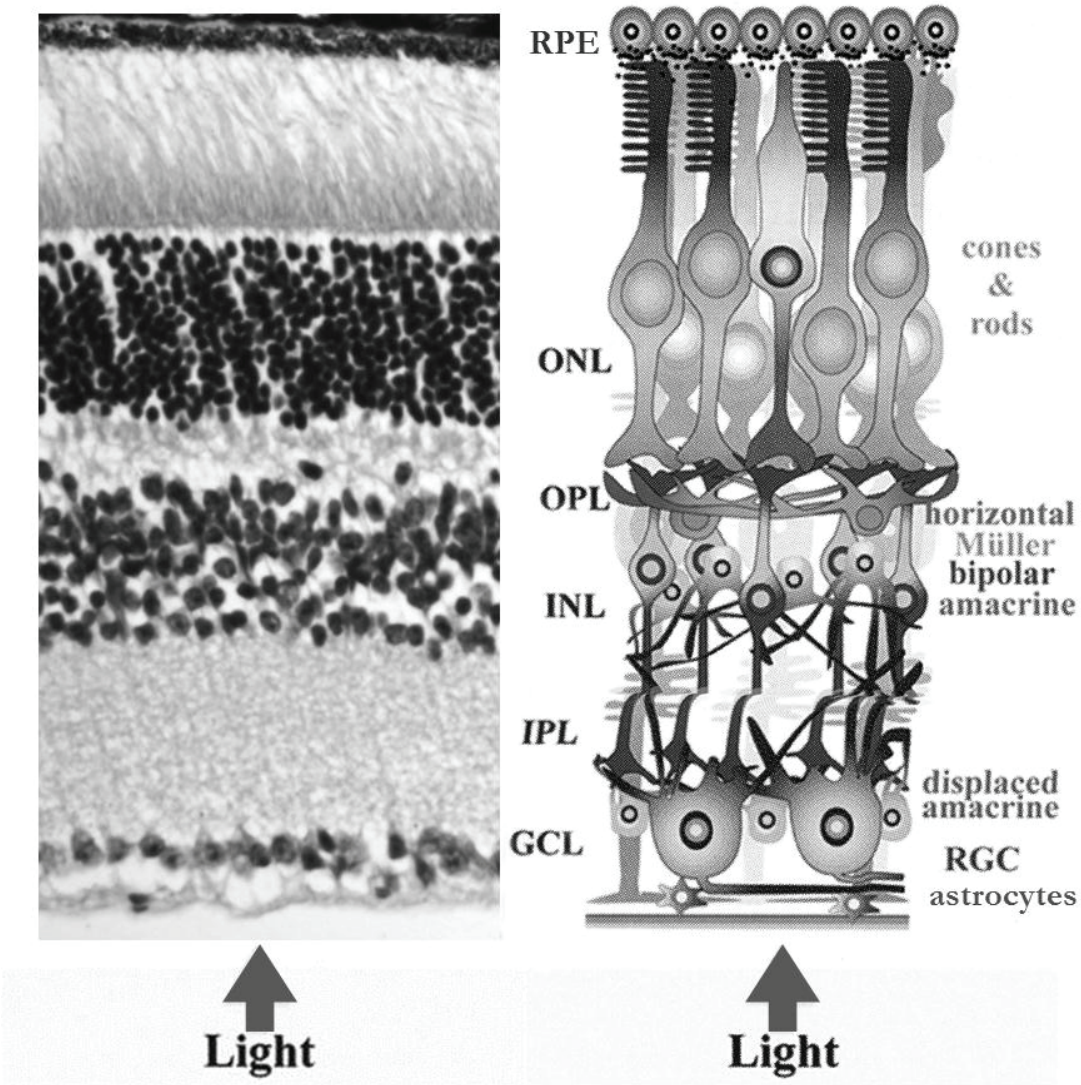

Figure is adapted from [110].

multiple photoreceptors (Fig. 1.10). Bipolar cells are classified as either rod or cone bipolar cells and receive input from the photoreceptors. Although the mouse retina contains mostly rod photoreceptors, there are approximately twice as many cone as rod bipolar cells [111]. A partial explanation for this phenomenon is each cone photoreceptor is associated with several cone bipolar cells, while several rod photoreceptors output their signal to a single rod bipolar cell. The bipolar cells are connected to both the primary neurons (photoreceptors) and the tertiary neurons (ganglion cells) and transmit the signal between them. The amacrine cells regulate and receive input from the bipolar cells and can also transmit the visual signal to the ganglion cells.

The ganglion cell layer (GCL) contains the tertiary neurons of the retina. This cell layer also contains several different cell types, including retinal ganglion cells (RGC), astrocytes, and displaced amacrine cells. The RGCs are the final layer of neurons of the retina and receive the visual signal from the bipolar cells and amacrine cells. The axons of the ganglion cells form the optic nerve, which carries the visual signal to the brain.

Between each layer of neurons exists a plexiform layer that contains the synaptic junctions formed between the neurons. The outer plexiform layer (OPL) contains the synaptic connections between the photoreceptors and bipolar cells. In the mouse, this layer is relatively thin (~12 μm). The inner plexiform layer (IPL), formed between the INL and GCL, is much thicker (~60 μm) and contains the neural connections between the amacrine and bipolar cells of the INL with the RGCs (unpublished data generated by Hussong).

In addition to neurons, the retina also contains epithelial cells and glia. Epithelial cells form a monolayer of cells at the posterior of the retina and are called the retinal pigment epithelium (RPE). The RPE function to support and maintain the photoreceptors and are an integral component of the visual cycle [112]. The RPE supply the retina with nutrients, ions, and growth factors. The enzyme-mediated reactions required for the regeneration of rhodopsin chromophore take place in the RPE (see Section 1.3.2). In addition, the RPE phagocytize the distal tips of the photoreceptors daily. This phagocytosis helps maintain healthy photoreceptors by preventing the build up of

Figure 1.10. Intercellular signaling in the retina

Light is captured by the photoreceptors (PR) whose nuclei are found in the outer nuclear layer (ONL). The PRs convert light into a neural impulse, which is transmitted to the horizontal (HC) and bipolar cells (BC). The HCs modulate the signal from the photoreceptors and also transmit the signal to the BCs. BCs are regulated by signals from the amacrine cells (AC) and either pass the neural impulse directly to the ganglion cells (GC) or to the ACs. The ACs receive signals from the BCs and either transfer the signal to additional BCs or to the GCs. The axons of the GCs, which form the optic nerve, carry the visual signal to the brain.

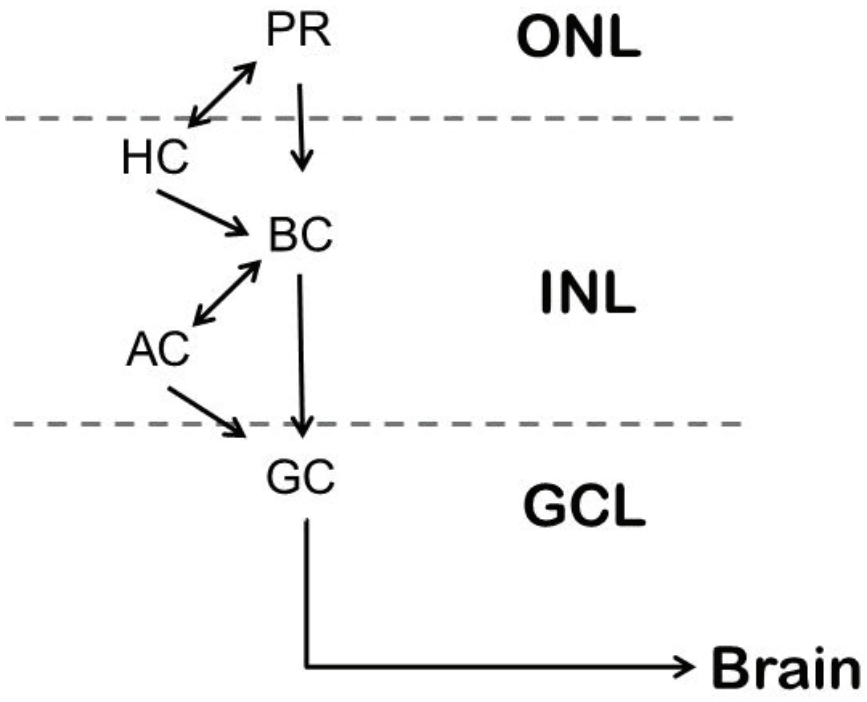

damaged proteins and membranes [112].

Glial cells include Müller cells and astrocytes and function as support cells in the retina. Glia cells play a crucial role in retinal function by recycling released neurotransmitters (e.g., glutamate) in the retina [113, 114]. In addition, they are critical in maintaining synaptic plasticity and synaptogenesis [114].

1.3.3. Retinal function

- **Photoreceptors**

Phototransduction is the process that converts light energy detected by the photoreceptors into a neural impulse in the photoreceptors (Figure 1.11). Rhodopsin is the visual pigment in rod photoreceptors. When light strikes rhodopsin, it isomerizes to the all-*trans* state (R*). R* then binds to the α subunit of the G-protein transducin (Gt, *Gnat1*). The binding of R* triggers the exchange of GDP for GTP thus activating transducin. Transducin is released and R* is free to activate additional transducin proteins. The activated form of transducin then diffuses laterally along the membrane and sequesters the inhibiting subunit of a phosphodiesterase (PDE) effectively activating the complex. PDE hydrolyzes cyclic GMP (cGMP) to 5'GMP. The reduction of intracellular cGMP causes the closure of the gated ion channels. Closing the ion channels stops the influx of cations into the outer segment of the photoreceptor and the retina becomes hyperpolarized [115]. The hyperpolarization of the retina is measured by the electroretinogram in the form of the a-wave (see section 1.5.3). The closure of the ion channels also halts the synaptic release of glutamate [116].

Following light exposure, rhodopsin must undergo several deactivation reactions to return it to its resting state (Fig. 1.12). Rhodopsin is first deactivated by phosphorylation via rhodopsin kinase (activated by recoverin) then bound to arrestin forming the MII-P-ARR complex. Following deactivation, the chromophore of rhodopsin, all-*trans*-retinal, is separated from opsin and transported to the RPE to be regenerated.

The regeneration of rhodopsin chromophore (11-*cis*-retinal), or the rod visual cycle, involves a series of chaperone-mediated, enzymatic reactions that take place in the RPE. In the rod photoreceptors, all-*trans*-retinal is released from opsin and reduced to

Figure 1.11. Phototransduction in rod photoreceptors

Rhodopsin (R*) is activated by light. Activated rhodopsin binds to the α-subunit of transducin (Gt). Gt sequesters the inhibitory subunit of phosphodiesterase (PDE). PDE hydrolyzes cyclic GMP (cGMP). The reduction in intracellular cGMP closes ion channels on the photoreceptors and inhibits synaptic glutamate release. Transducin is deactivated by the GTPase accelerating protein (GAP) complex containing Gβ5-L and RGS9-1. The hydrolysis of GTP deactivates transducin and returns it to its resting state.

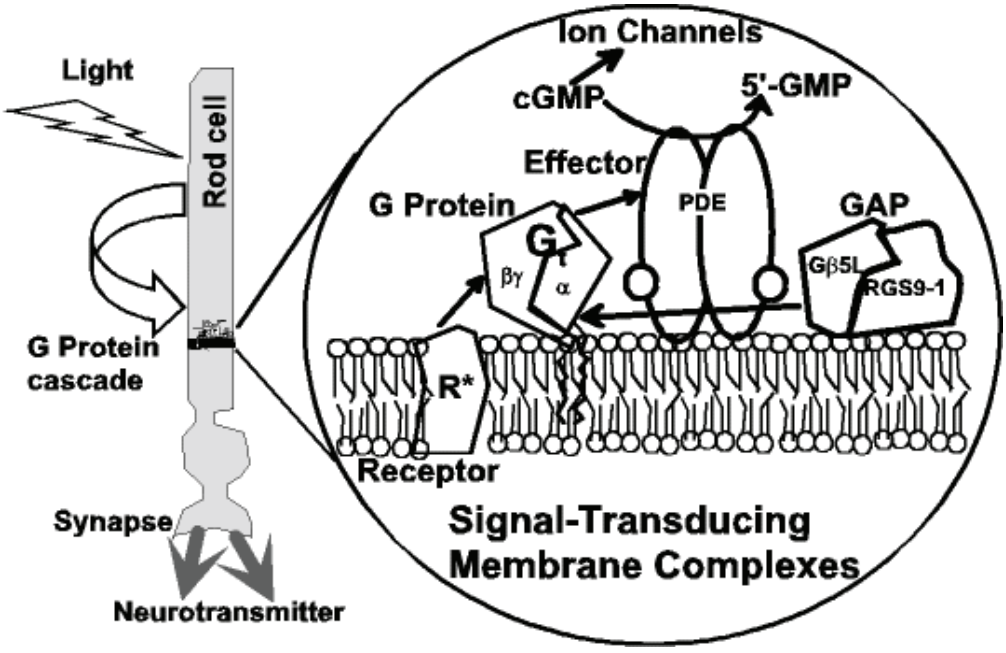

Figure is from [117].

Figure 1.12. Regeneration of rhodopsin following light exposure

Rhodopsin (RH*) is deactivated first by phosphorylation and binding to arrestin (ARR) to form the MII-P-ARR complex. The rhodopsin chromophore, 11-*trans*-retinal, is subsequently removed from opsin and transported to the retinal pigment epithelium (RPE). Isomerization is completed within the RPE. The regenerated 11-*cis*-retinal is rebound to opsin to reform rhodopsin (RH) to its resting state. Cellular retinaldehyde binding protein (CRALBP), interphotoreceptor binding protein (IRBP), lecithin retinol acyl transferase (LRAT), retinal dehydrogenase (RDH).

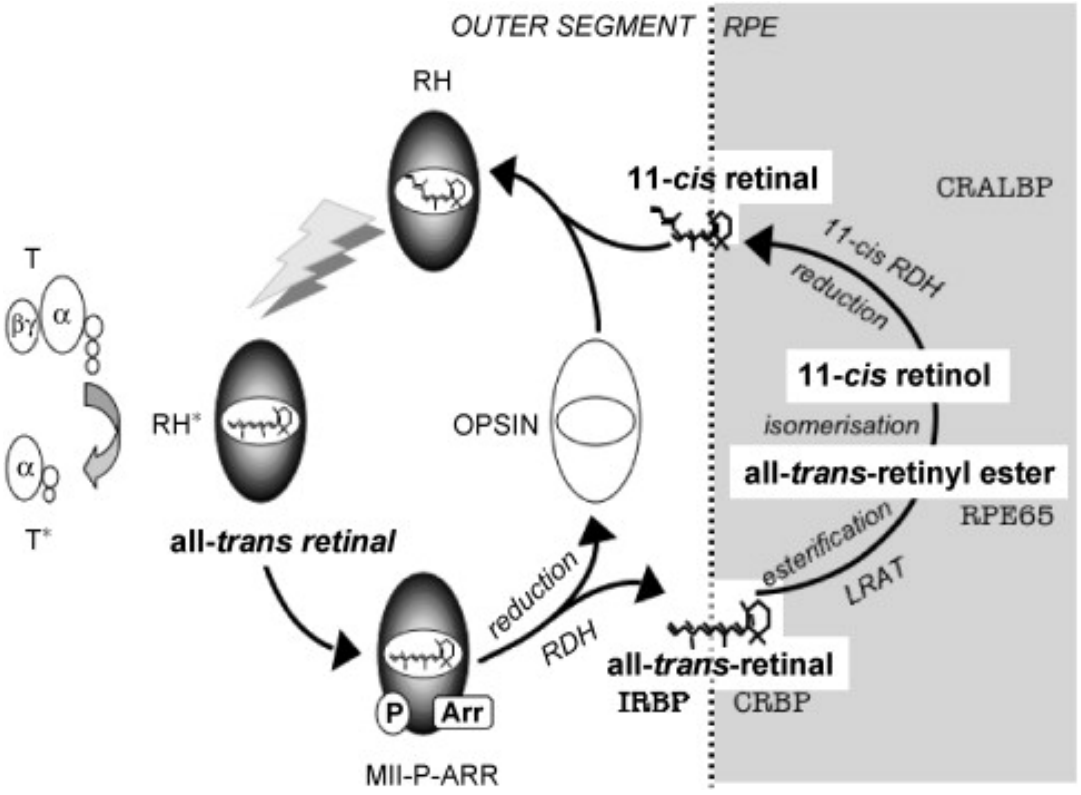

Figure is from [118].

all-*trans*-retinol using NADPH and catalyzed by a retinol dehydrogenase (RDH) [119]. The all-*trans*-retinol is then shuttled to the RPE by the chaperone interphotoreceptor retinoid binding protein (IRBP) [120]. Once in the RPE, the chromophore is transferred to the chaperone, cellular retinol-binding protein type I (CRBPI). While bound to CRBPI, the 11-*trans*-retinol is esterified by lecithin:retinol acyltransferase (LRAT) to a long chain fatty acid [121, 122]. RPE65, an isomerhydrolase, simultaneously hydrolyzes and isomerizes 11-*trans*-retinyl ester to form 11-*cis*-retinol [123-125]. Cellular retinaldehyde-binding protein (CRALBP) chaperones the 11-*cis*-retinol through the RPE [126], where it is oxidized to 11-*cis*-retinal by a *cis*-specific RDH. 11-*cis*-retinal is shuttled back to the photoreceptor by IRBP, where it is re-bound to opsin [119].

Once rhodopsin is deactivated, the termination of the light signal in the photoreceptor begins with the hydrolysis of GTP on transducin. After transducin activates PDE, it continues to diffuse laterally along the membrane and comes in contact with Gβ5L/RGS9-1, a GAP complex that hydrolyzes GTP and deactivates transducin. With the deactivation of transducin, PDE returns to its inhibited state and cellular cGMP levels return to normal. The available cGMP reopens the gated channels, allowing for the influx of cations. The photoreceptor depolarizes and glutamate release resumes.

- **Synaptic signaling**

In darkness, there is a continuous release of glutamate from the photoreceptors to the bipolar cells within the OPL (Figure 1.13). Synaptic vesicles encasing glutamate dock at the photoreceptor presynaptic terminal and are then transported via a ribbon synapse to the synaptic cleft that separates the photoreceptors from the bipolar cells (postsynaptic neuron) [127]. These ribbon structures serve two main purposes. First, they are able to accommodate the high load and rate of synaptic vesicle release from the photoreceptors [128, 129]. Secondly, the ribbon structures allow for the continual adjustment of glutamate release in order to create a graded response to light. This ability to generate a graded response allows for high sensitivity to varying levels of light and optimization of the synaptic transfer of information to the bipolar cells [127].

With light, the cation channels close, causing a hyperpolarization of the photoreceptors. This terminates the synaptic flow of glutamate to the bipolar cells. The

Figure 1.13. Synaptic signaling between the photoreceptors and bipolar cells of the retina

In darkness, there is a continuous flow of glutamate from the photoreceptors to the bipolar cells. Glutamate bound to the metabotropic glutamate receptor 6 (mGluR6) activates the G protein, Gαo. This pathway keeps the cation channel, transient receptor potential member 1 (TRPM1) closed. When light hits the retina, the calcium channels close on the photoreceptors hyperpolarizing the retina, which halts glutamate export. Without glutamate bound to mGluR6, the TRPM1 cation channel opens. Postsynaptic density 95 (PSD95) is a scaffolding protein associated with the calcium channels. Synaptophysin is a synaptic vesicle protein.

Figure 1.13. Synaptic signaling between the photoreceptors and bipolar cells of the retina

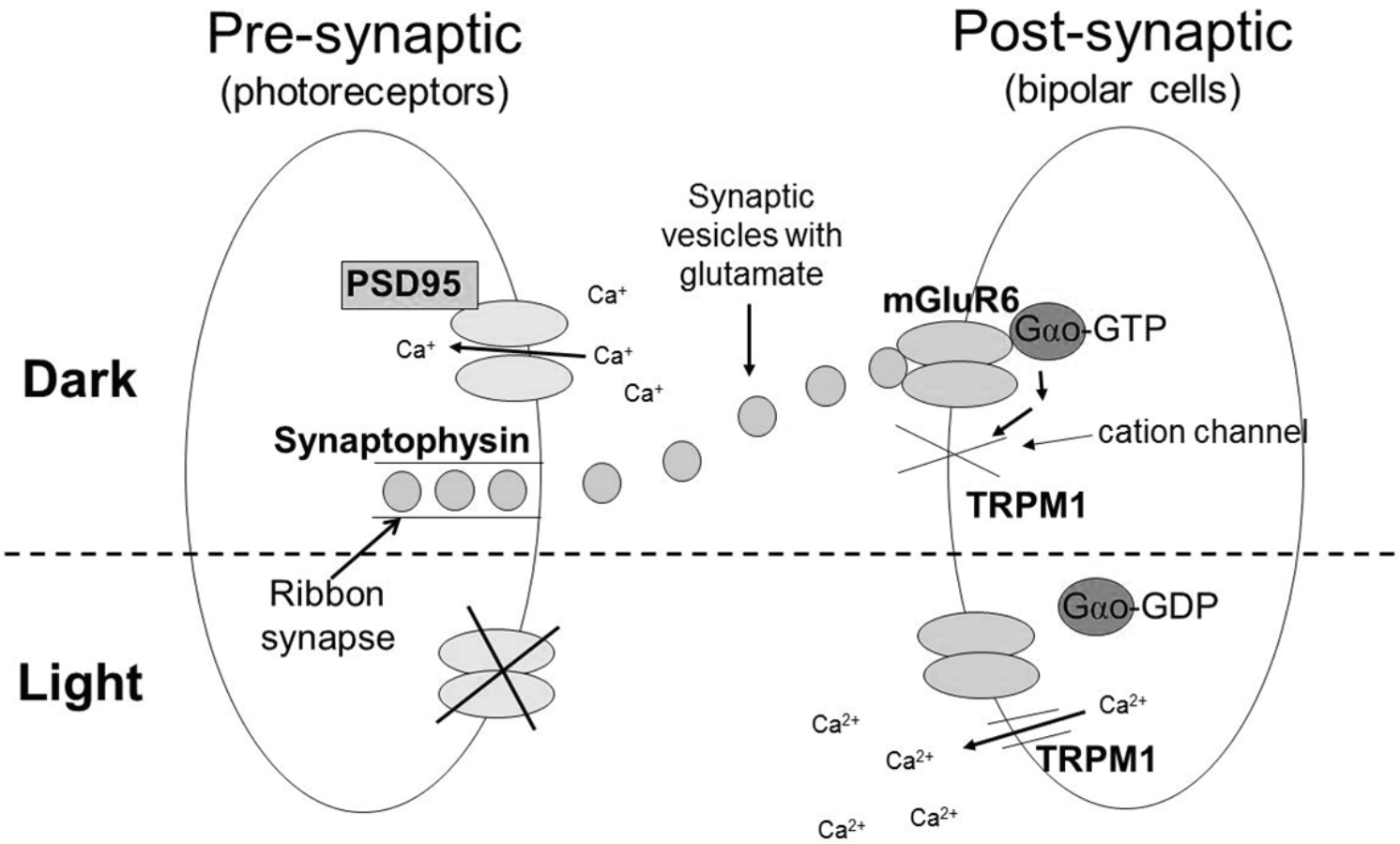

absence of glutamate in the synaptic cleft triggers a signaling cascade in the bipolar cells.

- **Inner retinal signaling**

The metabotropic glutamate receptor 6 (mGluR6, *Grm6*) is the primary glutamate receptor on bipolar cells. In darkness, when glutamate is bound, mGluR6 initiates a G-protein cascade that keeps the postsynaptic cation channels closed. Gαo1 is the primary effector of mGluR6, but the signaling pathway to the cation channel remains unclear [130, 131].

When light strikes the retina, the flow of glutamate from the photoreceptors is halted and glutamate is released from mGluR6. Without stimulation from the glutamate receptor, Gαo1 is rapidly deactivated by a GTPase accelerating protein (GAP). Recent evidence has shown that this GAP complex is formed by Gβ5-S and RGS7 or RGS11 [132]. The deactivation of Gαo1 relieves the inhibition of the ion channels. The transient receptor potential-like channel member 1 (TRPM1), the primary bipolar cell cation channel, opens and depolarizes the bipolar cells [133, 134]. The opening of the bipolar cation channels and subsequent depolarization can be measured by the electroretinogram and appears as the positive b-wave (see Section 1.5.3).

When the retina is no longer exposed to light, the flow of glutamate from the photoreceptors resumes. Glutamate binds to mGluR6 and activates Gαo1. This reinitiates the G protein cascade that closes the TRPM1 cation channel, returning the retina to a resting state.

- **Visual transmission from the bipolar cells**

The neural signal is transmitted from the rod bipolar cells to AII amacrine cells (Figure 1.10) [135]. Amacrine cells act as intermediaries between rod and cone bipolar cells. The signal is then passed from the cone bipolar cells to the ganglion cells. Amacrine cells also have the capacity to transmit the visual signal to the ganglion cells. Lastly, the ganglion cells transmit the neural signal to the axons leading to the optic nerve, and finally to the brain [136].

1.4. Aging

One of the many definitions of aging is the "progressive deterioration during the adult period of life that underlies an increasing vulnerability to challenges and a decreasing ability of the organism to survive" [137]. Because of aging's universal effect on all organisms, people have been studying aging for centuries.

There are several different models that can be used to study aging. Human aging has been studied in centenarians and in individuals with accelerated aging diseases, such as progeria, to identify specific links to long and short lifetimes, respectively. Cell culture can be used to study some aspects of aging, such as telomere maintenance. Model organisms such as *C. elegans* and mice are commonly used to study aging. Advantages of using these model organisms include the reduced variability between animals and much shorter lifespans as compared to a human population. The ability to genetically modify (either knock-out, mutated, or knock-in) specific genes in animal models has allowed for controlled testing of specific hypotheses about aging.

There are many hypotheses regarding the causes of aging. The most encompassing of these is the free radical theory of aging (FRTA). Although widely accepted as a viable explanation for the aging process, recent publications have begun to question the validity of this theory [138].

1.4.1. The free radical theory of aging

The free radical theory states that an organism accumulates oxidative damage with time and the amount amassed determines the rate of aging. The rate that damage accumulates depends upon a balance of (1) the generation of oxidants, (2) the antioxidant defenses, and (3) the ability of the cell to repair the damage incurred (Figure 1.14) [reviewed by [139]].

The most significant source of reactive oxygen species (ROS) in the cell is from the mitochondrial electron transport chain [reviewed by [139]]. In this respect, the FRTA is closely related to the "rate of living theory" that states the lifespan of an animal is

Figure 1.14. Contributing factors in the free radical theory of aging

The ultimate outcome of aging depends on three main factors: (1) the generation of oxidants (e.g., reactive oxygen species), (2) the defense mechanisms to prevent damage (e.g., antioxidants), and (3) the ability to repair the damage that occurs (e.g., protein degradation).

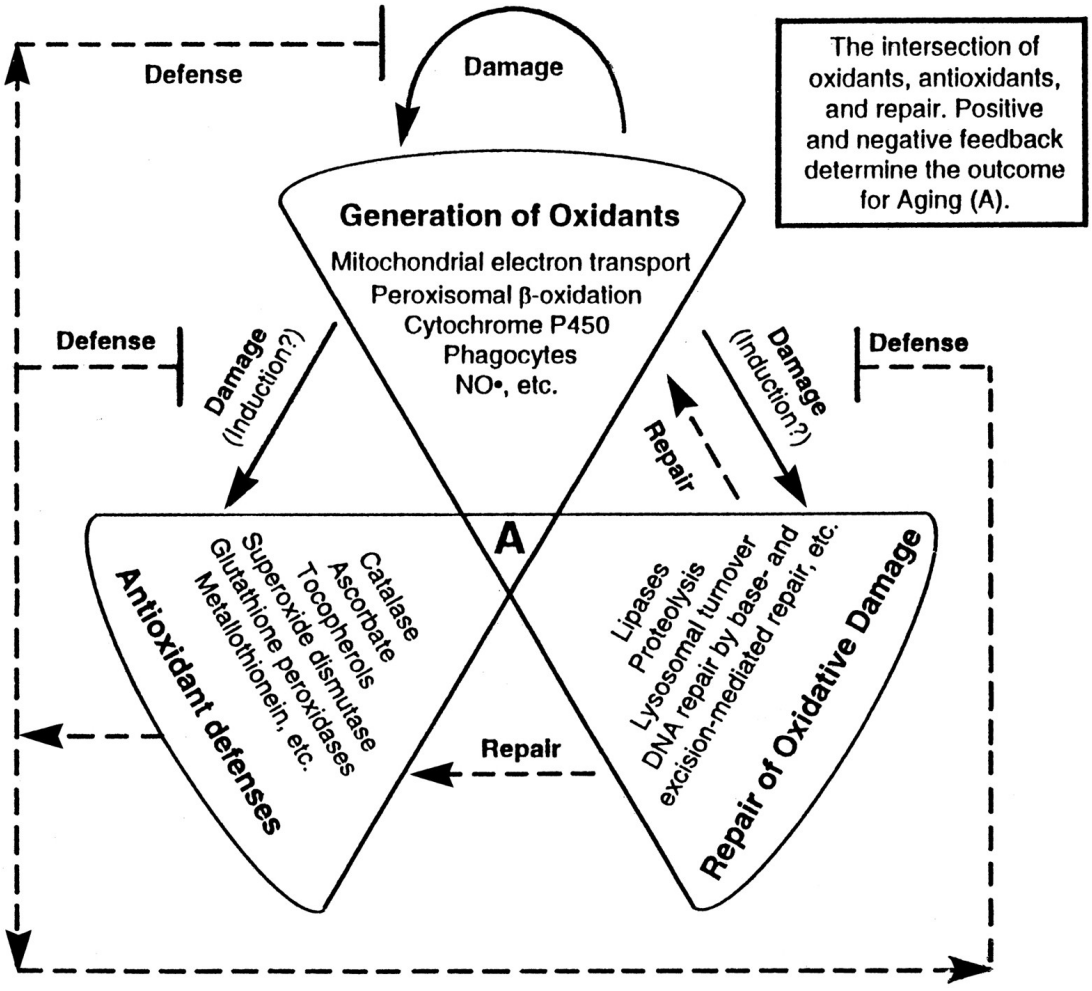

Figure is from [139].

dependent on the rate of cellular respiration. ROS can also be induced in the retina by environmental factors, such as light exposure, and phagocytosis in the RPE [87, 140].

The levels of ROS are controlled by antioxidants. For example, CuZn superoxide dismutase (SOD1) enzymatically converts superoxide anion to hydrogen peroxide. Catalase or glutathione peroxidase can further degrade hydrogen peroxide to water. Antioxidants are the first line of defense against the accumulation of oxidative damage.

ROS are able to modify many different components of the cell (Figure 1.15). These include DNA, lipids, carbohydrates, and proteins. The most common DNA oxidative modification is 8-oxoguanosine, which is considered a biomarker for aging [141].

ROS oxidize lipids in a process called lipid peroxidation. Lipid peroxidation can destabilize membranes and transmembrane proteins, as well as produce highly reactive by-products, such as 4-hydroxy-2-nonenal (HNE) [142], that can further damage other lipids and proteins in the cell. Damage to the mitochondrial membranes can cause loss of membrane potential and the increased production of ROS (mitochondrial dysfunction hypothesis). An increase in ROS produced in the mitochondria can also lead to increased mitochondrial DNA damage because of its close proximity to the electron transport chain (mitochondrial DNA damage hypothesis).

Carbohydrates are also modified by ROS and form advanced glycation end products (AGE). AGE products can then modify proteins and alter their function [143]. The accumulation of AGE products is also considered a hallmark of aging (advanced glycation end product hypothesis).

Lastly, cellular proteins can be modified by reactive oxygen species. Proteins can be modified directly, i.e., become carbonylated. Additionally, proteins can be modified by other molecules, e.g., HNE and AGE products. When proteins become oxidized, they undergo a conformational change that can expose hydrophobic regions of the proteins. These conformational changes often lead to the formation of protein aggregates. One of the proteasome's major roles is to degrade damaged proteins in the cell. Increased oxidative stress increases the load of proteins that need to be degraded. If the proteasome fails to keep cellular protein homeostasis, the cell may go into senescence

Figure 1.15. Targets of reactive oxygen species

Reactive oxygen species are generated in the cell, primarily from the mitochondria, but can also be induced from the environment. Antioxidants such as superoxide dismutase (SOD) and catalase (CAT) enzymatically break down reactive oxygen species before they can cause damage to cellular components. Reactive oxygen species can affect many components in the cell, including DNA, carbohydrates, mitochondria, lipids, and proteins.

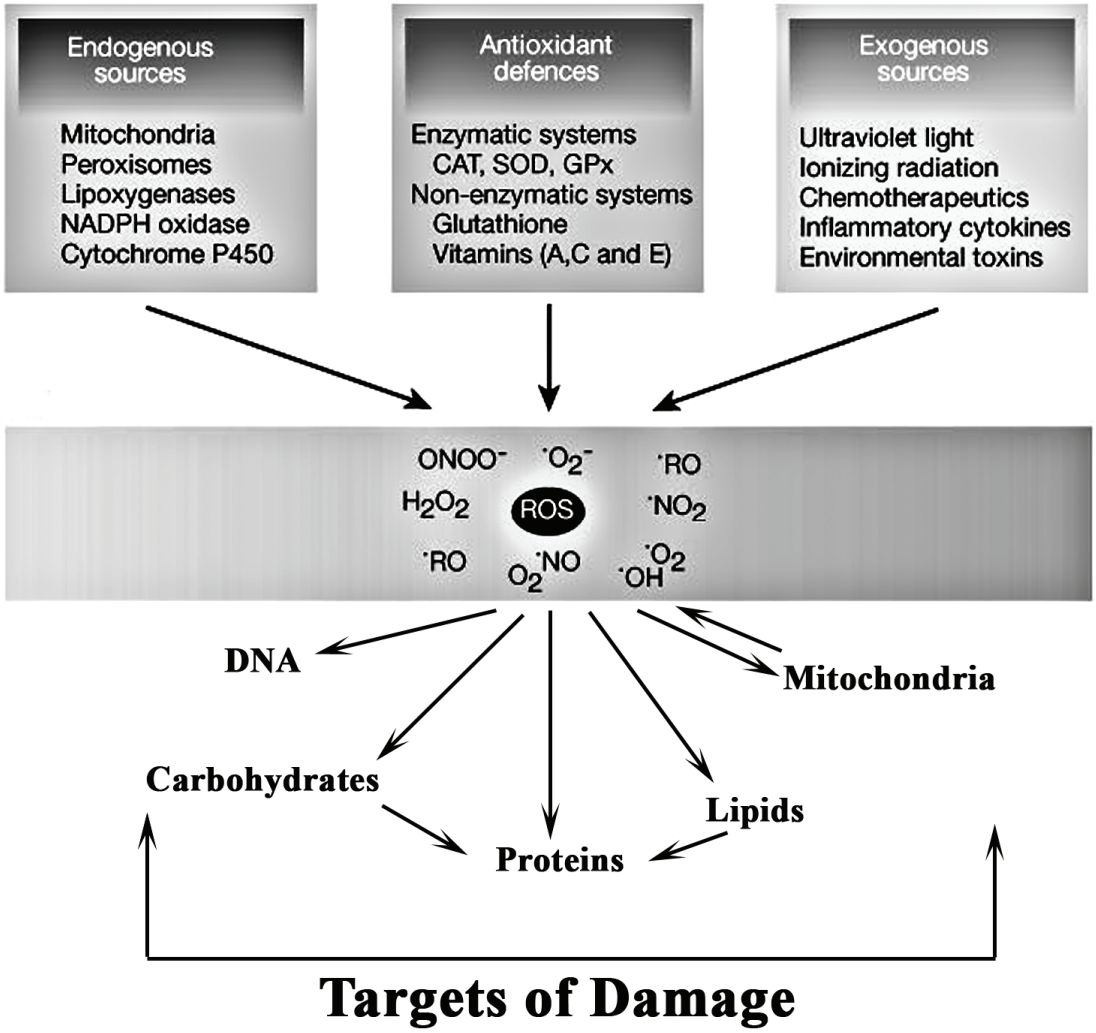

Figure is adapted from [144].

(aging). The following sections discuss the importance of proteasome in oxidative stress and aging.

1.4.2. Degradation of oxidized proteins by proteasome

The accumulation of damaged proteins with age is dependent on the rate of damage, and also on the rate at which the damaged proteins can be removed. Proteasomal degradation is the main pathway for removal of oxidant-damaged proteins in the nucleus and cytosol [46]. This statement is supported by data from both *in vitro* and *in vivo* (cultured cells) where the 20S proteasome selectively degrades oxidized proteins (Figure 1.16) [47, 93, 145].

Oxidized proteins are targeted to the 20S proteasome for degradation in one of several ways. Oxidation of proteins causes conformational changes that can expose hydrophobic regions, which are recognized by the 20S proteasome, and target them for degradation [146, 147]. Loss of secondary structure caused by oxidant-induced conformational changes can also target proteins to the 20S proteasome [146, 148]. A third targeting mechanism is the exposure of a 'PEST' sequence on a protein. A PEST sequence is a protein region that is rich in proline, aspartate, serine, and threonine residues. Studies have shown that exposure of a PEST region signals degradation of some proteins [149]. Cellular chaperones such as Hsp90 are also thought to target unfolded proteins to the 20S proteasome [61].

1.4.3. Proteasome activity with age

In general, the age-related accumulation of damaged proteins correlates with decreased proteasome function. In old (22-24 months) and very old (26-28 months) F344 rat retina, there was approximately a 70% decrease in chymotrypsin-like activity as compared to young rat retina [150]. Several groups have reported a similar (50-60%) decrease in caspase-like activity in the rat liver [151-153]. In both rats and mice, there is a general decrease in chymotrypsin- and trypsin-like activities in most areas of the brain [154]. Proteasome from human lymphocytes also exhibited a decrease in peptide hydrolysis [155].

Figure 1.16. Role of proteasome in clearing oxidative damage

The 26S proteasome degrades ubiquitinated proteins. The 20S proteasome degrades oxidized proteins. Both the 26S and 20S proteasomes are sensitive to oxidative damage and subsequent inhibition. Oxidized proteins can form aggregates, which inhibit the proteasome.

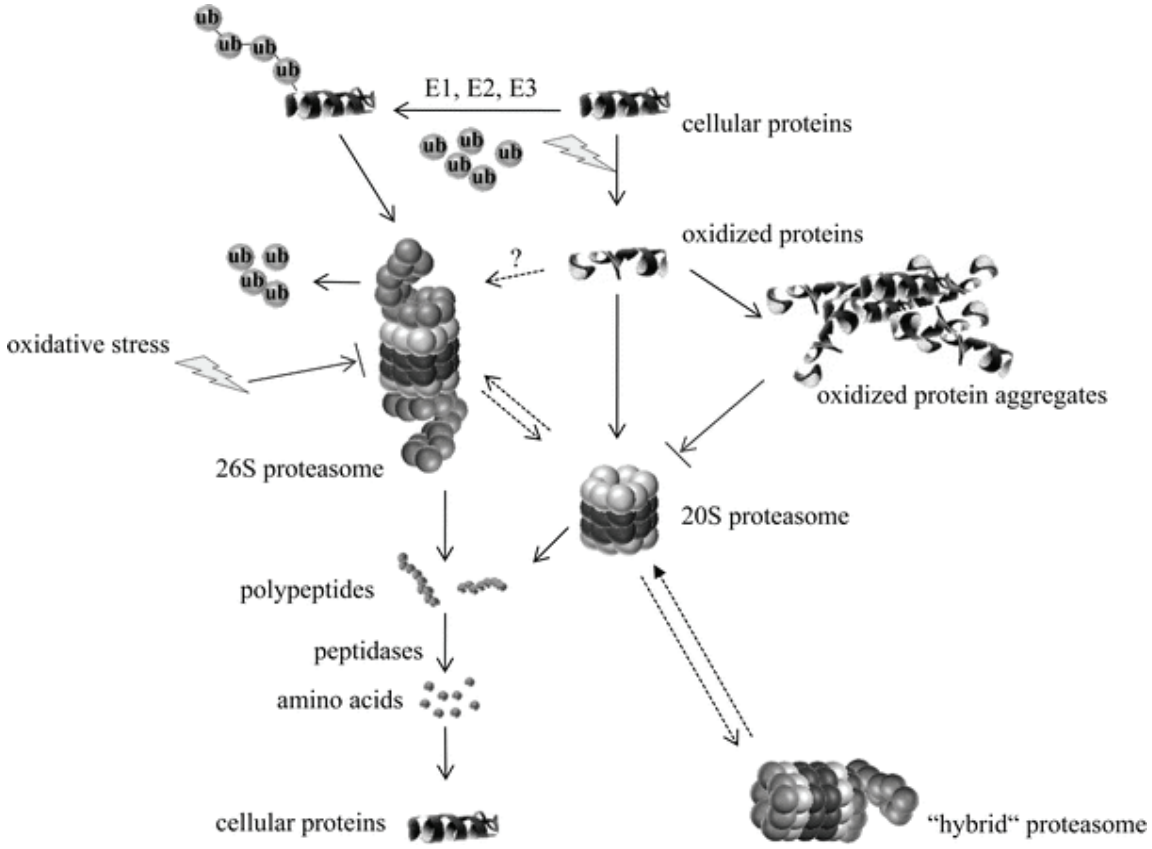

Figure is from [156].

Loss of 20S proteasome core activity is not the only explanation for the observed decrease in proteasome activity. The content of activators and inhibitors also factor in the outcome. For example, muscle tissue from aged rats demonstrated approximately a 50-60% decrease in proteasome activity [78, 79]. This decrease in muscle proteasome activity was partially explained by the significant decrease (~75%) in proteasome activators PA700 and PA28. However, isolated 20S core proteasome from aged rats also showed a reduced ability to degrade an oxidized protein substrate, suggesting additional effects in the 20S core particle.

Although there is a general decrease in proteasome activity with age, it is not universal. The changes observed in proteasome activity with age also depend on the tissue, species, and assay conditions used. For example, the changes in proteasome activity in rat liver described above, one group saw a change in chymotrypsin- and trypsin-activity and the other two groups did not [151-153]. Also, in Chapter 4, we did not see an age-related decrease in proteasome activity in the WT mouse retina as previously reported for rat retina [6, 150]. The disparate results could be attributed to the relative ages of the rats/mice used. Twenty-four-month-old mice have a higher survival rate than a 24-26-month-old rat.

1.4.4. Oxidative inhibition of the proteasome

Increased oxidative damage with age could be partially responsible for the decrease in proteasome activity. The proteasome can be inhibited by oxidative modification. For example, modification of the α6 subunit of the 20S core proteasome by 4-HNE results in the rapid inhibition of chymotrypsin-like activity [157]. Another study examined age-related modifications to 26S proteasome from lymphocytes. Both the 20S core and the PA700 regulatory complex subunits had increased oxidative modifications with age (glycation and HNE) [155]. Most of the modifications were present on the 20S core with only a few PA700 subunits affected [155].

The PA700 proteasome regulator is also sensitive to oxidative stress. The S6 ATPase subunit in particular is sensitive to carbonylation under oxidative stress conditions. An accumulation of ubiquitin-modified proteins was observed in cells devoid of the S6 ATPase subunit [158]. Other subunits of the PA700 were also susceptible to

oxidative modification with age [155]. These data suggest the oxidative modification of PA700, especially the S6 ATPase subunit, contributes to proteasome dysfunction with aging.

It has also been proposed that oxidant-induced protein aggregates in the cell can bind to and inhibit the proteasome [159, 160]. For example, epithelial cells fed lipofuscin, an aggregate of undegraded proteins and lipids that accumulates with age, showed decreased proteasome activity. In addition, cells dosed with $A\beta_{1\text{-}42}$, which forms plaques in Alzheimer's disease, showed decreased proteasome activity [161].

1.4.5. Proteasome activation as an anti-aging strategy

A decrease in proteasome activity can lead to the accumulation of damaged proteins in the cell. Therefore, proteasome activation has been proposed as an anti-aging strategy [reviewed by [162]].

Several studies have indicated that an increase of cellular proteasome activity is associated with an increase in lifespan. In human studies, fibroblasts cultured from centenarians were shown to have approximately 25% higher caspase-like activity as compared to fibroblasts cultured from an 80-year-old [163]. Human embryonic fibroblasts treated with oleuropeurin, an olive oil extract shown to increase proteasome activity, exhibited a 15% delay in replicative senescence in comparison to untreated cells [164].

Invertebrate studies have supported the findings from cultured cells. Overexpression of a proteasome activator subunit has been shown to increase lifespan in *Drosophila*. The overexpression of PA700 subunit Rpn11, which deubiquitinates protein substrates, resulted in a delay in the decrease of proteasome activity with age. This delay correlated with a 1.3-fold extension in lifespan [165]. The knock-down of Rpn11 in *Drosophila* had the opposite effect; a more pronounced accumulation of ubiquitinated proteins and decreased lifespan were observed. In addition, overexpression of Rpn11 suppressed neural degeneration by proteins that cause the polyglutamine diseases spinocerebellular ataxia type 3 and Huntington's disease in the *Drosophila* model [165].

Conversely, knock-down of the proteasome activator *aip-1* in *C. elegans* (homologue of mammalian arsenic inducible proteasomal 19S regulatory particle-

associated protein (AIRAP)) leads to decreased lifespan in *C. elegans*. The decrease in lifespan is accompanied by decreased proteasome activity and the accumulation of protein aggregates [166]. Taken together, these data support the idea that proteasome activity could be a determining factor in aging.

1.4.6. Immunoproteasome and age

Immunoproteasome has been shown to be upregulated with age in several tissues, including the immune-privileged brain and retina. In mouse retina, immunoproteasome subunits are upregulated 2- to 3-fold with age (Chapter 4) [6]. In aged rat and human hippocampus, immunoproteasome was significantly upregulated in comparison to young adult samples [84, 85]. Immunoproteasome is also upregulated with age in post-mitotic muscle tissue [78, 79].

As discussed in the previous section (Section 1.2.3), immunoproteasome is upregulated in response to a number of stressors, including oxidative stress. The presence of immunoproteasome under stress conditions was shown to have a protective effect and prevented the increase of oxidatively modified proteins [6, 92]. Therefore, the upregulation of immunoproteasome with age may be a compensatory mechanism to protect from the increased levels of oxidative stress and damage in the aging cell by degrading oxidized proteins more efficiently than standard proteasome [93, 94].

1.4.7. Age-related diseases and proteasome

Several age-related, neurodegenerative diseases are associated with the formation of protein aggregates and correlates with dysfunction of the proteasome. Because the proteasome is essential for normal cellular function, inhibition of proteasome could ultimately lead to cell death [156, 167]. In addition, it has been proposed that insufficient clearance of damaged or mutant proteins could be part of the pathogenesis of neurodegenerative diseases [167].

Proteasome activity is decreased with Alzheimer's disease and this decrease could be attributed to inhibition by either amyloid-β ($A\beta_{1\text{-}42}$) or tau, which both form protein aggregrates that are hallmarks of the disease [161, 168]. Normally $A\beta_{1\text{-}42}$ is degraded by the proteasome, preventing aggregate formation [169]. Conversely, $A\beta_{1\text{-}42}$ has been shown to inhibit the proteasome [161]. With the decrease in proteasome activity, $A\beta_{1\text{-}42}$

could build up in the cell and produce plaques. In cultured cells, neurofibrillary tau tangles are able to bind to and inhibit the proteasome [168]. Taken together, these hallmarks of Alzheimer's disease, neurofibrillary tau tangles and $A\beta_{1-42}$ plaques, are able to inhibit the proteasome, resulting in increased aggregates and neuronal dysfunction.

Huntington's disease is caused by a polyglutamine (polyQ) tract extension in the protein huntingtin. The fragments of mutant polyQ proteins are prone to aggregation. Huntingtin aggregates have been shown to inhibit proteasome activity, and thus could impair normal neuronal function [170].

Parkinson's disease is also associated with decreased proteasome activity and Lewy body (deposits of partially degraded proteins) formation in the substantia nigra. [171, 172]. Additionally, Parkinson's disease can arise from single mutations in several different proteins involved in the ubiquitin-proteasome pathway, such as mutations in parkin, an E3 ligase, or UCH-L1, a deubiquitinating enzyme [reviewed by [173]].

- **Immunoproteasome and age-related diseases**

Immunoproteasome is upregulated with several neurodegenerative diseases, including AMD (Chapter 2), ALS, Alzheimer's, and Huntington's disease [83, 85, 86, 174]. The function of immunoproteasome in these disease models is yet unknown. The upregulation of immunoproteasome in diseased brain and retina suggests alternative roles for immunoproteasome are possible.

1.4.8. Mouse model of aging

Research in *Drosophila melanogaster* and *C. elegans* has produced a large body of basic information regarding aging. These invertebrates have short lifespans (weeks), they are easily housed in the laboratory, and their genetics and environments are easily manipulated, allowing for the generation of large amounts of data in a short time [175]. However, to study the more complex processes and systems (i.e., brain and retina) involved in human aging, a mammalian model of aging must be used.

Mice are the most commonly used mammalian model of aging. Mice are also relatively simple to genetically manipulate and inexpensive to house [175]. The wild-type and immunoproteasome KO mice used in the aging studies of this thesis (Chapters 4 and 5) were pigmented mice on the C57BL/6 background.

Changes in retinal proteasome and morphology were determined at five different ages ranging from 2 to 24 months to follow the kinetics of the age-related changes. These ages were chosen in accordance to the "Principles of Animal Use for Gerontological Research" [176]. To avoid the changes involved with eye development, the youngest group was 2 months old. At this age, the mouse retina is fully mature and has not begun to show an age-related decline [177]. In addition, we also did not use mice that were 'too old' (at or below the 25th percentile for survival). The interest of our studies (Chapters 4 and 5) was to assess retinal changes with healthy aging. Using mice that are too old increases the probability that they are also afflicted with an age-related disease (e.g., cancer) [176]. The median lifespan of C57BL/6 mice is 2.5 years [178]. Therefore, a 24-month-old mouse is considered to be an 'old' mouse but has a high probability of being healthy. In addition, all mice were housed in a specific pathogen-free (SPF) environment to avoid consequences of diseases that could interfere with the changes involved with healthy aging [176].

1.4.9. Aging retina

- **Changes in retinal morphology with age**

The retina exhibits many changes over the lifespan of an organism. One of the most prominent age-related changes is cell loss. In the ONL and INL, nuclei are steadily lost with age (Chapter 5) (for retinal morphometry methods, see section 1.3.1). In aged, pigmented mice (C57BL/6J or B6D2F1/J), there is an 11-20% decrease in photoreceptors [7, 179, 180]. Albino mice (Balb/c) exhibit a greater loss (~40%) in photoreceptors with age [179]. Rod photoreceptors are particularly sensitive to age-related loss, both in mice and humans and are lost to a greater extent than cones [179, 181]. In addition to cell loss, photoreceptor outer segments become shorter with age [182].

The loss of photoreceptor cells with age is hypothesized to be secondary to RPE dysfunction [183]. As previously stated (Section 1.3.2), one of the RPE's main functions is to phagocytize the spent tips of the rod outer segments [112]. With age, there is increased accumulation of lipofuscin in the RPE. Lipofuscin is an amorphous combination of undigested proteins and lipids that accumulate in the lysosome [184]. In RPE, lipofuscin is thought to be remnants of phagocytized rod outer segments [185].

Increased lipofuscin causes a decrease phagocytosis of the rod outer segments and decreased lysosomal function [183, 186]. Because of the essential role the RPE cells play in photoreceptor maintenance, RPE dysfunction could lead to an increase in accumulated damage of the photoreceptors and ultimately cell loss.

Additional support for the importance of RPE phagocytosis and photoreceptor survival is the comparison between albino and pigmented mice. Albino mice lose more photoreceptors with age as compared to pigmented mice [179]. Decreased pigment (melanin) in cultured RPE cells led to increased accumulation of lipofuscin when fed photoreceptor outer segments [186]. Therefore, in addition to protecting from light-induced damage, melanin may also protect from oxidative damage induced by phagocytosis [140, 186].

The INL also loses nuclei with age [7, 187]. Aged mice lose approximately 13% of the nuclei in the INL from 2 to 24 months of age [7]. In addition to nuclei loss, remodeling of the synapse between the ONL and INL also occurs in aged animals [188]. Both rod bipolar cells and horizontal cells of the INL sprout abnormal processes beyond the OPL and into the ONL. These processes begin to grow at 12 months of age and continue past 24 months. Although the reason for this phenomenon is not yet known, it is possible that these aberrant growths could be a compensatory action to photoreceptor or synaptic dysfunction [188].

- **Retinal function decreases with age**

In correlation with morphological changes in the retina, the aged mouse exhibits decreases in vision and retinal function. Decreases in visual acuity have been monitored in adult (4 month-old) and aged (30 month-old) pigmented mice by measuring the optomotor response This technique uses black and white stripes of different width and contrast that rotate at different speeds to determine the visual acuity and contrast sensitivity of a mouse. The detection of the stripes is noted when the mouse "tracks" the stimulus by reflexively turning its head in the direction of movement. Aged mice exhibited a 50% decrease in both visual acuity and contrast sensitivity compared to adult mice [180].

Decreases in retinal function in aged mice have also been detected by electroretinography (method discussed in more detail in Section 1.5.3). The dark-adapted ERG response, both the a-wave (rod photoreceptor response) and b-wave (rod-originating bipolar cell response) was decreased approximately 50% with age in both pigmented and albino mice [179, 180]. Although aged albino mice had fewer photoreceptors, they had a similar ERG phenotype as compared to the aged pigmented mice.

1.5. Methodology

1.5.1. Cytotoxic T lymphocyte (CTL)-induced injury

In Chapter 3, CTL-induced injury to the retina and brain was accomplished using β-galactosidase (β-gal) transgenic mice (Figure 1.17). β-gal is a protein from *E. coli* and is not normally expressed in the mouse. As such, the cell-specific expression of β-gal can be controlled using promoters of genes expressed exclusively in cells of the retina and brain. Proteasome-dependent degradation of β-gal generates one well-defined antigenic peptide that is presented by MHC class I on the cell surface. Using activated T cells that recognize this specific β-gal epitope, specific cells of the retina and brain expressing β-gal can be targeted for destruction.

In this thesis (Chapter 3), two strains of transgenic β-gal mice were used. Hi-arr-β-gal mice express β-gal under the control of the arrestin promoter of rod photoreceptor cells (Figure 1.17) [189, 190]. β-galactosidase expressed via the promoter of glial fibrillary acidic protein (GFAP) targets both the retina and the brain of GFAP-β-gal mice (Figure 1.17) [191]. GFAP is a protein specifically expressed in glial cells and is expressed in astrocytes throughout the retina and brain.

To induce CTL-injury, activated T cells specifically targeted to an epitope of β-gal were injected into the transgenic mice [8]. Mice expressing β-gal on the arrestin promoter of rod photoreceptor cells (hi-arr-β-gal) experienced massive photoreceptor killing due to attack by the injected $CD8^+$ CTLs [8, 192, 193]. This injury upregulated immunoproteasome in the retina. CTLs targeted to the astrocytes of the brain (GFAP-β-gal mice) also produced an upregulation of immunoproteasome in the brain (Chapter 3)

Figure 1.17. Transgenic mice expressing β-galactosidase in retina and brain

Above: Hi-arr-β-gal mice express β-galactosidase (β-gal) under control of the arrestin promoter. (A) Wild-type retinal section stained with nuclear fast red. (B) Transgenic hi-arr-β-gal mouse retina stained with nuclear fast red. β-gal (purple) is expressed specifically in the photoreceptors.

Below: GFAP-β-gal mice express β-gal on the glial fibrillary acidic protein (GFAP). β-gal (blue) is expressed in the astrocytes of the (A) brain and (B) retina.

Ganglion cell layer (GCL); inner nuclear layer (INL), outer nuclear layer (ONL); outer photoreceptor segments (OS); photoreceptors (PR); retinal pigment epithelium (RPE).

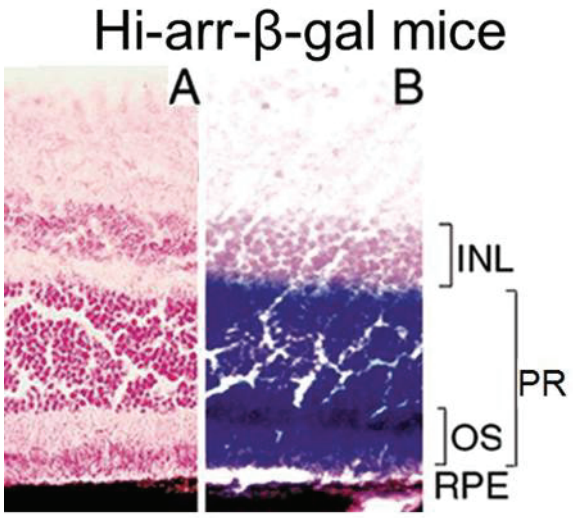

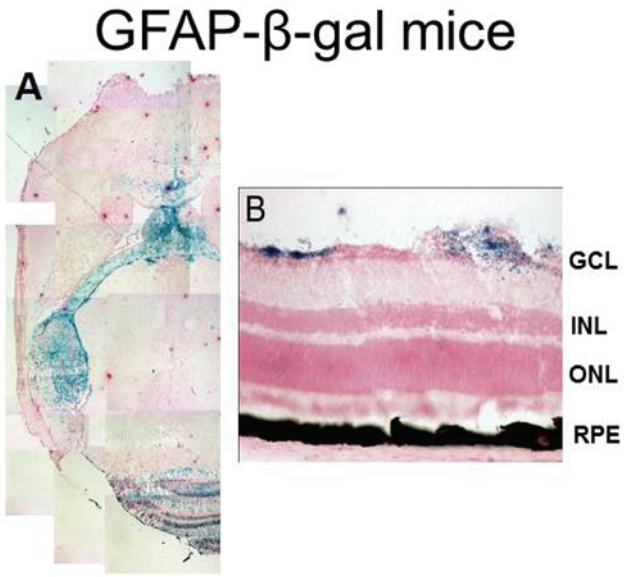

[8]. These data indicate that immunoproteasome responds to injury in both the immune-privileged brain and retina.

1.5.2. Retinal morphometry

As previously described (Section 1.3.2), the cells of the retina are stratified into discrete layers (Figure 1.9). The condition of the retina can be estimated from measurements of nuclei density in the nuclear layers, thickness of the plexiform layers, and length of the photoreceptor outer segments. Increased stress or the inability to maintain retinal homeostasis can lead to the thinning of the nuclear layers, thinning of the plexiform layers, and/or altering the length of the photoreceptor outer segments.

Retinal morphometry measurements were used in this thesis (Chapter 5) to determine if there were changes in the retinal morphology of immunoproteasome KO mice and to ascertain whether these changes were magnified with age. Morphometry measurements were done on paraffin-embedded retinal sections (6 μm). The retinal sections were stained with hematoxylin and eosin (H&E) to visualize the tissue (Figure 1.9).

One of the traditional methods for determining the ONL thickness is done by counting the number of vertical nuclei spanning the ONL [179]. However, this approach for determining the ONL thickness can have error associated with it. If the nuclei of the ONL are disorganized, it can be difficult to get an accurate count of nuclei spanning the nuclear layer. In addition, this measure is very discrete, and may not account for slight differences across the retinal section.

Another traditional method of determining ONL morphology simply measures the vertical thickness of the ONL. However, the accuracy of this method depends on the quality of the retinal sections, and measuring the retinal thickness (μm) can be misleading due to artifacts from sectioning. The mechanical force of cutting the retinal sections can stretch or compress the nuclear layers and cause inaccuracies in the measurements.

To overcome the potential artifacts associated with the traditional methods, the ONL and INL were assessed by using a nuclear density measurement. In brief, an area of the ONL was selected on a retinal section (Figure 1.18B). All of the nuclei in the section were counted. The nuclei density (nuclei/μm) was determined by dividing the number of

Figure 1.18. Retinal morphometry measurements

(A) Diagram of the retina. Retinal morphometry measurements were made at 500 and 1000 μm from the optic nerve. (B) Representative retina section illustrating how the ONL nuclei density (nuclei/μm) was measured. A section of the ONL was selected and the number of nuclei within the box was counted. The length of retinal section (μm) was measured. The number of nuclei counted was divided by the length of the retinal section (nuclei/μm).

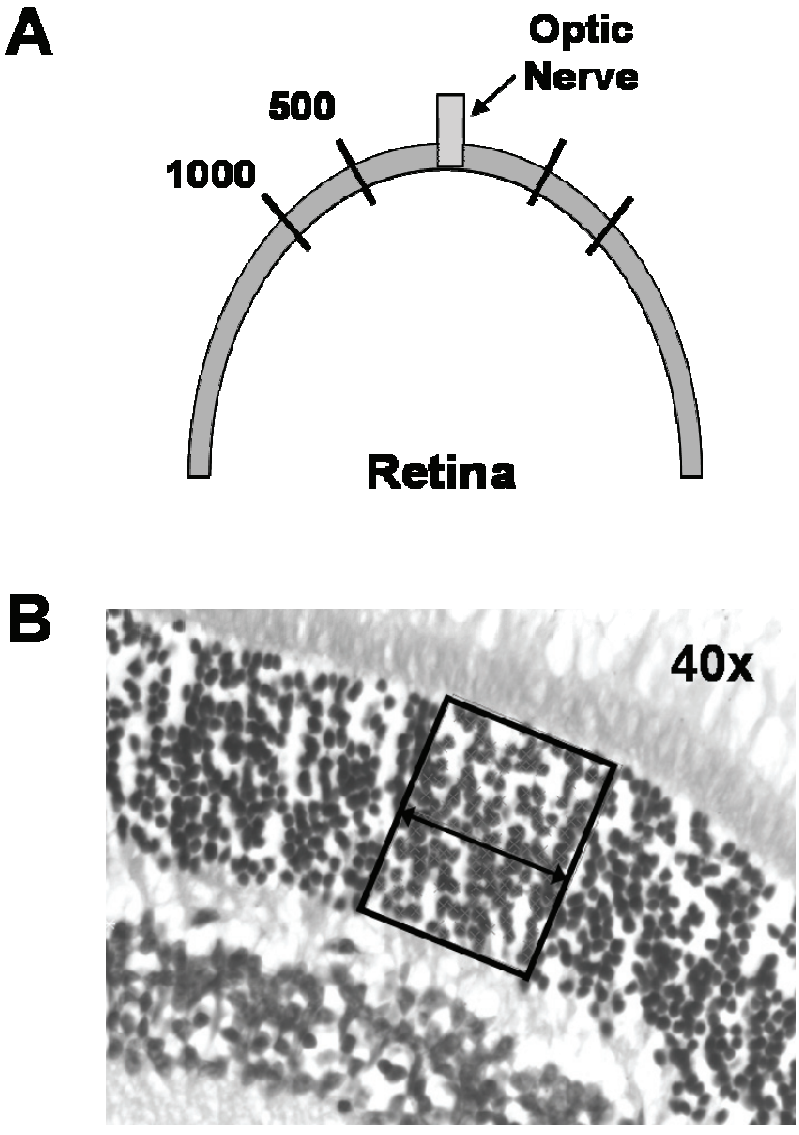

nuclei by the length of the retinal area counted. The same technique was used to determine the inner nuclear layer thickness. A detailed account of this procedure follows.

The optic nerve was used as a reference point to ensure the measurements were made in the same place for each individual mouse retina. The retinal layers were measured at 500 and 1000 μm on either side of the optic nerve (Figure 1.18A), which is important because retinal layer thickness can vary depending on the anatomical site. For example, the retina is the thickest near the optic nerve and gradually starts to thin until it reaches the pars plana. Measurements at 500 and 1000 μm were analyzed separately.

The thickness of the OPL was measured as the average distance between the nuclei of the ONL and INL. The IPL thickness was measured as the distance between the INL and the GCL. The photoreceptor outer segment length was measured from the ONL to the RPE in intact sections only. (In some of the retinal sections, the photoreceptor outer segments were separated from the RPE layer as an artifact of sectioning.) The GCL is mostly a single layer of cells (Figure 1.9). Therefore, the cell density for this layer was determined as the number of nuclei per micron.

1.5.3. Electroretinography

The electroretinogram (ERG) is a technique used to evaluate retinal function. This procedure measures the electrical response of the retina at the corneal surface following a light stimulus. Prior to the ERG, animals are dark-adapted for at least 14 hours and ERGs are conducted under low-intensity red light. This dark-adaption period is used to ensure that all of the available rhodopsin has been regenerated and is in its resting state. Mice are anesthetized with a ketamine/xylazine mixture and their eyes are dilated (1% tropicamide; 2% cyclopentolate) to ensure maximal light exposure to the retina. Two subdermal needle electrodes are used as a ground and a reference electrode (tail and cheek of measured eye, respectively). The ERG signal is measured using a silver DTL fiber electrode that is placed directly on the corneal surface. A Ganzfeld, which produces a finely calibrated flash of light of varying intensity and duration, is then placed over the head of the mouse.

The ERG recording protocol uses a graded series of light flashes of increasing intensity. The ERG waveform associated with each light intensity is an average of

several trials. At the low-light flashes, the signal is low, and therefore the signal to noise ratio (S/N) is low as well. To improve the S/N ratio, ten trials are averaged for the lowest light intensity. The intensity of the ERG signal increases with light intensity, improving the S/N so that only three trials are used at the highest light intensities.

To allow for rhodopsin regeneration, an interstimulus delay (time between trials) is employed. There is a direct correlation between light intensity and the extent of rhodopsin bleaching. Therefore, with increasing light intensity, the interstimulus delay is increased. This time ensures that all of the rhodopsin that had been activated by the previous flash has returned to its resting state. All of the rhodopsin in retina must be available for activation to receive an accurate ERG recording.

By varying the light flash intensity and background lighting, the function of both rods and cones can be distinguished. Under dark-adapted conditions, low intensity light flashes (0.0005 to 0.01 cd s/m^2), stimulate only the rod photoreceptors. This rod-only response is because the rhodopsin visual pigment in rods is extremely sensitive to light, whereas cone opsin has a higher detection limit. At higher light intensity flashes (0.05 to 50 cd s/m^2), the ERG waveform represents a mixed response, with contributions from both rods and cones.

In order to isolate the cone response, a light-adapted ERG can be performed. Contrary to the name's suggestion, the light-adapted ERG is still performed under dim, red light. By keeping the ambient lighting to low, red light, the level of light exposure to the mouse can be controlled. To light adapt the mouse, a backlight is turned on inside the Ganzfeld for a period of 10 minutes to ensure that all of the rhodopsin is bleached and that only the cone opsin is functioning. The backlight remains lit during the light-adapted ERG measurements. Similar to the dark-adapted ERG, the light-adapted ERG also uses a series of increasing light intensities and uses the average of 25 trials for each intensity. Unlike the dark-adapted ERG, the interstimulus delay is very short and does not increase with intensity. Cone opsin requires a much higher intensity light to isomerize and recovers ~100-fold faster than rhodopsin [194, 195].

The raw, dark-adapted ERG waveform has three main components that are measured directly (Fig. 1.19A). The first negative peak is the a-wave, which reflects the

Figure 1.19. Representative ERG waveforms

(A) Representative dark-adapted ERG waveform. The first negative peak is the a-wave, which represents the response from the photoreceptors. The large, positive peak is the b-wave. The amplitude from the trough of the a-wave to the peak of the b-wave represents the response from the bipolar cells. The wavelets that occur between the a- and b-waves are the oscillatory potentials. These wavelets are a measure of the amacrine cell response. (B) Representative light-adapted ERG waveform. This waveform represents the cone-only response from the retina. Similar to the dark-adapted ERG, there is an a- and b-wave.

Figure 1.19. Representative ERG waveforms

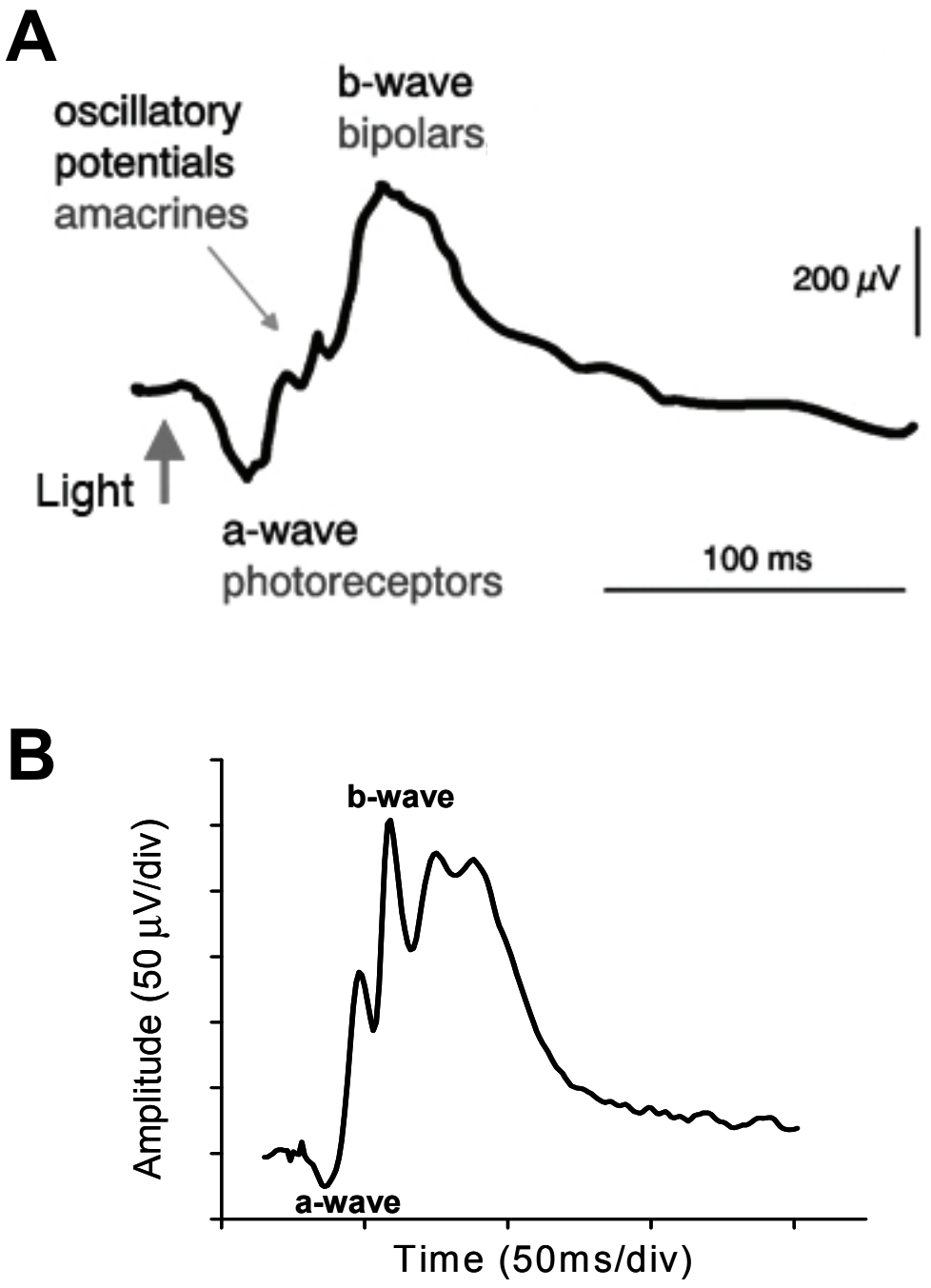

Figure is adapted from [7, 196].

photoreceptor response. It is a negative voltage response due to the hyperpolarization of the retina that results from the closing of the photoreceptor ion channels. The major positive peak is the b-wave, which reflects the bipolar cell or postreceptoral response. The positive electrical signal is generated by the opening of cation channels on the bipolar cells. The wavelets that occur between the a-wave and b-wave are the oscillatory potentials. This series of peaks reflects the function of the amacrine cells [197]. The light-adapted ERG has only an a- and b-wave that are directly measured (Figure 1.19B). The a- and b-waves of the ERG can be analyzed using both the amplitude and the implicit time (time between the light stimulus and peak). The amplitude, or magnitude of the response, can be a direct reflection of the number of functional cells generating the signal. Changes in the amplitude or implicit time could also indicate alterations in the signaling pathway, such as changes in content of signaling proteins. Differences in the structure of the retina could also create an abnormal ERG waveform. For example, changes in structural proteins could cause misalignment or malformation of synapses that could affect the b-wave. A bassoon (retinal structural protein) mutant and the *nob2* mutant both show defects in synaptic structure that could attribute decreased b-wave phenotype [198, 199].

The oscillatory potentials (OPs) cannot be directly measured on the raw ERG waveform because of the influence of the a- and b-waves. However, the OPs can be isolated by filtering out the slow a- and b-wave frequencies (65 to 235 Hz) while recording the ERG (Fig 1.20). There are usually 5-6 measurable OPs. The OPs are often analyzed together as a sum of all OP (SOP) amplitudes or implicit times. This method can only be employed if the OPs show a similar pattern across groups.

The oscillatory potentials may be used to assess the retinal metabolic needs and blood supply. Many retinal diseases that involve changes to the retinal blood supply, including glaucoma and diabetic retinopathy, show aberrant oscillatory potentials [200]. The amplitude, implicit time, and the frequency can be used to determine changes in retinal health.

Most studies report the raw ERG waveform measures, e.g., a- and b-wave amplitudes, and use these measures to determine the overall retinal function.

Figure 1.20. Isolation of oscillatory potentials from the raw ERG waveform

The oscillatory potentials (OPs) are isolated from the ERG waveform by filtering out the a- and b-waves. The OPs originate from the amacrine cells of the retina. The OPs are often analyzed as the summation of the amplitudes or implicit times for each individual OP.

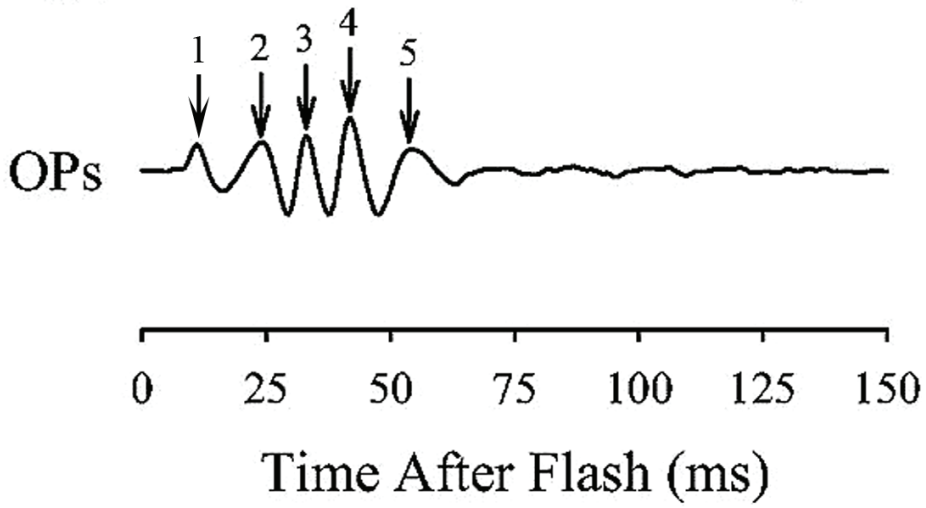

Figure adapted from [200].

Unfortunately, the accurate analysis of the ERG waveform is not as simple as measuring the peaks and troughs of the waveform. The raw ERG waveform is actually the addition of three different responses from the retina that are measured at the cornea. These components are known as PI, PII, and PIII (Fig. 1.21) [201]. PI is a slow, positive response measured from the cornea that originates from the RPE. The PII component is also positive, but is a much faster response. The third component, PIII, is a fast, negative response. Therefore the a-wave is the leading edge of the negative PIII while the b-wave is actually the summation of both the PII and PIII waves. Both the PII and PIII components can be isolated mathematically.

The PIII component originates from the photoreceptors. The PIII and a-wave amplitudes directly correlate with the number of functional photoreceptors. In mice, the dark-adapted a-wave generated by rods is much larger than the light-adapted a-wave originating from the cone photoreceptors. The smaller light-adapted a-wave amplitude reflects the relative photoreceptor populations. For example, in the mouse the ratio of rods to cones is 97:3 [108, 202]. The PIII is typically modeled using the Hood and Birch [203] formulation of the Lamb and Pugh model (Figure 1.22). Both time (t) and intensity (i) are considered in the following equation (Equation 1) to calculate Rm_{PIII}.

$$\text{Equation 1: } PIII(i,t) = (1-\exp(-0.5\ S_{rod} \times i \times (t - t_d)^2)) \times Rm_{PIII}.$$

The four highest flash intensities are used with this equation to calculate the Rm_{PIII}. In this formulation, Rm_{PIII} is the maximum dark-adapted photoreceptor response and S_{rod} is the sensitivity measurement. A representative graph for calculation of Rm_{PIII} is shown in Figure 1.22.

The PII component originates from the bipolar cells. There are several ways to extract this component from the raw ERG waveform. The most typical method of isolation is to subtract the PIII component from the ERG waveform (Figure 1.23). The extracted PII is then fit to a Naka-Rushton equation (Equation 2) (Figure 1.24).

$$\text{Equation 2: } PII(i)/Rm_{PII} = i/(i + kPII)$$

This equation is similar to Michaelis-Menten kinetics. The Naka-Rushton plot graphs the response vs. the intensity. The maximum response is the Rm_{PII} (similar to V_{max}) and the light intensity at one-half the maximum response is kPII (similar to K_m). The kPII value

Figure 1.21. Raw ERG waveform components

Representative ERG waveform from a cat. This figure shows the three different components that contribute to the final recorded ERG waveform. The PIII is a fast, corneal-negative response originating from the photoreceptors. The PII is corneal-positive and responds quickly to a light stimulus. The PII is generated by the bipolar cells. The PI component is also corneal-positive, but responds much slower than the PII. The PI component originates from the RPE.

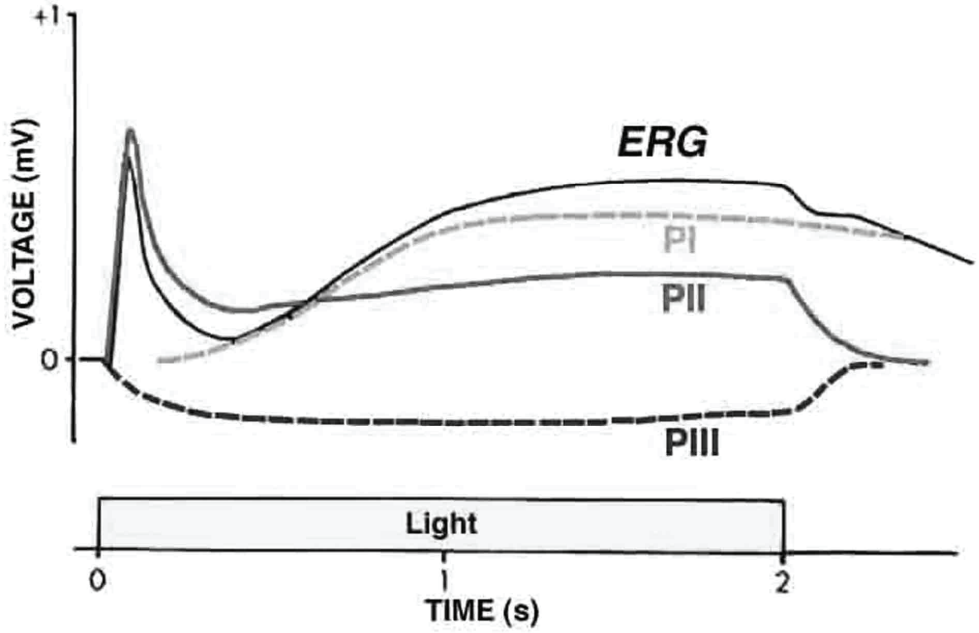

Figure adapted from [204].

Figure 1.22. Isolation of the PIII component by mathematical modeling

The circles represent data points collected from the raw ERG recording. The solid lines show the modeled PIII. The voltage where the PIII reaches its lowest point and becomes saturated is the maximum dark-adapted response of the photoreceptors (Rm_{PIII}).

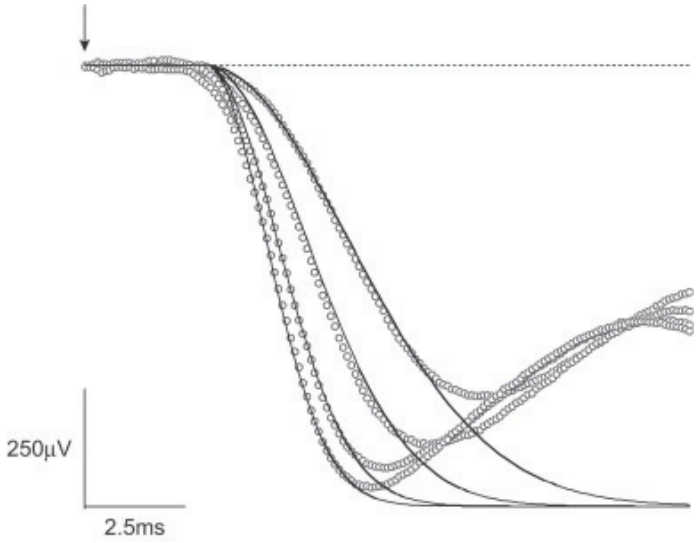

Figure is from [118].

Figure 1.23. Isolation of the PII component from the raw ERG waveform

The top figure shows the raw ERG waveform (solid) with the PIII contribution (dashed). The PII response (below) is isolated from the raw ERG waveform by subtracting the PIII response.

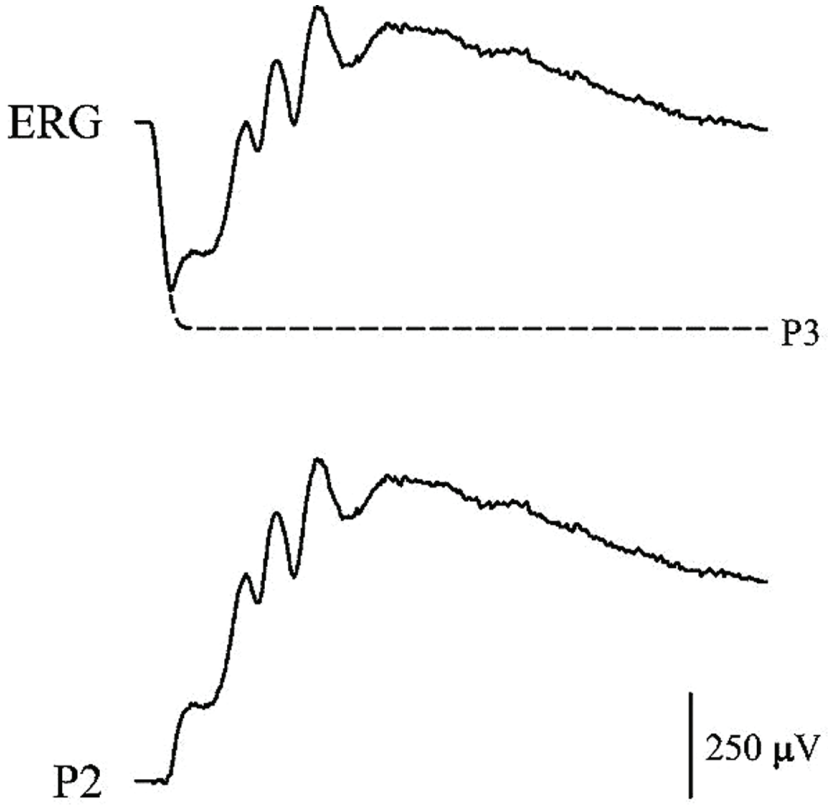

Figure is from [200].

Figure 1.24. Naka-Rushton plot

The Naka-Rushton plot is used to determine the maximum postreceptoral response. The Rm_{PII} is the maximum isolated bipolar cell response. The light intensity at one-half the maximum response is the sensitivity measure, kPII. Similarly, if the b-wave data from the raw ERG waveform is used, these measures are the Vm_{DA} (maximum dark-adapted response) and σ (sensitivity measure).

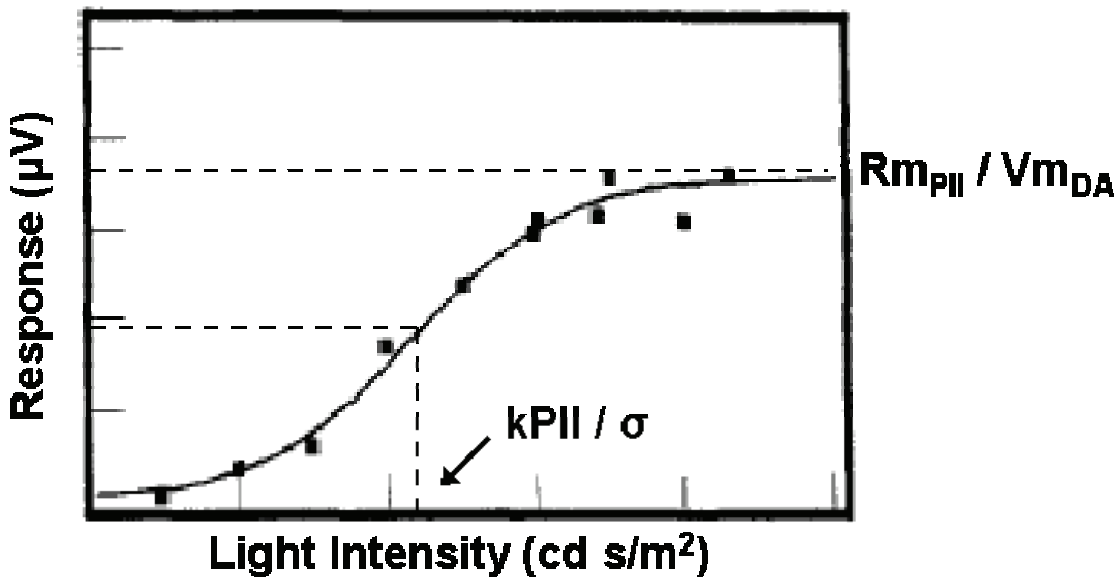

Figure is adapted from [205].

is a sensitivity measure of the bipolar cells.

The maximal dark-adapted b-wave response can also be analyzed as the Vm_{DA}. The Vm_{DA} is derived from a Naka-Rushton equation using the b-wave data measured from the raw ERG waveform in the following equation (Equation 3).

$$\text{Equation 3: } V(i)/Vm_{DA} = i/(i + \sigma)$$

In this equation, V is the voltage or response for each light intensity, *i*. The symbol σ is the light intensity at which voltage response reaches one-half the maximum and represents the sensitivity of the postreceptoral response.

- **Select mutations or KOs that produce an ERG phenotype**

There are numerous examples where the mutation or KO of a single protein significantly alters the ERG phenotype (Table 1.2). For example, KO or mutations in phototransduction proteins, rhodopsin (*Rho*) and PDE (*rd10*) result in decreased or abolished dark-adapted a-waves. Accelerated rod degeneration is also associated with both rhodopsin and PDE mutations [206, 207]. KOs of RPE65, the isomerase required for rhodopsin generation, have a phenotype similar to that of rhodopsin KOs, with increased retinal degeneration and no measurable a-wave [187, 208].

Mutations or KOs of subunits from presynaptic calcium channels ($Cacna2_{D4}$, $Cacna_{1f}$, Cgna) also exhibit an ERG phenotype. Even though these subunits are localized on photoreceptors and are incorporated into calcium channels that close in response to light, mutations demonstrate only a 20% decrease or no change in the a-wave amplitude. Interestingly, mutations in the calcium channels have a much greater effect on the b-wave phenotype; at least 75% decrease has been observed in the b-wave [198, 209-212]. These data suggest that mutations or KO of calcium channel subunits have a greater effect on visual transmission from the photoreceptors to the bipolar cells.

Changes in ERG phenotype of these presynaptic ion channel mutants not only reflect changes in ion channel function, but are also associated with changes in retinal structure. The KO of the $Cacna_{1f}$ has displaced synaptic connections between the photoreceptors and bipolar cells that could inhibit visual transmission. Mice with mutation in $Cacna2_{D4}$ exhibit accelerated rod degeneration, which also contributes to the observed ERG phenotype.

Table 1.2. Select mutations or KOs that produce an ERG phenotype

Presynaptic

Gene/Mutant Name	Protein Function	A-wave phenotype	B-wave phenotype	Other Phenotypes	Ref.
Rpe65$^{-/-}$	Regeneration of 11-*cis* retinal	No measurable a-wave	Decrease in b-wave amplitude and sensitivity	Retinal degeneration with age, loss in OS, ONL and OPL	[187, 208]
Rho$^{-/-}$, rhodopsin mutant	Rod visual pigment	Reduced DA a-wave – almost none	Decrease in DA amplitude and later (12-13wk) LA as well, DA increase in implicit time (>8wk)	Early degeneration of rods, used as a cone-only model and model of retinal degeneration	[207]
Cnga3$^{-/-}$, α-subunit of cone cyclic nucleotide-gated channel (CNG3)	Ion channel protein required for cone response to light		~75% decrease in LA b-wave amplitude; no change in DA amplitude	Cone degeneration; decreased visual acuity	[209]
Rpgr mutant – retinitis pigmentosa	Regulates GTPase RAN – localized in OS	decrease in a-wave amplitude in B/6 mice	In B/6 mice – DA – no difference LA – no diff. at 1,3,6,12 mo.; lower ampl. at 9 mo.	More severe defects in BALB/c mice but similar pattern	[213]
Gnat1$^{-/-}$, rod transducin α; aka *rd17*	Rod photoreceptor G protein	DA a-wave normal, slight reduction in LA a-wave	~65% decrease in DA b-wave amplitude; LA b-wave normal		[214]
Pde6b mutant; *rd10*	Phosphodiesterase subunit β in rods	Decrease in amplitude ~90%	Decreased in amplitude ~90%	Accelerated retinal degeneration, ERG phenotype never normal, ~90% at 2 months	[206]
Cacna2$_{D4}$, truncation frameshift mutation	Auxiliary subunit of L-type calcium channel on photoreceptors	Decrease in amplitude ~20%	Decrease in a/b wave diff. b/w a- & b-wave max; i.e., ~75% decrease in b-wave amplitude	Decrease in ONL; no change in INL; no change in number of cones	[212]
Cacna1f$^{-/-}$, *nob2*	L-type calcium channel protein on photoreceptors	Slight decrease	Almost non-existent b-wave	Displaced synaptic contacts between rod bipolar/horizontal cells and rods of ONL	[198, 210]

Table 1.2., continued

Gene/Mutant Name	Protein Function	A-wave phenotype	B-wave phenotype	Other Phenotypes	Ref.
$Cacna_{1D}$, null mutation	L-type calcium channel protein on photoreceptors	Normal	Normal	Expressed in RPE and cones	[211]
Postsynaptic					
$TRPM1^{-/-}$ - transient receptor potential member 1	Responding cation channel on bipolar cells		LA b-wave – none DA b-wave – very small	No change in Chx10, Goα, or mGluR6, no oscillatory potentials OPs	[133, 134]
$mGluR6^{-/-}$, metabotropic glutamate receptor, aka *Grm6*^{tm1Nak}	Glutamate receptor on bipolar cells		Almost no DA or LA b-wave present	No change in number of rod bipolar cells by PKCα labeling; still able to respond to visual cues, OFF bipolar response intact	[215]
Grm6, *nob3* mutation	Glutamate receptor on bipolar cells		Almost no DA or LA b-wave present	Normal morphology	[216]
Grm6, *nob4* mutation	Glutamate receptor on bipolar cells		Almost no DA or LA b-wave present		[216]
Synaptic Vesicle					
$SV2B^{-/-}$, synaptic vesicle protein 2B	Synaptic vesicle membrane protein	Normal	~30% decrease in b-wave amplitude	Decrease in other synaptic vesicle proteins	[217]
Structural Protein					
$RS1^{-/-}$, retinoschisin	Purported to be an adhesive protein to maintain retinal structural and fxnal integrity		50-85% decrease in b-wave amplitude	Decrease in b/a wave ratio; causes splitting of retinal layers; decrease in GCL, INL and ONL	[218]

Table 1.2., continued

Drystroglycan mutant – cre lox on GFAP and nestin (neuroepith.) promoters	Structural protein	Normal	Decrease in b-wave amplitude	No change in sensitivity (σ); no change in c-wave (RPE)	[219]
$Nyx^{-/-}$ aka *nob* Nyctalopin		Normal	Almost no b-wave	BALB/cByJ background; no significant difference in retinal layer thickness	[220]
BsnΔEx4/5 Bassoon	Ribbon synapse scaffolding protein	No change	Decrease in amplitude, increase in implicit time	Normal retinal anatomy Fewer ribbon synapses	[199]

Other

$CaBP4^{-/-}$ – calcium binding protein 4	Regulator of Ca^{2+} influx and glutamate release in photoreceptors	~50% decrease in a-wave amplitude	~80% reduction in DA b-wave amplitude ~45% reduction in LA b-wave amplitude	Modulates $Ca_v1.4$ L-type voltage-dependent calcium channel	[221]
$SOD1^{-/-}$ CuZn superoxide dismutase	CuZn SOD – antioxidant	Decrease	Decrease by ~40% both DA and LA	Decreased photopic flicker ERG amplitude; decreased ONL density, progressive with age; disorganized ONL, INL at 15 mo.	[222]
$Cpe^{-/-}$, Carboxypeptidase E	Cleaves neuropeptides producing active forms of neuropeptides	Normal	Decreased, both LA and DA, more prevalent with age	Normal retinal morphology, normal bipolar cell morphology	[223]
$Cpe^{fat/fat}$	Cpe is enzymatically inactive but sorting receptor function is intact	Normal	DA b-wave decreased ~50%	Normal bipolar cell morphology, decreased synaptic spherule vesicle size.	[223]

Mutations of proteins on the postsynaptic bipolar cells also have significant effects on the b-wave. The bipolar cell response is reflected in the ERG as the positive b-wave. Therefore, mutations or KOs of proteins that detect the signal from the photoreceptors and the ion channel that responds have a significant, no b-wave (*nob*) phenotype. Mutations in mGluR6 (*nob3, nob4*) and KO of this protein (*nob4*) have a *nob* phenotype [215, 216]. The knock-out of the recently discovered ON bipolar cell cation channel, TRPM1, also displays a *nob*-like phenotype and does not produce a measurable ERG b-wave[134].

Changes in retinal structure can also affect visual transmission as KOs of structural proteins bassoon, dystroglycan, and retinoschisin result in a decreased b-wave of the ERG [199, 218, 219]. This phenotype is likely caused by changes in retinal structure that interfere with the ability to transmit the visual signal efficiently between cell types. Ultrastructural changes in ion channels and/or synaptic spherules have been observed in bassoon and dystroglycan mutants [199, 219].

In summary, a wide variety of changes in the retinal proteome result in an ERG phenotype. As shown in Chapter 5, immunoproteasome KO mice exhibit a decreased b-wave (bipolar cell response). While no direct role in retinal function has been described for immunoproteasome, the proteasome is known to regulate the content of many different proteins required for normal retinal function (e.g., PSD95, mGluR, synaptophysin (see Figure 1.13)) [224, 225]. Therefore, immunoproteasome may be involved in specifically maintaining the protein homeostasis of a subset of synaptic proteins. For example, transcription factors required to express genes essential for proper retinal function could be controlled by the immunoproteasome.

Similarly, immunoproteasome could also be involved in maintaining a normal redox state in the retina. As described previously, immunoproteasome is implicated in protecting from oxidative stress (see Section 1.2.3). KOs of the antioxidant, CuZn superoxide dismutase (SOD1), also exhibit an ERG phenotype. However, $SOD1^{-/-}$ mice have an age-onset (at ~9 months) decrease in the a- and b-waves, whereas immunoproteasome KOs display a decreased b-wave at 2 months.

Previous studies have also suggested possible roles for immunoproteasome in signaling. Immunoproteasome could produce neuropeptides that are important in intercellular signaling in the retina [31, 99]. KO mice of carboxypeptidase E, a protease that cleaves neuropeptides, shows a similar decrease in the ERG b-wave as immunoproteasome KO mice (Chapter 5) [7, 223].

1.6. Thesis goals

The goal of my research was to test the hypothesis that immunoproteasome has alternative roles apart from its role in the immune system. The retina is an immune-privileged tissue and therefore immunoproteasome is unlikely to function in antigen presentation. Hence, the presence of immunoproteasome in the retina provided an excellent model system to determine new roles of the immunoproteasome that are not involved in the immune response.

Chapters 2 and 3 evaluated immunoproteasome's response to stress in immune-privileged, wild-type retina and brain. Immunoproteasome was shown to be upregulated with disease (age-related macular degeneration) in human tissue as determined by Western immunoblot (Chapter 2). Immunoproteasome's response to stress and injury was also evaluated in a mouse model. Even in the absence of injury, immunoproteasome's basal expression was 2-fold higher in the retina relative to the brain, which correlated with the elevated amount of stress experienced in the retina on a daily basis [87]. Localization of immunoproteasome expression to non-antigen presenting cells of both the brain and the retina further suggests immunoproteasome has a function outside of the immune system. Targeted CTL-injury (see Section 1.5.1) was used to cause damage specifically to the photoreceptors and astrocytes in the retina and brain, respectively (Chapter 3). Our data showed immunoproteasome is upregulated with injury in both neurons and glia.

After showing immunoproteasome is upregulated with stress, the next step was to ascertain the consequences of immunoproteasome deficiency in responding to stress. In Chapter 4, both the chronic stress of aging and acute oxidative stress were used as experimental conditions. These experiments utilized immunoproteasome KO mice devoid of either LMP7 or both LMP7 and MECL-1. Immunoproteasome content and proteasome activity was determined in immunoproteasome KO and WT mouse retina at five different ages from 2 to 24 months (Chapter 4). Retinal morphometry was also evaluated at these ages (Chapter 5). L7M1 mice showed elevated levels of apoptosis in the photoreceptors that increased with age, suggesting immunoproteasome-deficiency increased the retina's sensitivity to stress associated with aging.

Finally, to test the hypothesis that immunoproteasome is required for protecting against oxidative stress, we evaluated the level of cell death and immunoproteasome's response to acute oxidative stress in cultured RPE cells from WT and immunoproteasome-deficient (L7M1) mice (Chapter 4). Results showed that L7M1 RPE were more sensitive to oxidant-induced death, supporting the idea that immunoproteasome is a key element in a cell's protective mechanism to oxidative stress.

This thesis also evaluated whether immunoproteasome deficiency had an effect on retinal function (Chapter 5). Previous data (Chapter 3) showed that immunoproteasome was localized to the synaptic layers of the retina (OPL and IPL). The synaptic junctions between the photoreceptors and bipolar cells are critical for normal visual transmission [198, 199]. Therefore, protein changes in this layer (i.e., immunoproteasome) could have a significant effect on how the retina responds to light. To test the hypothesis that immunoproteasome has a role in maintaining normal retinal function, electroretinography was used (see Section 1.5.3). Results showed a decreased b-wave (bipolar cell) response to light. Further experiments were then done to elucidate the mechanism for the change in the ERG phenotype in immunoproteasome KO mice. Comparisons of retinal morphology (photoreceptor and bipolar cell populations) and Western blot analysis of key proteins in visual transmission showed no significant differences. So while the mechanism remains unclear, the data are consistent with a role for immunoproteasome in visual transmission.

The results from this thesis show that immunoproteasome is present in the immune-privileged brain and retina and is upregulated with injury and disease. Immunoproteasome-deficient RPE cells are more susceptible to oxidant-induced death as compared to WT. Taken together, these data provide compelling evidence that immunoproteasome has a role in retinal stress response. Furthermore, immunoproteasome-deficient mice were shown to have a decreased b-wave response to light as measured by ERG. Altogether, data from this thesis strongly supports the hypothesis that immunoproteasome has additional roles in the retina that do not involve immune function.

Chapter 2

Transformation of the Proteasome with Age-related Macular Degeneration

This chapter is essentially unmodified from the published journal article: Ethen, C.M., Hussong, S.A., Reilly, C., Feng, X., Olsen, T.W., Ferrington, D.A. Transformation of the proteasome with age-related macular degeneration. FEBS Letters, 2007. 581(5): 885-890.

Stacy Hussong was responsible for collecting data for Figure 2.3 for this manuscript. Cheryl Ethen was involved in the experimental design, data collection, analysis of Figures 2.1, 2.2, 2.4 as well as data analysis of Figure 2.3 and manuscript writing with writing assistance from Deborah Ferrington. Timothy Olsen and Xiao Feng contributed through the collection and categorization of donor tissue used in this study. Cavan Reilly provided advice about statistical analysis of the data.

The proteasome mediates pathways associated with oxidative stress and inflammation, two pathogenic events correlated with age-related macular degeneration (AMD). In human donor eyes corresponding to four stages of AMD, we found the proteasomal chymotrypsin-like activity increased in neurosensory retina with disease progression. Increased activity correlated with a dramatic increase in the inducible subunits of the immunoproteasome that was not due to an increase in CD45 positive immune cells in the retina. The novel observation of proteasome transformation may reflect retinal response to local inflammation or oxidative stress with AMD.

2.1. Introduction

The proteasome is a key intracellular protease that regulates pathways that are critical for cell survival. Different oligomeric forms of the proteasome exist, defined by both the composition of the catalytic subunits in the 20S core and associated regulatory complexes [13]. The 20S catalytic core is composed of four seven-member rings; constitutively expressed α-subunits form the outer rings and β-subunits form the inner rings. The β-subunits contain three pairs of active sites (β1, β2, β5) that perform distinct proteolytic activities [18]. The active sites have been identified as caspase-like, trypsin-like, and chymotrypsin-like for cleavage after acidic, basic, and hydrophobic amino acids, respectively.

Following exposure to cytokines, such as interferon γ (IFNγ), the constitutive catalytic subunits, β1, β2, and β5 can be replaced in nascent proteasomes by the inducible subunits β1i, β2i, and β5i [226]. The exchange of catalytic subunits to the inducible subunits forms the catalytic core of the immunoproteasome. Association of the 20S core containing inducible subunits with the proteasome activator PA28 forms the immunoproteasome, a specialized form of the proteasome known to generate immunogenic peptides [227].

Age-related macular degeneration (AMD) is the leading cause of vision loss and blindness in individuals over the age of 65 [228, 229]. Considerable evidence implicates retinal oxidative stress [230] and inflammation [231] as critical pathogenic events with AMD, both of which are partially mediated by the proteasome [46, 232]. We have previously utilized the Minnesota Grading System (MGS) for eyebank eyes [233] to track molecular changes in the neurosensory retina proteome over the course of the disease [234, 235]. We found altered expression of proteins linked to the proteasome [235], thus prompting a more in-depth analysis to investigate how this essential protein changes with the disease.

2.2. Materials and Methods

2.2.1. Materials

Peptide substrates were purchased from Sigma, Calbiochem, and BioMol. Proteasome inhibitors were from Peptides International. Antibodies and their respective companies are as follows: proteasomal subunits and activators (Affinity Bioreagents and Affiniti), HSP90 (Santa Cruz), CD45 and jurkat cell lysate (Epitomics), goat anti-rabbit or -mouse, donkey anti-goat or -rabbit alkaline phosphatase and HRP conjugated secondary antibodies (BioRad and Pierce).

2.2.2. Grading donor eyes

Eyes obtained from the Minnesota Lions Eye Bank were acquired with consent of the donor or donor family to be used for medical research in accordance with the principals outlined in the Declaration of Helsinki. Criteria established by the MGS [233] were used to determine the stage of AMD according to established guidelines. MGS4 is subdivided into individuals with (exudative AMD) or without (atrophic AMD) neovascularization. All MGS4 donors used in this study had exudative AMD. Eyes from Caucasian donors were screened for and excluded if other retinal diseases were observed.

2.2.3. Preparation of retinal homogenates

Dissection of the sensory retina was performed as reported previously [234]. The macula was harvested using a 6mm trephine punch. The periphery includes retina outside this 6mm macular region.

2.2.4. Rat retinal protein stability

Five-month-old Fischer 344 rats were purchased from the Veterinary Medical Unit at the Minneapolis Veterans Affairs Medical Center's aging rodent colony, which is maintained by the University of Minnesota. An animal protocol was approved by the Institutional Animal Care and Use Committee of the University of Minnesota. In these experiments, the post-mortem conditions of human donor eyes were replicated using rat eyes. In brief, one eye from each rat was immediately enucleated and served as a control for the paired eyes that were dissected two to twenty-four hours post-mortem. Bodies were maintained at room temperature for 2.5 hours then refrigerated until enucleation at 4.5 hours post-mortem. After enucleation, eyes were stored in a moist chamber at 4°C

until retinal dissection was performed. Retinas were dissected and frozen at –80˚ C and were later processed as outlined above for human retinas [234].

2.2.5. Measurement of proteasome activity

The fluorogenic peptides LLE-AMC (200 μM), LLVY-AMC (75 μM), and VGR-AMC (150 μM) were used as model substrates to test the caspase-like, chymotrypsin-like, and trypsin-like activities of the proteasome, respectively [157]. Retinal homogenates (3 μg) were pre-incubated in the absence or presence of proteasome inhibitor MG132 (200 μM), or lactacystin (50 μM) in reaction buffer prior to the addition of substrate. Proteasome activity was measured as described previously [79]. All samples were assayed in triplicate.

2.2.6. Western immunoblotting of 1D gels

Following 6% or 13% SDS-PAGE, retinal proteins were transferred to PVDF membranes as described [235]. For each antibody, 35 μg of protein was resolved, which was within the linear range of response. PVDF membranes were probed with the monoclonal antibodies (HSP90 and α7) or polyclonal antibodies that recognize proteasomal subunits (C2, β5, β5*i*, β1, and β1*i*) or regulators (PA28α, PA200, PA700-S4). The monoclonal antibody, CD45, was used to test for evidence of infiltration of immune cells. Jurkat cell lysates were used as a positive control. Appropriate secondaries were used in conjunction with BCIP-NBT or chemiluminescence to visualize the immunoreaction. Membranes were imaged with a GS800 Densitometer or ChemiDoc (BioRad), followed by quantification with Quantity One (BioRad). All 1D densities were normalized to a standard used on all blots [234].

2.2.7. Proteasome content

The immune reactions of the α7 subunit for 20S proteasome purified from rat liver [47] and human retinal homogenates were compared to determine the relative amount of proteasome in retinal homogenates.

2.2.8. Statistical analysis

Data are reported as mean ± standard error of the mean (SEM). The SEM for ratios β5i/β5, β1i/β1, and β5i/CD45 were corrected for the propagation of errors. The relationship between MGS stage and either activity or immunoblot density were

compared using linear regression. Outliers were removed if they were > 2.5 standard deviations (SD) from the mean. All statistical tests were two-sided with $\alpha = 0.05$.

2.3. Results

2.3.1. Experimental design

The MGS [233] was used to classify donor eyes into four progressive stages (MGS1-4) of AMD. MGS1 serves as the control group. MGS2 represents early stage AMD, MGS3 is an intermediate stage, and MGS4 is considered end stage (late) AMD. The macula and periphery of the neurosensory retina from human donor eyes were analyzed separately to determine if the preferential deterioration of the macula observed clinically is manifested at the molecular level.

2.3.2. Proteasome stability post-mortem

Demographic and clinical information for donor eyes obtained from the Minnesota Lions Eye Bank is similar to those published previously [234, 235]. Post-mortem conditions prior to tissue preparation did not differ between the four MGS groups, including the time from death to tissue freezing (average ± SD= 16.6 ± 4.0). Due to the broad range in tissue freezing times among donors in our study (range= 7.5-22.0 hrs), we tested proteasome activity and content in rats that replicated the average handling conditions for donor eyes (see section 2.2.4). Using fluorogenic peptides, we found proteasome chymotrypsin-like, trypsin-like, and caspase-like activity decreased with time to freezing up to eight hours (Figure 2.1). Activity remained stable from eight to twenty-four hours post-mortem, which corresponds to the time range for donor eyes. Furthermore, the content of α7 remained constant during this time, implying there was no appreciable degradation of 20S (data not shown). Based on these results, differences in freezing times for donor eyes should not influence our experimental results.

2.3.3. Increased retinal proteasome activity with AMD

Using fluorogenic peptide substrates, activity of the three catalytic sites of the proteasome was measured in human retinal homogenates from both the macula and periphery at four stages of AMD. The chymotrypsin-like activity was significantly increased with disease progression in both the macula ($p=0.038$) and the periphery

(p=0.031), while the trypsin-like and caspase-like activities remained unchanged (Figure 2.2). Since it is primarily the chymotryptic-like activity that determines the rate of protein breakdown [236], the increased activity likely results in an increased rate of protein degradation as AMD progresses.

2.3.4. Proteasome content remains constant

One possible explanation for the increased activity is that proteasome content is upregulated. Content was estimated from the levels of the α7 subunit, which is a constitutive component of the 20S catalytic core and therefore a good estimate of the total content [79]. Densitometric analysis following immunoblotting showed no change in total content of proteasome with progression of the disease (Figure 2.3A) in either the macula (p=0.65) or periphery (p=0.33). These results were confirmed using another α-subunit, α6 (data not shown). Comparing the immune reactions of the α7 subunit in a standard of 20S proteasome purified from liver with the retinal homogenates, we estimated the content of proteasome to be 2.02 ± 0.08 μg/mg protein (mean ± SEM, n=40). Thus, the uniform content through disease progression suggests that the increase in activity is due to an increase in proteasome specific activity.

2.3.5. Increased cytokine-induced catalytic subunits with AMD

It has been previously shown that the inducible β-subunits of the 20S core can alter the proteolytic activity of the proteasome [52, 237]. Therefore, we examined the levels of both the constitutive β1 and β5 subunits along with their inducible counterparts, β1i and β5i, to determine whether a change in subunit composition could explain the increased specific activity with disease progression. Because the total level of proteasome is not altered with disease, we expect that if inducible subunits increased, there would be a corresponding decrease in constitutive subunits. We found that the exchange of constitutive β-subunits for their inducible counterparts occurs between MGS1 and MGS4 (Figure 2.3B, C) in both the macula and periphery. These results are consistent with higher expression of the immunoproteasome with AMD progression.

To address the possibility that the observed increase of inducible subunits is due to infiltrating immune cells containing high levels of immunoproteasome, we assayed the level of CD45 in retinal tissue. CD45 is expressed in all bone-marrow derived immune

cells including resident microglia and infiltrating immune cells in the retina. If there was significant infiltration of immune cells into the retinal tissue, we should see a concomitant increase in levels of CD45 and immunoproteasome subunits. In samples from the macula and periphery, we observed that although there was no increase in CD45 (Figure 2.4A), there was a dramatic increase in content of immunoproteasome subunit β5i (Figure 2.4B). To account for the level of CD45 in each donor, we calculated the ratio of β5i and CD45 immune density (Figure 2.4C). These results closely replicate the graph of β5i content alone. Although we cannot definitively say whether immune cells have entered the neurosensory retina, given the limitations of the sensitivity of this assay, we feel confident that the increased content of immunoproteasome subunits at late stage AMD is not simply due to the contribution from infiltrating immune cells but rather reflects changes in retinal proteasome composition.

2.3.6. Proteasome regulatory proteins

Additional mechanisms for increased proteasome specific activity includes the association of the 20S core with regulatory complexes such as PA28 and PA700 [238]. Using antibodies that recognize the α-subunit of PA28 and the S4 subunit of PA700, we measured the relative concentration of these proteasome activators (Figure 2.5). No change in PA700 S4 was observed in the macula ($p=0.54$) or periphery ($p=0.83$). PA28α content was uniform in the periphery ($p=0.42$), but was increased ($p=0.07$) by MGS4 in the macula. Thus, in the macula, increased PA28α content is consistent with higher content of immunoproteasome subunits [52].

Two additional auxiliary proteins, PA200 and HSP90, have been shown to regulate proteasome activity. PA200 is a proteasomal activator whose biological roles are currently poorly understood [238]. PA200 content was significantly decreased in the macula ($p=0.0001$) and demonstrated a strong trend in the periphery ($p=0.058$). HSP90 has been shown to have the dual function of inhibiting the constitutive proteasome and activating the immunoproteasome [238]. Although HSP90 was highly variable between donors, no significant correlation with disease stage in either the macula ($p=0.95$) or periphery ($p=0.89$) was detected.

2.4. Discussion

Most aging studies focused on the proteasome report an age-related decline in activity, which has been suggested as an explanation for accumulation of oxidized proteins in aged tissue [239]. In the current study, MGS4 donors were statistically older ($p=0.01$) (86 ± 13 yrs, mean ± SD, n=10) than donors in MGS1-3 (71 ± 6 yrs, mean ± SD, n=30). Since the increase in chymotrypsin-like activity by MGS4 is contrary to the expected age-related decrease in activity, we concluded the increased activity reflects alterations due to the disease.

Inflammation has been proposed to play an important role in AMD pathology based upon proteomic [240] and immunohistochemical [231] evidence that detected complement proteins in drusen and by the identification of a risk-conferring complement factor H polymorphism [241-244]. The complement system is a key element of the innate immune response. Local inflammation leads to the production of cytokines [245] that can upregulate both immunoproteasome subunits and the proteasome activator PA28 [226]. Therefore, the dramatic upregulation of immunoproteasome subunits β1i and β5i observed in both the macular and peripheral neurosensory retina, as well as increased PA28 in the macular region, supports the presence of local inflammation at end stage of AMD. However, the uncoordinated regulation of PA28 and inducible subunit expression suggests other mechanisms may be involved.

The expression of inducible subunits in disease-free MGS1 immune-priviledged retina implies that the immunoproteasome may participate in non-immune functions. This idea is further supported by the presence of non-cytokine response elements in the promoter region in the mouse β5i gene [34]. An emerging hypothesis is that immunoproteasome plays a protective role during oxidative stress [90, 92]. Data in support of this hypothesis includes upregulation of inducible subunits by nitric oxide [91] and an increase in oxidized proteins with a β1i knockout model [92]. A major finding with AMD is the accumulation of oxidized proteins in retinal tissue [230]. Therefore, increased immunoproteasome may reflect a compensatory, albeit insufficient, response to the oxidative stress since oxidized proteins accumulate with the disease.

The prominent increase of immunoproteasome at end stage does not explain the gradual disease-related increase in chymotryptic activity. This prompted further investigation of cellular regulators of proteasome function. Levels of proteasome activators measured in this study revealed increased PA28 and decreased PA200, although the physiological significance of the latter remains uncertain [238]. Several inhibitors that we did not investigate may also play a role in regulating proteasome activity. Some of the recently discovered inhibitors PI31, Tat, HBx, and PR39 compete with PA28 for the same binding sites on α-subunits of the 20S core [238]. PR39 is reported to stimulate angiogenesis and suppress inflammation by inhibiting proteasome mediated degradation of HIF1α [238, 245] and will be of interest for future studies.

Regulation of the proteasome is of profound importance for cellular function. We interpret the presence of immunoproteasome at later stages of AMD as an indicator of local inflammation or increased oxidative stress in the neurosensory retina. Further studies are required to understand the underlying mechanisms behind immunoproteasome upregulation and the functional consequences of proteasome transformation in AMD pathology.

Figure 2.1. Post-mortem proteasome activity.

One eye from each F344 rat was immediately enucleated and served as a control for the paired eye; paired eyes replicated eye bank conditions. Retinal homogenates were assayed for proteasome activity by measuring the hydrolysis of fluorogenic peptides LLE-AMC (circles & solid line), VGR-AMC (triangles & dashed line), and LLVY-AMC (squares & uneven dashed line). The bracket represents the time range for human donor eyes in this study. Data are activity relative to the control eye. Values are the mean ± SEM. n= 2-3 rats per time point.

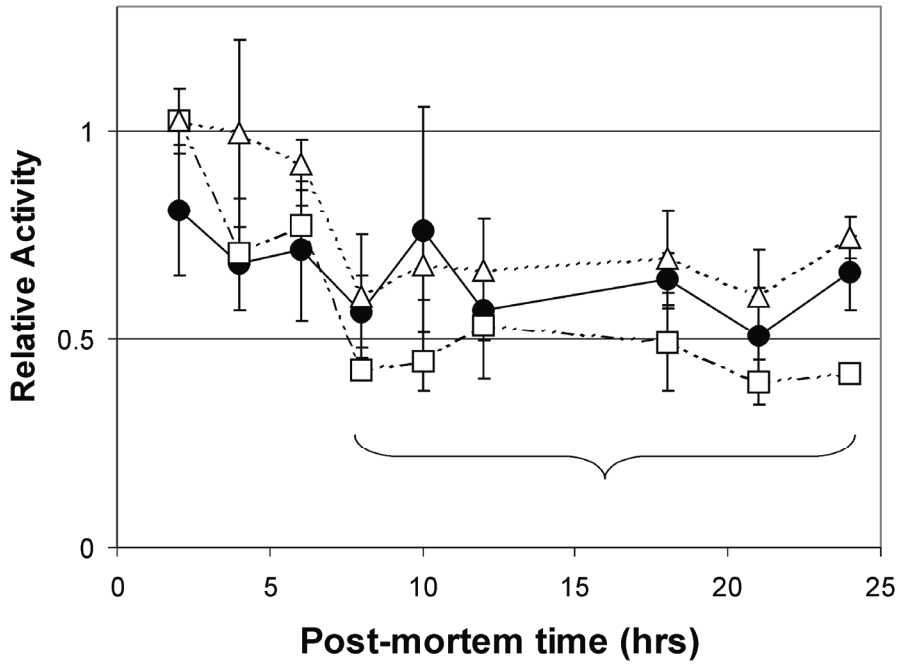

Figure 2.2. Proteasome activity in donor retinas with AMD.

Hydrolysis of fluorogenic peptides measuring the caspase-like (LLE), trypsin-like (VGR), and chymotrypsin-like (LLVY) activities, were determined in the macula (A) and periphery (B) from donors at MGS1 (grey), MGS2 (diagonal), MGS3 (vertical), MGS4 (black). *P = 0.038, ^P = 0.031, n = 6-9 for each group tested in both the macula and periphery.

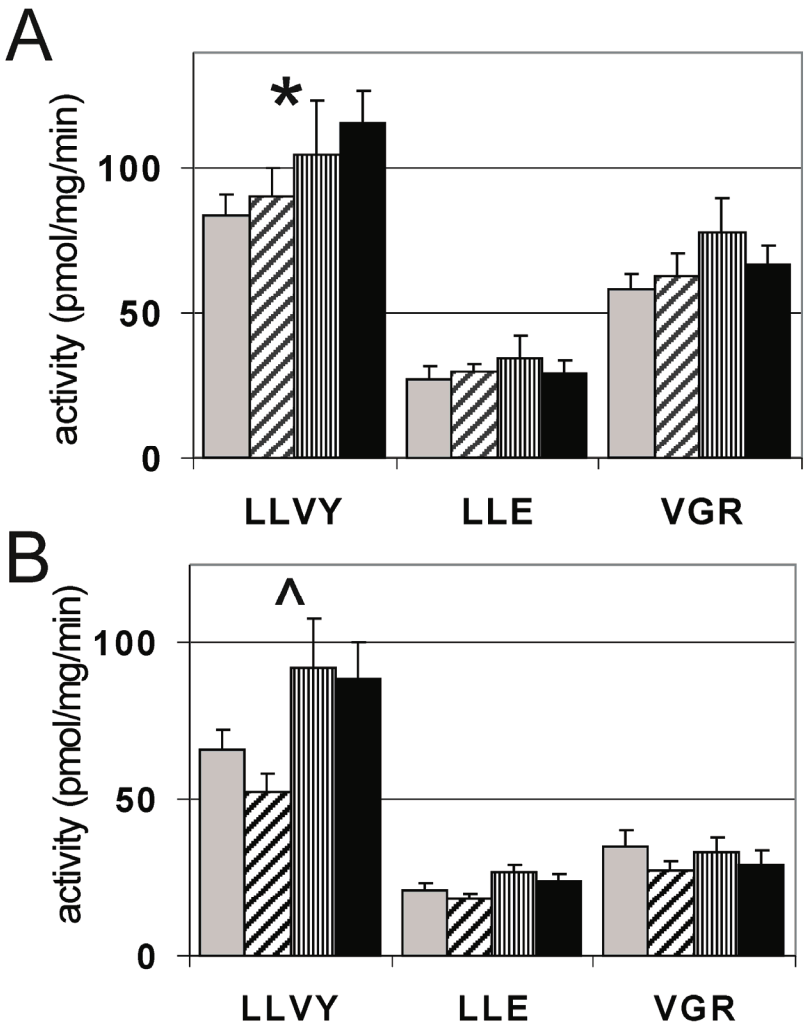

Figure 2.3. Content of 20S proteasomal subunits in AMD retinal tissue.
Relative content of proteasome subunit α7 and representative immunoblot (A) in the macula (M) and periphery (P). Exchange of constitutive subunits β1 and β5 for inducible subunits β1i and β5i in the macula (B) and periphery (C) at MGS1 (grey), MGS2 (diagonal), MGS3 (vertical), MGS4 (black). Corresponding representative immunoblots from donors at MGS1-4 are shown to the left. *P = 0.001, ^P = 0.007, $^{+}$P = 0.047, ^{O}P = 0.037, n = 6-10 for each group tested in both the macula and periphery.

Figure 2.3. Content of 20S proteasomal subunits in AMD retinal tissue.

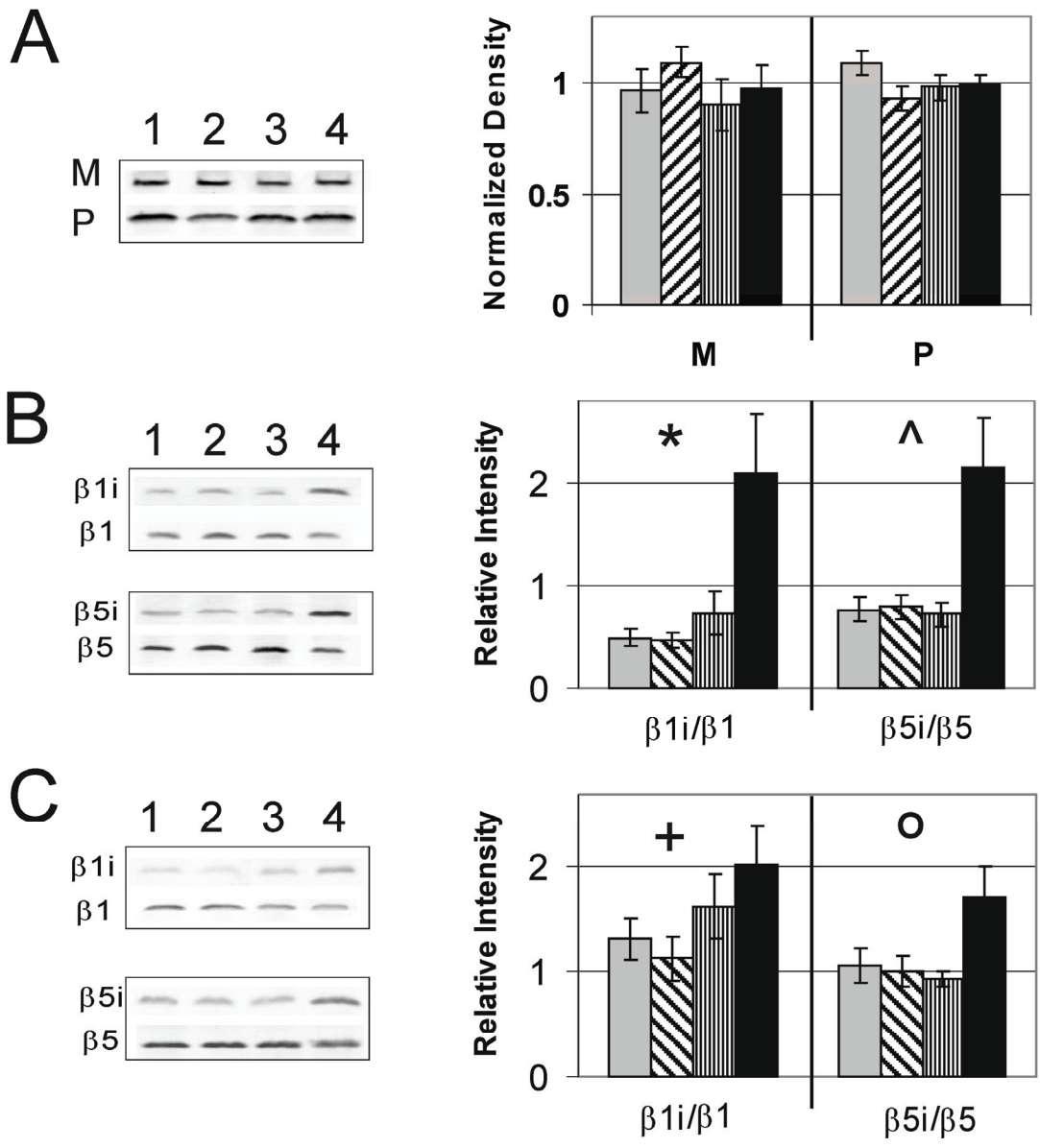

Figure 2.4. CD45 and immunoproteasome subunit levels.

(A) Relative content of CD45, present in bone-marrow derived immune cells, was measured at progressive levels of MGS from the macular (M, white wavy bars) and peripheral (P, gray bars) regions of the retina. The inset shows representative immunoblots. (B) Relative content of β5i from donor tissue used in (A). The inset shows representative immunoblots. (C) β5i levels normalized to the content of CD45 were calculated as the ratio of the densities (β5i/CD45) for each donor. n=2-4 for each group tested in both the macula and periphery.

Figure 2.4. CD45 and immunoproteasome subunit levels.

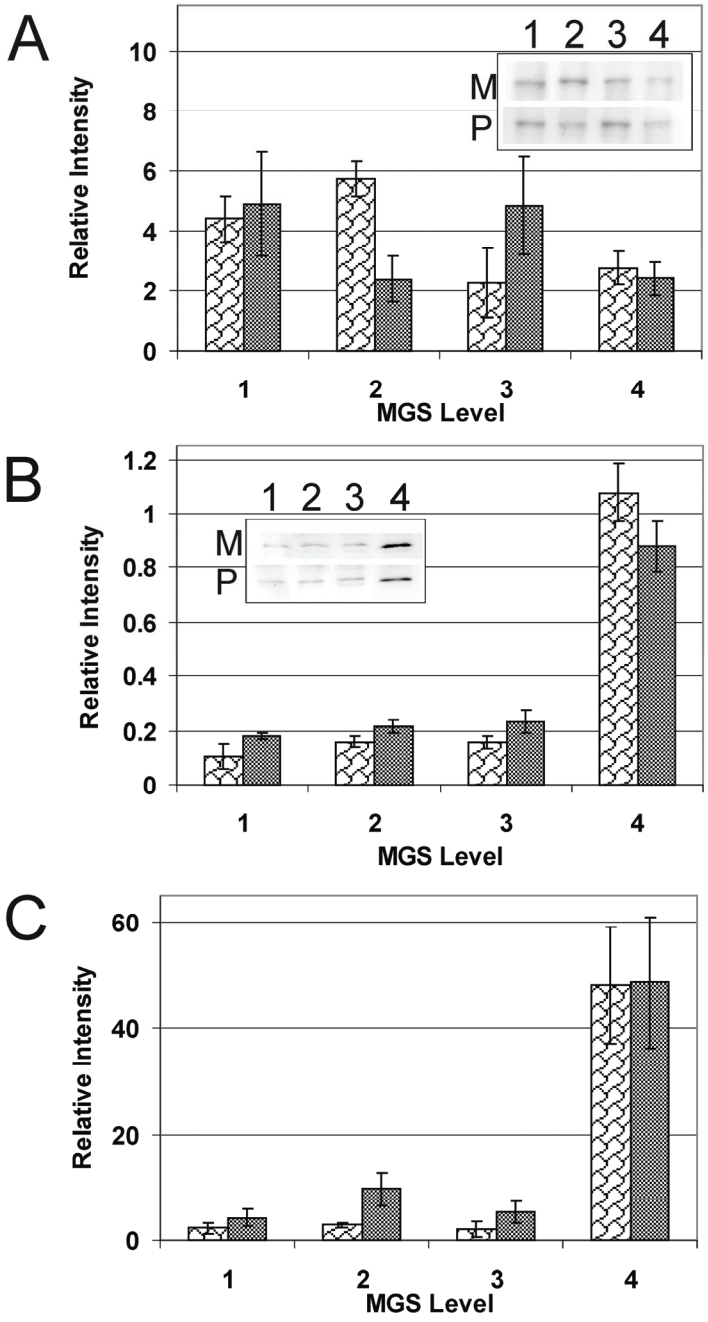

Figure 2.5. Content of proteasomal regulatory proteins.

Relative content of regulatory complexes PA28, PA700, PA200 and HSP90 were measured in the macula (A) and periphery (B) from donors at MGS1 (grey), MGS2 (diagonal), MGS3 (vertical), MGS4 (black). *P = 0.0001, ^P = 0.071, $^{+}$P = 0.058, n = 6-10 for each group tested in both the macula and periphery.

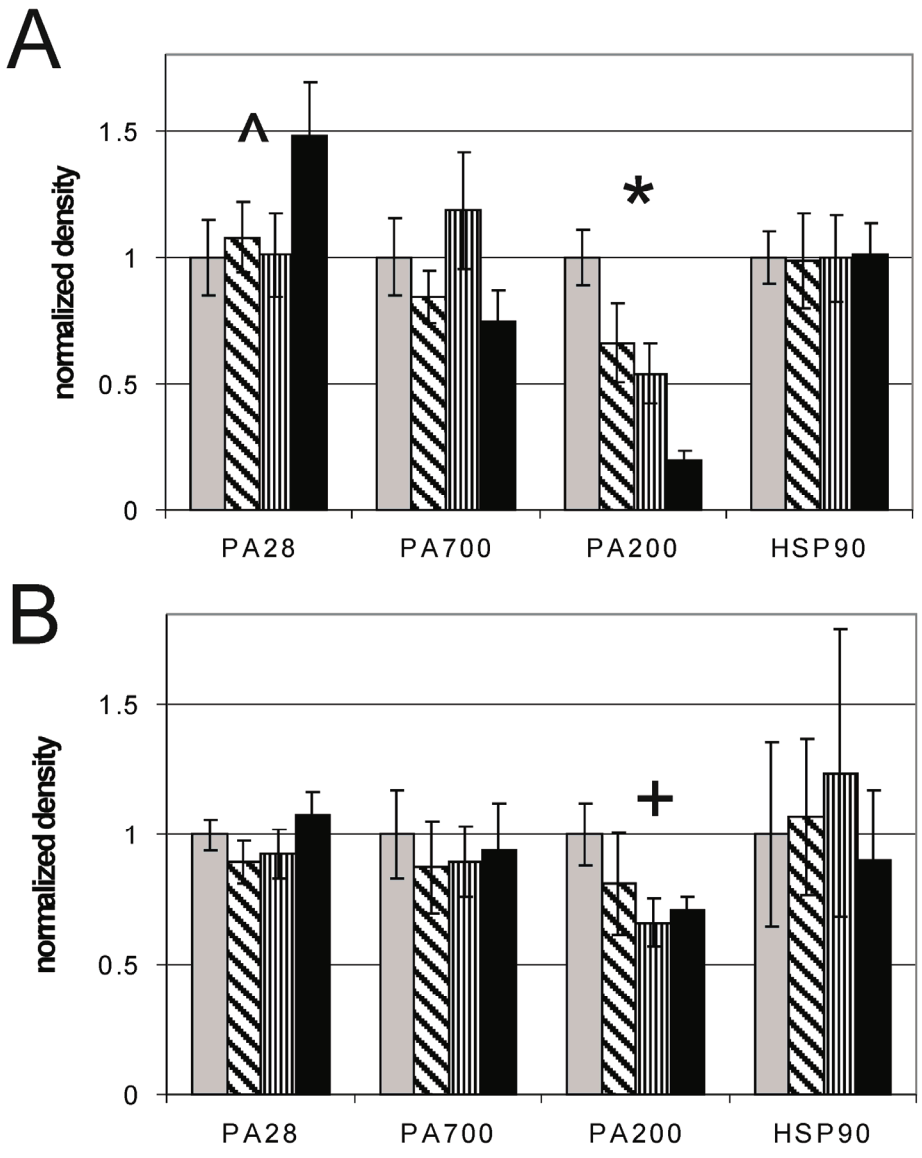

Chapter 3

Immunoproteasome Responds to Injury in the Retina and Brain

This chapter is essentially unmodified from the published journal article: Ferrington, D.A., Hussong, S.A., Roehrich, H., Kapphahn, R.J., Kavanaugh, S.M., Heuss, N.D., Gregerson, D.S. Immunoproteasome responds to injury in the retina and brain. Journal of Neurochemistry, 2008. 106(1): 158-169.

Stacy Hussong was responsible for data collection for Figure 3.3 (c,d) and Figure 3.4. Heidi Roehrich performed all of the tissue sectioning, staining, and imaging for the immunohistochemistry and immunofluorescence experiments. Rebecca Kapphahn was involved in proteasome activity measurements in Figure 3.4. Shannon Kavanaugh collected the data for Figure 3.1. Neal Heuss conducted all animal experiments and tissue collection. The data analysis and manuscript writing was completed by Deborah Ferrington with writing assistance from Dale Gregerson.

It is well known that immunoproteasome generates peptides for MHC Class I occupancy and recognition by cytotoxic T lymphocytes (CTL). The present study focused on evidence for alternative roles for immunoproteasome. Retina and brain were analyzed for expression of immunoproteasome subunits using immunohistochemistry and Western blotting under normal conditions and after injury/stress induced by CTL attack on glia (brain) or neurons (retina). Normal retina expressed substantial levels of immunoproteasome in glia, neurons, and retinal pigment epithelium. The basal level of immunoproteasome in retina was 2-fold higher than in brain; CTL-induced retinal injury further upregulated immunoproteasome expression. Immunoproteasome upregulation was also observed in injured brain and corresponded with expression in Purkinje cells, microglia, astrocytes, and oligodendrocytes. These results suggest that the normal environment of the retina is sufficiently challenging to require on-going expression of immunoproteasome. Further, immunoproteasome upregulation with retinal and brain injury implies a role in neuronal protection and/or repair of damage.

3.1. Introduction

The proteasome is an intracellular protease complex that regulates processes essential for cell survival, including cell cycle regulation, control of signal transduction and gene expression, and protein quality control [13]. The 20S proteasome makes up the catalytic core of all proteasome species (i.e., 26S, immunoproteasome) that are defined by both the composition of the 20S catalytic subunits and the association of various regulatory complexes, such as PA700 and PA28. Three subtypes of 20S catalytic cores have been described. The standard proteasome core contains the catalytic subunits β1, β2, and β5 and is the major core in tissues outside the immune system. These standard subunits can be replaced in nascent proteasomes with the inducible subunits, LMP2 (β1i), MECL (β2i), and LMP7 (β5i), which form the core of the immunoproteasome. The third type of core particle, the intermediate-type 20S proteasome, contains a mixture of the standard and immunoproteasome catalytic subunits [17, 246]. Analysis of the three types of catalytic cores has shown that they differ substantially in their enzymatic characteristics and cleavage of model substrates [17, 246]. Furthermore, while most cells contain a heterogeneous population of 20S cores, the relative ratio of different subtypes is cell specific [246, 247] and can be altered under different cellular conditions. For example, we have previously reported a 3-fold upregulation of the immunoproteasome subunits in aged muscle undergoing significant muscle atrophy[78, 79]. These findings support the hypotheses that the proteasome population is highly dynamic, and that each proteasome subtype may perform specialized functions that allow the cell to respond to changing conditions. Understanding how proteasome composition changes with specific environmental perturbations will provide valuable insight into the strategic functions of each proteasome subtype.

This study focused on evidence for alternative roles for the immunoproteasome in the brain and retina. While its role in generating immunogenic peptides for antigen presentation has been clearly established [248, 249], the expression of immunoproteasome in non-inflamed immune-privileged tissue such as retina [150, 250], brain [83, 85], and lens epithelial cells [82] implies other non-immune functions are possible. Notably, the upregulation of immunoproteasome in diseased retina [86] and

brain [83, 85] suggests the immunoproteasome responds to challenges that induce stress and injury. In the current study, we show that in normal retina, immunoproteasome expression is approximately two-fold higher than in normal brain. In response to injury, immunoproteasome is significantly upregulated in both retina and brain. These results suggest additional non-immune functions for the immunoproteasome that provide protection from damage and/or facilitate repair of injured tissue.

3.2. Materials and Methods

3.2.1. Animals

The two beta-galactosidase (β-gal) transgenic mice (B10.A background) have been described [193, 251, 252]. β-gal expression in the rod photoreceptor cells of hi-arr-β-gal mice is under control of the arrestin promoter [189, 190]. The GFAP-β-gal mice express β-gal in astrocytes of brain, retina, and optic nerve, under the control of the glial fibrillary acidic protein (GFAP) promoter [191]. Mice used in this study were 2-3 months old. Mice were handled in accordance with guidelines of the Institutional Animal Care and Use Committee of the University of Minnesota and the National Institutes of Health.

3.2.2. Generation, activation, and transfer of β-gal-specific CD8 T cells

CD8 T cells specific for an immunodominant, H-2L^d-restricted epitope of β-gal (TPHPARIGL) [253], were prepared from vaccinia virus VSC 56-vaccinated female B10.A mice. Use of the virus, and generation and maintenance of the T cells were done as previously described [193, 254, 255]. For I.V. inoculations (1 to 15 x 10^6 cells), the cells were resuspended in phosphate-buffered saline at 5 x 10^7 cells/ml.

3.2.3. Immunohistochemistry

Eyes and brains were removed and either immediately snap-frozen in Tragacanth (Sigma, St. Louis, MO) or tissues were fixed by perfusion with 4% paraformaldehyde and cryoprotected with 30% sucrose. Prior to antibody labeling, tissue sections (12 μm) were fixed in cold acetone for 30 min and washed in PBS. Non-specific immunoglobulin binding was blocked for 30 min with normal donkey serum. The tissue sections were stained with the primary antibody (Table 3.1) for 30 min at room temperature, then incubated with biotinylated secondary antibody for 30 min followed by incubation with

an avidin-biotin complex (Vector Laboratories, Burlingaine, CA). Antibody binding was visualized using 3', 3'–diaminobenzidine as the chromogen (DAB kit, Vector Laboratories). To confirm the specificity of the primary antibody, controls included pre-absorption with the corresponding synthetic peptide or omission of the primary antibody. Some sections were lightly counterstained with nuclear fast red (Vector Laboratories).

3.2.4. Immunofluorescence

For co-localization experiments, sections were incubated for 1 hour with blocking reagent followed by an overnight staining with the primary antibody (Table 3.1). After washing, the sections were incubated for 2 hours in the dark with the corresponding fluorescent secondary antibody (Rhodamin Red, 1:200, Jackson ImmunoResearch, West Grove, PA or Alexa Fluor 488, 1:200, Molecular Probes, Carlesbad, CA). For double labeling, sections underwent a further cycle of primary and secondary staining. After washing, the slides were cover slipped with Immuno Mount (Thermo Electron Corporation, Waltham, MA). Images were captured using the Bioquant Nova Prime V6 software (Nashville, TN).

3.2.5. Comparison of proteasome content

To compare the relative content of immunoproteasome in the retina and brain, minimal sample processing was used to capture essentially all proteasomes. To minimize day-to-day assay variability and differences between animals, tissues from individual mice were analyzed in parallel, with paired t-tests used to test statistical differences between tissues. Both retinas and the brain from each mouse were homogenized in 5x the tissue volume in DNase buffer (20mM Tris (pH 7.0), 1 mM $CaCl_2$, 5 mM $MgCl_2$, 150 units/ml DNase) using a glass homogenizer with a Teflon pestle and incubated for 20 minutes. The sample was then diluted to 25x the original tissue volume in 20 mM Tris (pH 7.0), 6 M urea, 2% sodium dodecyl sulfate (SDS) and homogenized. Protein concentrations were determined using the Bicinchoninic Acid Protein Assay (Pierce, Rockford, IL) with bovine serum albumin as the standard. Multiple lanes containing increasing amounts of protein from either the retina or brain (20-60 μg) were resolved using a 13% SDS gel, transferred to a polyvinylidene difluoride (PVDF) membrane, and probed with antibodies to α7, LMP2, LMP7, β1, and β5. Immunoblots were imaged

using a ChemiDoc (BioRad). Densitometry was performed on the immune reactions using Quantity One (BioRad) and density was plotted as a function of protein load. The relative content of individual proteasome subunits was determined by comparing the slope of the immune reactions (density/μg protein) for the retina and brain from each mouse. A paired t-test was performed comparing slopes from the retina and brain, with the level of significance set at $p \leq 0.05$.

3.2.6. Sample preparations

Retinas were processed as outlined [150, 250, 256], using an homogenization buffer containing 20 mM Tris (pH 7.4), 20% sucrose, 2 mM $MgCl_2$, 10 mM glucose, and 2% CHAPS. The supernatant containing soluble retinal proteins from the final step of processing was retained. Brains were homogenized in the retina buffer and centrifuged at 4000 g at 4°C for 20 min. Pellets were rehomogenized, centrifuged, and supernatants from the two spins were combined and centrifuged at 11,800 g for 20 min. The supernatant was then centrifuged at 100,000 g for 16 hours and the pellet was suspended in 20 mM Tris (pH 7.5), 5 mM $MgCl_2$, and 20 mM KCl. Aliquots of protein from the final processing step for retina and brain were stored at -80˚C. Protein concentration was determined using the Bicinchoninic Acid Protein Assay.

3.2.7. Western blotting

Western blotting was performed as described [150, 256]. A sample of 20S purified from liver was run along with samples on each blot. Membranes were incubated for 16 hours at 4˚C with one of the primary antibodies (Table 3.1). Appropriate secondary antibodies were used in conjunction with chemiluminescence to visualize the immune reactions.

Immunoblots were imaged using a ChemiDoc (BioRad) and quantified using Quantity One (BioRad). Samples were normalized to a reference sample run on each blot. To insure that the β-subunits were incorporated into the mature 20S complex, the migration of the β-subunits in samples were aligned with the β-subunits of 20S proteasome purified from liver that was run on each blot. The relative content of proteasome subunits or GFAP in tissue post- CTL injury is plotted relative to the control

tissue. Note that the third immunoproteasome catalytic subunit MECL is not included in our analysis because the specificity of the antibody was not adequate.

3.2.8. Proteasome activity measurements

Proteasome activity was measured using 75 μM LLVY-AMC (EMD Biosciences, San Diego, CA) as the fluorogenic peptide substrate [150].

3.2.9. Statistical analysis

Immunoproteasome content in retina and brain (Figure 3.1) was compared using a paired t-test. Other analyses for testing statistical significance between treatment groups used a Student's unpaired t-test analysis or analysis of variance (ANOVA) with a Tukey post-hoc test. Statistical software in Origin v. 7.5 was used for the analysis. The level of significance was set at $p \leq 0.05$. Data are reported as mean ± SEM for all groups.

3.3. Results

3.3.1. Immunoproteasome in the retina and brain

There are many similarities between retina and brain, especially with respect to parenchymal composition (i.e., neurons, glia, microglia) and the blood-tissue barriers. However, there are also substantial differences, including the retina's exposure to light, the shedding and degradation of spent tips of photoreceptors, and the rapid recycling of bleached photoreceptor molecules [257]. These conditions place a heavy burden of environmental stress and metabolic demands on the retina; consequently, we predicted that endogenous levels of retinal immunoproteasome would be higher than in brain. To test this hypothesis, proteasomal subunit content in the retina and brain was analyzed by Western blotting using subunit-specific antibodies. Since the α-subunits are present in the 20S catalytic core of all proteasome subtypes, the immune reaction of the α7 subunit provided a measure of the total proteasome content. Blots were also probed for two immunoproteasome (LMP2, LMP7) and standard (β1, β5) catalytic subunits.

To evaluate the content of immunoproteasome in retina and brain, minimal tissue processing (i.e., homogenization in buffers containing DNAse and detergents without centrifugation) was used so that essentially all protein in the tissue could be captured. To minimize the effect of variability between animals, subunit content was measured in

retina and brain from five individual mice and paired t-tests were performed to compare the relative tissue content of immunoproteasome (Figure 3.1). Based on densitometry of the α7 immune reaction, total proteasome content was slightly higher in the retina compared with brain (1.38 ± 0.15), but this increase did not reach statistical significance (p=0.12). When calculating the relative amount of immunoproteasome, the content of LMP2 and LMP7 was consistently higher in the retina of all five mice. Comparing retina to brain, the relative content of LMP2 and LMP7 was elevated 2.2 ± 0.4 (p=0.05) and 2.5 ± 0.5 (p=0.001) fold, respectively. The content of β1 and β5 were not different between retina and brain. These results show that there was approximately two-fold more immunoproteasome in the retina, consistent with our hypothesis that endogenous levels of retinal immunoproteasome are higher than in brain.

3.3.2. Localization of retinal immunoproteasome

To determine if immunoproteasome was localized to specific regions of the retina, immunohistochemistry was performed on retinal sections. Using antibody specific for the α5 subunit to track all proteasome subtypes, diffuse staining was observed throughout the retina (Figure 3.2A), which was expected based on proteasome's ubiquitous presence in all cells. The notably darker staining in the photoreceptor cell inner segments (IS) suggests higher total proteasome content in this region. Specificity of the reaction was shown in control experiments where the antigenic peptide of the α5 subunit was incubated with the α5 antibody prior to staining led to the loss of staining. Omission of the primary antibody further confirmed the specificity (Figure 3.2B,C). Retinal sections stained with anti-β5 antibody showed a pattern of staining identical to the α5 antibody (data not shown).

For immunoproteasome, intense staining with the LMP7 antibody was less concentrated in the IS and more heavily stained in the inner and outer plexiform layers (IPL, OPL) (Figure 3.2D). The specificity of the anti-LMP7 reaction was confirmed by the difference in intensity when the antibody was pre-incubated with 20S immunoproteasome purified from spleen, or the primary antibody was omitted (Figure 3.2E,F). Since the IS region also contains the Mueller cell end feet, we double-labeled retinal sections with antibodies to glial fibrillary acidic protein (GFAP) to stain the

Mueller cells, or arrestin to stain photoreceptors, to further define the cell type containing the immunoproteasome. The absence of overlapping stains for GFAP and arrestin show that distinct cell populations can be labeled (Figure 3.2J-L). Conversely, co-localization of arrestin and LMP7 confirms immunoproteasome is present in the inner segments (Figure 3.2G-I). Additionally, robust staining for LMP7 is also observed in the retinal pigment epithelium (RPE). In Figures 3.2M-O, minimal overlap in staining for LMP7 and GFAP is seen, including in the outer limiting membrane, suggesting immunoproteasome is present, albeit in very low abundance in the Mueller end feet and is concentrated in the photoreceptor cell inner segments.

3.3.4. Upregulation of retinal immunoproteasome following injury from cytotoxic T lymphocytes

The hypothesis is that immunoproteasome plays a role in protecting from damage and/or repairing injury. Therefore, the prediction is that immunoproteasome will be upregulated in response to challenges that induce injury. To test this idea, the retina was injured using an experimental model that mimics autoimmune retinitis, where photoreceptor injury is mediated by cytotoxic T lymphocytes (CTL) specific for beta-galactosidase (β-gal). Previously, we showed loss of photoreceptors following CTL injection into transgenic mice expressing β-gal in photoreceptor cells [192, 193]. In the current experiments, the protocol included sacrificing β-gal transgenic mice at 17 to 21 days after injection of CTLs. At this time, the initial inflammation and photoreceptor cell injury has occurred and the active inflammation has resolved. Staining of retinal sections with anti-LMP7 and neutral red counterstain showed the expected retinal morphology and pattern of staining for immunoproteasome in untreated mice (Figure 3.3A). In β-gal transgenic mice treated with CTLs, complete loss of the photoreceptor layer and intense overall staining with the anti-LMP7 antibody was observed (Figure 3.3B).

The content of GFAP was used as a marker of retinal stress or injury. This protein is expressed mainly in glial cells and was previously reported to be upregulated in the injured retina [258]. Western blotting of retinal homogenates showed GFAP content was increased ~13-fold over control levels (Figure 3.3C-D). This level of stress response is consistent with the significant damage observed on retinal sections. The reaction for

proteasomal subunits showed that both LMP2 and LMP7 subunits were upregulated approximately 4-fold, while content of α7, β1, and β5 remained unchanged. Measurement of total proteasome activity in retinal homogenates was maintained; activity for control and CTL-treated mice was 16 ± 1 pmol/mg/min and 15 ± 1 pmol/mg/min, respectively. Taken together, these results suggest upregulation of immunoproteasome content as a mechanism for maintaining proteasome-dependent functions following retinal injury.

3.3.5. Immunoproteasome upregulation in the brain following CTL-induced injury

We extended our investigation of immunoproteasome to the brain to determine if the CTL injury-induced upregulation was unique to the retina or was a more universal response in other immune-privileged tissue. The CTLs were injected into transgenic mice expressing β-gal in brain astrocytes. Mice were killed during the time of acute onset of CTL-mediated attack (day 6 post-CTL-transfer) and after active inflammation had subsided (day 21 post-CTL-transfer).

To evaluate proteasome changes in response to CTL-induced injury, proteasome activity was measured using a fluorogenic peptide substrate, and Western immunoblotting was done to evaluate the complement of proteasomal subunits. Proteasome activity demonstrated a significant 1.7-fold increase during the acute phase of attack (day 6) but returned to control values by 21 days post-CTL injection (Figure 3.4, left panel). Results from Western immunoblots showed GFAP content was increased 2- to 6-fold post CTL-transfer, indicating a stress response that was elicited by CTL-induced injury continued and was magnified after active inflammation had subsided (Figure 3.4, right panel). Quantitative assessment of LMP2 and LMP7 indicates content is increased 2.8- and 1.9-fold, respectively, at day 6 post-injection. Immunoproteasome content returned to near normal values by 21 days post-injection. Total proteasome content, estimated from the α7 reaction, increased 1.8-fold by 21 days. There was no significant change in the β1 and β5 subunits. These results show that, like the retina, immunoproteasome can be upregulated in the brain in response to injury.

Immunohistochemistry was performed to determine if immunoproteasome was localized to specific brain regions and specific cells. In non-injured brain, very minimal

anti-LMP7 staining of parenchymal tissue and a few anti-LMP7 positive cells in the meninges were observed (Figure 3.5I, J). Positive staining in the meninges is expected due to the presence of many $CD11b^+$ immune cells (Figure 3.5A). $CD11b^+$ microglia were present in the parenchyma, but not readily observed in thin sections (Figure 3.5B). During the acute phase of attack (day 6), there was significant staining with anti-LMP7 antibody, indicating immunoproteasome was upregulated in the leptomeninges, in active lesions, and in parenchymal tissue distant from lesions (Figure 3.5 K-M). Part of this staining was due to activation and injury of microglia, as well as the recruitment of inflammatory cells (Figure 3.5C-E). Interestingly, anti-LMP7 staining of the leptomeninges returned to normal levels by 21 days post-injury while remaining highly positive for $CD11b^+$ cells (Figure 3.5N,F). However, anti-LMP7 positive cells were often more prominent and widespread in the damaged lesion than were the anti-$CD11b^+$ cells (Figure 3.5O,G). This result raised the possibility that non-bone marrow-derived cells were expressing LMP7, as seen in the normal retina.

To estimate the contribution of the immune cells in the meninges to the overall content of immunoproteasome in the brain, we compared the immune densities of LMP2 and LMP7 in preparations from either the entire brain (pia/leptomeninges plus parenchymal tissue) or from brain tissue from which the pia was removed in normal (untreated) mice. We found the densities for immunoproteasomal subunits were only 25% lower in preparations in which pia was removed (data not shown). These results suggest that while the meninges contained significant amounts of immunoproteasome, non-bone marrow-derived elements of the parenchymal tissue also contained measurable amounts of immunoproteasome.

To more clearly define the cell-type contributing to the increased staining in CTL-injured brain, brain sections were double-labeled with anti-LMP7 and antibodies to proteins specific for astrocytes (GFAP), bone marrow-derived cells (CD45), and oligodendrocytes (myelin basic protein, MBP) (Figure 3.6). In the cerebellum, where the majority of the CTL-induced damaged has been previously observed [192], minor staining with anti-LMP7 is observed in normal mouse brain (Figure 3.6A, a-c). In the injured brain, a robust pattern of staining with anti-LMP7 is observed in the cerebellar

loops under low magnification (Figure 3.6A, d-f). At higher magnification, intensely stained individual cells are obvious (Figure 3.6A, g-i). Based on their location and appearance, these anti-LMP7 positive/GFAP negative cells in the acutely inflamed brain are Purkinje cells.

Other cells examined in the cerebellum include bone marrow-derived immune cells and astrocytes. The expected co-localization of anti-CD45 with anti-LMP7 in immune cells was observed (Figure 3.6B, j-l). Co-localization of anti-GFAP and anti-LMP7 was also observed (Figure 3.6B, m-o) indicating that astrocytes also express immunoproteasome in the injured brain. Notably, only one of the two adjacent anti-LMP7-positive cells stained with anti-GFAP, indicating multiple cell types contain immunoproteasome. Micrographs from the stria brain region stained with anti-LMP7 and anti-MBP showed that oligodendrocytes also contained immunoproteasome (Figure 3.6B, p-r). These results show immunoproteasome was upregulated in multiple non-immune cells in the injured brain.

3.4. Discussion

In this study, we investigated the possibility that the immunoproteasome performs functions unrelated to its well-characterized role in generating immunogenic peptides for presentation to CD8 T cells as part of immune surveillance. Our hypothesis is that immunoproteasome's alternative roles include protecting from injury and repairing damage. In the current study, we used injury protocols that evoked damage in the retina and brain. Our *in vivo* data provide convincing evidence through both increased staining of tissue sections and immune reactions on Western blots that injury induces an upregulation in immunoproteasome content in both retina and brain that was not limited to immune cells.

A critical distinction is whether the increases in immunoproteasome are solely due to the cellular elements of the innate and adaptive immune systems, or if the increases can be attributed in part to non-myeloid components of retina and brain. The retina contains $CD11b^+$ microglia that resemble, morphologically and phenotypically, the $CD11b^+$ microglia of brain [259, 260]. Myeloid-derived cells have the well-known

ability to upregulate immunoproteasome in response to numerous stimuli. Cultured CNS microglia were found to express mainly the standard proteasome subunits with very low LMP2 and LMP7, but no MECL [261]. Addition of IFNγ or endotoxin induced expression of MECL, but LMP7 was unchanged. Microglia play a critical role in maintaining tissue homeostasis, especially after injury. For example, optic nerve crush and light-induced retinal degeneration lead to microglial activation and migration to the ganglion cell layer and outer nuclear layer, respectively, where dying retinal cells are phagocytosed [262-264]. While the contribution of cells of the innate immune system to total immunoproteasome complement can not be ignored, the microglia, even under conditions of significant injury, are drastically limited in number relative to the total cellular content of the retina. We also presented evidence showing immunoproteasome is present in neurons (photoreceptor and Purkinje cells), glia (Mueller cells and astrocytes), and oligodendrocytes and conclude that these non-immune cells produce a substantial portion of the immunoproteasome.

3.4.1. Immunoproteasome in the retina and brain

Although immunoproteasome structure and function have been extensively studied in the immune system, a paucity of information is available for immunoproteasome in the CNS. Our laboratory provided the first reports of readily detectable levels of LMP2 and LMP7 in both rat and human retina [86, 150, 250]. Studies of immunoproteasome subunits in homogenates of young, non-diseased human, rodent, and bovine brains were consistent with our observation that immunoproteasome is expressed in low amounts in the uninjured brain of young mice [83, 85, 247]. In parallel analysis of proteasome subunits, our results show that while the standard proteasome subunits β1 and β5 in the brain and retina are approximately equal, the relative proportion of LMP2 and LMP7 immunoproteasomal subunits were ~two-fold higher in the normal retina compared with normal brain. This is despite the presence of the meninges in the brain, especially the pia, which is rich in cells of the innate immune system that could contribute to brain immunoproteasome content [265].

It is important to mention that our measures of β-subunit content included only subunits that were integrated into the mature 20S particle. Newly synthesized β-subunits

contain a pro-peptide that is cleaved upon incorporation into the 20S core [266], and therefore the unprocessed and processed subunits can be distinguished by their difference in migration on high percentage polyacrylamide gels. Alignment of β-subunits in samples with the β-subunits in 20S purified from liver was done on each Western blot to ensure that we were measuring only subunits integrated into the mature 20S particle. In contrast, the α-subunits do not contain a pro-peptide, so our measures of the α7 subunit include both subunits incorporated into the 20S core and those that have not incorporated. The inability to discriminate between the "free" and incorporated α7 subunits could explain why there is not complete correspondence between changes in β-subunits and α7 content.

This study and others have shown that disease and injury can upregulate immunoproteasome content in the CNS. Retinal injury induced by CTLs resulted in a four-fold increase in both LMP2 and LMP7, which is consistent with the reported increase in retinal immunoproteasome subunit content in diseased human retinas with age-related macular degeneration [86]. With brain injury induced by CTLs, a two-fold increase in both LMP2 and LMP7 was observed. Increased expression of the immunoproteasomal subunits has been reported in the hippocampus of human brain with aging and with Alzheimer's disease [85], in HD94 mice, a model of Huntington's Disease (HD) [83], and a 4-fold increase in only the LMP7 subunit after traumatic brain injury in rats [267].

Proteasome activity was measured to determine how the injuries affected function. In the brain, proteasome activity increased at early injury (6 days), then returned to control levels at late injury (21 days). In retina, activity was measured only at late injury and showed proteasome activity was equal between control and treated retina, which is consistent with our results from late injury in the brain. A limitation of using peptide hydrolysis as a measure of proteasome activity is that it does not distinguish between different proteasome subtypes and therefore, the contribution of immunoproteasome to total proteasome activity is not known. However, our results suggest upregulation of immunoproteasome content is a mechanism for maintaining proteasome function following injury.

To study the cellular distribution immunoproteasome, immunohistochemistry was used to localize the cells showing immunoproteasome expression. In control retinas, immunoproteasome staining was heaviest in the RPE, and specific neuronal regions (i.e., IS, OPL and IPL). The localization of immunoproteasome to specific retinal regions may provide important insight regarding its non-immune functions (see below).

Staining for immunoproteasome in injured brain was mostly in the leptomeninges and in lesions where astrocytes, microglia, oligodendrocytes and neuronal Purkinje cells stained intensely for immunoproteasome. Other laboratories have reported immunoproteasome staining in neurons, astrocytes, and the vascular endothelium of elderly and diseased brains and in degenerating neurons in the cortex and striatum of HD patients [83, 85]. The mechanisms responsible for inducing immunoproteasome expression in injured, aged, or diseased tissue has not been defined, but may reflect the occurrence of oxidative stress and inflammation that are common to these conditions. The induction of immunoproteasome subunits in cultured neurons following peroxide treatment is consistent with oxidative stress as a potential regulator of immunoproteasome expression [89].

3.4.2. Regulation of gene expression

Induction of immunoproteasome subunit expression by interferon gamma (IFNγ) has been well established for both cultured immune cells [268, 269] and cultured non-immune cells, such as neurons[270] and epithelial cells of the retina [254]. This cytokine-induced expression results from binding of the Stat transcription factor to multiple interferon gamma consensus/activation sequences in the promoter region of the LMP2, LMP7 and MECL-1 genes [32, 271, 272]. However, using IFNγ-/- mice, Barton [273] showed that constitutive expression of immunoproteasome occurred independent of IFNγ under basal conditions. The presence of promoter consensus sequences for multiple transcription factors that are not regulated by IFNγ [34, 36] provides additional evidence for a cytokine-independent regulation.

3.4.3. Potential alternative roles

The induction of immunoproteasome in the CNS under conditions of disease and injury suggest roles in protecting from injury and repairing damage. One possibility is

that immunoproteasome is more efficient at degrading specific protein substrates that are present in greater abundance as a result of injury or disease that leads to increased production of free radicals. For example, immunoproteasome may be involved in protecting the cell by efficiently degrading oxidized proteins. Consistent with this idea, oxidized proteins accumulate in the brain and liver of LMP2 deficient mice [92].

Immunoproteasome may perform roles related to normal cell functions, such as cell signaling or synaptic remodeling. Data from cultured lymphocytes of $LMP2^{-/-}$ mice and in splenocytes from nonobese diabetic mice that were devoid of the LMP2 protein suggest an important putative role for LMP2 in activation of NF-κB. Cell lines lacking LMP2 showed defects in proteolytic processing of both the NF-κB precursor and IκB inhibitory protein, linking immunoproteasome with cell signaling [10, 11].

The localized, intense staining for LMP7 in the retinal IPL and OPL, which are the sites of neuronal synapses, implies that immunoproteasome may participate in neuronal maintenance or synaptic vesicle formation. Although a role for distinct proteasome subtypes has not yet been defined, considerable evidence suggests proteasome modulates synaptic plasticity by translocating to the site of remodeling [274] and degrading proteins in the synaptic junction (i.e., NMDA receptor subunits, glutamate transporters, postsynaptic density scaffolding molecules) [224, 275, 276].

In summary, we show that while immunoproteasome is present in both retina and brain, the content is approximately 2-fold higher in the normal uninjured retina suggesting a role for immunoproteasome in maintaining retinal homeostasis. Furthermore, immunoproteasome is significantly upregulated with injury/stress *in vivo* in both the retina and brain. These data support the idea that an alternative role for immunoproteasome is in protecting from injury and/or repairing damage in the CNS.

Table 3.1. Antibodies used for immunohistochemistry or Western immunoblotting.

Antibody [a]	Type [b]	Assay [c]	Dilution	Company
20Sα5	P	I	1:1000	Affinity BioReagents, Golden, CO, USA
20Sα7	M	W	1:1000	Biomol, Phymouth Meeting, PA, USA
20Sβ1i (LMP2)	P	W	1:1000	Affinity BioReagents, Golden, CO, USA
20Sβ5i (LMP7)	P	I	1:1000	Biomol, Phymouth Meeting, PA, USA
20Sβ5i (LMP7)	P	W	1:1000	Affinity BioReagents, Golden, CO, USA
20Sβ1 (20SY)	P	W	1:1000	Affinity BioReagents, Golden, CO, USA
20Sβ5 (20SX)	P	W	1:1000	Affinity BioReagents, Golden, CO, USA
20Sβ5 (20SX)	P	I	1:200	Affinity BioReagents, Golden, CO, USA
Arrestin (A9C6)	M	I	1:1000	Dale Gregerson, U. of Minnesota, USA
GFAP	M	I	1:2000	Chemicon, Temecula, CA, USA
GFAP	P	W	1:100	Sigma, St. Louis, MO, USA
MBP	M	I	1:500	Chemicon, Temecula, CA, USA
CD45	M	I	1:20	Biolegend, San Diego, CA, USA

[a] Glial fibrillar acidic protein (GFAP), myelin basic protein (MBP); [b] Monoclonal (M), polyclonal (P); [c] Immunohistochemistry or Immunofluorescence (I), Western blotting (W).

Figure 3.1. Quantitative analysis of proteasomal subunits in murine retina and brain.

Western blotting was used to determine the relative content of the α7 subunit and the catalytic subunits for the immunoproteasome (LMP7, LMP2) and standard proteasome (β1, β5) in retina and brain from five mice (labeled 1-5). Relative content of proteasome subunits is the retinal reaction density normalized to the brain reaction density for each mouse. * Retina significantly higher than brain by paired t-test, $p \leq 0.05$.

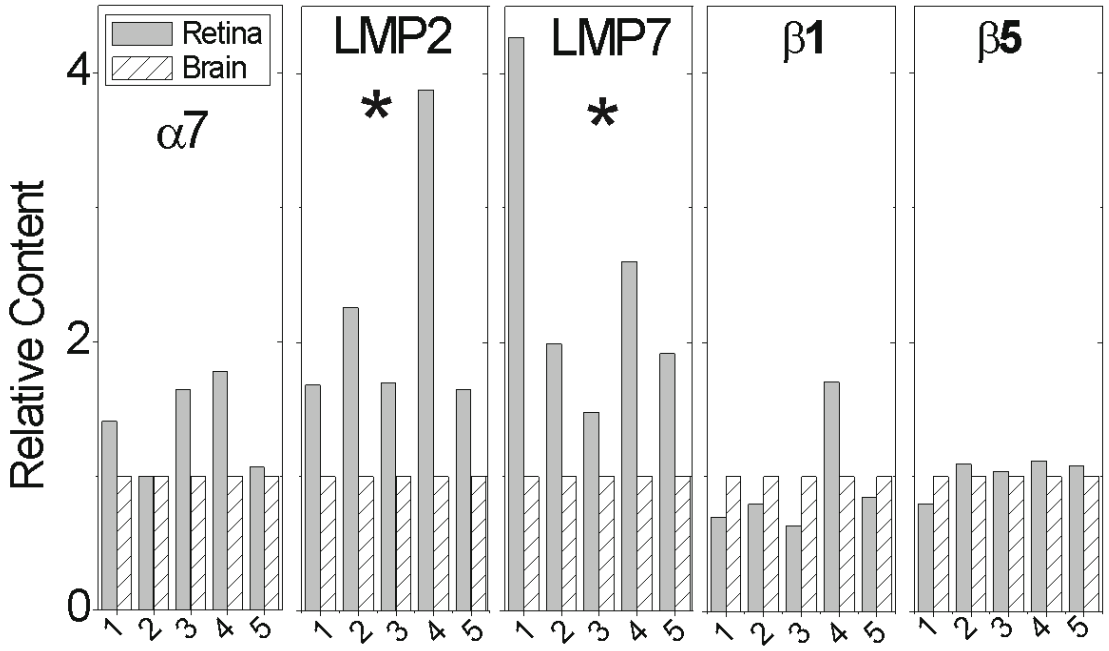

Figure 3.2. Immunolocalization of retinal immunoproteasome.

(A) Retinal sections stained with an antibody that recognizes the α5 subunit showed the distribution of all proteasome subtypes. The specificity of the antibody was demonstrated by the inhibition in staining when antibody is pre-incubated with the antigenic peptide (B) or without the primary antibody (C). (D) Retinal sections stained with an antibody specific for the LMP7 subunit showed the distribution of the immunoproteasome. The specificity of the LMP7 antibody is demonstrated by the inhibition in staining when antibody was pre-incubated with 20S immunoproteasome purified from spleen (E) or when the primary antibody was omitted (F). Bar in (D) indicates 100 μm. Micrographs (A-F) were taken at a magnification of 10X. (G-O) Immunofluorescence of retinal sections stained with antibodies specific for the immunoproteasome (LMP7), photoreceptors (arrestin), and Mueller cells (GFAP). (G) Anti-arrestin (green) labeled the photoreceptor cells from the OS to OPL. (H) Anti-LMP7 (red) intensely stained the RPE, OS and IPL. (I) Overlay showing the IS stain yellow/orange, indicated co-localization of arrestin and immunoproteasome. (J) Anti-arrestin (green) shows labeling as in G. (K) Anti-GFAP (red) staining the Mueller cells, including the Mueller end feet in the region of the IS. (L) Overlay showed that separate cell populations of photoreceptors and Mueller cells are distinctly labeled with very little overlap. (M) Anti-GFAP (green) stained for Mueller cells between the IS and OPL. (N) Anti-LMP7 (red) stained immunoproteasome. (O) Immunoproteasome staining was concentrated in the inner segments. The OLM was labeled yellow, which suggests that the Mueller cell end feet contain some immunoproteasome. GCL, ganglion cell layer; INL, inner nuclear layer; IPL, inner plexiform layer; IS, inner segments; OLM, outer limiting membrane; ONL, outer nuclear layer; OPL, outer plexiform layer;. OS, outer segments; RPE, retinal pigment epithelium.

Figure 3.2. Immunolocalization of retinal immunoproteasome.

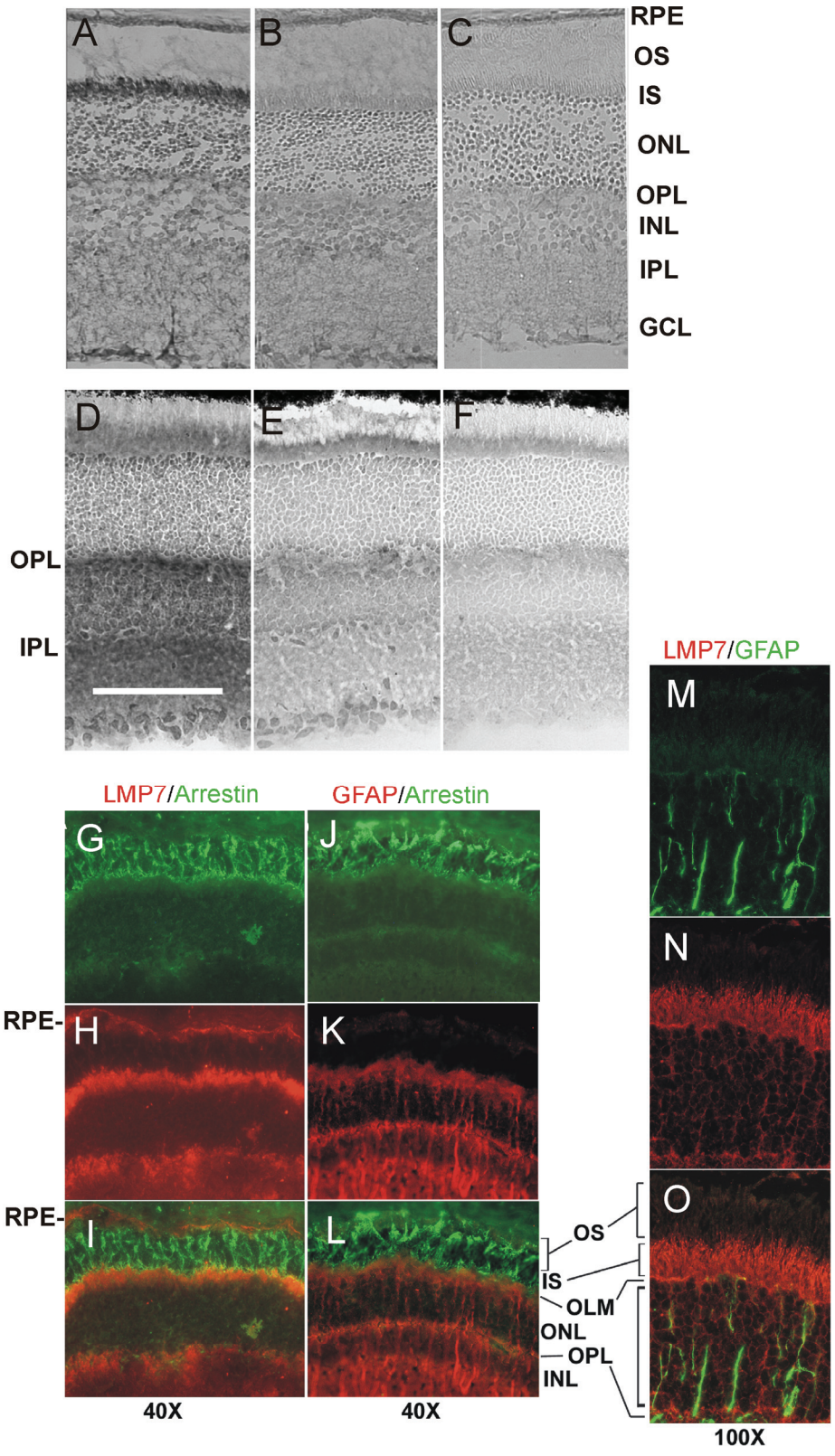

Figure 3.3. Immunoproteasome upregulation in CTL-injured retina.
(A,B) Retinal sections were stained with anti-LMP7 and counterstained with neutral red in control mice (A) and following 21 days after injection of CTLs into transgenic mice expressing β-gal in the photoreceptors (B). Both images were taken with a 20X objective. Bar is 100 μm. INL, inner nuclear layer; IPL, inner plexiform layer; ONL, outer nuclear layer; OPL, outer plexiform layer; OS, outer segments. (C) Western immunoblot probed for proteins to evaluate retinal stress (GFAP), and the content of total proteasome (α7), and catalytic subunits of immunoproteasome (LMP7, LMP2) and standard proteasome (β1, β5). Protein load was 35 μg per lane. (D) Summary of Western blot densities. Relative density is the average density for each group normalized to the control (untreated) density. Data are mean ± SEM. N=4 per group. *Significantly different by t-test, $p \leq 0.05$.

Figure 3.3. Immunoproteasome upregulation in CTL-injured retina.

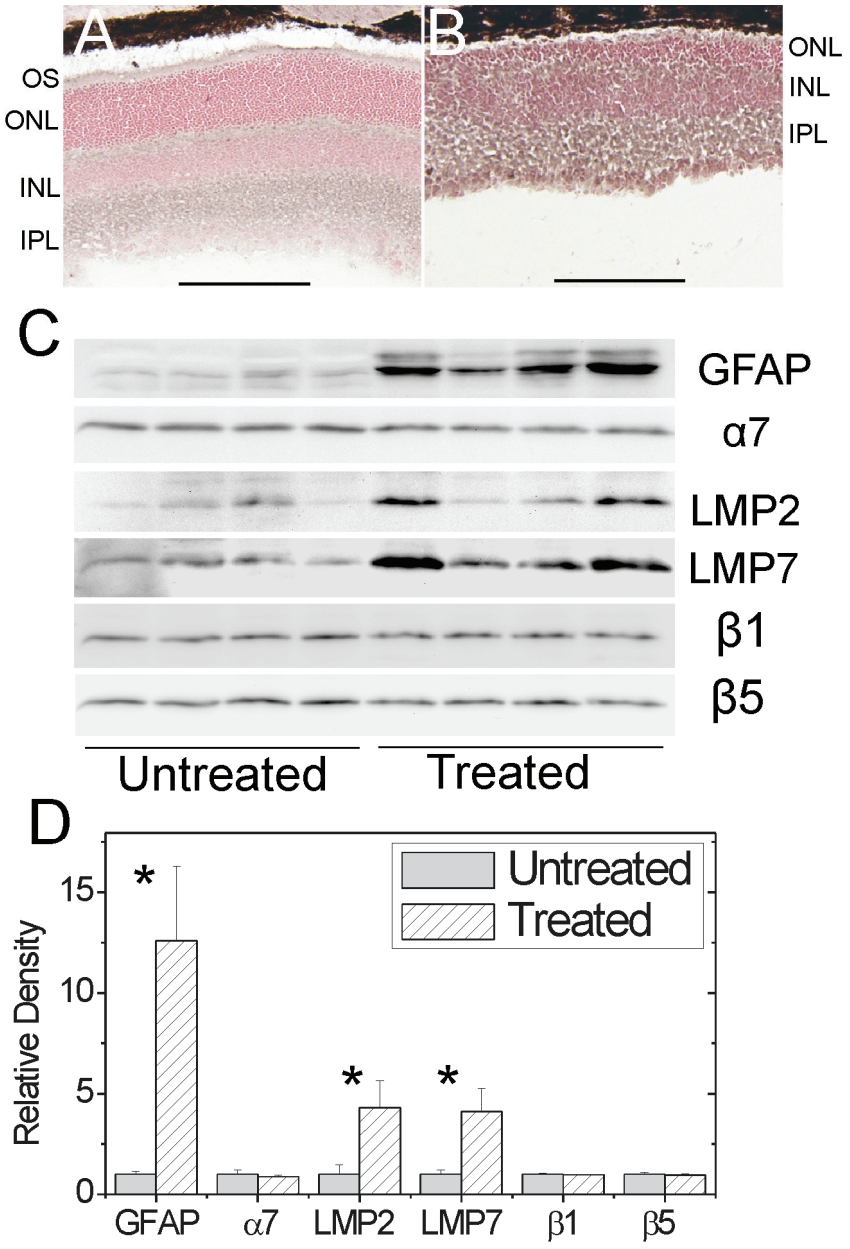

Figure 3.4. Immunoproteasome upregulation in CTL-injured brain.
(Left panel) Proteasome activity measured using the LLVY-AMC peptide substrate in controls, and at 6 and 21 days post-CTL injection. *p=0.005, 6 days different than control and 21 days. (Right panel) Summary of densitometry from Western blots probed for proteins to evaluate stress (GFAP), total proteasome content (α7), and catalytic subunits of immunoproteasome (LMP7, LMP2) and standard proteasome (β1, β5). Relative density is the average density for each group normalized to the control density. Symbols indicate significant differences by Tukey's post-hoc analysis; *control different than 21 days, ** control different than 6 days, @ 6 days different than 21 days. Data are mean ± SEM. N=6 (control), 5 (6 days), and 3 (21 days).

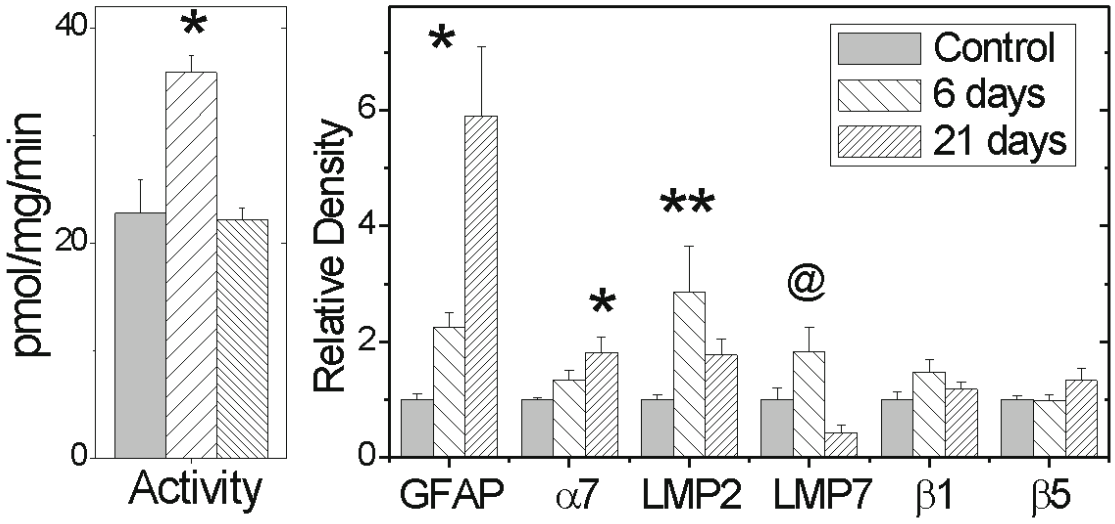

Figure 3.5. Immunoproteasome upregulation in specific regions of CTL-injured brain.

Brain sections stained with anti-CD11b (A-H), anti-LMP7 (I-P), or secondary antibody only (Q-S) showing the leptomeninges, sites of active lesions, and parenchymal tissue far from lesions. Mice were either untreated (Normal) or treated with CTLs and examined at 6 days post-transfer (6 d) when acute inflammation was ongoing or at 21 days post-transfer (21 d) when inflammation had subsided.

Figure 3.5. Immunoproteasome upregulation in specific regions of CTL-injured brain.

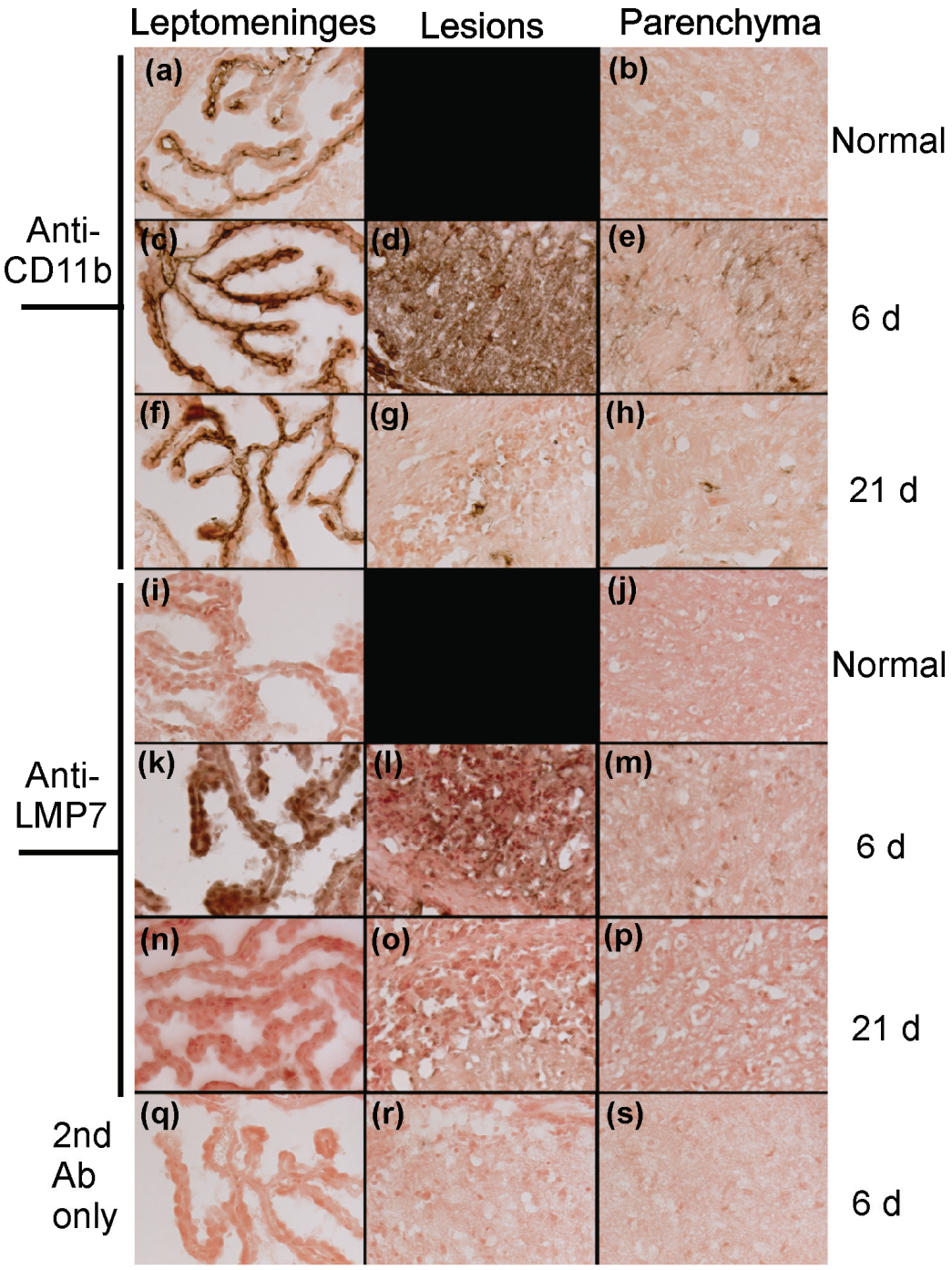

Figure 3.6. Localization of immunoproteasome to specific non-immune cells in the brain.

(A) Staining with anti-LMP7 and GFAP in the cerebellum of normal mice (a-c) and mice 6 days post-CTL injection (d-i). Panels d to f are low magnification images of the cerebellar region showing intense staining of the Purkinje cells with anti-LMP7. High magnification images from the boxed area are shown in panels g to i. Magnification was 100x (a-c, g-i) and 20x (d-f). (B) Staining of brain sections in a mouse 6 days post-CTL injection. Co-localization of staining for anti-LMP7 and cell specific antibodies show immunoproteasome is found in bone marrow-derived immune cells (CD45 positive) and astrocytes (GFAP positive) in the cerebellum, and oligodendrocytes (MBP positive) in the stria. Magnification was 100x (j-l), 53x (m-o), and 63x (p-r). GFAP, glial fibrillar acidic protein; MBP, myelin basic protein.

Figure 3.6. Localization of immunoproteasome to specific non-immune cells in the brain.

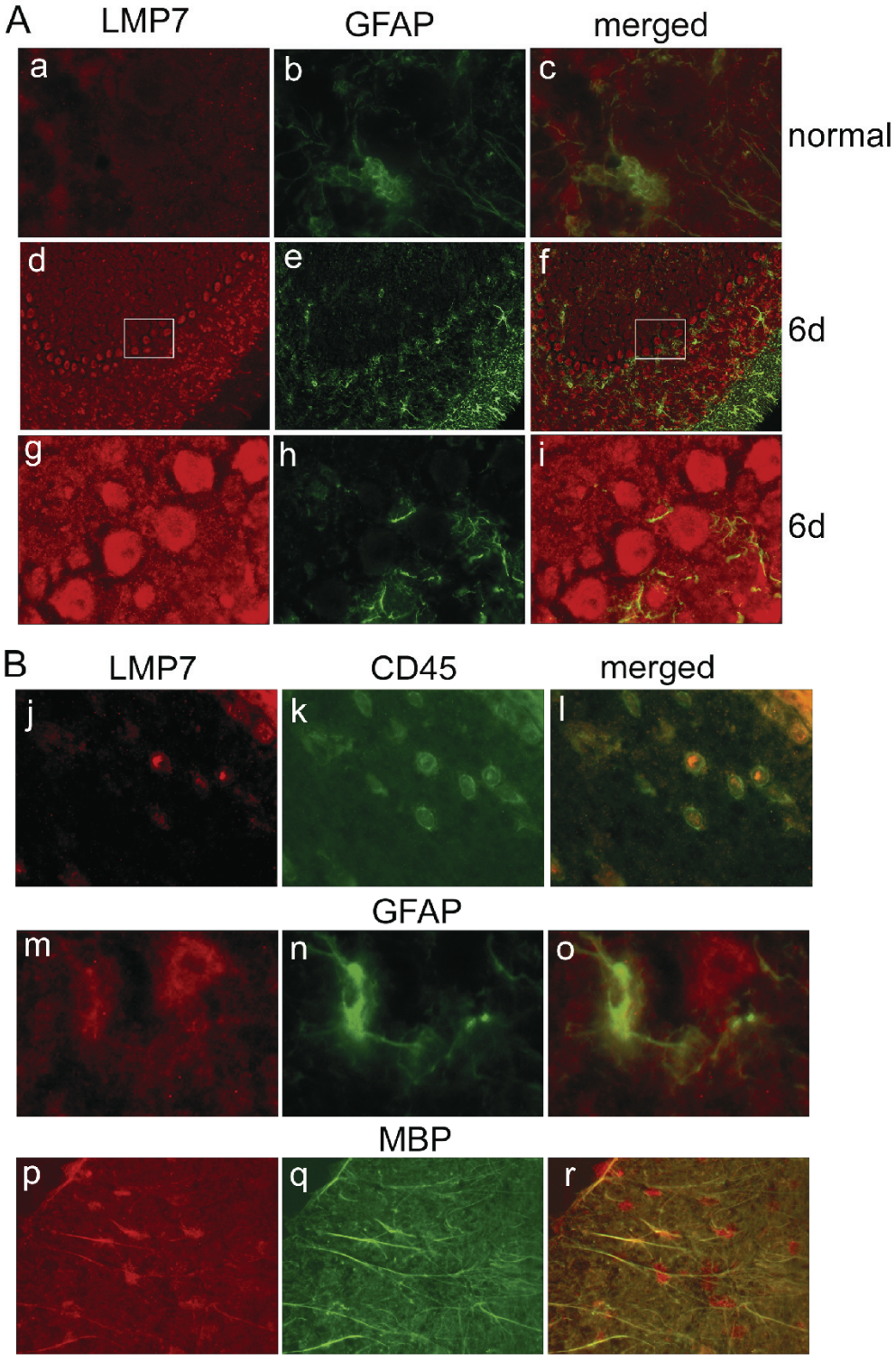

Chapter 4

Immunoproteasome Deficiency Alters Retinal Proteasome's Response to Stress

This chapter is essentially unmodified from the published journal article: Hussong, S.A., Kapphahn, R.J., Phillips, S.L., Maldonado, M., Ferrington, D.A. Immunoproteasome deficiency alters retinal proteasome's response to stress. Journal of Neurochemistry, 2010. 113(6): 1481-1490.

Stacy Hussong was responsible for experimental design, data collection, data analysis, and manuscript writing with the assistance of Deborah Ferrington. Rebecca Kapphahn collected and analyzed the data in Figure 4.1S, and proteasome activity measurements for Figures 4.3, 4.4, and 4.S4. Stacia Phillips performed all of the cell culture experiments and collected the data for Figure 4.5. Marcela Maldonado collected the Western blot data for Figure 4.S4.

Our previous work demonstrated that immunoproteasome is upregulated in the retina and brain in response to injury that does not involve an inflammatory response [8]. These results suggest additional non-immune functions for the immunoproteasome in the cellular stress response pathway. The current study further investigates the potential involvement of the immunoproteasome in responding to the chronic stress of aging or oxidant exposure in the retina and cultured retinal pigment epithelial (RPE) cells from knock-out mice missing either one (*lmp7*$^{-/-}$, L7) or two (*lmp7*$^{-/-}$/*mecl-1*$^{-/-}$, L7M1) immunoproteasome subunits. We show that aging and chronic oxidative stress upregulates immunoproteasome in the retina and RPE from WT mice. No upregulation of LMP2 was observed in retinas or RPE lacking MECL-1 and/or LMP7, suggesting that the full complement of immunoproteasome subunits is required to achieve maximal upregulation in response to stress. We also show that RPE deficient in immunoproteasome are more susceptible to oxidation-induced cell death, supporting a role for immunoproteasome in protecting from oxidative stress. These results provide key mechanistic insight into novel aspects of proteasome biology and are an important first step in identifying alternative roles for retinal immunoproteasome that are unrelated to its role in the immune response.

4.1. Introduction

The proteasome is a multi-subunit proteolytic complex that is involved in the degradation of many cytosolic and nuclear proteins that regulate pathways critical for cell survival. The 20S proteasome, which makes up the catalytic core, is composed of four heptameric rings of α and β subunits that form the outer and inner rings, respectively, of the barrel-shaped structure. The 20S core contains three catalytically active β-subunits that have distinct cleavage specificities. These activities, referred to as caspase-like, trypsin-like and chymotrypsin-like, are associated with the β1, β2, and β5 standard subunits. Alternatively, the standard subunits can be replaced in nascent proteasomes by their immunoproteasome counterparts, LMP2, MECL-1, and LMP7.

Three types of core particles that are defined by the composition of their catalytic subunits have been described. The standard proteasome, containing β1, β2, and β5, is the predominant core in most tissues outside the immune system. The immunoproteasome, containing LMP2, MECL-1, and LMP7, is the major proteasome species in immune tissue but is also found in limited abundance outside the immune system [8, 25, 79, 150]. The third type of 20S core, referred to as the intermediate-type 20S, contains a mixture of both the standard and immunoproteasome subunits [17, 246].

Analysis of 20S cores containing different subunit compositions has shown a substantial difference in peptide hydrolysis and cleavage of model protein substrates [17, 246]. Thus, the repertoire of peptides generated within a cell is determined by the population of proteasome subtypes. It is well established that the immunoproteasome is most efficient at generating immunogenic peptides for antigen presentation [248, 249]. However, the expression of immunoproteasome subunits in neurons (photoreceptor and Purkinje cells), glia (Mueller cells and astrocytes), and oligodendrocytes of the retina and brain implies other non-immune functions are possible [8, 83-86, 150, 250]. Additionally, immunoproteasome upregulation in the central nervous system with acute injury, disease, and age suggests a role in responding to stress and injury [8, 83-86]. Taken together, these results lead to the hypothesis that immunoproteasome is performing functions unrelated to its role in the immune system.

To directly test the effect of immunoproteasome deficiency in the retina, we have utilized immunoproteasome knock-out mice, missing either one (*lmp7* $^{-/-}$) or two (*lmp7* $^{-/-}$ */mecl-1* $^{-/-}$) immunoproteasome subunits. Previous research on these mice has mainly focused on defining defects in their immune function using antigen-presenting tissue and cell lines [29, 30, 105, 106]. The current work is the first to test whether the inability to make specific immunoproteasome subunits has a negative impact on retinal proteasome's response to the chronic stresses of aging and oxidant exposure.

4.2. Materials and Methods

4.2.1. Animals

C57BL/6 wild-type (WT) mice were purchased from the National Institute on Aging-maintained colony (Harlan Sprague Dawley, Indianapolis, IN). Breeders for mice deficient in one (*lmp7* $^{-/-}$, L7) or two (*lmp7* $^{-/-}$*/mecl-1* $^{-/-}$, L7M1) catalytic subunits of the immunoproteasome were generously donated by J. J. Monaco (University of Cincinnati). Descriptions of gene deletions and mouse characteristics have been previously published [29, 105, 106]. All mice are on the C57BL/6 genetic background. Mice were housed in an animal facility maintained at 20 ^{o}C with a 12-hour light and dark cycle. Ages 2, 9, 15, 20 and 24 months were used in this study. Mice were handled according to the guidelines of the Institutional Animal Care and Use Committee of the University of Minnesota and the National Institutes of Health. Animals were sacrificed with CO_2 and perfused with phosphate-buffered saline (PBS) with 2 U/mL heparin prior to tissue collection.

4.2.2. RNA isolation and quantitative RT-PCR

Total RNA was isolated from mouse retina using the RNeasy Mini Kit (Qiagen, Valencia, CA). Isolated RNA was quantified by spectrophotometry (λ = 260nm). cDNA was synthesized in a reverse transcription assay using 70 ng of total RNA. The RT reaction was performed in a GeneAmp PCR System 9700 (Applied Biosystems, Foster City, CA). RT-PCR conditions and primer sets are provided in the supplementary information (Table 4.S1). Proteasome subunit expression was normalized to acidic ribosomal phosphoprotein P0 (ARBP) expression for each sample. Normalized gene

expression was determined using the modified Livak method employed by the iQ5 software (BioRad).

4.2.3. Retinal protein processing

Retinas were processed as previously described [8, 150, 250, 256], using a homogenization buffer comprised of 20 mM Tris (pH 7.4), 20% wt/vol sucrose, 2 mM $MgCl_2$, 10 mM glucose, and 2% wt/vol 3-[(3-cholamidopropyl) dimethylamino]-1-propanesulfonate (CHAPS). The supernatant containing the soluble retinal proteins from the final processing step was saved. Homogenates were stored at -80 ^{o}C. Protein concentrations were determined using the bicinchoninic acid (BCA) protein assay (Pierce, Rockford, IL) with bovine serum albumin as the standard.

4.2.4. Cell culture

RPE cells from WT and L7M1 mice were harvested and immortalized as previously described [255]. For chronic oxidative stress, cells were cultured in 100 mm petri dishes with growth medium containing Dulbecco's Modified Eagle Medium (DMEM), 1X nonessential amino acids, 0.4 mM $_{L}$-glutamine, 25 mM glucose, 50 U/mL penicillin, 50 U/mL streptomycin and 10% fetal calf serum. Confluent cells were treated daily with culture medium containing 2% fetal calf serum and 0, 0.3, 0.5, or 1.0 mM hydrogen peroxide. The responses from 0.3 and 0.5 mM peroxide did not differ from each other so were combined for the low-dose oxidative stress treatment group. Only WT RPE cells were treated with 1.0 mM peroxide (high dose oxidative stress). Cells were treated for a period of one to six days, harvesting one dish of cells each day. Cell viability assay following hydrogen peroxide exposure was performed in 96-well plates as previously described [255].

4.2.5. RPE homogenization

RPE were collected by rinsing the plates in PBS followed by the addition of the lysis buffer containing 25 mM Tris (pH=7.8), 10 mM KCl, 2.5 mM EDTA, 0.5% nonyl phenoxylpolyethoxylethanol-40 (NP-40), 10% glycerol, and 1 mM dithiothreitol (DTT). Cells were scraped from the plate and the lysate was stored at -20 ^{o}C for 16 hr. The lysate was thawed and centrifuged at 16,000 x g for 20 min at 4 ^{o}C. The final supernatant

was collected and stored at -80 ^{o}C. Protein concentrations were determined using the BCA assay.

4.2.6. 20S proteasome purified from spleen

20S proteasome was purified from WT or L7M1 mouse spleen as described previously using ammonium sulfate precipitation followed by sequential column separation (DEAE-5PW, Mini Q) of proteins [79]. Each preparation used spleens from approximately ten animals. The final purified proteasome was suspended in a buffer containing 10mM Tris-HCl (pH 7.2) and stored at -80^{o}C. Protein concentration was determined using the BCA assay.

4.2.7. Western blot analysis

Western blotting was performed as previously described [8, 150, 256]. Primary antibodies and Western blot conditions are provided in the supplementary material (Table 4.S2). The presence of the third immunoproteasome subunit (MECL-1) was not evaluated due to an inadequate reaction with commercially available antibodies. Density values for the proteasome subunits, regulators, and ubiquitin-modified proteins were normalized to the mean value of 2 mo. WT mice. To obtain an estimate of how peroxide affects immunoproteasome content, the density of the control (no treatment) cells from each day was subtracted from the density of the hydrogen peroxide treated RPE.

4.2.8. Proteasome activity measurements

Proteasome activity was assayed using fluorogenic peptide substrates as previously described [8, 150]. Proteasome activity measured in purified 20S and proteasome-enriched homogenate from spleen was normalized to the α7 content for each sample.

4.2.9. Statistical analysis

Differences between three or more groups were tested by 2-way or 1-way ANOVA. When there was significant interaction between groups in the 2-way ANOVA, data was analyzed as 1-way ANOVA tests for each strain and each age. When appropriate, a Tukey-Kramer multiple comparison post-hoc test was performed. A two-sample T-test was performed for comparison of two groups. To observe the time dependent increase of immunoproteasome in response to hydrogen peroxide, data were

evaluated using linear regression. Statistical analysis was performed using NCSS 2001 and significance was set at $p<0.05$.

4.3. Results

4.3.1. Proteasome subunit gene expression

Proteasome subunit gene expression was evaluated in 2 month-old mice to confirm the genetic disruption of the *lmp7* and *mecl-1* genes in the retinas of immunoproteasome KO mice and to determine whether ablation of these genes affected the expression of other proteasome subunits. PCR amplification of retinal mRNA confirmed the disruption of *lmp7* in the L7 and L7M1 mice (Figure 4.S1A). Additionally, *mecl-1* was not expressed in L7M1 retinas (Figure 4.S1A,B). Quantitative analysis of catalytic subunit expression using qRT-PCR showed no significant difference between strains (Figure 4.S1B,C). Expression of the constitutively expressed α7 subunit, used as a measure of total proteasome content, was also consistent between strains. These results indicate that the genetic ablation eliminated expression of *lmp7* and *mecl-1* genes, but does not alter the expression of other proteasome subunits in young mice.

4.3.2. Altered subunit content with age and between strains

To determine how aging and ablation of specific immunoproteasome subunits affected retinal catalytic core subunit composition, Western blotting was performed using subunit-specific antibodies (Figure 4.1A). Western blot data showed no significant difference in the α7 subunit, which is a measure of total proteasome content, with either age or between strains (Figure 4.1B). At 2 months, catalytic subunit expression was equivalent among strains (Figure 4.1C-F). With aging, all strains exhibited a 35-percent decrease in β1 standard subunit content by 24 months and no change in β5 content (Figure 4.1E,F). With aging of WT mice, a significant age-dependent 2- and 3-fold increase in immunoproteasome subunits LMP7 and LMP2 was observed (Figure 4.1C,D). In contrast, LMP2 content in L7 and L7M1 retinas was not altered with age.

4.3.3. Age- and strain-related changes in proteasome catalytic activity

To determine the effect of age and immunoproteasome-deficiency on proteasome activity, fluorogenic peptide substrates were used to monitor the caspase-, chymotrypsin- and trypsin-like activities that are associated with the β1/LMP2, β5/LMP7, and β2/MECL-1 subunits, respectively. All assays were performed in the presence and absence of the proteasome inhibitor, MG132, to distinguish proteolysis that was specific to the proteasome.

For all mouse strains, proteasome activity was essentially equal for each peptide from ages 2 to 15 months, suggesting that elimination of specific subunits did not significantly alter retinal proteasome function (Figure 4.2A-C). For both WT and L7 retinas, proteasome activity did not change with age for all peptides. In contrast, L7M1 retinas exhibited a significant increase at 20 and 24 months for the chymotrypsin-like activity and trypsin-like activity was significantly increased by 24 months. These results suggest inherent differences in the response to aging of retinal proteasome from L7M1 compared with L7.

The relative content of ubiquitin-modified proteins was evaluated by Western blot as an indirect measure of proteasome function. No difference in ubquitinated proteins was noted between strains or with age (Figure 4.S2). These data suggest that proteasome activity is adequate to degrade the ubiquitin-associated proteins.

4.3.4. Relative content of proteasome activators

The increase in proteasome activity in L7M1 could possibly be attributed to an increased content of the proteasome activators PA28 (11S) and PA700. These regulatory complexes are capable of significantly increasing proteasome activity [78, 277]. Data from Western blots showed there was no difference in content of either PA28 or PA700 with aging or between strains (Figure 4.S3). These results rule out differences in content of these two proteasome regulators as an explanation for the increased activity in aged L7M1 retinas.

4.3.5. Activity for standard and immunoproteasome

Another potential explanation for the age-related increase in L7M1 activity is differences in catalytic subunit composition. At 24 months, WT retinas contain more

immunoproteasome and L7M1 retinas contain mainly the standard proteasome. Importantly, proteasome total content is not different between groups. Previous work has shown that the presence of the immunoproteasome subunits in the 20S core can significantly alter peptide hydrolysis [24, 237, 246, 278]. However, the data is conflicting since both increases and decreases in chymotrypsin- and trypsin-like activity have been attributed to the immunoproteasome due to potential artifacts introduced by cytokine treatment or by comparing proteasomes from different tissues [23-26].

To eliminate potential confounding variables due to treatment or tissue-specific regulators, we used proteasome purified from the spleen of WT and L7M1 mice, which contain predominately immunoproteasome and standard proteasome, respectively (Figure 4.3A). This experimental system allowed us to test whether the proteasome subunit composition could explain the differences in proteasome activity with age. Since both types of proteasome were isolated from spleen, variations in proteasome activity should depend primarily on the proteasome species.

Standard proteasome from L7M1 mice showed higher chymotrypsin-like and caspase-like activities (Figure 4.3B). Trypsin-like activity was not different between standard and immunoproteasome. Experiments performed with L7M1 and WT spleen homogenates produced essentially identical results (Figure 4.S4). Based on these data, we would predict an age-dependent decrease in activity for both L7M1 and WT mice since the β1 standard subunit is significantly decreased at 24 months. Additionally, the elevated content of immunoproteasome, which exhibits lower activity, in aged WT retinas also suggests activity should be decreased with aging. The discrepancy in our experimental data comparing spleen and retina suggests that factors other than subunit composition are involved in regulating proteasome activity in the retina with aging.

4.3.6. Proteasome response to oxidative stress in the RPE

One of the prevalent factors associated with aging is increased oxidative stress, which has been shown to alter proteasome subunit composition and activity [89]. To test the effect of chronic oxidative stress, we used cultured RPE cells derived from WT and L7M1 retinas. Prior to exposure to peroxide, both cell lines of cultured RPE contained approximately equivalent amounts of total proteasome (α7) and LMP2 (Figure 4.4A). As

expected, cells from L7M1 mice contain no LMP7. Following exposure to a daily, dose of peroxide, WT RPE showed a dose- and time-dependent increase in LMP2 and LMP7 subunits (Figure 4.4B,C). In contrast, no change in LMP2 content was observed in L7M1 cells using the low dose conditions (Figure 4.4B). Of note, the higher peroxide dose was not tolerated by the L7M1 cells.

These results highlight two important points. First, they suggest chronic oxidative stress as a potential mechanism for induction of immunoproteasome subunits in the WT retina. Second, the absence of an oxidation-induced increase in LMP2 in RPE from L7M1 cells as well as in the retina from aged L7M1 mice (Figure 4.1) suggest LMP2 upregulation during chronic stress requires expression of the full complement of immunoproteasome subunits. Our results show that under conditions of minimal stress (i.e., in 2 month old mouse retina or untreated cells), a basal level of immunoproteasome is present. However, cells deficient in one or two immunoproteasome subunits are unable to respond to stress (i.e., aging or low-level oxidation) by upregulating LMP2. These *in vivo* and *in vitro* results provide corroborative evidence for a cooperative mechanism of co-incorporating immunoproteasome subunits into nascent 20S core particles under conditions of stress in WT cells.

To determine how the oxidation-induced upregulation in immunoproteasome content affects proteasome function, activity was measured in WT RPE exposed to a daily dose of peroxide (Figure 4.4D). We observed a time dependent decrease in chymotrypsin-like activity that correlated with the increased content of both LMP2 ($r = -0.86$, $p=0.03$) and LMP7 ($r = -0.79$, $p=0.06$). The lower chymotrypsin-like activity measured in WT RPE expressing elevated immunoproteasome agrees with results in spleen where immunoproteasome exhibited lower chymotrypsin-like activity compared with standard proteasome (Figure 4.3). Taken together, these results suggest that factors other than subunit composition are involved in regulating proteasome activity in the retina, which is composed of a complex network of neurons and glia.

4.3.7. Consequences of immunoproteasome deficiency

Immunoproteasome upregulation under conditions of chronic oxidative stress (i.e., aging and peroxide treatment) suggests immunoproteasome could provide protection

from oxidative damage. To directly test this hypothesis, we compared the relative resistance of cultured RPE cell lines derived from WT and L7M1 mice to an oxidative challenge. Cell viability was measured 24 hours after exposure to varying doses of peroxide (Figure 4.5). Exposure to peroxide caused a dose-dependent decrease in cell viability for both cell lines. However, the immunoproteasome-deficient cells were significantly more susceptible to oxidation-induced cell death as determined by the peroxide dose required to obtain a 50% reduction in cell viability (LD_{50}). The mean LD_{50} was significantly lower in L7M1 1.26 ± 0.03 mM) compared to WT (1.44 ± 0.02 mM) RPE as determined from 5 separate experiments (p=0.002). These data suggest the absence of immunoproteasome makes cells more susceptible to oxidation-induced cell death and supports the hypothesis that immunoproteasome plays a role in protecting from oxidative damage.

4.4. Discussion

4.4.1. Summary

This study investigated the effect of chronic stress, i.e., aging or exposure to peroxide, on the proteasome in WT and immunoproteasome-deficient retinas and cultured RPE. We showed that aging and oxidative stress upregulates immunoproteasome in the retina and RPE from WT mice. LMP2 was not upregulated in mice lacking MECL-1 and/or LMP7, suggesting that the full complement of immunoproteasome subunits is required to achieve maximal upregulation in response to stress. Furthermore, we showed that RPE cells deficient in immunoproteasome were more susceptible to peroxide-induced cell death. These results provide important novel information about proteasome biology and suggest immunoproteasome may play an essential role in protecting from oxidative stress in the immune-privileged retina.

4.4.2. Plasticity of proteasome subunit composition: response to chronic stress

In the current work, we showed that total proteasome (α7) content was not altered with aging (Figure 4.1). However, aged WT mice exhibited increased levels of LMP2 and LMP7, suggesting transformation of a portion of the population from standard to immunoproteasome. This altered proteasome composition could be induced by age-

related changes in the retinal environment, such as increased oxidative stress [250, 279] and inflammation [280, 281]. Consistent with this idea, induction of immunoproteasome was demonstrated in cultured RPE (Figure 4.4) and neurons [89] following chronic oxidative stress. Additionally, induction of immunoproteasome subunits by cytokines is a well-established response in cultured immune cells [268], neurons [83], and the RPE [254]. It is also possible that other signals, present only in the aged retina, are stimulating immunoproteasome expression since the promoter regions for *lmp2*, *lmp7*, *mecl*-1 contain putative consensus sequences for multiple transcription factors that are not associated with cytokine-induced stimulation [34-36, 282].

4.4.3. Altered subunit plasticity in KO mice under conditions of stress

In the current study, we found no difference in LMP2 incorporated into the 20S core under conditions of minimal stress, i.e., from retinas of 2 month-old WT, L7, and L7M1 mice (Figure 4.1), or in cultured cells derived from WT and L7M1 mice prior to exposure to peroxide (Figure 4.4). Additionally, LMP2 was observed in spleen proteasome from L7M1 mice, albeit at lower levels than found in WT spleen (Figure 4.3). These results are consistent with reports from lymphoblastoids isolated from L7 and L7M1 mice where a slight decrease in LMP2 incorporation was observed [45]. These data support the idea that even in the absence of MECL-1 and/or LMP7, a basal level of LMP2 can be incorporated into the 20S core.

Both the chronic stress of aging and oxidant exposure resulted in increased LMP2 incorporation in either retinas or cultured RPE from WT mice (Figure 4.1, 4.4). This response to stress was not replicated in the immunoproteasome-deficient tissue, suggesting that the full complement of immunoproteasome subunits is required to obtain the maximum induction of immunoproteasome in response to stress. These results support an important role for LMP7 in the incorporation of LMP2 into the 20S core under conditions of stress [45].

4.4.4. Activity of the standard and immunoproteasome

Significantly higher proteasome activity was observed in aged L7M1 retina containing nearly all standard proteasome as compared with aged WT retinas containing elevated levels of immunoproteasome. Importantly, an age-related decrease in the β1

standard subunit was observed in both WT and L7M1 retinas. We investigated whether difference in proteasome subunit composition could explain the strain-dependent variation in activity since proteasome subunit composition can significantly influence its catalytic activity [24, 237, 246, 278]. However, the literature is wrought with conflicting results when comparing activities attributed to standard versus immunoproteasome in different tissues. This may be due to cell-specific differences in endogenous regulators. An additional complication is that peptide hydrolysis does not distinguish between proteasome subtypes. This is especially problematic in tissues containing a mixture of both standard and immunoproteasomes.

To obtain an unambiguous measure of activity for proteasome subtypes, we compared peptide hydrolysis from the 20S isolated from spleen from WT and L7M1 mice. These preparations contained nearly pure populations of either the immunoproteasome or standard proteasome (Figure 4.3). Our results show that standard proteasomes have higher chymotrypsin- and caspase-like activities compared with immunoproteasome, but trypsin-like activity was not different between groups. Proteasome activity measured in RPE cells under chronic oxidative stress corroborates these results. We observed a decreased chymotrypsin-like activity correlated with immunoproteasome induction (Figure 4.4). Our results are consistent with reports where activity in KO mice was compared in tissues (either spleen or virus infected liver) containing mainly the immunoproteasome [28-30]. Taken together, these data unequivocally support the idea that the standard proteasome has increased peptide hydrolysis for the β1 and β5 subunits. However, these data also indicate that the strain-dependent difference in WT and L7M1 retina is due to factors other than subunit composition such as the presence of multiple cell types or endogenous regulators.

4.4.5. Potential alternative roles for immunoproteasome

We have shown that retinal cells respond to injury [8], disease [86], oxidative stress (Figure 4.4), and the chronic stress of aging (Figure 4.1) by upregulating the immunoproteasome. We have also shown that cells deficient in immunoproteasome are more susceptible to peroxide-induced cell death (Figure 4.5). These results imply a previously unrecognized role for immunoproteasome as a key component of the retinal

stress response. A recent publication documenting a role for LMP2 in the cardioprotection afforded by ischemic preconditioning also supports the link between the immunoproteasome and the cell's response to stress [98]. These experiments, showing that ischemic preconditioning-induced degradation of phosphatase and tensin homologue deleted on chromosome 10 (PTEN) and the downstream activation of the kinase Akt is disrupted in LMP2$^{-/-}$ hearts, suggests immunoproteasome could participate in signaling that is critical for cell survival.

A putative role for LMP2 in NFκB activation, one of the primary stress response mechanisms, has also been suggested. In cell lines lacking LMP2, defects in proteolytic processing of NFκB precursors and IκB inhibitory protein were observed [10, 11]. Moreover, a recent report of enhanced processing of NFκB precursors and IκBα by immunoproteasome isolated from inflamed, diseased intestines provide corroborative evidence supporting a role for immunoproteasome in NFκB signaling [96]. While a strict requirement for immunoproteasome in regulating the NFκB pathway is unlikely since immunoproteasome deletion is not lethal, it is possible that immunoproteasome's action may influence the kinetics or termination of signals that are key for cell survival under stress.

Since standard and immunoproteasomes generate different peptides [246], it is possible that some peptides uniquely produced by the immunoproteasome could be biologically active and regulate cell signaling [31]. Upregulation of immunoproteasome under conditions of stress alters the spectrum of peptides within the cell, which could ultimately influence the cell survival. Peptides generated by immunoproteasome in immune-privileged tissue, such as the retina, are more than likely not produced for antigen presentation. They may instead be biologically active peptides that play a key role in retinal survival.

4.4.6. Summary and conclusions

Data from this study showed that aging and chronic oxidative stress upregulates immunoproteasome in the retina and cultured RPE from WT mice. We also reported that the cells deficient in immunoproteasome were more susceptible to oxidation-induced cell death. These results suggest a previously unrecognized role for the immunoproteasome

in protecting from oxidation-induced damage and provide key insight into novel aspects of proteasome biology. Defining the consequences associated with the inability to upregulate immunoproteasome under conditions of stress is an important first step in identifying alternative roles for immunoproteasome in the retina.

Figure 4.1. Age- and strain-related changes in proteasome subunit protein expression.

(A) Representative Western blots of proteasome subunits in WT (■), L7 (○) and L7M1 (Δ) retina. Purified 20S proteasome from mouse spleen was used as a positive control. (B-F) Summary of Western blot densities for proteasome subunits. One-way ANOVA results are provided in panel D. Two-way ANOVA results are provided in panels B, C, E, and F. When there was significant interaction (SxA), one-way ANOVA comparisons were performed for each strain and each age. Results of Tukey-Kramer post-hoc comparisons are indicated by letters, numbers or symbols. (B) α7 content. No significant difference with age or between mouse strains. (C) LMP2 content. One-way ANOVA results by strain with age: (WT, $p<0.001$) a, different from WT 2 mo.; b, different from WT 9 mo. One-way ANOVA results by age between strains: (15 mo., $p=0.009$; 20 mo., $p<0.001$; 24 mo. $p=0.003$) 1, different from L7M1 and L7 at 15 mo.; 2, different from L7 and L7M1 at 20 mo.; 3, different from L7 at 24 mo. (D) LMP7 content in WT mice. a, different from WT 2 mo. (E) β1 content. #, different from 2 mo. (F) β5 content. No significant difference with age or between mouse strains. All values are mean ± SEM and are shown relative to WT 2 mo. WT n=3-15; L7 n=4; L7M1 n=5-10 per group.

Figure 4.1. Age- and strain-related changes in proteasome subunit protein expression.

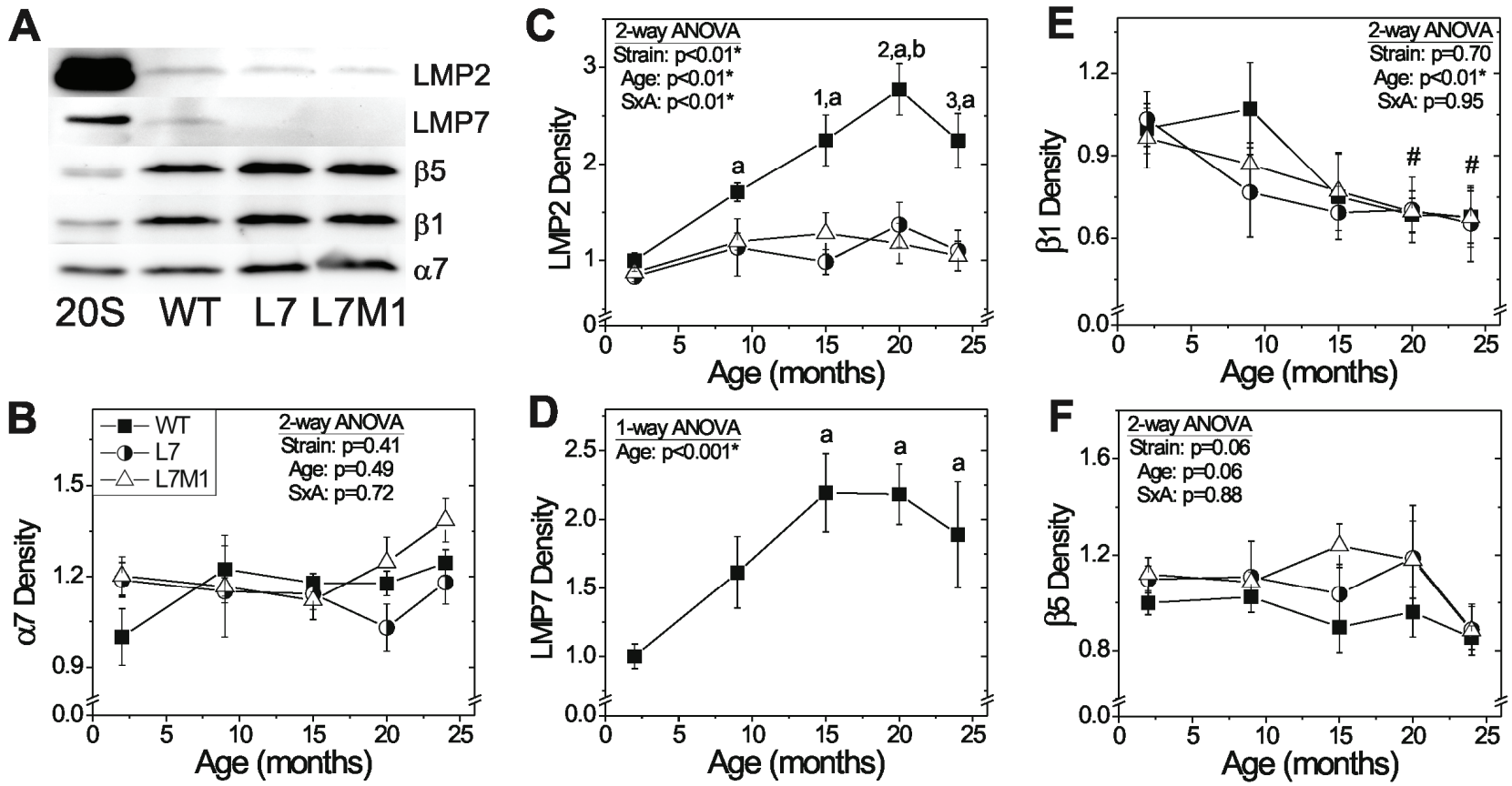

Figure 4.2. Age- and strain-related changes in proteasome catalytic activity. Two-way ANOVA results are shown in each panel. When there was significant interaction (SxA), one-way ANOVA comparisons were performed for each strain and each age. Results of Tukey-Kramer post-hoc comparisons are indicated by letters or numbers. (A) Chymotrypsin-like (CT-L) activity of WT (■), L7 (○) and L7M1 (Δ) retina. One-way ANOVA results by strain with age: (L7M1, p=0.01) a, different from L7M1 9 mo.; b, different from L7M1 2 and 15 mo. One-way ANOVA results by age between strains showed no significant difference at any age. (B) Trypsin-like (T-L) activity. One-way ANOVA results by strain with age: (L7M1, p=0.04) a, different from L7M1 2mo. One-way ANOVA results by age between strains (24 mo., p=0.01) 1, different from WT and L7 at 24 mo. (C) Caspase-like (C-L) activity. Two-way ANOVA showed no difference between strains or with age. All values are mean ± SEM. WT n=3-8; L7 n=4-5; L7M1 n=4-12 per group.

Figure 4.2. Age- and strain-related changes in proteasome catalytic activity.

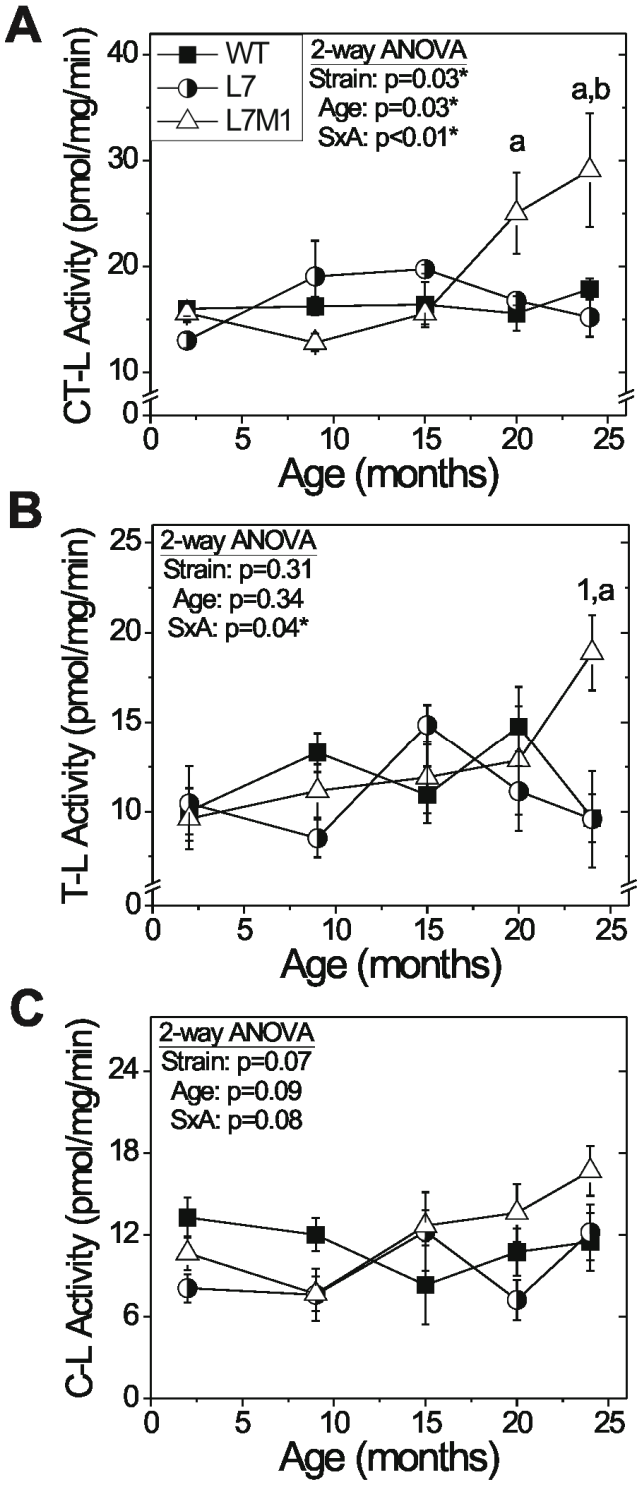

Figure 4.3. Catalytic activity of standard and immunoproteasome.

(A) Representative Western blot of purified 20S proteasome from WT or L7M1 spleen. (B) Catalytic activity of purified 20S spleen proteasome from WT (solid) or L7M1 (cross-hatched) spleen using fluorogenic peptide substrates to test chymotrypsin-like (CT-L), trypsin-like (T-L), and caspase-like (C-L) activities. Two-sample T-tests were performed; *, indicates significance at $p<0.05$. All values are mean ± SEM, n=4 per group.

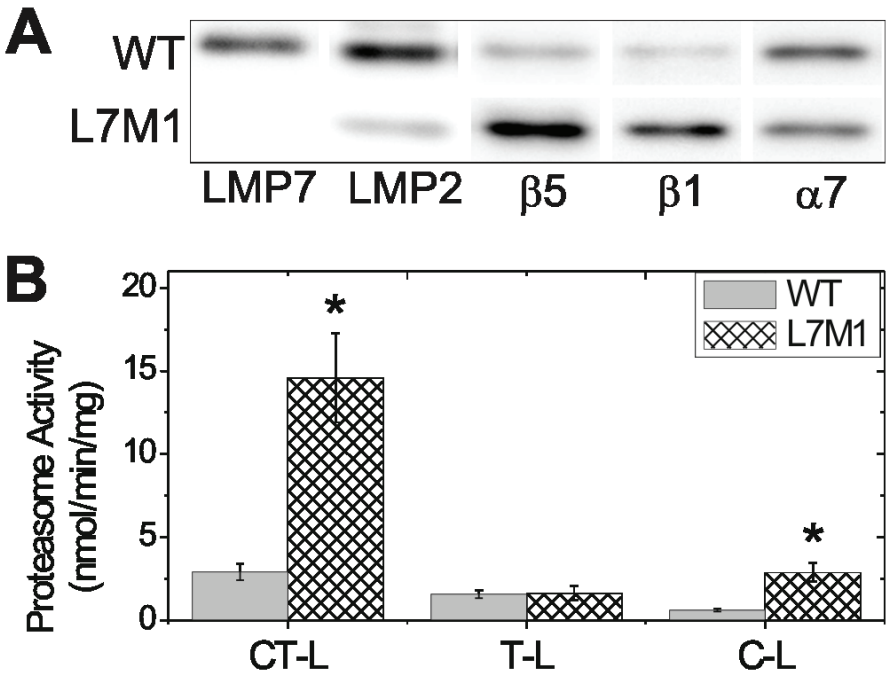

Figure 4.4. Immunoproteasome response to chronic oxidative stress in the RPE. (A) Representative Western blot of proteasome subunits in cultured WT (1) and L7M1 (2) RPE cells. Cultured RPE were treated daily with either a high (WT (■)) or low (WT (○) and L7M1 (Δ)) dose of hydrogen peroxide. (B) LMP2 and (C) LMP7 content was measured by Western blot following one to six days of chronic oxidative stress. The density of the control (no treatment) cells from each day was subtracted from the density of the hydrogen peroxide treated RPE. Subunit density was analyzed using linear regression. *, $p<0.05$. #, $p<0.10$. Values are mean ± SEM, n=2-4 separate experiments per group. (D) Chymotrypsin-like (CT-L) activity in WT cultured RPE treated with a high dose of hydrogen peroxide for one to six days. Activity was measured in triplicate (mean ± SD).

Figure 4.4. Immunoproteasome response to chronic oxidative stress in the RPE.

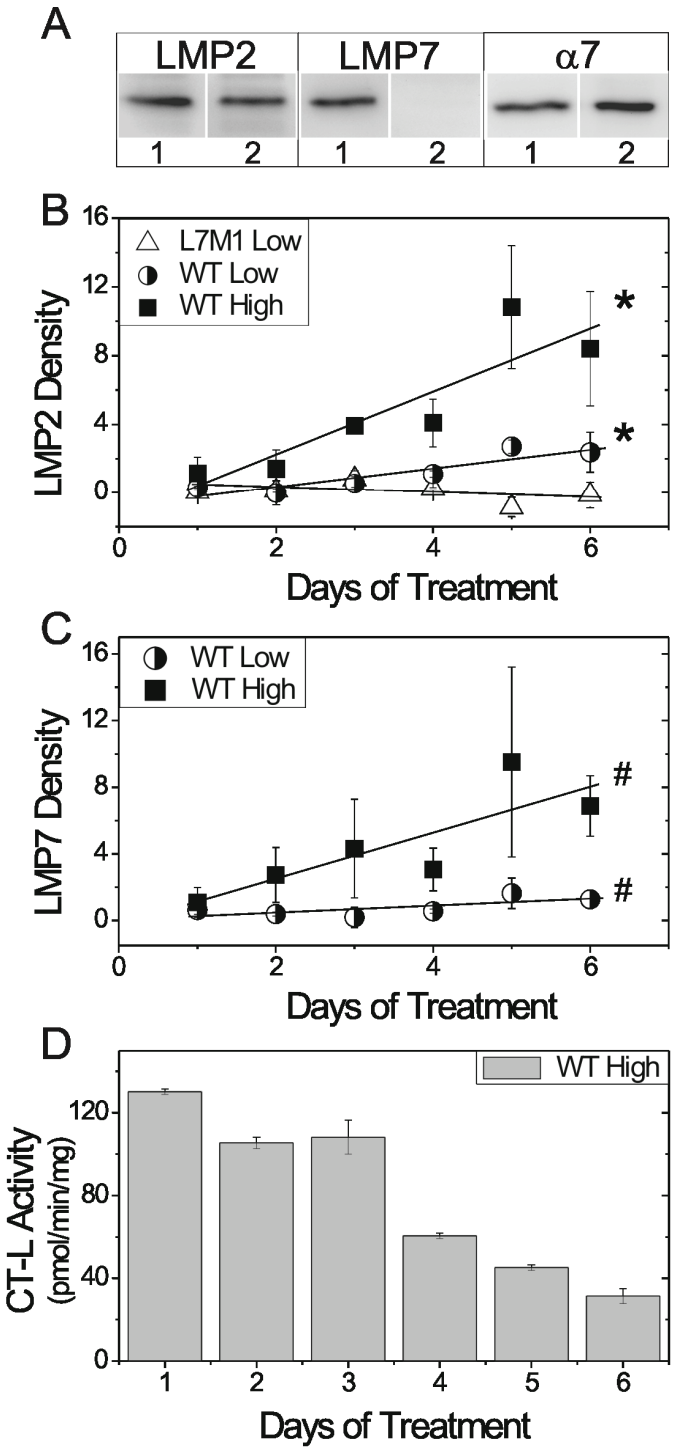

Figure 4.5. RPE cell viability after exposure to hydrogen peroxide.
Cultured WT (■) and L7M1 (Δ) RPE cells were exposed to hydrogen peroxide at the indicated doses and cell viability was measured 24 hours later. Two-way ANOVA results showed lower cell viability in L7M1 compared with WT RPE (p=0.002). All values are mean ± SEM. WT n=5 and L7M1 n=4 separate experiments each with eight replicates.

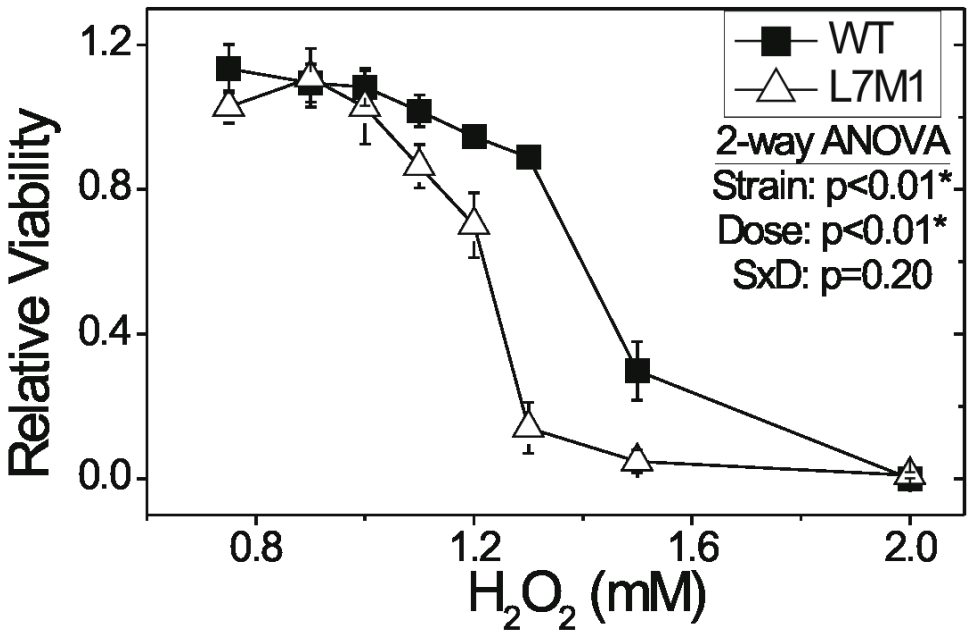

4.5. Supplementary Materials

4.5.1. Real-time RT-PCR conditions

The RT reaction was performed with the following parameters: 60 minutes at 44 °C followed by 15 minutes at 70 °C. The reaction contained 2.5 ng/μL random hexamer, 25 ng/μL oligo dT 18 mer (Integrated DNA Technologies, Coralville, IA), 500 μM dNTPs (Bioline, Taunton, MA), 1X RT Buffer, 10 mM dithiothreitol (DTT), 10 U superase inhibitor (Ambion, Austin, TX), and 100 U Superscript II reverse transcriptase (Invitrogen, Carlsbad, CA) in a 20 μL total reaction volume. Quantification of cDNA was performed with the Quant-iT PicoGreen dsDNA assay kit (Invitrogen). The cDNA (6 ng) was then used as the template for Real-Time PCR performed in an iQ5 Multicolor Real-Time PCR detection system (BioRad, Hercules, CA). PCR reactions were carried out using a two-step amplification with a melt curve using the following cycle parameters: 7 minutes at 95 °C, followed by 35 cycles of 10 s at 95 °C and 30 s at 55 °C. For each gene, the reaction was conducted in triplicate in a 25 μL reaction volume containing 1X PCR buffer, 3 mM $MgCl_2$, 800 μM dNTPs (Bioline), 10 nM fluorescein (USB Corporation, Cleveland, OH), 0.025X SYBR Green (Invitrogen), 0.1% Triton X-100, 100 ng/μL bovine serum albumin (Sigma, St. Louis, MO), 5% DMSO (Sigma), 0.03 U/μL Immolase DNA polymerase (Bioline), and 200 nM of each primer set (Integrated DNA Technologies) (see Table S1).

4.5.2. Proteasome-enriched homogenates from spleen

Single spleen homogenates from 2 mo. mice were prepared similar to methods described previously [79]. Frozen spleen was homogenized in buffer containing 20mM Tris (pH 7.4), 20% (wt/vol) sucrose, 2 mM $MgCl_2$, 10 mM glucose, and 2% (wt/vol) CHAPS. Tissue homogenate was centrifuged at 4600 x g for 15 min at 4 ^{o}C. The pellet was rehomogenized and centrifuged as above. Supernatants were combined and centrifuged at 12,000 x g for 15 min at 4 ^{o}C. The final supernatant was centrifuged at 100,000 x g at 4 ^{o}C for 16 h. Pellets enriched for proteasome were resuspended in 50 mM Tris-HCl, 5mM $MgCl_2$ (pH 7.5). Protein concentration was determined using the BCA assay.

4.5.3. Western blotting

Western blot membranes were incubated with a primary antibody (Table S2) for 14-16 h at 4 ^{o}C. The appropriate secondary antibody conjugated to HRP (Pierce) was applied to the membrane. Membranes were developed using SuperSignal West Dura Extended Duration chemiluminescence substrate (Pierce). Images were taken using a ChemiDoc XRS (Bio-Rad) and densitometry was performed using Quantity One (Bio-Rad). Samples were normalized to a standard run on each blot. To confirm incorporation of proteasome β-subunit in the proteasome complex, Western blot antibody reactions were aligned with the 20S proteasome purified from mouse spleen that was run on each blot to ensure that only the processed form of the subunit was measured.

Table 4.S1. Primers used for Real-Time RT-PCR

Gene	Accession #	Product (bp)	Primer Sequence
LMP7	NM-010724	101	For 5'-GGGACAAGAAGGGACCAGGA-3 Rev 5'-TGCCGGTAACCACTGTCCATCA-3'
LMP2	NM_013585	133	For 5'-CATCATGGCAGTGGAGTTTG-3' Rev 5'-TGAGAGGGCACAGAAGATG-3'
MECL-1	NM_013640	120	For 5'-AAGACCGGTTCCAGCCAAACATGA-3' Rev 5'-TGATCACACAGGCATCCACATTGC -3'
β5	NM_011186	145	For 5'-CGAATCGAAATGCTTCACGG -3' Rev 5'-GAAGGTACGGGTTGATCTCT -3'
β1	NM_008946	132	For 5'-GCCTTAGCTGTTCGTCGAG -3' Rev 5'-TAGAACCACGCCCCCATTAAA -3'
β2	NM_011187	122	For 5'-GTGTCGGTGTTTCAGCCAC -3' Rev 5'-GTGCCAGTTTTCCGAGCTTTC -3'
α7	NM_011184	143	For 5'-AAACAGTAGTACAGCGATTGGG-3' Rev 5'-CTGCAACTGCCATTCCAACA-3'
ARBP	NP_031501	102	For 5'-CTTTCTGGAGGGTGTCCGCAA -3' Rev 5'-ACGCGCTTGTACCCATTGATGA -3'

Accession number is from NCBI database. Forward (For); Reverse (Rev); acidic ribosomal phosphoprotein P0 (ARBP).

Table 4.S2. Antibodies used for Western blotting

Antibody	Type	Dilution	Company
α7	M	1:1000	Biomol, Phymouth Meeting, PA
LMP2	M	1:1000	Biomol, Phymouth Meeting, PA
LMP7	P	1:1000	Biomol, Phymouth Meeting, PA
β1	P	1:1000	Affinity BioReagents, Golden, CO
β5	P	1:1000	Affinity BioReagents, Golden, CO
PA28α	P	1:1000	Biomol, Phymouth Meeting, PA
PA700 S4	P	1:200	Affinity BioReagents, Golden, CO
Ubiquitin	M	1:1000	Stressgen, Ann Arbor, MI

All antibodies were isotype IgG. Monoclonal, host species mouse (M); polyclonal, host species rabbit (R).

Figure 4.S1. mRNA expression of proteasome subunits in 2 mo. mouse retina. (A) Representative 2% agarose gel of PCR products for immunoproteasome subunits (LMP2, LMP7, and MECL-1), α7 proteasome subunit, and ARBP (reference gene). 1=WT, 2=L7M1, 3=L7. Size marker units are in base pairs. Summary of qRT-PCR results for the (B) α7 subunit, immunoproteasome subunits (LMP2, MECL-1), and (C) standard catalytic proteasome subunits (β5, β1, β2). Values are mean ± SEM and are expressed relative to WT. WT n=5-8; L7 n=4-9; L7M1 n=9.

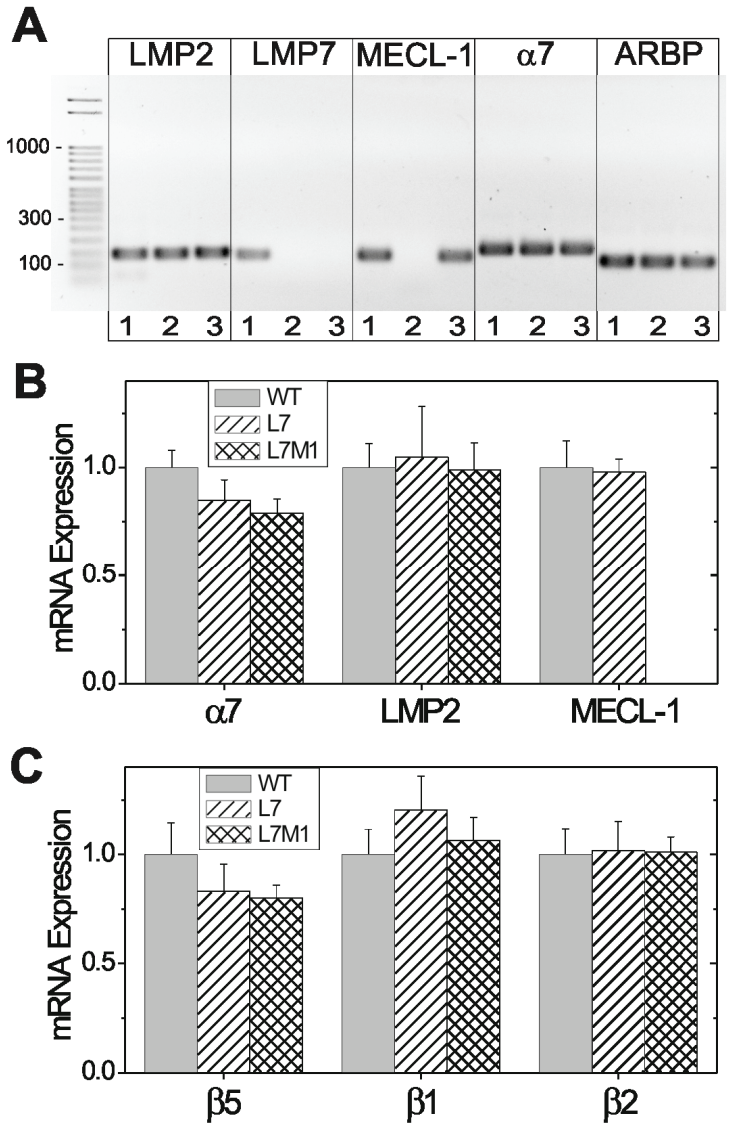

Figure 4.S2. Age- and strain-related content of ubiquitin-modified proteins. Summary of Western blot densitometry for WT (■), L7 (○) and L7M1 (Δ) retina. Two-way ANOVA results showed no significant difference with age or between strains of ubiquitin-modified proteins. All values are mean ± SEM and are shown relative to WT 2 mo. WT n=4-6; L7 n=3-7; L7M1 n=3-6 per group.

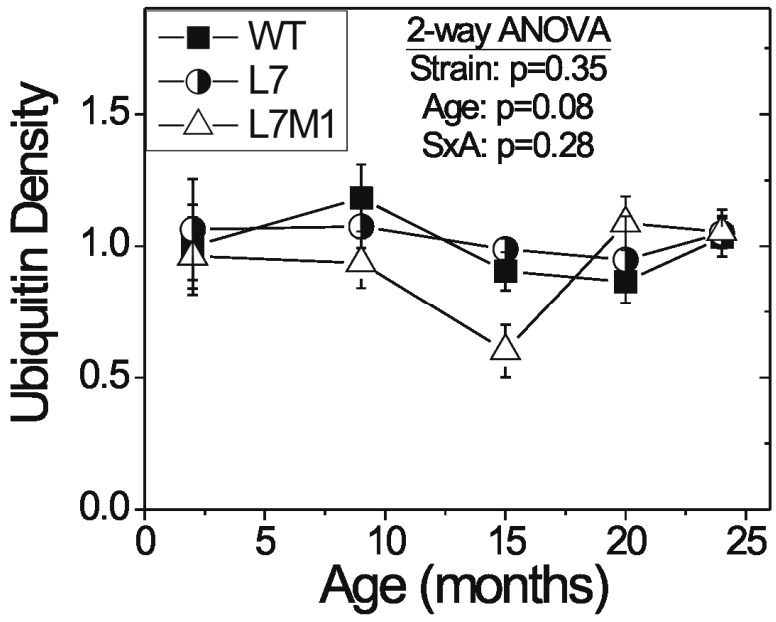

Figure 4.S3. Age- and strain-related measures of content of proteasome activators. Summary of Western blot densitometry for WT (■), L7 (○) and L7M1 (Δ) retina. Two-way ANOVA results are provided in panels A and B. (A) PA700 S4 subunit content. No significant difference with age or between mouse strains. (B) PA28α subunit content. No significant difference with age or between mouse strains. All values are mean ± SEM and are shown relative to WT 2 mo. WT n=3-15; L7 n=4-7; L7M1 n=2-7 per group.

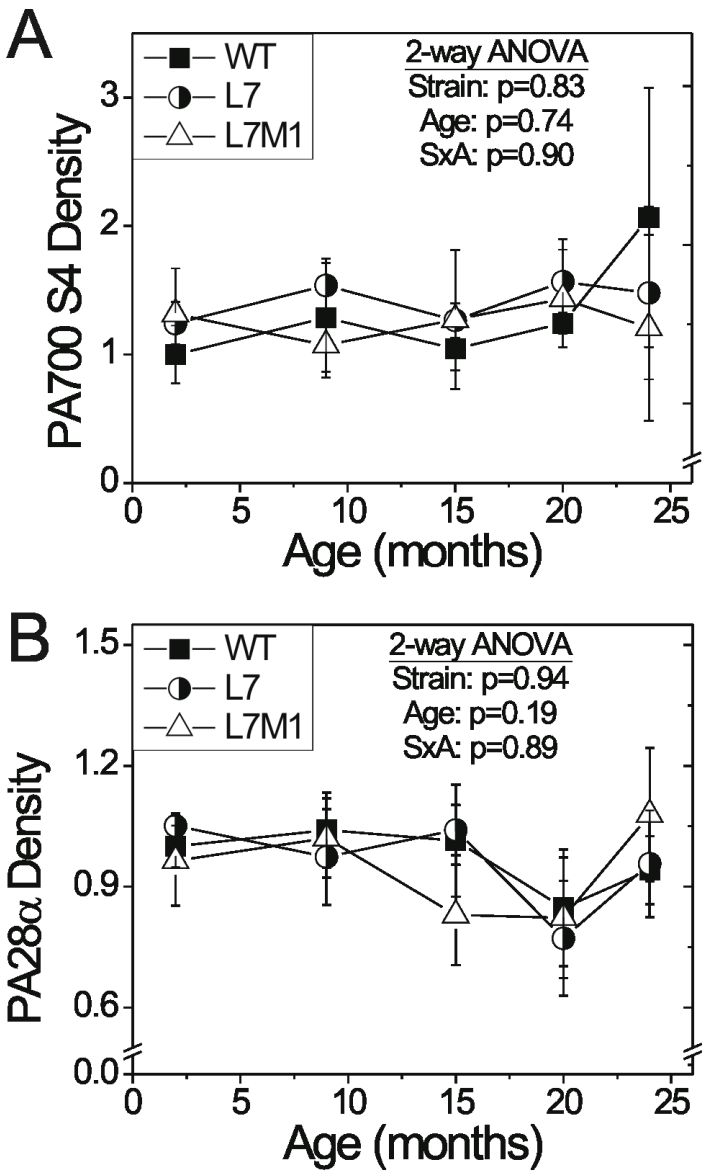

Figure 4.S4. Catalytic activity of standard and immunoproteasome.

(A) Representative Western blot of proteasome-enriched homogenates from WT or L7M1 spleen. (B) Catalytic activity of proteasome-enriched homogenates from WT (solid) or L7M1 (cross-hatched) spleen using fluorogenic peptide substrates to test chymotrypsin-like (CT-L), trypsin-like (T-L), and caspase-like (C-L) activities. Two-sample T-tests were performed; *, indicates significance at $p<0.05$. All values are mean ± SEM, n=4 per group.

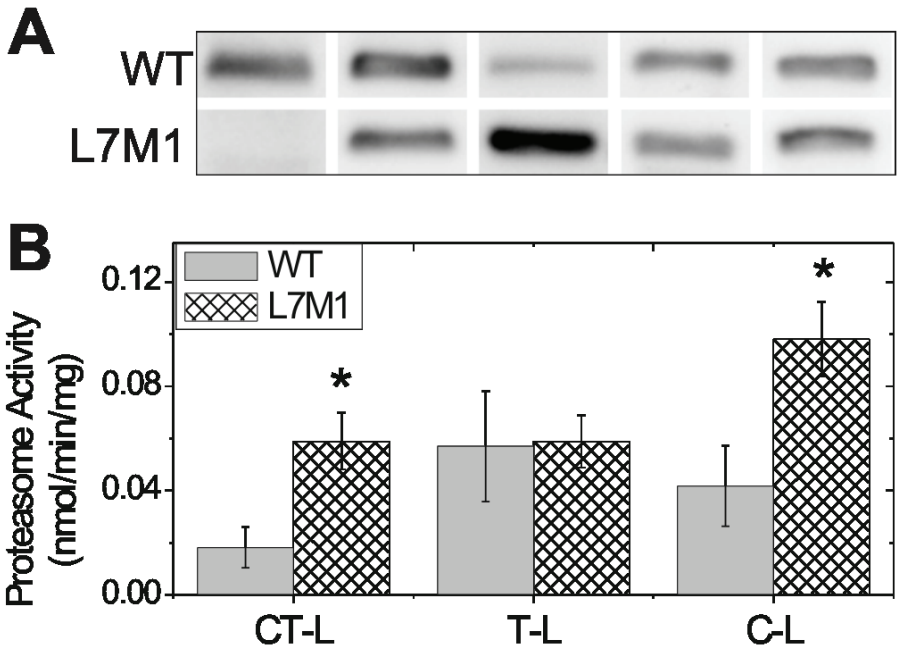

Chapter 5

A Novel Role for Immunoproteasome in Retinal Function

This chapter is essentially unmodified from the accepted journal article: Hussong, S.A., Roehrich, H., Kapphahn, R.J., Maldonado, M., Pardue, M.T., Ferrington, D.A. A novel role for immunoproteasome in retinal function. Investigative Ophthalmology and Visual Science, 2010. doi: 10.1167/iovs.10-6032.

Stacy Hussong was responsible experimental design, data collection, data analysis, and manuscript writing with assistance from Deborah Ferrington. Heidi Roehrich performed all of the retinal sectioning and staining as well as the data collection for Figure 5.1C. Rebecca Kapphahn generated data for Figure 5.7. Marcela Maldonado collected data for Figures 5.7 and 5.8. Machelle Pardued instructed Stacy Hussong on the electroretinogram technique and also assisted with data analysis.

Purpose: Immunoproteasome is a proteasome subtype with a well-characterized role in the immune system. The presence of high concentrations of immunoproteasome in the photoreceptors and synaptic regions of the immune-privileged retina implies a role in visual transmission. In this study, immunoproteasome knock-out (KO) mice lacking either one (*lmp7*$^{-/-}$, L7) or two (*lmp7*$^{-/-}$*/mecl-1*$^{-/-}$, L7M1) catalytic subunits of the immunoproteasome were used to test the hypothesis that immunoproteasome is required to maintain normal retinal function.

Methods: Wild-type (WT) and immunoproteasome KO mice lacking either one (L7) or two (L7M1) catalytic subunits of the immunoproteasome were studied to determine the importance of immunoproteasome in maintaining normal retinal function and morphology. Changes in retinal morphology were assessed for mice ages 2 to 24 months. Retinal function was measured with electroretinography (ERG), and relative content of select retinal proteins was assessed using immunoblots.

Results: Retinal morphometry showed no major abnormalities comparing age-matched WT and KO mice. No significant difference was observed in the content of proteins involved in vision transmission. ERGs from KO mice exhibited an approximate 25-percent decrease in amplitude of the dark- and light-adapted b-waves and faster dark-adapted b-wave implicit times.

Conclusions: Immunoproteasome deficiency causes defects in bipolar cell response. These results support a previously unrecognized role for immunoproteasome in vision transmission.

5.1. Introduction

The proteasome proteolytic complex plays a fundamental role in processes essential for cell viability, such as cell cycle regulation, control of signal transduction and gene expression, and the degradation of oxidized and misfolded proteins [46, 283]. The 20S catalytic core of the proteasome is a barrel-shaped structure, consisting of four heptameric rings. The two outer rings contain the constitutively expressed α subunits that interact with a number of regulatory complexes, i.e., PA28, PA700. The two inner rings contain the β subunits. Three of the β subunits (β1, β2, β5) contain the catalytic sites that perform distinct proteolytic activities referred to as caspase-like (β1), trypsin-like (β2) and chymotrypsin-like (β5). These catalytic subunits form the core of the standard proteasome. In nascent proteasomes, the standard subunits can be replaced by LMP2 (β1i), MECL-1 (β2i), and LMP7 (β5i) to form the core of the immunoproteasome. A third type of catalytic core, referred to as the intermediate-type proteasome, contains a mixture of both standard and immunoproteasome catalytic subunits [17, 246].

While the standard proteasome is the predominant core particle in most tissues, the immunoproteasome is the major proteasome species found in tissues and cells of the immune system [25]. However, immunoproteasome is also found in limited abundance in cells outside the immune system, including neurons (photoreceptors and Purkinje cells) and glia (Mueller cells and astrocytes) of the retina and brain [8, 83, 85]. A recent focus of our lab [6, 8, 86, 150, 250] and others [83-85, 89] has been to define conditions that provoke the upregulation of immunoproteasome in the central nervous system. Data derived from this experimental approach provide some indication that immunoproteasome's function goes beyond its well-defined role in immune surveillance [248, 249]. For example, immunoproteasome is upregulated in the central nervous system in response to acute injury, disease, and age, suggesting a role in responding to stress and injury [6, 8, 83-86, 104, 150, 250]. Additionally, immunoproteasome expression in the non-injured retina and brain [6, 8, 83-86, 250], and its recent localization to synapse in the brain [104] and outer plexiform layer in the retina [8] implies a role in normal, neuronal function.

The present study utilized immunoproteasome knock-out (KO) mice missing either one (*lmp7*$^{-/-}$) or two (*lmp7*$^{-/-}$/*mecl-1*$^{-/-}$) immunoproteasome subunits to test the hypothesis that immunoproteasome is required to maintain normal retinal function. We found that while immunoproteasome deficiency had only minor effects on overall retinal morphology, a significant defect in retinal function as measured by electroretinography (ERG) was observed.

5.2. Materials and Methods

5.2.1. Animals

C57BL/6 wild-type (WT) mice were either purchased from the National Institute on Aging-maintained colony (Harlan Sprague Dawley, Indianapolis, IN) or produced in our colony. Breeders for mice deficient in one (*lmp7* $^{-/-}$, L7) or two (*lmp7* $^{-/-}$/*mecl-1* $^{-/-}$, L7M1) catalytic subunits of the immunoproteasome were generously donated by J.J. Monaco (University of Cincinnati). Descriptions of gene deletions and mouse characteristics have been previously published [29, 105, 106]. All mice were on the C57BL/6 genetic background. Mice were housed in an animal facility maintained at 20 ^{o}C with a 12-hour light and dark cycle. Mice at 2, 9, 15, 20 and 24 months of age were used for the aging analysis. For the remaining studies, only 2-month-old animals were assessed. Mice were handled according to the guidelines of the Institutional Animal Care and Use Committee of the University of Minnesota and the National Institutes of Health. Animal procedures conformed to the ARVO Statement for the Use of Animals in Ophthalmic and Vision Research. Animals were sacrificed with CO_2 and perfused with phosphate-buffered saline (PBS) with 2 U/mL heparin prior to tissue collection.

5.2.2. Retinal protein processing

Retinas were processed as previously described [6, 8, 150, 250, 256], using a homogenization buffer containing 20mM Tris (pH 7.4), 20% w/v sucrose, 2 mM $MgCl_2$, 10 mM glucose, and 2% w/v 3-[(3-cholamidopropyl) dimethylamino]-1-propanesulfonate (CHAPS). The supernatant containing the soluble retinal proteins from the final processing step was saved and stored at -80 ^{o}C. Protein concentrations were determined

using the bicinchoninic acid (BCA) assay (Pierce, Rockford, IL) with bovine serum albumin as the standard.

5.2.3. Western and slot blot immunoassays

Western blotting was performed as previously described [6, 8, 150, 256]. Slot blot immunoassays were executed as previously described using a Bio-Dot SF (Bio-Rad, Hercules, CA) and 0.2 μm polyvinylidene fluoride membrane (Millipore, Billerica, MA) [256]. Membranes were incubated with a primary antibody (Table 5.1) for 14-16 hr at 4^{o}C. The appropriate secondary antibody conjugated to horseradish peroxidase (HRP) (Pierce, Rockford, IL) was applied to the membrane. Reactions were developed using SuperSignal West Dura Extended Duration chemiluminescence substrate (Pierce, Rockford, IL). Images were taken using a ChemiDoc XRS (Bio-Rad, Hercules, CA) and densitometry was performed using Quantity One (Bio-Rad, Hercules, CA). Samples were normalized to a standard retina preparation run on each blot. For slot immunoblots, background was subtracted using a buffer-only sample.

5.2.4. Histology and immunohistochemistry on retinal sections

For all histological analysis, tissue was fixed in 10% buffered formalin (Fischer Scientific, Pittsburgh, PA) and paraffin-embedded. Retinal sections (6 μm) were taken through the optic nerve. Prior to staining, retinal sections were deparaffinized through a graded series of xylene and ethanol. For retinal morphometry measures and counts, sections were stained with hematoxylin and eosin (H&E). Terminal deoxynucleotidyl transferase-mediated dUTP nick-end labeling (TUNEL) was accomplished using the In Situ Cell Death Detection Kit, Fluorscein (Roche, Indianapolis, IN). For antibody staining, the tissue sections were rehydrated and then submitted to antigen retrieval by heating in 10 mM sodium citrate, 0.05% Tween 20 (pH 6.0) for 24 minutes at 94 ^{o}C. Sections were blocked for 30 minutes in 10% normal donkey serum and then incubated in the primary antibodies overnight (Table 5.1). The reaction was visualized using appropriate secondary antibodies. To confirm the specificity of the primary antibody, sections were incubated in the absence of the primary antibody, using the secondary antibody alone. TUNEL-labeled and antibody stained slides were cover slipped with

VECTASHIELD Mounting Medium containing 4',6-diamidino-2-phenylindole (DAPI) (Vector Laboratories, Burlingame, CA).

5.2.5. Retinal morphology measurements

The photoreceptor lengths and outer nuclear layer (ONL) and inner nuclear layer (INL) nuclei densities were measured on H&E stained sections. Bipolar cell densities were determined from the dual staining of retinal sections with ceh-10 homeo domain containing homolog (Chx10) (all bipolar cells) and protein kinase C, alpha (PKCα) (rod bipolar cells only) antibodies followed by DAPI staining of nuclei [284]. Nuclei densities and photoreceptor lengths were measured at 500 and 1000 μm on either side of the optic nerve. ONL, INL, and bipolar cell densities were determined by counting the nuclei of a specified area and dividing by the length of the measured region. Photoreceptor length was measured from the retinal pigment epithelium (RPE) to the edge of the ONL. Measurements were performed using BIOQUANT NOVA PRIME 6.90.10 (BIOQUANT Image Analysis, Nashville, TN).

The number of apoptotic nuclei was determined from counting the entire number of TUNEL-positive nuclei in the ONL of retinal sections dually-stained with TUNEL and DAPI. The averaged counts from four sections was used for each mouse and the data are reported as the number of TUNEL-positive nuclei in the outer nuclear layer per retinal section.

5.2.6. Electroretinograms

Electroretinography (ERG) was performed as described by Phillips et al. [285]. Two-month-old mice were dark-adapted overnight and ERGs were recorded using an Espion^2 Electrophysiology System with Espion V4.0.51 software (Diagnosys LLC, Lowell, MA). Mice were anesthetized with ketamine (80 mg/kg) and xylazine (16 mg/kg). The cornea was subsequently anesthetized (0.5% tetracaine) and pupils were dilated (1% tropicamide; 2% cyclopentolate). Body temperature was regulated using the ATC1000 Animal Temperature Controller (World Precision Instruments, Sarasota, FL). The active electrode was a silver DTL fiber that contacted the cornea through a layer of 0.5% carboxymethylcellulose. Subdermal needle electrodes (Grass Technologies, West Warwick, RI) were placed in the cheek and tail to serve as reference and ground,

respectively. A ColorBurst Ganzfeld (Espion) supported by a ringstand was positioned directly over the animal's head and produced a series of light flashes ranging from -3.3 to 1.7 log cd s/m^2. Dark-adapted ERG recordings were averaged from 3 to 10 separate light flashes at each of the 10 intensities. The interstimulus time increased from 4 to 65 seconds with increasing light flash intensity. Mice were light-adapted for 10 minutes using a background light of 1.4 log cd/m^2. Isolated cone responses were recorded using a seven-step intensity series (-0.3 to 1.7 log cd s/m^2) presented at 4 Hz with a constant background light of 1.4 log cd/m^2. Light-adapted ERGs were averaged over twenty-five separate light flashes for each intensity. When ERG recordings were completed, mice were either immediately sacrificed by CO_2 inhalation or treated with 2 mg/kg yohimbine to reverse the effects of the xylazine and prevent corneal lesions [286].

5.2.7. Electroretinogram data analysis

ERG a-wave amplitudes were measured from the baseline to the first negative peak. The a-wave amplitude was also measure at 7 ms for the four brightest flash intensities to avoid any effect of b-wave changes in the summed response [287]. The b-wave amplitude was determined by measuring from the trough of the a-wave to the peak of the first positive wave. When the a-wave was absent, the b-wave was measured from baseline to the first positive peak. The implicit time was measured from the incidence of the flash to the leading edge of the a- and b-wave peaks, respectively.

To determine the isolated photoreceptor contribution (PIII), the dark-adapted waveform data were fitted to the Hood and Birch formulation of the Lamb and Pugh model of rod phototransduction activation to determine the PIII contribution [288]. In this model, Rm_{P3} is the maximal saturated photoreceptor response and is proportional to the number of ion channels in the outer segments that close in response to light and S is the rod photoreceptor sensitivity to light.

The post-receptoral b-wave response was modeled to examine the response of the rod bipolar cells. Data from the dark-adapted b-wave was used in conjuction with the Naka-Rushton equation to measure the maximum scotopic b-wave response (Vm) and the post-receptoral sensitivity (log σ) [288].

The oscillatory potentials (OP) were isolated from the waveform by digitally filtering signals with a band-pass of 65 to 235 Hz.[200] Each OP amplitude was measured from the peak to the trough immediately preceding it. The implicit time was measured in milliseconds from the incidence of the flash to peak of each OP. The individual OPs displayed a similar pattern so the summed OP amplitudes and implicit times were calculated from OPs 1-6.

5.2.8. Statistical analysis

Statistical analysis for ERG a-wave, b-wave, and summed OP amplitudes and implicit times was performed across flash intensities and between mouse strains using repeated measures ANOVA tests using a Greenhouse-Geisser correction (SPSS, Chicago, IL). For all other experiments, data were analyzed using NCSS 2001 (Kaysville, UT). Differences between three or more groups were tested as 2-way, 1-way, or repeated measures ANOVA as indicated. When the two-way ANOVA showed significant interaction (SxA), one-way ANOVA tests were performed for each age and each strain. When appropriate, a Tukey-Kramer post-hoc test was performed. When data failed normality assumptions of the one-way ANOVA, a Kruskal-Wallis (KW) one-way ANOVA on ranks was performed followed by a Z-value multiple comparison test. Significance was set at $p<0.05$ for all statistical measures.

5.3. Results

5.3.1. Altered retinal morphology with aging and immunoproteasome deficiency

In comparing H & E stained retinal sections from two-month-old mice, the overall retinal morphology was essentially the same across strains (Figure 5.1A). To quantitatively assess whether retinal morphology is altered with age or strain, the density of the outer (ONL) and inner (INL) nuclear layers was measured. The ONL contains the nuclei of the photoreceptors and therefore, the density of nuclei is a measure of the relative content of photoreceptors. ONL nuclei density decreased by 11% with age at both 500 and 1000 μm from the optic nerve (Figure 5.1B). At 500 μm from the optic nerve, the number of ONL nuclei was dependent on age and strain [2-way ANOVA , $F(8,133) = 2.74$, $p=0.008$]. At 1000 μm, only a significant decrease in ONL nuclei across

age was observed [two-way ANOVA $F(4,133) = 4.64$, $p=0.002$]. Thus, only minor defects in retinal morphology are evident in L7M1 mice which exhibit approximately 6% fewer nuclei in the ONL compared to WT and L7 (Figure 5.1B).

To determine if the differences in ONL nuclei density with aging and between strains were due to a loss of cells via apoptosis, retinal sections were stained with TUNEL and the number of nuclei undergoing apoptosis in the ONL was counted (Figure 5.1C). (The number of apoptotic cells in the other nuclear layers of the retina was negligible (data not shown)). Overall, age- and strain-dependent decreases in ONL nuclei density correlated with significant increases in apoptotic nuclei [two-way ANOVA, $F(8,124) = 2.41$, $p=0.02$]. For all strains, the number of apoptotic nuclei was approximately 2-fold higher by 15 months compared with 2 months. Levels of apoptosis reached its peak at 20 months when the number of apoptotic nuclei was 2.5-fold higher than 2 month-old animals [one-way ANOVA, (WT, $H(4)=16.93$, $p=0.002$), (L7, $F(4,27)=4.14$, $p<0.01$), (L7M1, $F(4,48)=15.66$, $p<0.001$)]. These data are consistent with an apoptotic mechanism of cell death with aging. Additionally, apoptosis levels in L7M1 ONL were, on average, 1.7-fold higher than both WT and L7 [one-way ANOVA, (2 months, $F(2,32)=7.21$, $p=0.003$), (15 months, $H(2) = 16.47$, $p<0.001$), (20 months, $F(2,16)=9.55$, $p=0.002$)]. The increased apoptosis levels correlate with the observed decrease in ONL density. The elevated apoptosis in L7M1 retinas that was not replicated in L7 suggests the MECL-1 subunit, which is present in the L7 and WT mice, may be crucial in preventing apoptotic cell death of photoreceptors.

Nuclei density in the inner nuclear layer (INL), which contains bipolar, amacrine, and horizontal cell nuclei, decreased approximately 13% with age at both 500 [two-way ANOVA, $F(4,132)=9.51$, $p<0.001$)] and 1000 μm [two-way ANOVA, $F(4,133)=4.01$, $p=0.004$)] from the optic nerve (Figure 5.1D). However, there were no significant differences between strains in the INL density (500 μm, $p=0.21$; 1000 μm, $p=0.16$). The age-related loss of nuclei observed in both the ONL and INL is consistent with previously reported data in aged C57BL/6 mice [179, 187].

5.3.2. Decreased retinal function with immunoproteasome-deficiency

To determine the effect of immunoproteasome deficiency on retinal function, we performed dark- and light-adapted ERGs on two-month-old WT, L7, and L7M1 mice. At this age, there is no difference in retinal morphology (Figure 5.1), so any change in the ERG can be attributed to the absence of specific immunoproteasome subunits rather than secondary effects associated with aging.

Comparing WT and immunoproteasome KO mice, dark-adapted ERGs from WT showed significantly larger waveforms (Figure 5.2A). At the two highest flash intensities, the dark-adapted a-wave amplitude, reflecting the function of the photoreceptors, was 20% lower in both L7 and L7M1 mice as compared to WT (repeated measures ANOVA, $F(4.95,61.8)=3.61$, $p=0.006$) (Figure 5.2B). More dramatic differences were seen in the dark-adapted b-wave amplitudes, reflecting the electrical activity of the bipolar cells. Dark-adapted b-wave amplitudes of immunoproteasome-deficient mice were 22% to 27% lower than WT at all flash intensities above -0.70 log cd m/s^2 ($F(4.25,53.17)=4.00$, $p=0.006$) (Figure 5.2C). A plot of the relationship between a- and b-wave amplitudes further confirms that the b-wave is more dramatically altered at all intensities in immunoproteasome-deficient retinas (Figure 5.2D). Defects in the a-wave are observed only at the highest intensities.

Cone-mediated, light-adapted b-wave amplitudes were also significantly higher in WT compared with immunoproteasome-deficient retinas (Figure 5.3A). Amplitude plotted across flash intensity showed the L7 amplitude was 19% to 34% lower than both the WT and L7M1 at flash intensities of greater or equal to 0.35 log cd m/s^2 ($F(4.22,52.8) = 6.56$, $p<0.001$) (Figure 5.3B). L7M1 light-adapted b-wave amplitude was significantly lower (11% and 16%, respectively) than WT at the two brightest flash intensities ($p<0.001$) (1.30 and 1.70 log cd m/s^2).

The implicit times for the dark-adapted a- and b-wave and light-adapted b-wave were also evaluated to determine if immunoproteasome deficiency had an effect on the response rate after a light stimulus. There was no significant difference between strains in either the dark-adapted a-wave ($p=0.09$) or light-adapted b-wave ($p=0.86$) implicit

times (Figure 5.4A,C). Notably, the dark-adapted b-wave response was significantly faster in both immunoproteasome KO strains ($F(2,25) = 4.30$, $p=0.03$) (Figure 5.4B).

The decrease in the dark-adapted b-wave implicit time could lead to a premature truncation of the a-wave [287]. To determine if the decrease in the dark-adapted a-wave could be an artifact of a faster b-wave, the a-wave amplitude was reanalyzed at 7 ms at the four highest flash intensities for all strains. This time point occurs before the first negative peak in all ERG waveforms. At 7 ms, the dark-adapted a-wave amplitudes were not significantly different between WT and the KO mice ($p=0.45$) suggesting no difference in photoreceptor response to light (Figure 5.2E).

To confirm the results of the raw waveform analysis, we also evaluated the isolated components of the ERG measurements by fitting the waveform data to models as described in methods. The isolated scotopic photoreceptor contribution (PIII) provides the maximal photoreceptor response (Rm_{P3}), which is proportional to the number of ion channels in the rod outer segments that close in the response to light, and the retinal photoreceptor sensitivity to light (S) (Figure 5.5A). When the ERG waveforms were fit to this model, there was a 35% decrease in the maximal rod photoreceptor response (Rm_{P3}) in both L7 and L7M1. However, due to the high variability between animals, this apparent difference between strains was not significant ($p=0.058$). There was no difference in retinal sensitivity (S) between strains ($p=0.38$). These data agree with the dark-adapted a-wave analyzed at 7ms; indicating that there is no change in the photoreceptor response in L7 and L7M1 mice.

The post-receptoral b-wave response was modeled to measure the maximum scotopic, b-wave response (Vm_{DA}) and the post-receptoral sensitivity ($\log \sigma$). The sensitivity of the post-receptoral response was not significantly different in $\log \sigma$ ($p=0.86$) (Figure 5.5B). The L7 and L7M1 mice exhibited a 30% decrease in the maximal dark-adapted b-wave (Vm_{DA}) ($H(2) = 12.90$, $p=0.002$) as compared to WT (Figure 5.5B). These data are consistent with the raw b-wave amplitude measures indicating a significant difference in the bipolar cell response of the retinas deficient in immunoproteasome.

The effects of immunoproteasome-deficiency on OP amplitude and implicit time were also examined. The individual OPs displayed a similar pattern between strains so the summed OP amplitudes and implicit times were analyzed. No significant difference in summed OP amplitudes ($p=0.42$) or implicit times ($p=0.06$) was observed between strains (Figure 5.6A,B).

5.3.3. Assessment of cells and proteins involved in the ERG response

To begin exploring potential mechanisms responsible for the loss in retinal function exhibited by KO mice, we quantified the cells specifically involved in producing the ERG signal (i.e., photoreceptor and bipolar cells) as well as the content of select proteins involved in visual transmission. The relative content of photoreceptor proteins (rhodopsin (rods) and opsin (cones)) was determined using slot blot immunoassays. In two-month-old mice, no difference in rhodopsin ($p=0.99$) or opsin ($p=0.63$) content was observed between strains (Figure 5.7A). Consistent with these results, no difference in photoreceptor outer segment length (measured on H&E stained retinal sections) was observed comparing immunoproteasome-deficient retinas with WT ($p=0.26$; data not shown).

The b-wave response is mainly produced from the bipolar cells whose nuclei are located in the INL. Retinal morphology data did not show a difference in nuclei density in the INL between mouse strains (Figure 5.1C). However, the INL contains nuclei of multiple cell types (i.e. amacrine, horizontal, and bipolar cells) and thus counts of nuclei density are not specific for bipolar cells [108]. To determine if there was a specific loss in rod or cone bipolar cells, counts of total bipolar and rod-specific bipolar cells were performed on retinal sections double-stained with antibodies to Chx10 (bipolar cell marker) and PKCα (rod bipolar cell marker). Rod bipolar cells were identified by the colocalization of Chx10 and PKCα [284]. Conversely, cone bipolar cells only stain with Chx10. No significant difference in either total ($p=0.67$) or rod ($p=0.33$) bipolar cell density was observed between strains (Figure 5.8). Therefore, changes in total or photoreceptor-specific bipolar cell content does not account for the observed decrease in bipolar cell response in L7 and L7M1 mice.

Although the overall content of the cell types that produce the ERG signal are not changed with immunoproteasome-deficiency, the proteins involved in transmitting the visual signal could be affected. Proteasome is a key regulator of the protein content of some of the synaptic proteins, such as PSD95, synaptophysin and several glutamate receptors [224, 225]. It is plausible that immunoproteasome regulates the content of a subset of these proteins. To determine if immunoproteasome-deficiency affects synaptic protein content, we examined the presynaptic protein PSD95, the synaptic vesicle protein synaptophysin, and the post-synaptic proteins metabotropic glutatmate receptor 6 (mGluR6) and transient receptor potential member 1 (TRPM1) by Western blot. There was no significant difference in either the content of PSD95 ($p=0.44$) or synaptophysin ($p=0.51$) (Figure 5.7B). As a caveat, it is important to mention that both PSD95 and synaptophysin are located both in the inner (IPL) and outer plexiform layers (OPL), which could reduce the sensitivity of this assay in detecting changes localized to the OPL [289, 290].

TRPM1 is a bipolar cell protein that was recently identified as the cation channel that generates the b-wave.[133, 134] The 184 kD isoform makes the cation channel but the function of the other isoforms remains unclear.[133] There was no difference in the protein content of any of the TRPM1 isoforms, including the 184 kDa cation channel ($p\geq0.11$) (Figure 5.7C).

The bipolar cell glutamate receptor, mGluR6, is the initiator of the G-protein cascade that ultimately opens the TRPM1 cation channel. There was an approximate 30% decrease in mGluR6 in L7 and L7M1 retinas as compared to WT. Due to large variability in the sample group, a nonparametric test was required, and therefore this decrease was not significant. ($p=0.13$) (Figure 5.7B).

5.4. Discussion

The current study utilized immunoproteasome KO mice lacking either one (*lmp7*$^{-/-}$, L7) or two (*lmp7*$^{-/-}$/*mecl-1*$^{-/-}$, L7M1) catalytic subunits of the immunoproteasome to test the hypothesis that immunoproteasome is required to maintain normal retinal function. Retinal morphometry (Figure 5.1) and quantitative measures of several retinal cell types

(photoreceptor and bipolar cells) (Figure 5.7, 5.8) showed no major abnormalities in overall retinal morphology in KO mice. Evaluation of retinal function by ERG showed significantly decreased amplitude in the dark- and light-adapted b-waves, suggesting immunoproteasome deficiency is associated with both rod and cone pathway defects (Figure 5.2-5.4). Correlation plots of a- and b-wave amplitudes (Figure 5.2) and altered implicit times (Figure 5.4) further imply abnormal signal transmission resulting from defects in the secondary neurons. Analysis of the content of a subset of proteins involved in signal transmission showed no significant decrease. Taken together, the data suggest that immunoproteasome deficiency causes defects in bipolar cell response. These results support a previously unrecognized role for immunoproteasome in vision transduction.

Immunoproteasome has a well-described role in the immune system. Therefore, it is possible that the loss in retinal function observed in L7 and L7M1 mice could be due to changes in the systemic immune system that could affect overall retinal health. Based on the literature, there is no evidence that these mice are immunologically impaired (i.e. develop autoimmune disease or immunodeficiency). In fact, only minor changes in T-cell populations and proliferation in L7 and L7M1 mice have been reported.[105, 106] Under our laboratory conditions, the mice are healthy and breed well. Additionally, there is no evidence of retinal inflammation based on the lack of gross morphological changes up to 24 months of age (Figure 5.1). Overall, there is currently no evidence that the lack of specific immunoproteasome subunits can substantially impair the systemic immune function. However, subtle, currently undescribed changes in the immune system that have an effect on retinal function are possible.

Another potential mechanism behind the altered ERG waveforms in immunoproteasome KO mice could be that the content of some proteins involved in phototransduction or visual transmission are regulated by the immunoproteasome. The direct knock-out of many of these visual transmission proteins (i.e. RPE65, rhodopsin, TRPM1, mGluR6) causes a severe ERG phenotype (greater than 75% decrease in amplitudes) [134, 187, 207, 208, 210, 212, 214, 215, 221]. In immunoproteasome knock-out mice, we observed only a 25% decrease in the dark-adapted b-wave. In the current study, we evaluated the content of select proteins in each pathway and found a 30%

decrease in mGluR6 in the KO mice. Although this change was not significant, it suggests there could be subtle changes in protein content of other proteins as well. The synergistic effect of altering the content of several proteins involved in visual transmission could have an effect on retinal function. Ongoing comparative analysis of the retinal proteome will provide important molecular details of how immunoproteasome deficiency impacts the retina.

In addition to the proteins directly involved in signal transduction or transmission, changes in proteins required for maintaining retinal structural integrity can also caused altered ERG waveforms. Mutations or elimination of the structural proteins bassoon, dystroglycan, and retinoschisin resulted in a decrease in the b-wave that was associated with the inability to efficiently transmit the visual signal from the photoreceptors to the bipolar cells [199, 218, 219]. The gross retinal morphology of bassoon and dystroglycan mutants both appear normal, however, ultrastructural changes in ion channels or synaptic spherules are present [199, 219]. In-depth investigation of synaptic junction morphology of immunoproteasome KO retinas could help determine if subtle changes in alignment of synapses between photoreceptors and bipolar cells are responsible for their decreased visual transmission.

Altered ERG waveforms have also been observed with reduction or elimination of proteins not directly linked to vision, but which are ubiquitously involved in maintaining retinal homeostasis. One of the critical requirements for maintaining retinal homeostasis is the tight regulation of cellular redox status, which reflects the balance between production and elimination of harmful reactive oxygen and nitrogen species. These reactive molecules upset homeostasis when they damage DNA, lipids and proteins. In the retina, the highly abundant copper-zinc superoxide dismutase (CuZn SOD) is a key antioxidant for maintaining retinal homeostasis via elimination of superoxide [291]. Recent studies of retinal function in CuZn SOD KO mice (*sod1*$^{-/-}$) showed ~30% reduction in both a- and b-wave amplitudes that correlated with a 15-20% decrease in ONL and INL nuclear density [222]. Additionally, ribozyme-induced reduction of the manganese SOD (MnSOD; *sod2*), which is localized to the mitochondria, also caused a similar reduction in a- and b-wave amplitudes and ONL nuclear density [292].

Conversely, the neuroprotective effect of boosting cellular antioxidant capacity via induced expression of antioxidant enzymes or the introduction of antioxidant supplements in various retinal degeneration models suggests a critical role for tight regulation of redox status in retinal function [293-295].

In our previous work, we have shown that retinal cells respond to elevated levels of oxidative stress due to disease [86], aging [6], and exposure of cultured cells to peroxide [6] by upregulating the immunoproteasome. These results imply an important role for immunoproteasome in responding to and protecting from oxidative damage. Consistent with this idea, retinal pigment epithelial cells from L7M1 mice were more susceptible to peroxide-induced death compared with WT cells [6]. There are several possible means by which immunoproteasome protects cells from oxidative damage. As has been suggested previously, immunoproteasome could be involved in the degradation of oxidatively modified proteins [90]. Inadequate turnover of damaged proteins caused by immunoproteasome deficiency could allow dysfunctional proteins involved in visual transmission to accumulate. Immunoproteasome could also participate in cell signaling in response to oxidative stress by regulating the content of key proteins in the cascade. Activation of the kinase Akt [98] and transcription factor NFκB [10, 11] are two examples where regulation of stress-induced signaling has been linked to immunoproteasome.

Proteasome degrades protein substrates into peptides ranging in size from 3 to 22 amino acids [67]. Some of these peptides could be biologically active and regulate proteins or pathways critical for normal vision transmission. The importance of neuropeptides and hormones generated by carboxypeptidase E in maintaining normal vision transmission was demonstrated in carboxypeptidase E KO mice, which exhibit decreased b-wave amplitudes and altered synaptic vesicle biogenesis [35, 296]. Previous reports have shown that the standard, intermediate-type, and immunoproteasome produce peptides that are unique to each proteasome sub-type [30, 246]. While WT retina most likely contains all three proteasome subtypes, L7 and L7M1 retina (that still have the full complement of LMP2) contains only populations of standard and intermediate-type proteasomes [6]. Therefore, the difference in proteasome subpopulations may result in

diminished ERG response in KO mice through the absence of biologically active peptides uniquely produced by the immunoproteasome.

In conclusion, using immunoproteasome-deficient mice, we have demonstrated an essential role for the immunoproteasome in normal vision transmission. These results, along with our previous reports suggesting a role for immunoproteasome in responding to stress and injury [6, 8], provide unequivocal evidence that immunoproteasome functions beyond its well described role in immune surveillance. Thus, the name "immunoproteasome" is misleading, since it acknowledges only one aspect of the ever-increasing roles discovered for this intriguing protein.

Table 5.1. Antibodies used for immunoblotting and immunohistochemistry

Antibody [a]	Type [*]	Assay [†]	Dilution	Company
Rhodopsin	M	B	1:1000	BIODESIGN International, Saco, ME
Opsin: Red/green	C	B	1:500	Millipore, Billerica, MA
PKCα	R_M	I	1:1000	Abcam, Cambridge, MA
Chx10	S	I	1:200	Abcam, Cambridge, MA
PSD95	R_P	B	1:1000	Cell Signaling Technology, Danvers, MA
Synaptophsin	M	B	1:1000	Millipore, Billerica, MA
mGluR6	R_P	B	1:1000	Neuromics, Edina, MN
TRPM1	R_P	B	1:1000	Abcam, Cambridge, MA

Protein kinase C, alpha (PKCα); Ceh-10 homeo domain containing homolog (Chx10); Postsynaptic density protein 95 (PSD95); Metabotropic glutamate receptor 6 (mGluR6); Transient receptor potential cation channel subfamily M, member 1 (TRPM1).

[*]Monoclonal, host species mouse (M), IgG; monoclonal, host species rabbit (R_M), IgG; polyclonal, host species rabbit (R_P), IgG; polyclonal, host species chicken (C), IgY; polyclonal, host species sheep (S), IgG.

[†]Immunohistochemistry (I); Western or slot blot immunoassays (B).

Figure 5.1. Age- and strain-related changes in retinal morphology and apoptosis. (A) Representative paraffin-embedded retinal sections stained with hematoxylin and eosin (H&E) from 2-month-old WT, L7 and L7M1 mice. Images were taken with a 20x objective. Bar in WT panel indicates 50 μm. GCL, ganglion cell layer; INL, inner nuclear layer; IPL, inner plexiform layer; IS, inner segments, ONL, outer nuclear layer; OPL, outer plexiform layer; OS, photoreceptor outer segments. (B-D) Summary of retinal morphology and TUNEL measurements for WT (■), L7 (○) and L7M1 (Δ) retinas. Two-way ANOVA results are provided in each panel. When there was significant interaction (SxA), one-way ANOVA comparisons were performed for each strain and each age. Results of Tukey-Kramer post-hoc comparisons are indicated by letters, numbers, or symbols. (B) ONL nuclei density measured at 500 and 1000 μm from the optic nerve. Two-way ANOVA for the nuclei densities at 500 μm showed significant interaction ($F(8,133) = 2.74$, $p<0.01$). One-way ANOVA results by strain with age: (WT, $p<0.001$; L7M1, $p=0.001$) a, different from WT 2 months; b, different from WT 15 months; x, different from L7M1 2 months. One-way ANOVA results by age between strains: (9 months, $p=0.008$, 15 months, $p<0.001$) 1, different from L7 and WT at 9 months; 2, different from WT at 15 months. Two-way ANOVA for the nuclei densities at 1000 μm showed a significant decline with age ($F(4,133) = 4.64$, $p=0.002$); #, different from 2 months. (C) TUNEL positive nuclei in the ONL. Two-way ANOVA for TUNEL positive nuclei in the ONL showed significant interaction ($F(8,124) = 2.41$, $p=0.02$). One-way ANOVA results by strain with age: (WT, $p=0.002$; L7, $p<0.01$; L7M1 $p<0.001$) a, different from WT 2 months, b, different from WT 9 months, x, different from L7 2 months, y, different from L7M1 2 and 9 months; z, different from L7M1 24 months. One-way ANOVA results by age between strains: (2 months, $p=0.003$; 15 months, $p<0.001$; 20 months, $p=0.002$) 1, different from L7 and WT. (D) INL nuclei density decreased with age at both 500 μm (Two-way ANOVA $F(4,132) = 9.51$, $p<0.001$) and 1000 μm (Two-way ANOVA $F(4,133) = 4.01$, $p=0.004$) from the optic nerve; #, different from 2 months. However there were no differences between strains at either 500 μm ($p=0.21$) or 1000 μm ($p=0.16$). Data is shown as mean ± SEM. WT n=7-18; L7 n=5-11; L7M1 n=6-19 per group.

Figure 5.1. Age- and strain-related changes in retinal morphology and apoptosis.

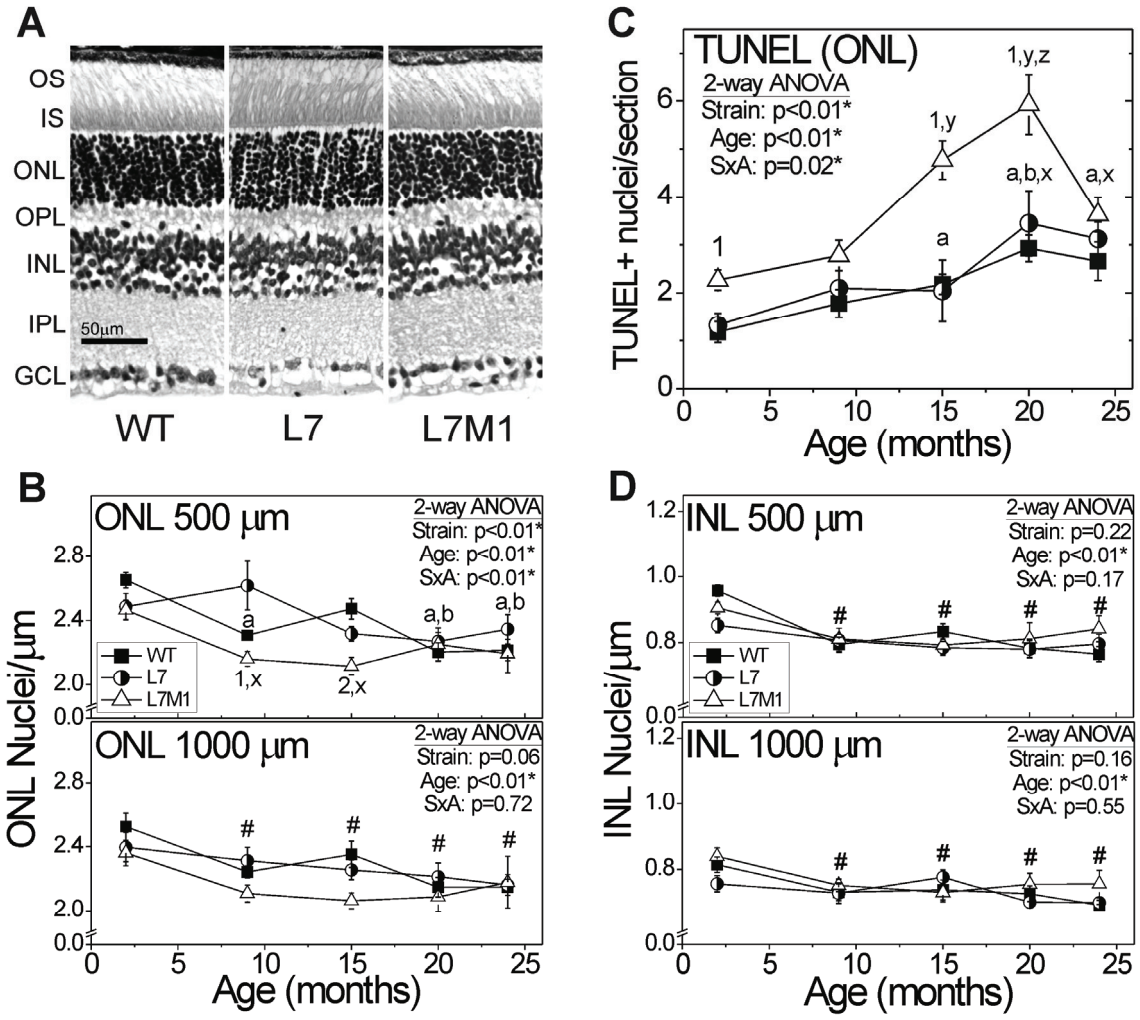

Figure 5.2. Strain-related changes in dark-adapted retinal response measured by electroretinography.

(A) Representative dark-adapted waveforms for 2 mo. WT, L7, and L7M1 mice. (B-D) Average dark-adapted amplitudes from ERGs performed on WT (■), L7 (○) and L7M1 (Δ) mice. (B-C) Repeated measures ANOVA tests were performed: *, WT different from L7M1 and L7. (B) Dark-adapted a-wave amplitudes ($F(4.95,61.8) = 3.61$, $p=0.006$). (C) Dark-adapted b-wave amplitudes ($F(4.25,53.17) = 4.00$, $p=0.006$). (D) Dark-adapted b-wave plotted against the dark-adapted a-wave. (E) Dark-adapted a-wave amplitude at 7 ms ($p=0.45$). WT n=11-12; L7 n=6; L7M1 n=10.

Figure 5.2. Strain-related changes in dark-adapted retinal response measured by electroretinography.

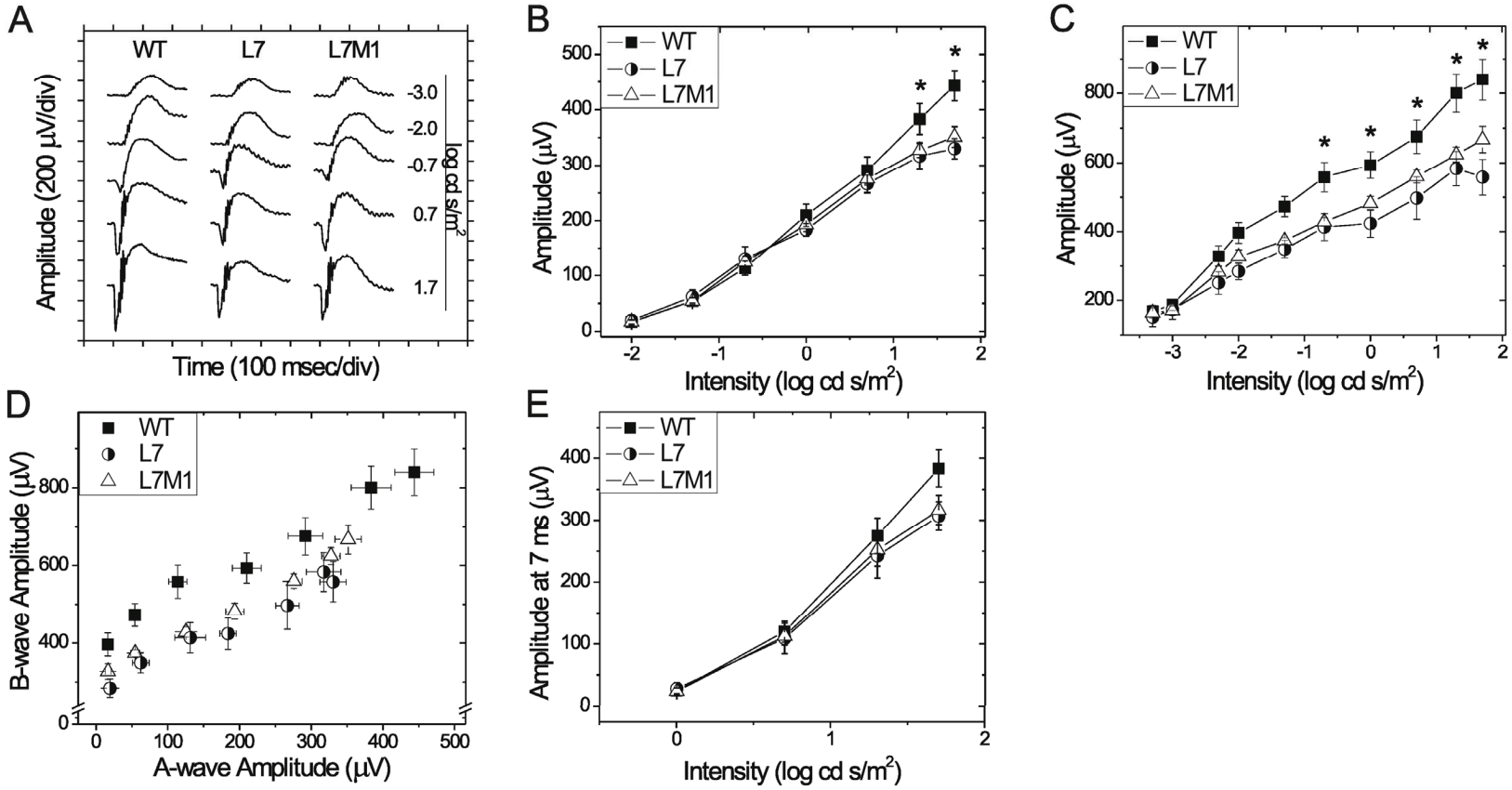

Figure 5.3. Strain-related changes in light-adapted retinal response measured by electroretinography.

(A) Representative light-adapted waveforms for 2 mo. WT, L7, and L7M1 mice. (B) Average light-adapted b-wave amplitudes from ERGs performed on WT (■), L7 (○) and L7M1 (Δ) mice. Repeated measures ANOVA tests were performed: *, WT different from L7M1 and L7; @, L7 different from WT and L7M1. L7 and L7M1 KO mice had significantly lower amplitudes compared to WT ($F(4.22,52.8) = 6.56$, $p<0.001$). Data are shown as mean ± SEM. WT n=12; L7 n=6; L7M1 n=10.

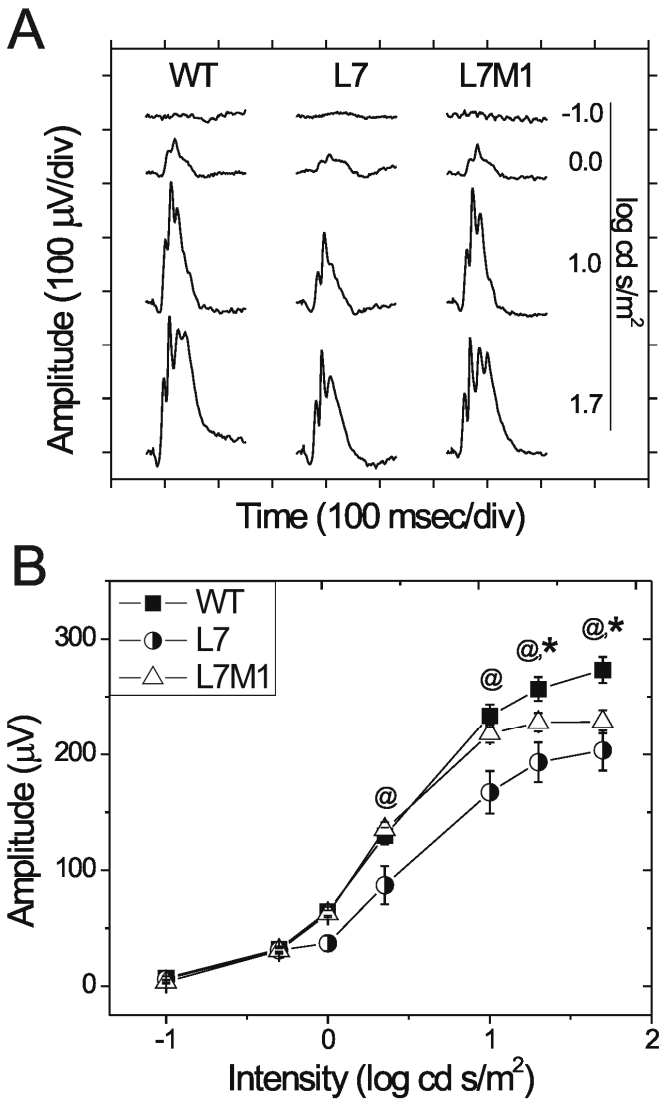

Figure 5.4. Strain-related changes in ERG implicit time.

(A-C) Average implicit times from ERGs performed on WT (■), L7 (○) and L7M1 (Δ) mice. Repeated measures ANOVA tests were performed. (A) Dark-adapted a-wave implicit times ($p=0.09$). (B) Dark-adapted b-wave implicit times. Repeated measures ANOVA revealed a strain effect: ($F(2,25) = 4.30$, $p=0.03$) *, different from WT. (C) Light-adapted b-wave implicit times ($p=0.86$). Data are shown as mean ± SEM. WT n=12; L7 n=6; L7M1 n=10.

Figure 5.4. Strain-related changes in ERG implicit time.

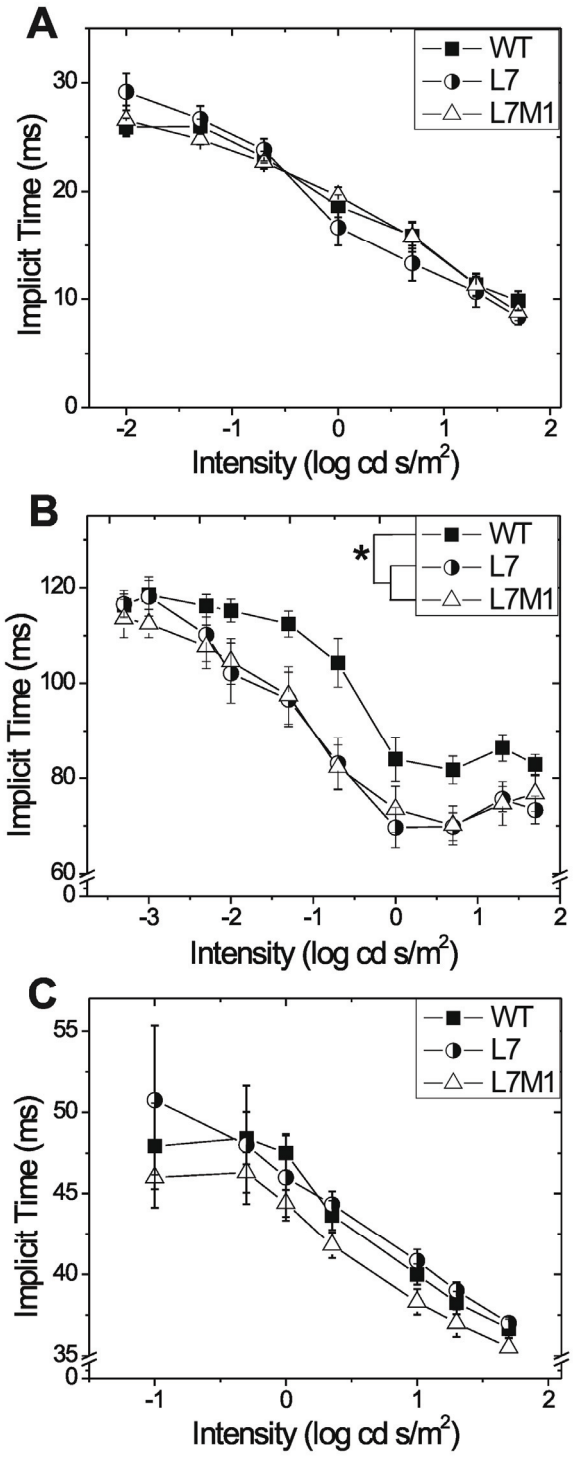

Figure 5.5. Strain-related changes in ERG parameters.

Average ERG parameters derived from mathematical models from WT (solid), L7 (striped) and L7M1 (cross-hatched) mice. One-way ANOVA or KW one-way ANOVA followed by Tukey-Kramer or Z-value multiple comparison tests were performed; *, different from WT at $p<0.05$. (A) Isolated rod photoreceptor response (Rm_{P3}; p=0.058) and sensitivity (S; p=0.38) of WT (solid), L7 (striped) and L7M1 (cross-hatched) retinas. (B) Maximal dark-adapted post-receptoral response (bipolar cells) (Vm_{DA}; H(2) = 12.90, p=0.002) and sensitivity (log σ; p=0.86). Data are shown as mean ± SEM. WT n=11; L7 n=6; L7M1 n=9.

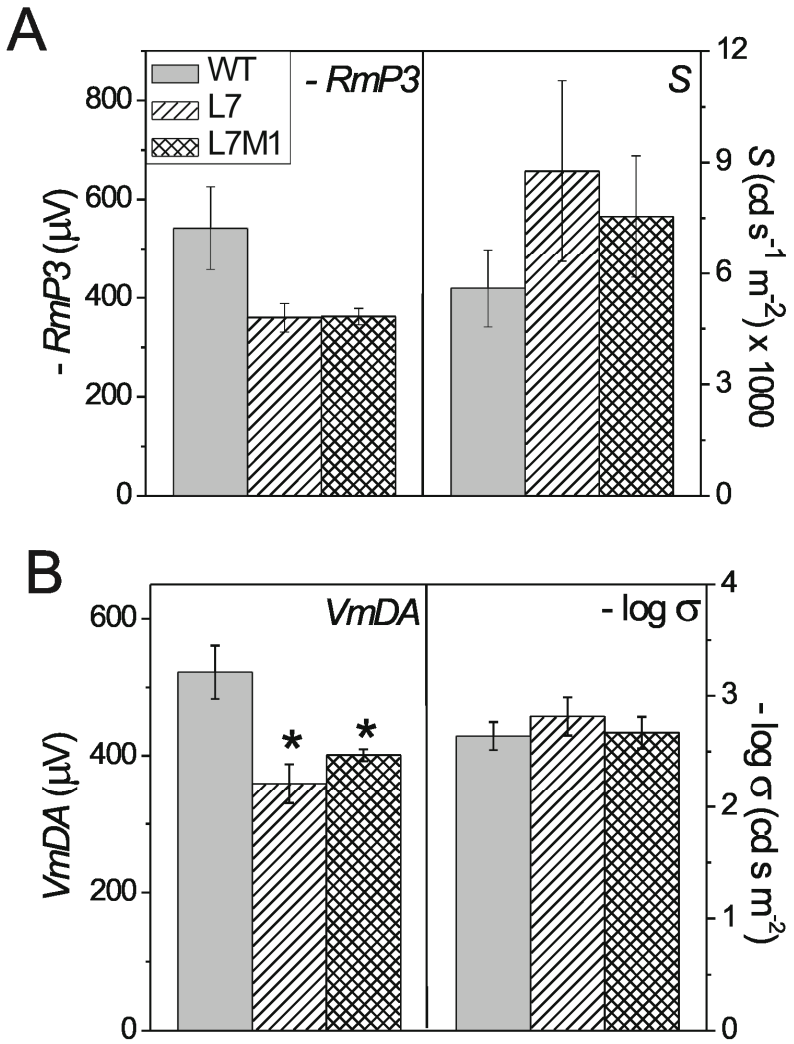

Figure 5.6. Summary of filtered oscillatory potentials.

(A) Summed amplitudes of oscillatory potentials 1-6 from WT (■), L7 (○) and L7M1 (Δ) mice. Repeated measures ANOVA tests showed no significant difference between strains (p=0.42). (B) Summed implicit times (ITs) for oscillatory potentials 1-6. Repeated measures ANOVA tests showed no significant difference between strains (p=0.06). Data are shown as mean ± SEM. WT n=11; L7 n=6; L7M1 n=9.

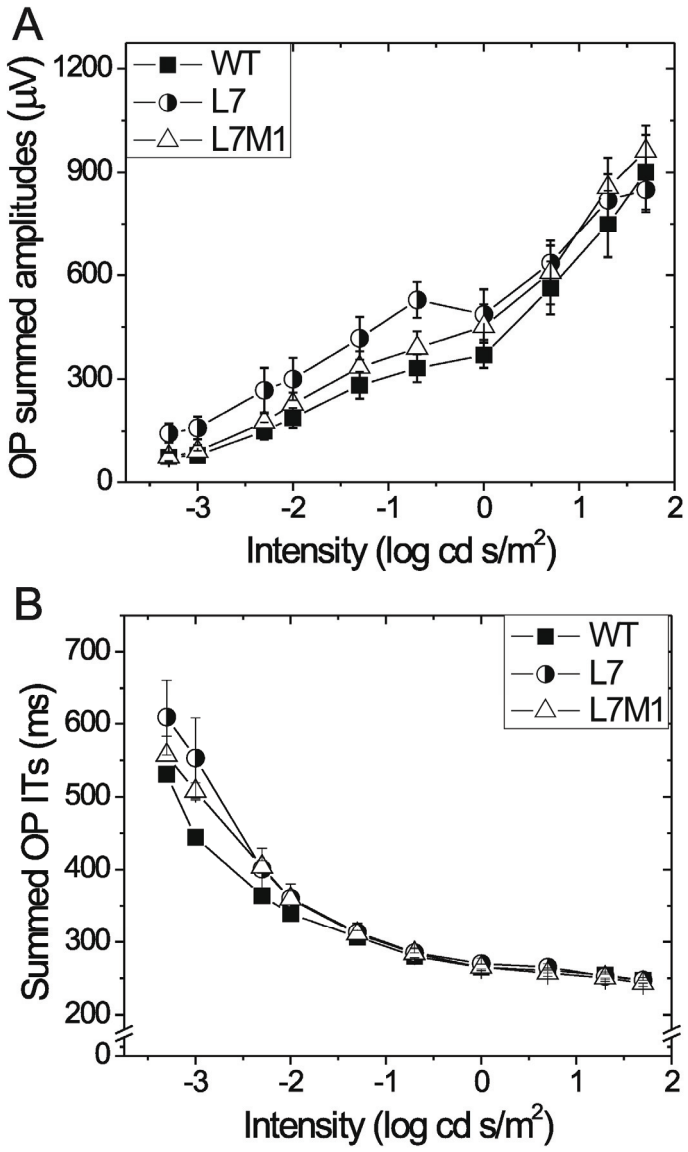

Figure 5.7. **Content of photoreceptor and synaptic proteins.**
Summary immunoblot data for retinal photoreceptor and synaptic proteins from two-month-old WT (solid), L7 (striped) and L7M1 (cross-hatched) mice. One-way ANOVA or KW one-way ANOVA was performed for each protein. (A) Relative content measured from slot immunoblots for photoreceptor proteins: rhodopsin and opsin. There were no significant differences between strains in either relative opsin ($p=0.63$) or rhodopsin ($p=0.99$) content. (B) Relative Western blot density for synaptic proteins: PSD95, synaptophysin, and mGluR6. There was no significant difference between strains for PSD95 ($p=0.44$), synaptophysin ($p=0.51$) or mGluR6 ($p=0.14$). (C) Relative Western blot density for three TRPM1 isoforms: 184 kDa, 83 kDa, and 60 kDa. ANOVA showed no significant difference between strains for any isoform ($p=0.56$; $p=0.11$; $p=0.18$, respectively). Data are shown as mean ± SEM. WT n=6-19; L7 n=4-18; L7M1 n=6-14 per group.

Figure 5.7. Content of photoreceptor and synaptic proteins.

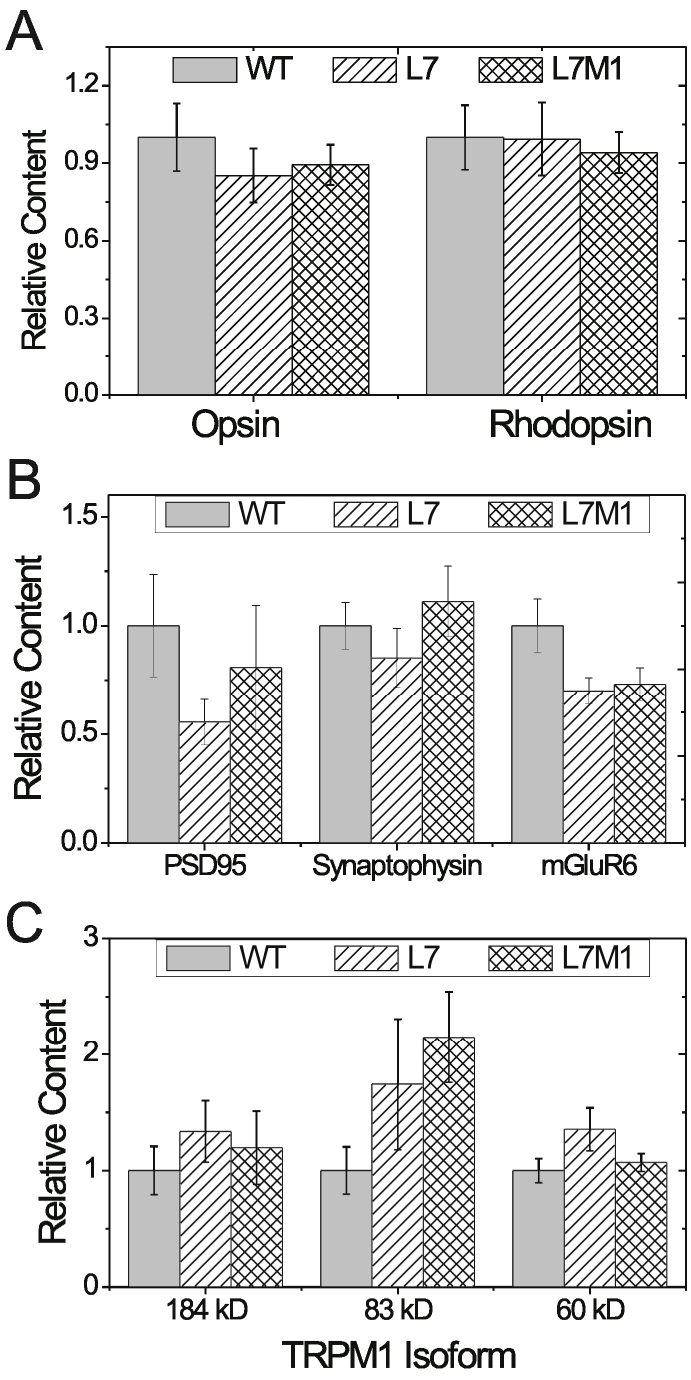

Figure 5.8. Unaltered bipolar cell densities in two-month-old WT, L7, and L7M1 retina.

Summary of bipolar cell densities and distribution of rod and cone bipolar cell populations. One-way ANOVA tests were performed on total (striped) and rod (gray) bipolar cell density. No significant difference was detected between strains for either total (p=0.67) or rod (p=0.33) bipolar cell density. Data are shown as mean ± SEM. WT n=5; L7 n=6; L7M1 n=6.

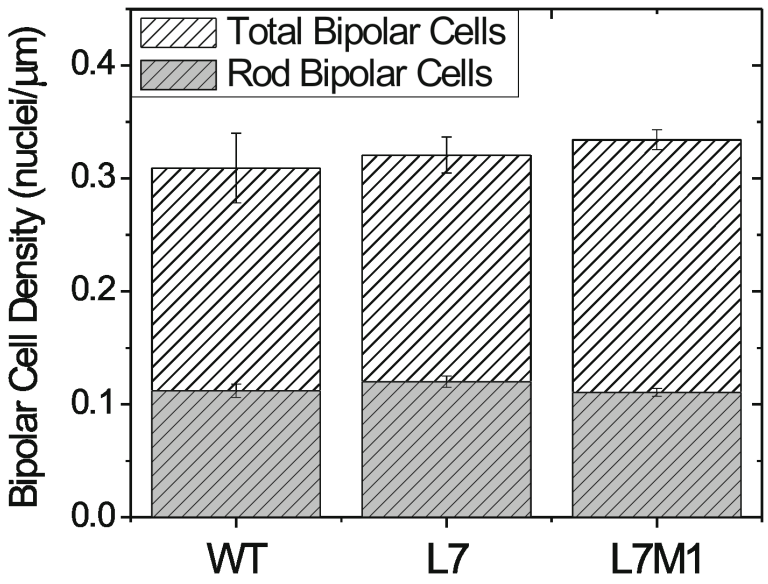

Chapter 6

Summary and Future Directions

6.1. Summary

Previously, the immunoproteasome was thought to function exclusively in the generation of antigenic peptides. However, more recent data, including data from this thesis, supports alternative roles for this intriguing protein complex [6-11, 93-95, 98]. These studies have suggested that immunoproteasome may have a more basic physiological role in the cell.

Data from this thesis shows that immunoproteasome is localized in non-antigen presenting cells of the brain and retina. Both the brain and retina are immune-privileged tissues and thus have a dampened immune response. Therefore, immunoproteasome is unlikely to function as part of the immune system, especially in non-antigen presenting cells. Our data support the hypothesis that immunoproteasome is a key player in responding to stress. Data that support this hypothesis include the 2-fold higher content of immunoproteasome in retina compared with brain. The difference in immunoproteasome content likely reflects the higher basal stress experienced by the retina versus the brain [87]. Immunoproteasome was also upregulated in response to disease (age-related macular degeneration, Chapter 2), injury (CTL-induced injury, Chapter 3), the chronic stress of aging (Chapter 4), and acute oxidant-induced stress (Chapter 4) in the immune-privileged retina. Taken together, these data support the hypothesis that immunoproteasome upregulation is a generalized response to stress.

One of the most interesting links produced from this research was the critical requirement for immunoproteasome during oxidative stress. Support for this link includes the increased susceptibility of immunoproteasome-deficient cultured cells to peroxide and the increased apoptosis in aged L7M1 retina. Also supporting the link between immunoproteasome and the protection from oxidative stress are two high-profile papers that were recently published [93, 94]. The authors showed the immunoproteasome was able to degrade oxidized proteins more efficiently than standard proteasome, revealing a possible mechanism for immunoproteasome's protective ability during oxidative stress.

Another physiological role that has emerged from this research is the requirement for immunoproteasome in maintaining retinal function. Using electroretinography,

results showed that L7 and L7M1 mice had a significantly reduced b-wave (bipolar cell) response as compared to WT (Chapter 5). In investigating the mechanism, data revealed that the difference in response was not due to a change in the photoreceptor or bipolar cell population. Nor was it due to a change in content of select synaptic proteins (e.g., PSD95, synaptophysin, mGluR6, or TRPM1). However, many other proteins are involved in visual transmission and the immunoproteasome could be involved in regulating their content. Immunoproteasome could also have an effect on retinal function by regulating signaling pathways in the retina such as NFκB or Akt, or through the production of neuropeptides. Further studies are needed to determine the mechanism behind the requirement for immunoproteasome in maintaining normal visual transmission.

This thesis also explored the connection between immunoproteasome subunit content and the rate of peptide hydrolysis by the proteasome (Chapter 4). Previous studies as to whether standard or immunoproteasome had higher activity have been controversial. The controversy is due to inadequate systems for comparing activity and appears to depend on cell treatment and/or the tissue type in the experiment. To eliminate these complicating factors, we isolated standard and immunoproteasome from spleen by utilizing our immunoproteasome KO mice (L7M1). WT spleen contains mainly immunoproteasome. In contrast, spleen from L7M1 mice is missing two out of the three immunoproteasome subunits and has lower expression of the third (LMP2) subunit. Therefore, L7M1 spleen contains mainly standard proteasome. Using this model system, results showed that standard proteasome had higher chymotrypsin- and caspase-like activity as compared to immunoproteasome. These data are in contrast to some of the previous reports that state the immunoproteasome had higher chymotrypsin-like activity [22, 23].

6.2. Future directions

- **Immunoproteasome and visual transmission**

This thesis has shown evidence that immunoproteasome is required for normal visual transmission (Chapter 5). Future experiments will focus on determining the

mechanism of immunoproteasome's involvement in retinal function. One potential function for immunoproteasome is the regulation of the development of the synapse between the photoreceptors and bipolar cells. Ultrastructural changes to ion channels and/or synaptic spherules are known to cause an ERG phenotype [198, 199]. Therefore, future experiments are planned to determine if immunoproteasome-deficiency causes changes in synaptic structure using electron microscopy.

Taken together, immunoproteasome's localization to the OPL and the decreased b-wave response in immunoproteasome KO mice indicate that immunoproteasome is important in visual transmission. The exact localization of immunoproteasome has yet to be determined, which could provide insight into the role of immunoproteasome in retinal function. The OPL contains the synapses between the photoreceptors, horizontal cells, and bipolar cells. Localization of immunoproteasome to a specific cell type using immunofluorescence cell-specific markers, will aid in understanding the role of immunoproteasome in visual transmission. Once immunoproteasome cellular localization is determined, experiments will be conducted to express immunoproteasome subunits with cell-specific promoters to determine if retinal function can be rescued in immunoproteasome KO mice.

From this thesis we have also learned that immunoproteasome is protective against oxidative stress (Chapter 4) and is involved in maintaining normal retinal function (Chapter 5). Future studies will evaluate whether immunoproteasome's role in stress response plays a role in maintaining retinal function. As stated previously, the retina is exposed to high stress levels on a daily basis due to its high exposure to light and metabolic demands [87]. Therefore, as shown in the SOD1 KO mice, increased oxidative stress, with age, causes a decrease in the a- and b-waves of the ERG. Future experiments will determine whether immunoproteasome KO mice also have an exacerbated ERG phenotype with age.

For these future experiments, we have also generated a strain of KO mice that have the SOD1, LMP7, and MECL-1 genes genetically ablated (triple KO). These mice were developed by crossing an SOD1 KO mouse strain to the L7M1 strain of immunoproteasome KO mice. Both strains of mice were on the C57BL/6 background so

no backcrossing was required. SOD1 is one of the most abundant antioxidant enzymes in the retina [291]. Therefore, SOD1 KO mice have a higher basal level of oxidative stress [291]. Since L7M1 cultured cells have been shown to be more sensitive to oxidative stress, it is expected that the triple KO mouse strain will have an accelerated phenotype due to the greater level of oxidative stress (SOD1 KO) and the decreased ability to cope with that stress (L7M1).

To test this hypothesis, future experiments will evaluate the ERG phenotype with age in WT, L7M1, SOD1 KO and triple KO mice. In tandem with the ERG phenotype, changes in retinal morphometry will also be determined. In the triple KO mouse strain, an accelerated decrease in the a- and b-waves of the ERG is expected, in comparison to the other strains. In addition, an accelerated decrease in nuclei density of the ONL and INL layers of the retina is also anticipated.

- **Involvement of immunoproteasome in Akt and NFκB signaling pathways with acute retinal injury**

Future experiments are also planned to elucidate the mechanism involved in immunoproteasome's protective abilities. Previous data has implicated that the immunoproteasome has a role in several signaling pathways, including the NFκB (Figure 1.5) [9-11, 95, 96] and the Akt (Figure 1.6) pathways [98]. Future experiments are planned to further test the immunoproteasome's involvement in these pathways.

Optic nerve crush is an injury model for glaucoma that specifically affects the retinal ganglion cells. This injury involves partial axotomy of the optic nerve, which is comprised of the axons of the ganglion cells. In WT animals, there is a predictable time course of ganglion cell death via apoptosis accompanied by cell loss. Both the NFκB and IGF-1 pathways are affected with this type of injury. NFκB nuclear content has been shown to be 2-fold higher with glaucoma [297] and the IGF-1/Akt pathway has been suggested to play an integral role in controlling apoptosis in retinal ganglion cells [103].

The LMP2 immunoproteasome subunit in particular has been shown to be an important player in both the NFκB and Akt pathways. Therefore a breeding colony of the *lmp2*$^{-/-}$ (L2) strain of immunoproteasome KO mice has been obtained. The response to optic nerve crush will be compared in WT, L2, and L7M1.

Future experiments are planned to test both the NFκB and Akt signaling pathways. Specifically, the cytoplasmic and nuclear content of p65, one of the NFκB transcription factors, will be determined to test the level of NFκB activation. Immunoproteasome, especially LMP2, has been suggested to be involved in the activation of NFκB and hence we hypothesize there will be little change in the activation levels of p65 with optic nerve crush.

Previous reports have shown that IGF-1 is significantly down-regulated with optic nerve crush, resulting in a decrease in phosphorylated Akt (activated, pAkt) (see Figure 1.6). This decrease in pAkt is suggested to be responsible for the increase in retinal ganglion cell apoptosis with optic nerve injury by controlling the pro- and anti-apoptotic proteins of the Bcl-2 family [103]. Therefore, future experiments will determine the content and phosphorylation state of proteins involved in this pathway (i.e., Akt, pAkt, Bad, pBad, Bcl-2, Bax). We hypothesize that the L2 and L7M1 KO mice will show a differential response in the optic nerve injury time course as compared to WT. As LMP2 has previously been shown to be involved in pAkt activation [98], the hypothesis is that pAkt will be lower in control LMP2 mice and there will be a delay in the decrease of pAkt.

Furthermore, using RPE cell lines isolated from WT, L2, and L7M1 mice, experiments are planned to test the role of immunoproteasome in the NFκB pathway. The cell culture technique is very useful to test the cellular response to different stimuli in a controlled environment.

References

1. Ciehanover, A., Y. Hod, and A. Hershko, *A heat-stable polypeptide component of an ATP-dependent proteolytic system from reticulocytes.* Biochem. Biophys. Res. Commun., 1978. **81**(4): p. 1100-1105.
2. Etlinger, J.D. and A.L. Goldberg, *A soluble ATP-dependent proteolytic system responsible for the degradation of abnormal proteins in reticulocytes.* Proc. Natl. Acad. Sci. USA, 1977. **74**(1): p. 54-58.
3. Wilk, S. and M. Orlowski, *Cation-sensitive neutral endopeptidase: Isolation and specificity of the bovine pituitary enzyme.* J. Neurochem., 1980. **35**(5): p. 1172-1182.
4. Orlowski, M. and S. Wilk, *A multicatalytic protease complex from pituitary that forms enkephalin and enkephalin containing peptides.* Biochem. Biophys. Res. Commun., 1981. **101**(3): p. 814-822.
5. Wilk, S. and M. Orlowski, *Evidence that pituitary cation-sensitive neutral endopeptidase is a multicatalytic protease complex.* J. Neurochem., 1983. **40**(3): p. 842-849.
6. Hussong, S.A., et al., *Immunoproteasome deficiency alters retinal proteasome's response to stress.* J. Neurochem., 2010. **113**(6): p. 1481-1490.
7. Hussong, S.A., et al., *A novel role for immunoproteasome in retinal function.* Invest. Ophthalmol. Vis. Sci., 2010. **DOI: 10.1167/iovs.10-6032**.
8. Ferrington, D.A., et al., *Immunoproteasome responds to injury in the retina and brain.* J. Neurochem., 2008. **106**(1): p. 158-169.
9. Hensley, S.E., et al., *Unexpected role for the immunoproteasome subunit LMP2 in antiviral humoral and innate immune responses.* J. Immunol. 2010 Apr 15;184(8):4115-22., 2010. **184**(8): p. 4115-4122.
10. Hayashi, T. and D.L. Faustman, *NOD mice are defective in proteasome production and activation of NF-κB.* Mol. Cell. Biol., 1999. **19**(12): p. 8646-8659.
11. Hayashi, T. and D.L. Faustman, *Selected contribution: Association of gender-related LMP2 inactivation with autoimmune pathogenesis.* J. Appl. Physiol., 2001. **91**(6): p. 2804-2815.
12. Glickman, M.H. and A. Ciechanover, *The ubiquitin-proteasome proteolytic pathway: destruction for the sake of construction.* Physiol Rev. 2002 Apr;82(2):373-428., 2002. **82**(2): p. 373-428.
13. Coux, O., K. Tanaka, and A.L. Goldberg, *Structure and functions of the 20S and 26S proteasomes.* Annu Rev Biochem, 1996. **65**: p. 801-847.
14. Zavrski, I., et al., *Proteasome: an emerging target for cancer therapy.* Anticancer Drugs, 2005. **16**(5): p. 475-481.
15. Dahlmann, B. *Ubiquitons & Zomes*. [Product Guide] 2006 July, 27,2006]; Available from: www.biomol.com/ubiquitons&zomes.
16. Groll, M. and R. Huber, *Substrate access and processing by the 20S proteasome core particle.* Int. J. Biochem. Cell Biol., 2003. **35**(5): p. 606-616.
17. Klare, N., et al., *Intermediate-type 20 S proteasomes in HeLa cells: "asymmetric" subunit composition, diversity and adaptation.* J. Mol. Biol., 2007. **373**(1): p. 1-10.

18. Groll, M., et al., *The catalytic sites of 20S proteasomes and their role in subunit maturation: a mutational and crystallographic study.* Proc. Natl. Acad. Sci. USA, 1999. **96**(20): p. 10976-10983.
19. Brannigan, J.A., et al., *A protein catalytic framework with an N-terminal nucleophile is capable of self-activation.* Nature, 1995. **378**(6555): p. 416-419.
20. Orlowski, M. and S. Wilk, *Catalytic activities of the 20 S proteasome, a multicatalytic proteinase complex.* Arch. Biochem. Biophys., 2000. **383**(1): p. 1-16.
21. Marques, A.J., et al., *Catalytic mechanism and assembly of the proteasome.* Chem. Rev., 2009. **109**(4): p. 1509-1536.
22. Gaczynska, M., K.L. Rock, and A.L. Goldberg, *Gamma-interferon and expression of MHC genes regulate peptide hydrolysis by proteasomes.* Nature, 1993. **365**(6443): p. 264-267.
23. Gaczynska, M., et al., *Peptidase activities of proteasomes are differentially regulated by the major histocompatibility complex-encoded genes for LMP2 and LMP7.* Proc. Natl. Acad. Sci. USA, 1994. **91**(20): p. 9213-9217.
24. Boes, B., et al., *Interferon γstimulation modulates the proteolytic activity and cleavage site preference of 20S mouse protesomes.* J. Exp. Med., 1994. **179**(3): p. 901-909.
25. Eleuteri, A.M., et al., *Bovine spleen multicatalytic proteinase complex (proteasome). Replacement of X, Y, and Z subunits by LMP7, LMP2, and MECL1 and changes in properties and specificity.* J. Biol. Chem., 1997. **272**(18): p. 11824-11831.
26. Driscoll, J., et al., *MHC-linked LMP gene products specifically alter peptidase activities of the proteasome.* Nature, 1993. **365**(6443): p. 262-264.
27. Ustrell, V., G. Pratt, and M. Rechsteiner, *Effects of interferon gamma and major histocompatibility complex-encoded subunits on peptidase activities of human multicatalytic proteases.* Proc. Natl. Acad. Sci. USA, 1995. **92**(2): p. 584-588.
28. Van Kaer, L., et al., *Altered peptidase and viral-specific T cell response in LMP2 mutant mice.* Immunity, 1994. **1**(7): p. 533-541.
29. Basler, M., et al., *An altered T cell repertoire in MECL-1-deficient mice.* J. Immunol., 2006. **176**(11): p. 6665-6672.
30. Stohwasser, R., et al., *20S proteasome from LMP7 knock out mice reveals altered proteolytic activities and cleavage site preferences.* FEBS Lett., 1996. **383**(1-2): p. 109-113.
31. Yewdell, J.W., *Immunoproteasomes: regulating the regulator.* Proc. Natl. Acad. Sci. USA, 2005. **102**(26): p. 9089-9090.
32. Cruz, M., et al., *DNA sequence, chromosomal localization, and tissue expression of the mouse proteasome subunit Lmp10 (Psmb10) gene.* Genomics, 1997. **45**(3): p. 618-622.
33. Foss, G.S., et al., *Constituitive and interferon-γ-induced expression of the human proteasome subunit multicatalytic endopeptidase complex-like 1.* Biochim. Biophys. Acta., 1998. **1402**: p. 17-28.
34. Zanelli, E., et al., *Genomic organization and tissue expression of the mouse proteasome gene Lmp-7.* Immunogenetics, 1993. **38**(6): p. 400-407.

35. Zhou, P., et al., *Genomic organization and tissue expression of mouse proteasome gene Lmp-2.* Genomics, 1993. **16**(3): p. 664-668.
36. James, A.B., A.M. Conway, and B.J. Morris, *Regulation of the neuronal proteasome by Zif268 (Egr1).* J. Neurosci., 2006. **26**(5): p. 1624.
37. Marqués, L., et al., *STAT1 regulates lipopolysaccharide- and TNF-alpha-dependent expression of transporter associated with antigen processing 1 and low molecular mass polypeptide 2 genes in macrophages by distinct mechanisms.* J. Immunol., 2004. **173**(2): p. 1103-1110.
38. Wright, K., et al., *Coordinate regulation of the human TAP1 and LMP2 genes from a shared bidirectional promoter.* . J. Exp. Med., 1995. **181**: p. 1459-1471.
39. Hirano, Y., et al., *A heterodimeric complex that promotes the assembly of mammalian 20S proteasomes.* Nature, 2005. **437**(7063): p. 1381-1385.
40. Hirano, Y., et al., *Dissecting beta-ring assembly pathway of the mammalian 20S proteasome.* EMBO J., 2008. **27**(16): p. 2204-2213.
41. Yashiroda, H., et al., *Crystal structure of a chaperone complex that contributes to the assembly of yeast 20S proteasomes.* Nat. Struct. Mol. Biol., 2008. **15**(3): p. 228-236.
42. Rosenzweig, R. and M. Glickman, *Chaperone-driven proteasome assembly.* Biochem. Soc. Trans., 2008. **36**: p. 807-812.
43. Groettrup, M., et al., *The subunits MECL-1 and LMP2 are mutually required for incorporation into the 20S proteasome.* Proc. Natl. Acad. Sci. USA, 1997. **94**(17): p. 8970-8975.
44. Griffin, T.A., et al., *Immunoproteasome assembly: Cooperative incorporation of interferon γ (IFN-γ)-inducible subunits.* J. Exp. Med., 1998. **187**(1): p. 97-104.
45. De, M., et al., *β2 subunit propeptides influence cooperative proteasome assembly.* J. Biol. Chem., 2003. **278**(8): p. 6153-6159.
46. Grune, T., et al., *Selective degradation of oxidatively modified protein substrates by the proteasome.* Biochem. Biophys. Res. Commun., 2003. **305**(3): p. 709-718.
47. Ferrington, D.A., et al., *Selective degradation of oxidized calmodulin by the 20 S proteasome.* J. Biol. Chem., 2001. **276**(2): p. 937-943.
48. Deveraux, Q., et al., *A 26 S protease subunit that binds ubiquitin conjugates.* J. Biol. Chem., 1994. **269**: p. 7059-7061.
49. Lam, Y.A., et al., *Specificity of the ubiquitin isopeptidase in the PA700 regulatory complex of 26 S proteasomes.* J. Biol. Chem., 1997. **272**: p. 28438-28446.
50. Verma, R., et al., *Role of Rpn11 metalloprotease in deubiquitination and degradation by the 26S proteasome.* Science, 2002. **298**: p. 611-615.
51. Yao, T. and R.E. Cohen, *A cryptic protease couples deubiquitination and degradation by the proteasome.* . Nature, 2002. **419**: p. 403-407.
52. Groettrup, M., et al., *The interferon-gamma-inducible 11 S regulator (PA28) and the LMP2/LMP7 subunits govern the peptide production by the 20 S proteasome in vitro.* J. Biol. Chem., 1995. **270**(40): p. 23808-23815.
53. Zhang, Z., A. Clawson, and M. Rechsteiner, *The proteasome activator 11 S regulator or PA28. Contribution by both alpha and beta subunits to proteasome activation.* J. Biol. Chem., 1998. **273**(46): p. 30660-30668.

54. Schwarz, K., et al., *The proteasome regulator PA28alpha/beta can enhance antigen presentation without affecting 20S proteasome subunit composition.* Eur. J. Immunol., 2000. **30**(12): p. 3672-3679.
55. Ustrell, V., et al., *PA200, a nuclear proteasome activator involved in DNA repair.* EMBO J., 2002. **21**(13): p. 3516-3525.
56. Khor, B., et al., *Proteasome activator PA200 is required for normal spermatogenesis.* Mol. Cell. Biol., 2006. **26**(8): p. 2999-3007.
57. McCullock, S., et al., *blm3-1 is an allele of UBP3, a ubiquitin protease that appears to act during transcription of damaged DNA.* J. Mol. Biol., 2006. **363**(3): p. 660-672.
58. McCutchen-Maloney, S.L., et al., *cDNA cloning, expression, and functional characterization of PI31, a proline-rich inhibitor of the proteasome.* J. Biol. Chem., 2000. **275**(24): p. 18557-18565.
59. Zaiss, D.M., et al., *The proteasome inhibitor PI31 competes with PA28 for binding to 20S proteasomes.* FEBS Lett., 1999. **457**(3): p. 333-338.
60. Zaiss, D.M., et al., *PI31 is a modulator of proteasome formation and antigen processing.* Proc. Natl. Acad. Sci. USA, 2002. **99**(22): p. 14344-14349.
61. Goasduff, T. and A.I. Cederbaum, *CYP2E1 degradation by in vitro reconstituted systems: role of the molecular chaperone hsp90.* Arch. Biochem. Biophys., 2000. **379**(2): p. 321-330.
62. Whittier, J.E., et al., *Hsp90 enhances degradation of oxidized calmodulin by the 20 S proteasome.* J. Biol. Chem., 2004. **279**(44): p. 46135-46142.
63. Lu, X., C. Michaud, and M. Orlowski, *Heat shock protein-90 and the catalytic activities of the 20 S proteasome (multicatalytic proteinase complex).* Arch. Biochem. Biophys., 2001. **387**(1): p. 163-171.
64. Wagner, B.J. and J.W. Margolis, *Age-dependent association of isolated bovine lens multicatalytic proteinase complex (proteasome) with heat-shock protein 90, an endogenous inhibitor.* Arch. Biochem. Biophys., 1995. **323**(2): p. 455-462.
65. Eleuteri, A.M., et al., *Interaction of Hsp90 with 20S proteasome: thermodynamic and kinetic characterization.* Proteins., 2002. **48**(2): p. 169-177.
66. Cascio, P., et al., *26S proteasomes and immunoproteasomes produce mainly N-extended versions of an antigenic peptide.* EMBO J., 2001. **20**(10): p. 2357-2366.
67. Kisselev, A.F., et al., *The size of peptides generated from protein by mammalian 26 and 20 S proteasomes: Implications for understanding the degradative mechanism and antigen presentation.* J. Biol. Chem., 1999. **274**(6): p. 3363-3371.
68. Schwarz, K., et al., *Overexpression of the proteasome subunits LMP2, LMP7, and MECL-1, but not PA28 alpha/beta, enhances the presentation of an immunodominant lymphocytic choriomeningitis virus T cell epitope.* J. Immunol., 2000. **165**(2): p. 768-778.
69. Yewdell, J.W., E. Reits, and J. Neefjes, *Making sense of mass destruction: quantitating MHC class I antigen presentation.* Nat. Rev. Immunol., 2003. **3**(12): p. 952-961.
70. Goslings, W.R., et al., *A small molecular weight factor in aqueous humor acts on C1q to prevent antibody-dependent complement activation.* Invest. Ophthalmol. Vis. Sci., 1998. **39**(6): p. 989-995.

71. Apte, R.S., et al., *Role of macrophage migration inhibitory factor in inhibiting NK cell activity and preserving immune privilege.* J. Immunol., 1998. **160**(12): p. 5693-5696.
72. Sugita, S., et al., *Retinal and ciliary body pigment epithelium suppress activation of T lymphocytes via transforming growth factor beta.* Exp. Eye Res., 2006. **83**(6): p. 1459-1471.
73. Sugita, S., et al., *B7+ iris pigment epithelial cells convert T cells into CTLA-4+, B7-expressing CD8+ regulatory T cells.* Invest. Ophthalmol. Vis. Sci., 2006. **47**(12): p. 5376-5384.
74. Zamiri, P., et al., *Thrombospondin plays a vital role in the immune privilege of the eye.* Invest. Ophthalmol. Vis. Sci., 2005. **46**(3): p. 908-919.
75. Stein-Streilein, J., *Immune regulation and the eye.* Trends Immunol., 2008. **29**(11): p. 548-554.
76. Piehl, F. and O. Lidman, *Neuroinflammation in the rat--CNS cells and their role in the regulation of immune reactions.* Immunol. Rev., 2001. **184**: p. 212-225.
77. Wang, H.M., et al., *The distribution and ontogeny of MHC antigens in murine ocular tissue.* Invest. Ophthalmol. Vis. Sci., 1987. **28**(8): p. 1383-1389.
78. Ferrington, D.A., A.D. Husom, and L.V. Thompson, *Altered proteasome structure, function, and oxidation in aged muscle.* FASEB J., 2005. **19**(6): p. 644-646.
79. Husom, A.D., et al., *Altered proteasome function and subunit composition in aged muscle.* Arch Biochem Biophys., 2004. **421**(1): p. 67-76.
80. Liu, Y., et al., *Molecular characterization, expression, and mapping of porcine LMP2 and MECL-1 genes.* DNA Seq., 2007. **18**(4): p. 257-264.
81. Cardozo, C., A.M. Eleuteri, and M. Orlowski, *Differences in catalytic activities and subunit pattern of multicatalytic proeinase complexes (proteasomes) isolated from bovine pituitary, lung and liver.* J. Biol. Chem., 1995. **270**(38): p. 22645-22651.
82. Singh, S., et al., *Immunoproteasome expression in a nonimmune tissue, the ocular lens.* Arch Biochem Biophys., 2002. **405**(2): p. 147-153.
83. Díaz-Hernández, M., et al., *Neuronal induction of immunoproteasome in Huntington's disease.* J. Neurosci., 2003. **23**(37): p. 11653-11661.
84. Gavilán, M.P., et al., *Age-related increase in the immunoproteasome content in rat hippocampus: molecular and functional aspects.* J. Neurochem., 2009. **108**(1): p. 260-272.
85. Mishto, M., et al., *Immunoproteasome and LMP2 polymorphism in aged and Alzheimer's disease brains.* Neurobiol. Aging, 2006. **27**(1): p. 54-66.
86. Ethen, C.M., et al., *Transformation of the proteasome with age-related macular degeneration.* FEBS Lett., 2007. **581**(5): p. 885-890.
87. LaVail, M.M., et al., *Genetic regulation of light damage to photoreceptors.* Invest. Ophthalmol. Vis. Sci., 1987. **28**(7): p. 1043-1048.
88. Puttaparthi, K. and J.L. Elliot, *Non-neuronal induction of immunoproteasome subunits in an ALS model: possible mediation by cytokines.* Exp. Neurol., 2005. **196**(2): p. 441-451.

89. Ding, Q., et al., *Role of the proteasome in protein oxidation and neural viability following low-level oxidative stress.* FEBS Lett., 2003. **546**(2-3): p. 228-232.
90. Teoh, C.Y. and K.J. Davies, *Potential roles of protein oxidation and the immunoproteasome in MHC class I antigen presentation: the 'PrOxI' hypothesis.* Arch Biochem Biophys., 2004. **423**(1): p. 88-96.
91. Kotamraju, S., et al., *Upregulation of immunoproteasomes by nitric oxide: Potential antioxidative mechanism in endothelial cells.* Free Radic. Biol. Med., 2006. **40**(6): p. 1034-1044.
92. Ding, Q., et al., *LMP2 knock-out mice have reduced proteasome activities and increased levels of oxidatively damaged proteins.* Antioxid. Redox. Signal., 2006. **8**(1-2): p. 130-135.
93. Pickering, A.M., et al., *The immunoproteasome, the 20S proteasome, and the PA28αβ proteasome regulator are oxidative stress-adaptive proteolytic complexes.* Biochem. J., 2010. **doi:10.1042/BJ20100878**.
94. Seifert, U., et al., *Immunoproteasomes preserve protein homeostasis upon interferon-induced oxidative stress.* Cell, 2010. **142**: p. 613-624.
95. Gong, P., et al., *The ubiquitin-like protein FAT10 mediates NF-kappaB activation.* J. Am. Soc. Nephrol., 2010. **21**(2): p. 316-326.
96. Visekruna, A., et al., *Proteasome-mediated degradation of IκBα and processing of p105 in Crohn disease and ulcerative colitis.* J. Clin. Invest., 2006. **116**(12): p. 3195-3203.
97. Karin, M. *Cancer research in flames*. 2005 [cited 2010; Available from: http://www.biox.cn/content/20051212/41326.htm.
98. Cai, Z.P., et al., *Ischemic preconditioning-induced cardioprotection is lost in mice with immunoproteasome subunit low molecular mass polypeptide-2 deficiency.* FASEB J., 2008. **22**(12): p. 4248-4257.
99. Linden, R., R.A.P. Martins, and M.S. Silveira, *Control of programmed cell death by neurotransmitters and neuropeptides in the developing retina.* Prog. Retin. Eye Res., 2005. **24**: p. 457-491.
100. Heink, S., et al., *IFN-gamma-induced immune adaptation of the proteasome system is an accelerated and transient response.* Proc. Natl. Acad. Sci. USA, 2005. **102**(26): p. 9241-9246.
101. Clark, R.A.F. and M. Pavlis, *Dysregulation of the mTOR Pathway Secondary to Mutations or a Hostile Microenvironment Contributes to Cancer and Poor Wound Healing.* J. Inv. Dermatol., 2009. **129**: p. 529-531.
102. Feng, Z., *p53 regulation of the IGF-1/AKT/mTOR pathways and the endosomal compartment.* Cold Spring Harb. Perspect. Biol., 2010. **2**(2): p. a001057.
103. Homma, K., et al., *Early downregulation of IGF-1 decides the fate of rat retinal ganglion cells after optic nerve injury.* Neurochem. Int., 2007. **50**(5): p. 741-748.
104. Nguyen, T.P., V.M. Soukup, and B.B. Gelman, *Persistent hijacking of brain proteasomes in HIV-associated dementia.* Am. J. Pathol., 2010. **176**(2): p. 893-902.
105. Fehling, H.J., et al., *MHC class I expression in mice lacking the proteasome subunit LMP-7.* Science, 1994. **265**(5176): p. 1234-1237.

106. Caudill, C.M., et al., *T cells lacking immunoproteasome subunits MECL-1 and LMP7 hyperproliferate in response to polyclonal mitogens.* J. Immunol., 2006. **176**(7): p. 4075-4082.
107. Nussbaum, A.K., et al., *Immunoproteasome-deficient mice mount largely normal CD8+ T cell responses to lymphocytic choriomeningitis virus infection and DNA vaccination.* J. Immunol., 2005. **175**(2): p. 1153-1160.
108. Jeon, C.J., E. Strettoi, and R.H. Masland, *The major cell populations of the mouse retina.* J. Neurosci., 1998. **18**(21): p. 8936-8946.
109. Thompson, S. *Photosensory Biology*. [Webpage] 2010 [cited 2010 September 24, 2010]; Post-doctoral webpage]. Available from: http://photosensorybiology.org/id34.html.
110. Mu, X. and W.H. Klein, *Gene regulatory networks and retinal ganglion cell development.*, in *Eye, Retina, and Visual System of the Mouse*, L.M. Chalupa and R.W. Williams, Editors. 2008, The MIT Press: Cambridge, MA. p. 321-332.
111. Strettoi, E. and M. Volpini, *Retinal organization in the bcl-2-overexpressing transgenic mouse.* J. Comp. Neurol., 2002. **446**(1): p. 1-10.
112. Strauss, O., *The retinal pigment epithelium in visual function.* Physiol. Rev., 2005. **85**(3): p. 845-881.
113. Bringmann, A., et al., *Role of retinal glial cells in neurotransmitter uptake and metabolism.* Neurochem. Int., 2009. **54**(3-4): p. 143-160.
114. de Melo Reis, R.A., et al., *Müller glia as an active compartment modulating nervous activity in the vertebrate retina: neurotransmitters and trophic factors.* Neurochem. Res., 2008. **33**(8): p. 1466-1474.
115. Lamb, T.D. and E.N.J. Pugh, *Phototransduction, dark adaptation, rhodopsin regeneration.* Invest. Ophthalmol. Vis. Sci., 2006. **47**(12): p. 5137-5152.
116. Copenhagen, D.R. and C.E. Jahr, *Release of endogenous excitatory amino acids from turtle photoreceptors.* Nature, 1989. **341**(6242): p. 536-539.
117. Wensel, T.G. *Theodore G. Wensel, Ph.D. - Verna and Marrs McLean Department of Biochemistry and Molecular Biology*. 2010 September 23,2010 September 15, 2010]; Available from: http://128.249.2.7/biochem/?PMID=3795.
118. Weymouth, A.E. and A.J. Vingrys, *Rodent electroretinography: methods for extraction and interpretation of rod and cone responses.* Prog. Retin. Eye Res., 2008. **27**(1): p. 1-44.
119. Saari, J.C. and J.W. Crabb, *Genetic and proteomic analyses of the mouse visual cycle.*, in *Eye, Retina, and Visual System of the Mouse*, L.M. Chalupa and R.W. Williams, Editors. 2008, The MIT Press: Cambridge, MA. p. 157-164.
120. Qtaishat, N.M., B. Wiggert, and D.R. Pepperberg, *Interphotoreceptor retinoid-binding protein (IRBP) promotes the release of all-trans retinol from the isolated retina following rhodopsin bleaching illumination.* Exp. Eye Res., 2005. **81**(4): p. 455-463.
121. Barry, R.J., F.J. Cañada, and R.R. Rando, *Solubilization and partial purification of retinyl ester synthetase and retinoid isomerase from bovine ocular pigment epithelium.* J. Biol. Chem., 1989. **264**(16): p. 9231-9238.
122. Saari, J.C. and D.L. Bredberg, *Lecithin:retinol acyltransferase in retinal pigment epithelial microsomes.* J. Biol. Chem., 1989. **264**(15): p. 8636-8640.

123. Jin, M., et al., *Rpe65 is the retinoid isomerase in bovine retinal pigment epithelium.* Cell, 2005. **122**(3): p. 449-459.
124. Moiseyev, G., et al., *RPE65 is an iron(II)-dependent isomerohydrolase in the retinoid visual cycle.* J. Biol. Chem., 2006. **281**(5): p. 2835-2840.
125. Redmond, T.M., et al., *Mutation of key residues of RPE65 abolishes its enzymatic role as isomerohydrolase in the visual cycle.* Proc. Natl. Acad. Sci. USA, 2005. **102**(38): p. 13658-13663.
126. Winston, A. and R.R. Rando, *Regulation of isomerhydrolase activity in the visual cycle.* Biochemistry, 1998. **37**(7): p. 2044-2050.
127. Sterling, P. and G. Matthews, *Structure and function of ribbon synapses.* Trends Neurosci, 2005. **28**(1): p. 20-29.
128. Heidelberger, R., et al., *Calcium dependence of the rate of exocytosis in a synaptic terminal.* Nature, 1994. **371**(6497): p. 513-515.
129. Heidelberger, R., W.B. Thoreson, and P. Witkovsky, *Synaptic transmission at retinal ribbon synapses.* Prog. Retin. Eye Res., 2005. **24**(6): p. 682-720.
130. Nawy, S., *The metabotropic receptor mGluR6 may signal through G(o), but not phosphodiesterase, in retinal bipolar cells.* J. Neurosci., 1999. **19**(8): p. 2938-2944.
131. Vardi, N., *Alpha subunit of Go localizes in the dendritic tips of ON bipolar cells.* J. Comp. Neurol., 1998. **395**(1): p. 43-52.
132. Chen, F.S., et al., *Functional redundancy of R7 RGS proteins in ON-bipolar cell dendrites.* Invest. Ophthalmol. Vis. Sci., 2010. **51**(2): p. 686-693.
133. Koike, C., et al., *TRPM1 is a component of the retinal ON bipolar cell transduction channel in the mGluR6 cascade.* Proc. Natl. Acad. Sci. USA, 2010. **107**(1): p. 332-337.
134. Morgans, C.W., et al., *TRPM1 is required for the depolarizing light response in retinal ON-bipolar cells.* Proc. Natl. Acad. Sci. USA, 2009. **106**(45): p. 19174-19178.
135. Strettoi, E., E. Raviola, and R.F. Dacheux, *Synaptic connections of the narrow-field, bistratified rod amacrine cell (AII) in the rabbit retina.* J. Comp. Neurol., 1992. **325**(2): p. 152-168.
136. Strettoi, E., *Synaptic organization of the mouse retina*, in *Eye, Retina, and Visual System of the Mouse*, L.M. Chalupa and R.W. Williams, Editors. 2008, The MIT Press: Cambridge, MA. p. 157-164.
137. Masoro, E.J., *Are age-related diseases an integral part of aging?*, in *Handbook of the biology of aging.*, E.J. Masoro and S.N. Austad, Editors. 2006, Academic Press: Burlington, MA. p. 43-62.
138. Pérez, V.I., et al., *Is the oxidative stress theory of aging dead?* Biochim. Biophys. Acta., 2009. **1790**(10): p. 1005-1014.
139. Beckman, K.B. and B.N. Ames, *The free radical theory of aging.* Physiol. Rev., 1998. **78**(2): p. 547-581.
140. Miceli, M.V., M.R. Liles, and D.A. Newsome, *Evaluation of oxidative processes in human pigment epithelial cells associated with retinal outer segment phagocytosis.* Exp. Cell Res., 1994. **214**(1): p. 242-249.

141. Kujoth, G.C., C. Leeuwenburgh, and T.A. Prolla, *Mitochondrial DNA mutations and apoptosis in mammalian aging.* Cancer Res., 2006. **66**(15): p. 7386-7389.
142. Benedetti, A., M. Comporti, and H. Esterbauer, *Identification of 4-hydroxynonenal as a cytotoxic product originating from the peroxidation of liver microsomal lipids.* Biochim. Biophys. Acta., 1980. **620**(2): p. 281-296.
143. Cecarini, V., et al., *Protein oxidation and cellular homeostasis: Emphasis on metabolism.* Biochim. Biophys. Acta., 2007. **1773**(2): p. 93-104.
144. Finkel, T. and N.J. Holbrook, *Oxidants, oxidative stress and the biology of ageing.* Nature, 2000. **408**(6809): p. 239-247.
145. Grune, T., et al., *Proteolysis in cultured liver epithelial cells during oxidative stress. Role of the multicatalytic proteinase complex, proteasome.* J. Biol. Chem. 1995 Feb 3;270(5):2344-51., 1995. **270**(5): p. 2344-2351.
146. Lasch, P., et al., *Hydrogen peroxide-induced structural alterations of RNAse A.* J Biol Chem. 2001 Mar 23;276(12):9492-502. Epub 2000 Dec 13., 2001. **276**(12): p. 9492-9502.
147. Pacifici, R.E., Y. Kono, and K.J. Davies, *Hydrophobicity as the signal for selective degradation of hydroxyl radical-modified hemoglobin by the multicatalytic proteinase complex, proteasome.* J. Biol. Chem., 1993. **268**(21): p. 15405-15411.
148. Balog, E.M., et al., *Site-specific methionine oxidation intiates calmodulin degradation by the 20S proteasome.* Biochemistry, 2009. **48**: p. 3005-3016.
149. Rechsteiner, M. and S.W. Rogers, *PEST sequences and regulation by proteolysis.* Trends Biochem. Sci., 1996. **21**(7): p. 267-271.
150. Kapphahn, R.J., E.J. Bigelow, and D.A. Ferrington, *Age-dependent inhibition of proteasome chymotrypsin-like activity in the retina.* Exp. Eye Res., 2007. **84**(4): p. 646-654.
151. Anselmi, B., et al., *Dietary self-selection can compensate an age-related decrease of rat liver 20 S proteasome activity observed with standard diet.* J. Gerontol. A. Biol. Sci. Med Sci., 1998. **53**(3): p. B173-B179.
152. Conconi, M., et al., *Age-related decline of rat liver multicatalytic proteinase activity and protection from oxidative inactivation by heat-shock protein 90.* Arch. Biochem. Biophys., 1996. **331**(2): p. 232-240.
153. Hayashi, T. and S. Goto, *Age-related changes in the 20S and 26S proteasome activities in the liver of male F344 rats.* Mech. Ageing Dev., 1998. **102**(1): p. 55-66.
154. Zeng, B.Y., et al., *Proteasomal activity in brain differs between species and brain regions and changes with age.* Mech. Ageing Dev., 2005. **126**(6-7): p. 760-766.
155. Carrard, G., et al., *Impact of ageing on proteasome structure and function in human lymphocytes.* Int. J. Biochem. Cell Biol., 2003. **35**(5): p. 728-739.
156. Grimm, S., A. Höhn, and T. Grune, *Oxidative protein damage and the proteasome.* Amino Acids, 2010. **DOI: 10.1007/s00726-010-0646-8**.
157. Ferrington, D.A. and R.J. Kapphahn, *Catalytic site-specific inhibition of the 20S proteasome by 4-hydroxynonenal.* FEBS Lett., 2004. **578**(3): p. 217-223.

158. Ishii, T., et al., *Oxidative modification of proteasome: identification of an oxidation-sensitive subunit in 26 S proteasome.* Biochemistry, 2005. **44**(42): p. 13893-13901.
159. Friguet, B. and L.I. Szweda, *Inhibition of the multicatalytic proteinase (proteasome) by 4-hydroxy-2-nonenal cross-linked protein.* FEBS Lett., 1997. **405**(1): p. 21-25.
160. Sitte, N., et al., *Proteasome inhibition by lipofuscin/ceroid during postmitotic aging of fibroblasts.* FASEB J., 2000. **14**(11): p. 1490-1498.
161. Oh, S., et al., *Amyloid peptide attenuates the proteasome activity in neuronal cells.* Mech. Ageing Dev., 2005. **126**(12): p. 1292-1299.
162. Chondrogianni, N. and E.S. Gonos, *Proteasome activation as a novel antiaging strategy.* IUBMB Life., 2008. **60**(10): p. 651-655.
163. Chondrogianni, N., et al., *Fibroblast cultures from health centenarians have an active proteasome.* Exp. Gerontol., 2000. **35**(721-728): p. 721.
164. Katsiki, M., et al., *The olive constituent oleuropein exhibits proteasome stimulatory properties in vitro and confers life span extension of human embryonic fibroblasts.* Rejuvenation Res., 2007. **10**(2): p. 157-172.
165. Tonoki, A., et al., *Genetic evidence linking age-dependent attenuation of the 26S proteasome with the aging process.* Mol. Cell. Biol., 2009. **29**(4): p. 1095-1106.
166. Yun, C., et al., *Proteasomal adaptation to environmental stress links resistnace to proteotoxicity with longevity in Caenorhabditis elegans.* Proc. Natl. Acad. Sci. USA, 2008. **105**(19): p. 7094-7099.
167. Ciechanover, A. and P. Brundin, *The ubiquitin proteasome system in neurodegenerative diseases: sometimes the chicken, sometimes the egg.* Neuron, 2003. **40**(2): p. 427-446.
168. Keck, S., et al., *Proteasome inhibition by paired helical filament-tau in brains of patients with Alzheimer's disease.* J. Neurochem. 2003 Apr;85(1):115-22., 2003. **85**(1): p. 115-122.
169. Lopez Salon, M., et al., *Relationship between beta-amyloid degradation and the 26S proteasome in neural cells.* Exp. Neurol., 2003. **180**(2): p. 131-143.
170. Zhou, H., et al., *Huntingtin forms toxic NH2-terminal fragment complexes that are promoted by the age-dependent decrease in proteasome activity.* J. Cell. Biol., 2003. **163**(1): p. 109-118.
171. McNaught, K.S., et al., *Altered proteasomal function in sporadic Parkinson's disease.* Exp. Neurol., 2003. **179**(1): p. 38-46.
172. McNaught, K.S. and P. Jenner, *Proteasomal function is impaired in substantia nigra in Parkinson's disease.* Neurosci. Lett., 2001. **297**(3): p. 191-194.
173. Paul, S., *Dysfunction of the ubiquitin-proteasome system in multiple disease conditions: therapeutic approaches.* Bioessays., 2008. **30**(11-12): p. 1172-1184.
174. Puttaparthi, K., L. Van Kaer, and J.L. Elliot, *Assessing the role of immuno-proteasomes in a mouse model of familial ALS.* Exp. Neurol., 2007. **206**: p. 53-58.
175. Sierra, F., et al., *Prospects for life span extension.* Annu. Rev. Med., 2009. **60**: p. 457-469.
176. Miller, R.A. and N.L. Nadon, *Principles of animal use for gerontological research.* J. Gerontol. A. Biol. Sci. Med. Sci., 2000. **55**(3): p. B117-B123.

177. Young, R.W., *Cell death during differentiation of the retina in the mouse.* J. Comp. Neurol., 1984. **229**(3): p. 362-373.
178. Yuan, R., et al., *Aging in inbred strains of mice: study design and interim report on median lifespans and circulating IGF1 levels.* Aging Cell, 2009. **8**(3): p. 277-287.
179. Gresh, J., et al., *Structure-function analysis of rods and cones in juvenile, adult, and aged C57BL/6 and Balb/c mice.* Vis. Neurosci., 2003. **20**(2): p. 211-220.
180. Kolesnikov, A.V., et al., *Age-related deterioration of rod vision in mice.* J. Neurosci., 2010. **30**(33): p. 11222-11231.
181. Curcio, C.A., et al., *Aging of the human photoreceptor mosaic: evidence for selective vulnerability of rods in central retina.* Invest. Ophthalmol. Vis. Sci., 1993. **34**(12): p. 3278-3296.
182. Cunea, A. and G. Jeffery, *The ageing photoreceptor.* Vis. Neurosci. 2007 Mar-Apr;24(2):151-5., 2007. **24**(2): p. 151-155.
183. Jackson, G.R., C. Owlsey, and C.A. Curcio, *Photoreceptor degeneration and dysfunction in aging and age-related maculopathy.* Ageing Res. Rev., 2002. **1**(381-396): p. 381-396.
184. Brunk, U.T. and A. Terman, *Lipofuscin: mechanisms of age-related accumulation and influence on cell function.* Free Radic. Biol. Med., 2002. **33**(5): p. 611-619.
185. Kennedy, C.J., P.E. Rakoczy, and I.J. Constable, *Lipofuscin of the retinal pigment epithelium: a review.* Eye (Lond). 1995;9 (Pt 6):763-71., 1995. **9**(6): p. 763-771.
186. Nilsson, S.E.G., et al., *Aging of cultured retinal pigment epithelial cells: oxidative reactions, lipofuscin formation and blue light damage.* Doc. Ophthalmol., 2003. **106**(1): p. 13-16.
187. Rohrer, B., et al., *Correlation of regenerable opsin with rod ERG signal in Rpe65$^{-/-}$ mice during development and aging.* Invest. Ophthalmol. Vis. Sci., 2003. **44**(1): p. 310-315.
188. Terzibasi, E., et al., *Age-dependent remodelling of retinal circuitry.* Neurobiol. Aging, 2009. **30**: p. 819-828.
189. Kikuchi, T., et al., *The proximal promoter of the mouse arrestin gene directs gene expression in photoreceptor cells and contains an evolutionarily conserved retinal factor-binding site.* Mol. Cell. Biol., 1993. **13**(7): p. 4400-4408.
190. Gregerson, D.S. and C. Dou, *Spontaneous induction of immunoregulation by an endogenous retinal protein.* Invest. Ophthalmol. Vis. Sci., 2002. **43**(9): p. 2984-2991.
191. Johnson, W.B., et al., *Indicator expression directed by regulatory sequences of the glial fibrillary acidic protein (GFAP) gene: in vivo comparison of distinct GFAP-lacZ transgenes.* Glia, 1995. **13**(3): p. 174-184.
192. McPherson, S.W., et al., *Bystander killing of neurons by cytotoxic T cells specific for a glial antigen.* Glia, 2006. **53**(5): p. 457-466.
193. McPherson, S.W., et al., *Resting CD8 T cells recognize beta-galactosidase expressed in the immune-privileged retina and mediate autoimmune disease when activated.* Immunology, 2003. **110**(3): p. 386-396.

194. Lyubarksy, A.L. and E.N.J. Pugh, *Recovery phase of the murine rod photoresponse reconstructed from electroretinographic recordings.* J. Neurosci., 1996. **16**(2): p. 563-571.
195. Lyubarsky, A.L., et al., *UV- and midwave-sensitive cone-driven retinal responses of the mouse: a possible phenotype for coexpression of cone photopigments.* J. Neurosci., 1999. **19**(1): p. 442-455.
196. Niemeyer, G. *The Baltic Eye Newsletter for Ophthalmologists*. [cited 2010; Available from: http://www.thebalticeye.com/ZURICH.html.
197. Wachtmeister, L., *Oscillatory potentials in the retina: what do they reveal.* Prog. Retin. Eye Res., 1998. **17**(4): p. 485-521.
198. Bayley, P.R. and C.W. Morgans, *Rod bipolar cells and horizontal cells form displaced synaptic contacts with rods in the outer nuclear layer of the nob2 retina.* J. Comp. Neurol., 2007. **500**(2): p. 286-298.
199. Dick, O., et al., *The presynaptic active zone protein bassoon is essential for photoreceptor ribbon synapse formation in the retina.* Neuron, 2003. **37**(5): p. 775-786.
200. Akula, J.D., et al., *The oscillatory potentials of the dark-adapted electroretinogram in retinopathy of prematurity.* Invest. Ophthalmol. Vis. Sci., 2007. **48**(12): p. 5788-5797.
201. Granit, R., *The components of the retinal action potential in mammals and their relation to the discharge in the optic nerve.* J. Physiol., 1933. **77**(3): p. 207-239.
202. Szél, A. and P. Röhlich, *Two cone types of rat retina detected by anti-visual pigment antibodies.* Exp. Eye Res., 1992. **55**(1): p. 47-52.
203. Hood, D.C. and D.G. Birch, *A quantitative measure of the electrical activity of human rod photoreceptors using electroretinography.* Vis. Neurosci., 1990. **5**(4): p. 379-387.
204. Perlman, I. *The electroretinogram: ERG.* 2001 June 27, 2007 [cited 2010 October 10, 2010]; NCBI Bookshelf. Historical view.]. Available from: http://www.ncbi.nlm.nih.gov/bookshelf/br.fcgi?book=webvision&part=ch35erg.
205. Gangadhar, D.V., B.M. Wolf, and H.L. Tanenbaum, *Naka-Rushton equation parameters in electroretinogram analysis of daunomycin effects on retinal function.* Doc. Ophthalmol., 1989. **72**: p. 61-70.
206. Chang, B., et al., *Two mouse retinal degenerations caused by missense mutations in the beta-subunit of rod cGMP phosphodiesterase gene.* Vision Res., 2007. **47**(5): p. 624-633.
207. Jaissle, G.B., et al., *Evaluation of the rhodopsin knockout mouse as a model of pure cone function.* Invest. Ophthalmol. Vis. Sci., 2001. **42**(2): p. 506-513.
208. Seeliger, M.W., et al., *New views on RPE65 deficiency: the rod system is the source of vision in a mouse model of Leber congenital amaurosis.* Nature Genet., 2001. **29**(1): p. 70-74.
209. Ding, X.Q., et al., *Impaired cone function and cone degeneration resulting from CNGB3 deficiency: down-regulation of CNGA3 biosynthesis as a potential mechanism.* Hum. Mol. Genet., 2009. **18**(24): p. 4770-4780.

210. Mansergh, F., et al., *Mutation of the calcium channel gene Cacna1f disrupts calcium signaling, synaptic transmission and cellular organization in mouse retina.* Hum. Mol. Genet., 2005. **14**(20): p. 3035-3046.
211. Wu, J., et al., *Voltage-dependent calcium channel CaV1.3 subunits regulate the light peak of the electroretinogram.* J. Neurophysiol., 2007. **97**(5): p. 3731-3735.
212. Wycisk, K.A., et al., *Structural and functional abnormalities of retinal ribbon synapses due to Cacna2d4 mutation.* Invest. Ophthalmol. Vis. Sci., 2006. **47**(8): p. 3523-3530.
213. Brunner, S., et al., *Cone versus rod disease in a mutant Rpgr mouse caused by different genetic backgrounds.* Invest. Ophthalmol. Vis. Sci., 2010. **51**(2): p. 1106-1115.
214. Maeda, T., et al., *A critical role of CaBP4 in the cone synapse.* Invest. Ophthalmol. Vis. Sci., 2005. **46**(11): p. 4320-4327.
215. Masu, M., et al., *Specific deficit of the ON response in visual transmission by targeted disruption of the mGluR6 gene.* Cell, 1995. **80**(5): p. 757-765.
216. Maddox, D.M., et al., *Allelic variance between GRM6 mutants, Grm6nob3 and Grm6nob4 results in differences in retinal ganglion cell visual responses.* J. Physiol., 2008. **586**(18): p. 4409-4424.
217. Morgans, C.W., et al., *Loss of synaptic vesicle protein SV2B results in reduced neurotransmission and altered synaptic vesicle protein expression in the retina.* PLoS ONE, 2009. **4**(4): p. e5230.
218. Takada, Y., et al., *Synaptic pathology in retinoschisis knockout (Rs1$^{-/y}$) mouse retina and modification by rAAV-Rs1 gene delivery.* Invest. Ophthalmol. Vis. Sci., 2008. **49**(8): p. 3677-3686.
219. Satz, J.S., et al., *Visual impairment in the absence of dystroglycan.* J. Neurosci., 2009. **29**(42): p. 13136-13146.
220. Pardue, M.T., et al., *A naturally occurring mouse model of X-linked congenital stationary night blindness.* Invest. Ophthalmol. Vis. Sci., 1998. **39**(12): p. 2443-2449.
221. Haeseleer, F., et al., *Essential role of Ca2+-binding protein 4, a Cav1.4 channel regulator, in photoreceptor synaptic function.* Nat. Neurosci., 2007. **7**(10): p. 1079-1087.
222. Hashizume, K., et al., *Retinal dysfunction and progressive retinal cell death in SOD1-deficient mice.* Am. J. Pathol., 2008. **172**(5): p. 1325-1331.
223. Zhu, X., et al., *Carboxypeptidase E is required for normal synaptic transmission from photoreceptors to the inner retina.* J. Neurochem., 2005. **95**(5): p. 1351.
224. Colledge, M., et al., *Ubiquitination regulates PSD-95 degradation and AMPA receptor surface expression.* Neuron, 2003. **40**(3): p. 595-607.
225. Wheeler, T.C., et al., *Regulation of synaptophysin degradation by mammalian homologues of Seven in Absentia.* J. Biol. Chem., 2002. **277**(12): p. 10273-10282.
226. Kloetzel, P.M., A. Soza, and R. Stohwasser, *The role of the proteasome system and the proteasome activator PA28 complex in the cellular immune response.* Biol. Chem., 1999. **380**(3): p. 293-297.

227. Rivett, A.J. and A.R. Hearn, *Proteasome function in antigen presentation: immunoproteasome complexes, peptide production, and interactions with viral proteins.* Curr. Protein Pept. Sci., 2004. **5**(3): p. 153-161.
228. Klein, R., B.E. Klein, and K.L. Linton, *Prevalence of age-related maculopathy. The Beaver Dam Eye Study.* Opthalmology, 1992. **99**(6): p. 933-943.
229. Klaver, C.C., et al., *Age-specific prevalence and causes of blindness and visual impairment in an older population: the Rotterdam Study.* Arch. Ophthalmol., 1998. **116**(5): p. 653.
230. Beatty, S., et al., *The role of oxidative stress in the pathogenesis of age-related macular degeneration.* Surv. Ophthalmol., 2000. **45**(2): p. 115-134.
231. Donoso, L.A., et al., *The role of inflammationin the pathogenesis of age-related macular degeneration.* Surv. Ophthalmol., 2006. **51**(2): p. 137-152.
232. Di Napoli, M. and F. Papa, *The proteasome system and proteasome inhibitors in stroke: controlling the inflammatory response.* Curr. Opin. Investig. Drugs, 2003. **4**(11): p. 1333-1342.
233. Olsen, T.W. and X. Feng, *The Minnesota Grading System of eye bank eyes for age-related macular degeneration.* Invest. Ophthalmol. Vis. Sci., 2004. **45**(12): p. 4484-4490.
234. Ethen, C.M., et al., *Declines in arrestin and rhodopsin in the macula with progression of age-realted macular degeneration.* Invest. Ophthalmol. Vis. Sci., 2005. **46**(3): p. 769-775.
235. Ethen, C.M., et al., *The proteome of central and peripheral retina with progression of age-related macular degeneration.* Invest. Ophthalmol. Vis. Sci., 2006. **47**(6): p. 2280-2290.
236. Kisselev, A.F., et al., *Proteasome active sites allosterically regulate each other, suggesting a cyclical bite-chew mechanism for protein breakdown.* Mol. Cell, 1999. **4**(3): p. 395-402.
237. Ehring, B., et al., *Effects of major-histocompatibility-complex-encoded subunits on the peptidase and proteolytic activities of human 20S proteasomes. Cleavage of proteins and antigenic peptides.* Eur. J. Biochem., 1996. **235**(1-2): p. 404-415.
238. Rechsteiner, M. and C.P. Hill, *Mobilizing the proteolytic machine: cell biological roles of proteasome activators and inhibitors.* Trends Cell. Biol., 2005. **15**(1): p. 27-33.
239. Carrard, G., et al., *Impairment of proteasome structure and function in aging.* Int. J. Biochem. Cell. Biol., 2002. **34**(11): p. 1461-1474.
240. Crabb, J.W., et al., *Drusen proteome analysis: an approach to the etiology of age-related macular degeneration.* Proc. Natl. Acad. Sci. USA, 2002. **99**(23): p. 14682-14687.
241. Edwards, A.O., et al., *Complement factor H polymorphism and age-relatedd macular degeneration.* Science, 2005. **308**(5720): p. 421-424.
242. Hageman, G.S., et al., *A common haplotype in the complement regulatory gene factor H (HF1/CFH) predisposes individuals to age-related macular degeneration.* Proc. Natl. Acad. Sci. USA, 2005. **102**(20): p. 7227-7232.
243. Haines, J.L., et al., *Complement factor H variant increases the risk of age-related macular degeneration.* Science, 2005. **308**(5720): p. 419-421.

244. Klein, R.J., et al., *Complement factor H polymorphism in age-related macular degeneration.* Science, 2005. **308**(5720): p. 385-389.
245. Nowak, J.Z., *Age-related macular degeneration (AMD): pathogenesis and therapy.* Pharmacol. Rep., 2006. **58**(3): p. 353-363.
246. Dahlmann, B., et al., *Different proteasome subtypes in a single tissue exhibit different enzymatic properties.* J. Mol. Biol., 2000. **303**(5): p. 643-653.
247. Noda, C., et al., *Tissue distribution of constitutive proteasomes, immunoproteasomes, and PA28 in rats.* Biochem. Biophys. Res. Commun., 2000. **277**(2): p. 348-354.
248. Rock, K.L., et al., *Inhibitors of the proteasome block the degradation of most cell proteins and the generation of peptides presented on MHC class I molecules.* Cell, 1994. **78**(5): p. 761-771.
249. Goldberg, A.L., et al., *The importance of the proteasome and subsequent proteolytic steps in the generation of antigenic peptides.* Mol. Immunol., 2002. **39**(3-4): p. 147-164.
250. Louie, J.L., R.J. Kapphahn, and D.A. Ferrington, *Proteasome function and protein oxidation in the aged retina.* Exp. Eye Res., 2002. **75**(3): p. 271-284.
251. Gregerson, D.S., et al., *Retinal expression of a neo-self antigen, beta-galactosidase, is not tolerogenic and creates a target for autoimmune uveitis.* J. Immunol., 1999. **163**(2): p. 1073-1080.
252. Gregerson, D.S. and J. Xiao, *Failure of memory (CD44 high) CD4 T cells to recognize their target antigen in retina.* J. Neuroimmunol., 2001. **120**(1-2): p. 34-41.
253. Dick, L.R., et al., *Proteolytic processing of ovalbumin and beta-galactosidase by the proteasome to yield antigenic peptides.* J. Immunol., 1994. **152**(8): p. 3884-3894.
254. Gregerson, D.S., et al., *RPE cells resist bystander killing by CTLs, but are highly susceptible to antigen-dependent CTL killing.* Invest. Ophthalmol. Vis. Sci., 2006. **47**(12): p. 5385-8394.
255. Ferrington, D.A., et al., *Different death stimuli evoke apoptosis via multiple pathways in retinal pigment epithelial cells.* Exp. Eye Res., 2006. **83**(3): p. 638-650.
256. Kapphahn, R.J., et al., *Retinal proteins modified by 4-hydroxynonenal: Identification of molecular targets.* Exp. Eye Res., 2006. **83**(1): p. 165-175.
257. Burnside, B. and L. Bost-Usinger, *The retinal pigment epithelial cytoskeleton*, in *The Retinal Pigment Epithelium*, M.F. Marmore and T.J. Wolfensberger, Editors. 1998, Oxford University Press: New York, NY. p. 41-67.
258. Chen, H. and A.J. Weber, *Expression of glial fibrillary acidic protein and glutamine synthetase by Müller cells after optic nerve damage and intravitreal application of brain-derived neurotrophic factor.* Glia, 2002. **38**(2): p. 115-125.
259. Gregerson, D.S. and J. Yang, *CD45-positive cells of the retina and their responsiveness to in vivo treatment with IFN-gamma or anti-CD40.* Invest. Ophthalmol. Vis. Sci., 2003. **44**(7): p. 3083-3093.

260. Gregerson, D.S., T.N. Sam, and S.W. McPherson, *The antigen-presenting activity of fresh, adult parenchymal microglia and perivascular cells from retina.* J. Immunol., 2004. **172**(11): p. 6587-6597.
261. Stohwasser, R., et al., *Biochemical analysis of proteasomes from mouse microglia: induction of immunoproteasomes by interferon-gamma and lipopolysaccharide.* Glia, 2000. **29**(4): p. 355-365.
262. Moore, S. and S. Thanos, *The concept of microglia in relation to central nervous system disease and regeneration.* Prog. Neurobiol., 1996. **48**(4-5): p. 441-460.
263. Panagis, L., et al., *Unilateral optic nerve crush induces bilateral retinal glial cell proliferation.* Eur. J. Neurosci., 2005. **21**(8): p. 2305-2309.
264. Zhang, C., et al., *Activation of microglia and chemokines in light-induced retinal degeneration.* Mol. Vis., 2005. **11**: p. 887-895.
265. McMenamin, P.G., *Distribution and phenotype of dendritic cells and resident tissue macrophages in the dura mater, leptomeninges, and choroid plexus of the rat brain as demonstrated in wholemount preparations.* J. Comp. Neurol., 1999. **405**(4): p. 553-562.
266. Chen, P. and M. Hochstrasser, *Autocatalytic subunit processing couples active site formation in the 20S proteasome to completion of assembly.* Cell, 1996. **86**(6): p. 961-972.
267. Yao, X., J. Liu, and J.T. McCabe, *Alterations of cerebral cortex and hippocampal proteasome subunit expression and function in a traumatic brain injury rat model.* J. Neurochem., 2008. **104**(2): p. 353-363.
268. Akiyama, K., et al., *cDNA cloning and interferon gamma down-regulation of proteasomal subunits X and Y.* Science, 1994. **265**(5176): p. 1231-1234.
269. Nandi, D., H. Jiang, and J.J. Monaco, *Identification of MECL-1 (LMP-10) as the third IFN-gamma-inducible proteasome subunit.* J. Immunol., 1996. **156**(7): p. 2361-2364.
270. Díaz-Hernández, M., et al., *Enhanced induction of the immunoproteasome by interferon gamma in neurons expressing mutant Huntingtin.* Neurotox. Res., 2004. **6**(6): p. 463-468.
271. Chatterjee-Kishore, M., et al., *Different requirements for signal transducer and activator of transcription 1 alpha and interferon regulatory factor 1 in the regulation of low molecular mass polypeptide 2 and transporter associated with antigen processing 1 gene expression.* J. Biol. Chem., 1998. **273**(26): p. 16177-16183.
272. Yawata, M., et al., *Nucleotide sequence analysis of the approximately 35-kb segment containing interferon-gamma-inducible mouse proteasome activator genes.* Immunogenetics, 2001. **53**(2): p. 119-129.
273. Barton, L.F., et al., *Regulation of immunoproteasome subunit expression in vivo following pathogenic fungal infection.* J. Immunol., 2002. **169**(6): p. 3046-3052.
274. Bingol, B. and E.M. Schuman, *Activity-dependent dynamics and sequestration of proteasomes in dendritic spines.* Nature, 2006. **441**(7097): p. 1144-1148.
275. Boehmer, C., et al., *Regulation of the glutamate transporter EAAT1 by the ubiquitin ligase Nedd4-2 and the serum and glucocorticoid-inducible kinase isoforms SGK1/3 and protein kinase B.* J. Neurochem., 2003. **86**(5): p. 1181-1188.

276. Ehlers, M.D., *Activity level controls postsynaptic composition and signaling via the ubiquitin proteasome system.* Nat. Neurosci., 2003. **6**(3): p. 231-242.
277. Dubiel, W., et al., *Purification of an 11 S regulator of the multicatalytic protease.* J. Biol. Chem., 1992. **267**(31): p. 22369-22377.
278. Nelson, J.E., et al., *Proteasome from cytokine-treated human cells shows stimulated BrAAP activity and depressed PGPH activity.* Biochem. Cell Biol., 2000. **78**(2): p. 115-118.
279. Li, D., F. Sun, and K. Wang, *Caloric restriction retards age-related changes in rat retina.* Biochem. Biophys. Res. Commun., 2003. **309**(2): p. 457-463.
280. Chan-Ling, T., et al., *Inflammation and breakdown of the blood-retina barrier during "physiological aging" in the rat retina: a model for CNS aging.* Microcirculation, 2007. **14**(1): p. 63-76.
281. Xu, H., M. Chen, and J.V. Forrester, *Para-inflammation in the aging retina.* Prog. Retin. Eye Res., 2009. **28**(5): p. 348-368.
282. Hayashi, M., et al., *The mouse genes encoding the third pair of β-type proteasome subunits regulated reciprocally by IFN-γ: structural comparison, chromosomal localization, and analysis of the promoter.* J. Immunol., 1997. **159**(6): p. 2760.
283. Goldberg, A.L., *Functions of the proteasome: the lysis at the end of the tunnel.* Science, 1995. **268**(5210): p. 522-523.
284. Morrow, E.M., C.M. Chen, and C.L. Cepko, *Temporal order of bipolar cell genesis in the neural retina.* Neural Dev., 2008. **3**: p. 2.
285. Phillips, M.J., et al., *Tauroursodeoxycholic acid preservation of photoreceptor structure and function in the rd10 mouse through postnatal day 30.* Invest. Ophthalmol. Vis. Sci., 2008. **49**(5): p. 2148-2155.
286. Guillet, R., et al., *Anesthetic-induced corneal lesions in developmentally sensitive rats.* Invest. Ophthalmol. Vis. Sci., 1988. **29**(6): p. 949-954.
287. Robson, J.G., et al., *Rod and cone contributions to the a-wave of the electroretinogram of the macaque.* J. Physiol., 2003. **547**(Pt. 2): p. 509-530.
288. Akula, J.D., et al., *Rod photoreceptor function predicts blood vessel abnormality in retinopathy of prematurity.* Invest. Ophthalmol. Vis. Sci., 2007. **48**(9): p. 4351-4359.
289. Brandstätter, J.H., O. Dick, and T.M. Boeckers, *The postsynaptic scaffold proteins ProSAP1/Shank2 and Homer1 are associated with glutamate receptor complexes at rat retinal synapses.* J. Comp. Neurol., 2004. **475**(4): p. 551-563.
290. Sharma, R.K., et al., *Development of the outer retina in the mouse.* Brain Res. Dev. Brain Res., 2003. **145**(1): p. 93-105.
291. Behndig, A., et al., *Superoxide dismutase isoenzymes in the human eye.* Invest. Ophthalmol. Vis. Sci., 1998. **39**(3): p. 471-475.
292. Justilien, V., et al., *SOD2 knockdown mouse model of early AMD.* Invest. Ophthalmol. Vis. Sci., 2007. **48**(10): p. 4407-4420.
293. Galbinur, T., et al., *Effect of para-aminobenzoic acid on the course of retinal degeneration in the rd10 mouse.* J. Ocul. Pharmacol. Ther., 2009. **25**(6): p. 475-482.
294. Lu, L., et al., *Increased expression of glutathione peroxidase 4 strongly protects retina from oxidative damage.* Antioxid. Redox. Signal., 2009. **11**(4): p. 715-724.

295. Sasaki, M., et al., *Neuroprotective effect of an antioxidant, lutein, during retinal inflammation.* Invest. Ophthalmol. Vis. Sci., 2009. **50**(3): p. 1433-1439.
296. Fricker, L.D. and S.H. Snyder, *Purification and characterization of enkephalin convertase, an enkephalin-synthesizing carboxypeptidase.* J. Biol. Chem., 1983. **258**(18): p. 10950-10955.
297. Agapova, O.A., P.L. Kaufman, and M.R. Hernandez, *Androgen receptor and NFκB expression in human normal and glaucomatous optic nerve head astrocytes in vitro and in experimental glaucoma.* Exp. Eye Res., 2006. **82**: p. 1053-1059.

Appendix

Copyright Permissions

Chapter 2: Ethen, C.M., Hussong, S.A., Reilly, C., Feng, X., Olsen, T.W., Ferrington, D.A. Transformation of the proteasome with age-related macular degeneration. FEBS Letters, 2007. 581(5): 885-890.

ELSEVIER LICENSE
TERMS AND CONDITIONS

Oct 10, 2010

This is a License Agreement between Stacy A Hussong ("You") and Elsevier ("Elsevier") provided by Copyright Clearance Center ("CCC"). The license consists of your order details, the terms and conditions provided by Elsevier, and the payment terms and conditions.

All payments must be made in full to CCC. For payment instructions, please see information listed at the bottom of this form.

Supplier	Elsevier Limited The Boulevard,Langford Lane Kidlington,Oxford,OX5 1GB,UK
Registered Company Number	1982084
Customer name	Stacy A Hussong
Customer address	2001 6th Street SE
	Minneapolis, MN 55405
License number	2525550877188
License date	Oct 10, 2010
Licensed content publisher	Elsevier
Licensed content publication	FEBS Letters
Licensed content title	Transformation of the proteasome with age-related macular degeneration
Licensed content author	Cheryl M. Ethen, Stacy A. Hussong, Cavan Reilly, Xiao Feng, Timothy W. Olsen, Deborah A. Ferrington
Licensed content date	6 March 2007
Licensed content volume number	581
Licensed content issue number	5
Number of pages	6
Type of Use	reuse in a thesis/dissertation
Portion	full article
Format	both print and electronic
Are you the author of this Elsevier article?	Yes
Will you be translating?	No
Order reference number	
Title of your thesis/dissertation	Identifying Novel Roles for the Immunoproteasome in the Retina
Expected completion date	Oct 2010
Estimated size (number of pages)	250
Elsevier VAT number	GB 494 6272 12

Chapter 3: Ferrington, D.A., Hussong, S.A., Roehrich, H., Kapphahn, R.J., Kavanaugh, S.M., Heuss, N.D., Gregerson, D.S. Immunoproteasome responds to injury in the retina and brain. Journal of Neurochemistry, 2008. 106(1): 158-169.

JOHN WILEY AND SONS LICENSE TERMS AND CONDITIONS

Aug 19, 2010

This is a License Agreement between Stacy A Hussong ("You") and John Wiley and Sons ("John Wiley and Sons") provided by Copyright Clearance Center ("CCC"). The license consists of your order details, the terms and conditions provided by John Wiley and Sons, and the payment terms and conditions.

All payments must be made in full to CCC. For payment instructions, please see information listed at the bottom of this form.

License Number	2492770787889
License date	Aug 19, 2010
Licensed content publisher	John Wiley and Sons
Licensed content publication	Journal of Neurochemistry
Licensed content title	Immunoproteasome responds to injury in the retina and brain
Licensed content author	Deborah A. Ferrington,Stacy A. Hussong,Heidi Roehrich,Rebecca J. Kapphahn,Shannon M. Kavanaugh,Neal D. Heuss,Dale S. Gregerson
Licensed content date	Jul 1, 2008
Start page	158
End page	169
Type of use	Dissertation/Thesis
Requestor type	Author of this Wiley article
Format	Print and electronic
Portion	Full article
Will you be translating?	No
Order reference number	

Chapter 4: Hussong, S.A., Kapphahn, R.J., Phillips, S.L., Maldonado, M., Ferrington, D.A. Immunoproteasome deficiency alters retinal proteasome's response to stress. Journal of Neurochemistry, 2010. 113(6): 1481-1490.

JOHN WILEY AND SONS LICENSE TERMS AND CONDITIONS

Aug 19, 2010

This is a License Agreement between Stacy A Hussong ("You") and John Wiley and Sons ("John Wiley and Sons") provided by Copyright Clearance Center ("CCC"). The license consists of your order details, the terms and conditions provided by John Wiley and Sons, and the payment terms and conditions.

All payments must be made in full to CCC. For payment instructions, please see information listed at the bottom of this form.

License Number	2492550249670
License date	Aug 19, 2010
Licensed content publisher	John Wiley and Sons
Licensed content publication	Journal of Neurochemistry
Licensed content title	Immunoproteasome deficiency alters retinal proteasome's response to stress
Licensed content author	Stacy A. Hussong,Rebecca J. Kapphahn,Stacia L. Phillips,Marcela Maldonado,Deborah A. Ferrington
Licensed content date	Jun 1, 2010
Start page	1481
End page	1490
Type of use	Dissertation/Thesis
Requestor type	Author of this Wiley article
Format	Print and electronic
Portion	Full article
Will you be translating?	No
Order reference number	

Chapter 5: Hussong, S.A., Roehrich, H., Kapphahn, R.J., Maldonado, M., Pardue, M.T., Ferrington, D.A. A novel role for immunoproteasome in retinal function. Investigative Ophthalmology and Visual Science, 2010. doi: 10.1167/iovs.10-6032.

- Subject: **RE: Permission to print published materials in a doctoral dissertation**
- From: Debbie Chin <dchin@arvo.org> +
- Date: Fri, 1 Oct 2010 13:20:16 -0400
- To: husso004@umn.edu +
- Report this message as spam.

Dear Dr. Hussong,

If you need a hard copy of this permission, please let me know. Also, please note that while your accepted article is currently online in our Recently Accepted Papers section at http://www.iovs.org/cgi/content/abstract/iovs.10-6032v1, the final version will be published in a few months.

Permission is hereby granted to reprint the following article in your doctoral dissertation for the University of Minnesota. ARVO is aware that ProQuest may supply single copies of your dissertation upon demand and that the thesis will be submitted to the University of Minnesota Digital Conservancy, giving open access to all students, faculty, and staff of the University of Minnesota.

Hussong, S.A., Roehrich, H., Kapphahn, R.J., Maldonado, M., Pardue, M., Ferrington, D.A. 2010. A Novel Role for Immunoproteasome in Retinal Function. Invest Ophthalmol Vis Sci. DOI: 10.1167/iovs.10-6032

A reprint of this material must include a full article citation and acknowledge the Association for Research in Vision and Ophthalmology as the copyright holder.

Best regards,
Debbie Chin

Please note our new address:
IOVS Editorial Office
1801 Rockville Pike, Suite 400
Rockville, MD 20852
Tel: +1.240.221.2926 | Fax: +1.240.221.0355
www.iovs.org